The Influence of Carbon Dioxide on Cellular Cyclic Adenosine Monophosphate

COOK, ZARA,CHARLOTTE

The Influence of Carbon Dioxide on Cellular Cyclic Adenosine Monophosphate

Author: Zara Cook

Supervisor: Dr. Martin Cann

November 19, 2012

Contents

List of Figures

List of Tables

Abstract

Inorganic carbon is fundamental to the physiology of all organisms, however elevated CO_2 is generally detrimental. Numerous class III adenylyl cyclases (AC) from both prokaryotic and mammalian organisms have been shown to respond to inorganic carbon *in vitro*, however, at present there is limited evidence *in vivo*. This thesis demonstrates *in cellulo* evidence that hypercapnia CO_2 blunts agonist induced cAMP signalling. The effect of CO_2 is independent of changes in intracellular and extracellular pH, independent of the mechanism used to activate the cAMP signalling pathway, and is independent of the cell line employed. Through a combination of pharmacological and genetic tools this effect of elevated CO_2 on cAMP signalling is demonstrated to require Ca^{2+} ion release from IP_3 receptors in the endoplasmic reticulum. Consistent with these findings, CO_2 caused an increase in cytoplasmic Ca^{2+} concentrations which require the presence of active IP_3 receptors and is absent under comparable acidotic conditions. Physiological relevance for this signalling mechanism is demonstrated through activity of the sodium dependant proton exchanger NHE3. This transporter exhibits well-characterised inhibition by cAMP dependant protein kinase PKA to increase bicarbonaturia *in vivo*. Overall these results provide conclusive evidence of potentially profound effects of inorganic carbon on intracellular cell signalling, which could lead to significant insight into the pathophysiology and treatment of numerous disorders including metabolic acidosis, reperfusion injuries, acute lung injury and obesity.

Acknowledgements

My doctorate has been carried out through the joint assistance of the Biological and Biomedical Sciences and the Chemistry Departments at the University of Durham and the Epithelial Research group at Newcastle University. I appreciate all the guidance and materials I have received enabling me to carry out this work. I would like to foremostly thank Dr. Martin Cann, my supervisor, Dr. Stepan Fenyk and Dr. Philip Townsend for their time and help in the laboratory and additionally Dr. Robert Dorazi, Dr. Victoria Money and Dr. Catherine Bruce for aiding my understanding of experimental techniques and for being so accommodating to my presence in the lab. For their work on iTRAQ sample preparation and data production I would like to acknowledge Dr. William Simon and Miss Joanne Robson from the Proteomics Facility of the School of Biological and Biomedical Sciences at Durham University and away from Durham, Dr. Mike Gray of the University of Newcastle for providing both materials and assistance. For their help, support and understanding through the writing up period I would also like to express my gratitude to Mr. James Keaveney and my mother, Mrs. Linda Cook. Finally I would like to mention The Welcome Trust who have provided funding for this project, without which it would not have been possible for me to come this far.

Declaration

The work presented in this thesis is my own original research, except where indicated by statement or citation, and has not been submitted for any other degree. The copyright of this thesis lies with the author. No quotations from it should be published without prior written consent and information derived from it should be acknowledged.

List of Abbreviations

AC	Adenylyl Cyclase
ADP	Adenosine Diphosphate
AKAP	A-Kinase Anchoring Proteins
AMP	Adenosine Monophosphate
2-APB	2-Aminoethyl diphenylborinate
APS	Ammonium Persulphate
ATP	Adenosine Triphosphate
BAPTA(-AM)	1,2 - bis (o-aminophenoxy) ethane - N, N, N′, N′ - tetraacetic acid (- acetoxymethyl)
BCECF(-AM)	2′,7′-bis(carboxyethyl)-5(6)-carboxyfluorescein (- acetoxymethyl)
BSA	Bovine Serum Albumin
CaM	Calmodulin
cAMP	3′-5′-cyclic Adenosine Monophosphate
CaMKK	Ca^{2+}/Calmodulin-dependent Protein Kinase Kinase
CA	Carbonic Anhydrase
CFTR	Cystic Fibrosis Trans-membrane conductance Regulator
cGMP	3′-5′-cyclic Guanosine Monophosphate
Ci	Inorganic Carbon
cNMP	cyclic Nucleoside Monophosphate
CRE	cAMP Response Element
CREB	CRE Binding protein
DAG	Diacylglycerol
DMEM	Dulbecco's Modified Eagle Medium
DMSO	Dimethyl Sulfoxide
DTT	Dithiothreitol
DT40	Chicken B Lymphocytes
DT40-IP_3 R1	DT40-K/O with gene for IP_3R1 re-introduced
DT40-K/O	DT40 cell line with all IP_3R genes disrupted
EGTA	Ethylene Glycol Tetra-acetic Acid
EIA	Enzyme Immunoassay
ELISA	Enzyme-linked Immunosorbent Assay
Epac	Exchange proteins activated by cAMP
ER	Endoplasmic Reticulum
FSK	Forskolin (adenylylyl cyclase activator)
GC	Guanylyl Cyclase
HBS	HEPES Buffered Saline
HEK293t	Human Embryonic Kidney cells
HEKPR1	HEK cells stably expressing human Parathyroid Hormone Receptor 1

HEPES	4-(2-hydroxyethyl)-1-piperazineethanesulfonic acid
IP_3	Inositol triphosphate
IP_3R	Inositol triphosphate receptor
IBMX	Isobutylmethylxanthine
IPTG	Isopropyl β-D-thiogalactoside
KO or K/O	Knock-out
LC	Liquid Chromatography
MAPK	Mitogen Activated Protein Kinase
MS	Mass Spectrometry
MS/MS	Tandem Mass Spectrometry
NAD(P)H	Nicotinamide Adenine Dinucleotide (Phosphate)
NAADP	Nicotinic Acid-Adenine Dinucleotide Phosphate
NEAA	Non-Essential Amino Acids
NHE	Na^+/H^+ Exchanger
Pi	Inorganic Phosphate
pHe	Extracellular pH
pHi	Intracellular pH
OK	Opossum Kidney cell line
PA	Propionic Acid
PBS	Phosphate Buffered Saline
RyR	Ryanodine Receptors
SDS	Sodium Dodecyl Sulphate
SERCA	Sarcoplasmic/Endoplasmic Reticulum Ca^{2+}-ATPases
Sto-609	1,8-napthoylene benzimidazole-3-carboxylic acid
TBST	Tris-Buffered Saline Tween-20
TCA	Tricholoacetic acid
TEMED	Tetramethylethylenediamine
tmAC	Transmembrane Adenylyl Cyclase
PDE	Phosphodiesterase
PIP2	Phosphatidylinositol 4,5-bisphosphate
PI3(K)	Phospho-tri-inositol (Kinase)
PKA/C	Phospho-Kinase A/C
PLC	Phospho-Lipase C
PPi	Inorganic Pyrophosphate
PT	Proximal Tubule
PTH	Parathyroid Hormone
sAC	soluble Adenylyl Cyclase
SDS	Sodium Dodecyl Sulphate
TEMED	N,N,N′,N′-tetramethyl-ethylenediamine

UMR-106	Rat osteosarcoma cell line
7TM	Seven Transmembrane Receptors

1 Chapter 1: Background Information

1.1 Overview

This thesis provides evidence that CO_2 can alter physiological processes through IP_3 mediated Ca^{2+} release and an associated decrease in intracellular cAMP levels. This chapter is aimed at providing the reader with a review of the topics required to greater appreciate the research findings. A review of both the cAMP and calcium signalling pathways will be provided, with particular focus on how inorganic carbon affects adenylyl cyclase isoforms and IP_3 mediated calcium release from the endoplasmic reticulum. Examples of the interactions between these two signalling pathways will also be provided. Following on from this signalling information, inorganic carbon will be considered and its role in the environment, as well as *in vivo*. The final section focuses on how systemic inorganic carbon levels are regulated, in addition to how disruption of these mechanisms can lead to pathophysiological acid-base disorders and their clinical implications. Particular focus in the final section will lie on the effects of hypercapnia in a clinical setting, as well as the renal control of HCO_3^- reabsorption, as it is this system that is most relevant for the experimental chapters to follow.

1.2 Cell Signalling

Cell signalling is part of a complex system of communication that governs basic cellular activities and coordinates cell actions. No cells live in complete isolation; in order for organisms to survive, cells need to be able to monitor their extra-cellular environments and adjust accordingly in order to promote survival. Commonly, the perception of both abiotic and biotic elements of the environment is provided through the use of protein receptors, which transduce a stimulus to an intracellular signalling network. Within this network, information is commonly conveyed either through protein-protein interactions, or is transmitted by diffusible elements, usually referred to as second messengers. Cells often employ a number of these signalling pathways and cross-talk between them is an important feature of their regulation. Responses to stimuli vary, but notably involve transcription, translation and post-translational effects. Errors in cellular information processing can lead to diseases such as cancer, autoimmune disorders and diabetes, as well as ultimately resulting in death.

1.3 Adenylyl Cyclase and cAMP

1.3.1 Introduction

Once an abiotic or biotic stimulus has been perceived at the plasma membrane of a cell, intracellular cascades of molecular responses usually ensue. One common method of signal propagation is through the accumulation of an intracellular second messenger, which acts as an intermediary between the receptor and target molecule. This section focuses on the generation of one such second messenger, 3′,5′-cyclic adenosine monophosphate (cAMP). Cyclic-AMP (Sutherland & Rall, 1958) is an important signalling molecule involved in a host of processes as diverse as controlling cellular shape in *Bordetella pertussis* infected cells (Ohnishi et al., 2008), osmoregulation, chemotaxis, phototaxis, pH regulation (Linder & Schultz, 2003), memory formation (Gerstner et al., 2009), olfaction (Kamenetsky et al., 2006) and cardiac contraction (Pignatti et al., 1993).

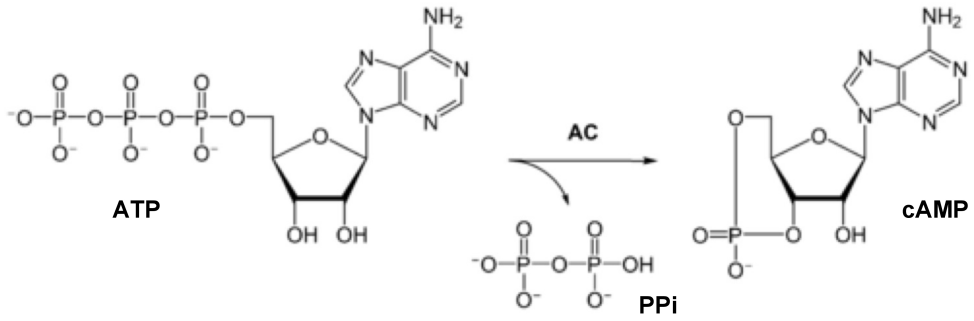

Figure 1: Reaction catalysed by adenylyl cyclase

Cyclic-AMP is generated by the enzyme adenylyl cyclase (AC) which catalyses the cyclisation of its substrate ATP to produce cAMP, in addition to an inorganic pyrophosphate by-product (Figure 1). This enzyme is present in all kingdoms of life, although its presence in plants is controversial (Kamenetsky et al., 2006; Gehring, 2010; Fenyk et al., 2012). Genes encoding AC are divided into six phylogenetically defined classes by primary amino acid sequence (Bârzu & Danchin, 1994). Briefly, class I ACs are found in the Enterobacteria such as *Escherichia coli* where they mediate catabolic repression; class II in exclusive toxin-producing bacteria such as *Bacillus anthracis* and *Bordetella pertussis*; class III in higher eukaryotes in addition to certain prokaryotic members; class IV in certain prokaryotic thermophiles such as *Aeromonas hydrophila*. Class V consists of a single member from the obligate anaerobe *Prevotella ruminicola*; and class VI ACs are found in the genomes of the

Rhizobiaceae (Cann et al., 2003). Class III is of most interest here as it encompasses the isoforms found in mammalian cells and the class on which most work on AC stimulation by inorganic carbon has been carried out (Section 1.3.6). From this point forth where ACs are mentioned they will thus be isoforms in this class. Mammalian ACs are further divided into ten isoforms with isoforms I-IX transmembranal across the plasma membrane and responsive to G-proteins (Section 1.3.2). In contrast group X, discovered in 1975 (Braun & Dods, 1975), is intracellular and deceivingly has been named soluble adenylyl cyclase (sAC) despite being located at specific organelles including the centrioles, mitotic spindle, mitochondria and within the nucleus (Zippin et al., 2003; Acin-Perez et al., 2011); and therefore is not typically 'soluble' (Section 1.3.3).

1.3.2 Transmembrane Adenylyl Cyclases

Transmembrane ACs (tmACs) consist of two sets of six transmembrane domains, each followed by an intracellular catalytic domain (Figure 1.3.2). The two catalytic domains are called C1a and C2a and contain similar (more than 50% similarity), but non-identical, sequences of around 230 amino acids and are responsible for ATP binding and catalysis (Tang & Hurley, 1998). C1a and C2a are then followed by two hyper-variable sequence regions, C1b and C2b respectively, which contain several regulatory sites (Hurley, 1999) and are not related between isoforms. As expected with such high sequence homology, the tertiary structure of C1a and C2a is almost identical, consisting of a three-layer α/β sandwich enabling hetero-dimerisation. The two domains orientate head-to-tail forming two potential ATP binding sites at their interface (Tang & Hurley, 1998). Only one of these sites is involved in substrate binding and catalysis, whilst the other acts as a binding site for the AC activator forskolin (Tesmer et al., 1997; Zhang et al., 1997), a plant diterpene from *Coleus forskolhii*. Forskolin activates all AC isoforms bar type IX from several species (Hatley et al., 2002; Cumbay & Watts, 2004; Yan et al., 1998; Hacker et al., 1998) and sAC (Forte et al., 1983) and works by promoting the affinity of the C1 and C2 domains (Dessauer et al., 1997). This domain interaction is particularly important as neither catalytic domain can function independently, as proven by experiments in *E.coli* using recombinant forms of the cytosolic domains of the mammalian type I and type II isoforms (Tang & Gilman, 1995).

In addition to forskolin, all tmACs are regulated by G-proteins, GTP activated proteins released from the intracellular domain of an upstream seven trans-membrane (7TM) receptor (Section 1.3.5). The AC activating G-protein Gα_s has a binding site which is $\sim$30 Å away from the AC catalytic site (Yan et al., 1997) and binding facilitates a 7 degree rotation of C1 with respect to C2, which

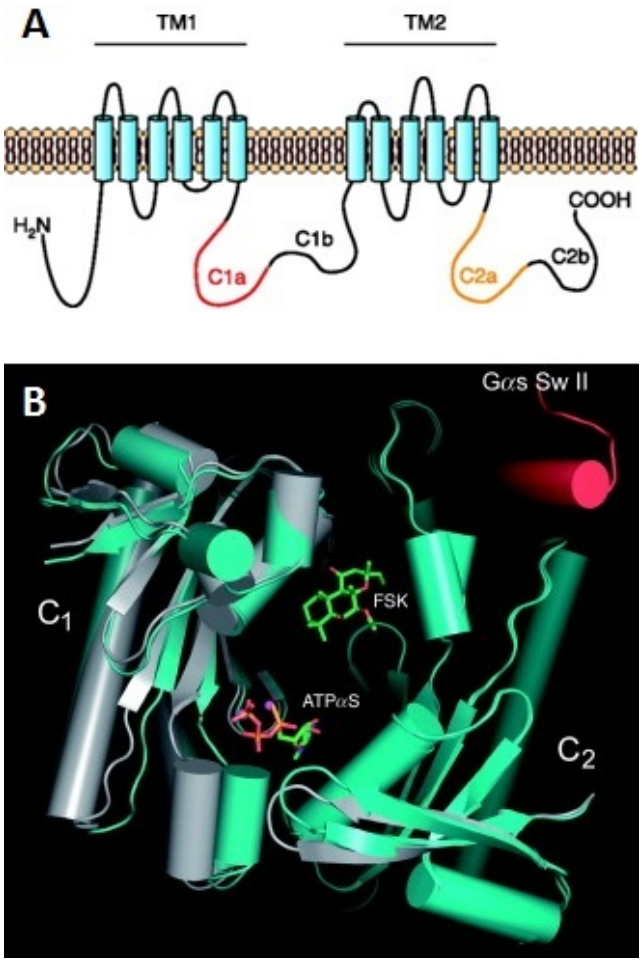

Figure 2: Structure of transmembrane adenylyl cyclase.

A. Diagrammatic representation of AC showing the NH_2 terminus, the first transmembrane region (TM1, cyan cylinders), the first cytoplasmic loop comprising C1a (red) and C1b (black), the second transmembrane cluster (TM2, cyan cylinders) the second cytoplasmic loop comprising C2a (orange) and C2b (black) and the C terminus. C1a and C2a are highly conserved catalytic ATP-binding regions, which dimerise to form the catalytic site. Figure adapted from *Willoughby et al.* (Willoughby & Cooper, 2007).

B. Ribbon diagram of the AC catalytic domains with α-helices shown as cylinders and β-strands as ribbons. The C2 domains of two AC molecules are superimposed with the open inactive enzyme crystallised in the absence of an ATP analogue in grey (PDB ID: 1AZS) and the closed active state crystallised with ATP bound to the AC catalytic site in cyan (PDB ID: 1CJT). Location of forskolin and $G\alpha_s$ switch II domain (red) binding is also included. With substrate ATP in the active site the two catalytic domains are held closer together which allows catalysis to proceed. Figure adapted from *Sprang et al.* (Sprang et al., 2007).

causes the AC active site to close around its ATP substrate (Tesmer et al., 1999). Binding of Gα_i to ACs I, V and VI (Kamenetsky et al., 2006), however, inhibits these isoforms by hindering this active site collapse and stabilising an inactive conformation of the enzyme (Tesmer et al., 1999).

AC Isoform	Tissue Distribution	Regulatory Factor		
		G protein Subunits	Protein Kinases	Ca^{2+}/CaM
AC 1	Brain, adrenal medulla	$G\alpha_s$ stimulated; $G\alpha_o$ and $G\beta\gamma$ inhibited	PKC weak stimulation, CaMIV inhibited	Stimulated
AC 2	Brain, skeletal muscle, lung, heart	Stimulated by $G\alpha_s$ and $G\beta\gamma$	PKC stimulated	
AC 3	Brain, olfactory epithelium	$G\alpha_s$ stimulated	PKC weak stimulation, CaMII inhibited	Stimulated
AC 4	Brain, heart, kidney, liver, lung, uterus	Stimulated by $G\alpha_s$ and $G\beta\gamma$	PKC inhibited	
AC 5	Heart, brain, kidney, liver, lung, uterus, adrenal	$G\alpha_s$ stimulated; $G\alpha_i$ and $G\beta\gamma$ inhibited	PKA inhibited, PKC stimulated	Inhibited
AC 6	Ubiquitous	$G\alpha_s$ stimulated; $G\alpha_i$ and $G\beta\gamma$ inhibited	PKA inhibited, PKC stimulated	Inhibited
AC 7	Ubiquitous, highly expressed in the brain	Stimulated by $G\alpha_s$ and $G\beta\gamma$	PKC stimulation	
AC 8	Brain, lung, testis, adrenal, uterus, heart	Stimulated by $G\alpha_s$		Stimulated
AC 9	Brain, skeletal muscle	Stimulated by $G\alpha_s$		
sAC	Brain, ovary, liver, lung, spleen, heart, embryo, testis, kidney	Not regulated by G protein subunits		Stimulated

Table 2: Regulatory properties and tissue distribution of mammalian adenylyl cyclase isoforms (Sunahara & Taussig, 2002; Sinclair et al., 2000).

Certain AC isoforms can also be regulated by other G-protein subunits including: $G\alpha_o$ and $G\beta\gamma$ (Section 1.3.5 and Table 2) and tissue specific subunits such as $G\alpha_{olf}$ which activates ACs in the olfactory system (Milligan et al., 1990). TmACs are further regulated by adenosine analogs, Ca^{2+}/calmodulin (Section 1.5), CO_2 (Section 1.3.6), protein kinases and via feedback inhibition from downstream protein kinase A (PKA). Each AC isoform responds to these factors differentially (Tang & Hurley, 1998) and a summary table of these interactions is provided as Table 2.

1.3.3 Soluble Adenylyl Cyclase

Compared to AC isoforms I-IX, sAC is structurally, molecularly and biochemically distinct (Buck et al., 1999) being neither transmembranal nor regulated by G-proteins (Braun & Dods, 1975). Although the enzyme still contains two catalytic domains (C1 and C2) these two domains exhibit low sequence homology compared to those of the tmACs and are more similar to bacterial ACs than other mammalian tmACs. This has led to the theory that sAC originated from the fusion of two distinct bacterial proteins rather than a duplication event (Buck et al., 1999; Kobayashi et al., 2004). As mentioned, sAC is not located at the plasma membrane but found within the cytoplasm, mitochondria and nucleus (Xie & Conti, 2004; Zippin et al., 2003; Acin-Perez et al., 2011). sAC thus provides an intracellular source of cAMP, closer to its downstream targets. For example, PKA is often found at similar intracellular locations to sAC (Zippin et al., 2003), anchored by AKAPs; A-kinase anchoring proteins (Alberts, 2002). This proximity is particularly advantageous as it reduces the possibility of loss of signal via the breakdown of cAMP by endogenous phosphodiesterases (PDEs), which restrict cAMP diffusion to less than 1 μm from its source (Zippin et al., 2003). sAC has been shown to respond directly to Ca^{2+} (not via calmodulin) and bicarbonate, synergistically when both are present (Garbers et al., 1982). As HCO_3^- is in a pH dependent equilibrium with CO_2 (Section 1.6) it is possible that sAC is regulated by either or both of these species and furthermore that other AC types could be similarly activated (Townsend et al., 2009). Discussion of this AC regulatory mechanism is provided in Section 1.3.6.

1.3.4 Catalysis Mechanism and Requirement for Divalent Metal Co-factors

Despite the differences in AC regulation and structure across the mammalian isoforms (Sections 1.3.2 and 1.3.3) the reaction mechanism of ATP cyclisation remains relatively constant (Figure 3). Catalysis requires the interaction of two divalent metal ion co-factors. For tmACs these ions are

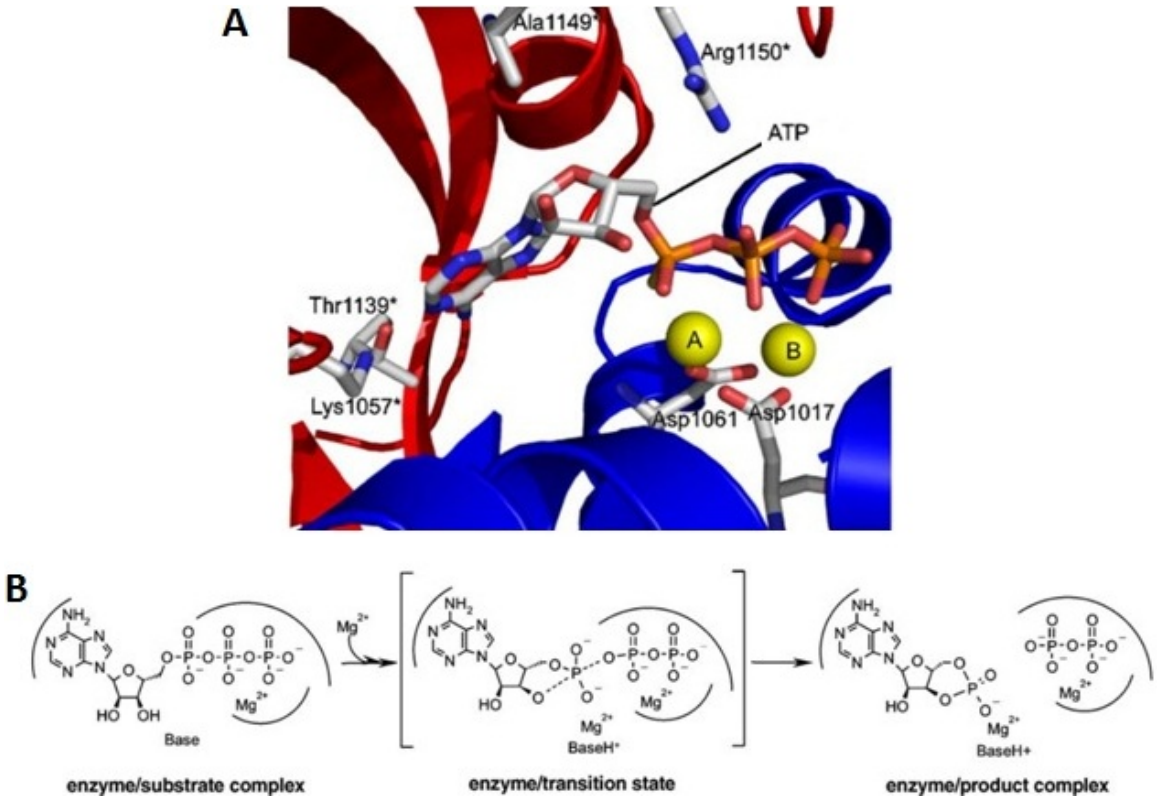

Figure 3: Adenylyl cyclase reaction mechanism and divalent ion co-factor requirement.

A. Active site of the sAC-like cyclase CyaC in complex with the ATP. AC catalytic domain C1 presented as red ribbons with C2 in blue and magnesium ions A and B as yellow spheres. ATP substrate coloured with the adenine base in grey and blue, the ribose sugar in grey and red and the three phosphates in orange and red. The ion-coordinating aspartate residues 1017 and 1061, the residues recognising the adenine ring (Thr1139* and Lys1057*), the phosphate binding arginine (1150*), and the alanine conserved in sACs and replaced by serine in tmACs (1149*) are labeled.

B. Catalytic mechanism of class III AC enzymes. Schematic view of the two-ion catalysed reaction, which starts with the substrate ATP and yields the products cAMP and pyrophosphate. The reaction proceeds through a magnesium stabilised penta-covalent transition state.

Figures adapted from *Kamenetsky et al.* (Kamenetsky et al., 2006)

usually both Mg^{2+}, although Mn^{2+} at one site is able to enhance the catalytic activity of most isoforms (Hatley et al., 2002). For sAC the co-factors are both normally Mn^{2+} (Braun & Dods, 1975), although other divalent cations can substitute, predominantly Mg^{2+} and Ca^{2+} (Geng et al., 2005). The ion co-factors are co-ordinated by two conserved aspartate residues located within the enzyme active site and are required to increase enzyme activity by both enabling the formation of complexes with the substrate ATP (de Haen, 1974) and chelating free inhibitory ATP molecules (Alvarez & Bruno, 1977; Hammes & Rodbell, 1976). ATP hydrolysis proceeds via a pseudo-bimolecular nucleophilic substitution (SN2) mechanism (Kamenetsky et al., 2006). Metal ion A acts to acidify the ATP ribose 3′-hydroxyl and stabilise the transition state between the 3′-hydroxyl and the α-phosphoryl group, whilst ion B anchors the ATP's β- and γ-phosphates (Tesmer et al., 1999) and enables production of the pyrophosphate product (PPi). The shape of the cAMP product is incompatible with the AC active site, whilst PPi fits by the metal ion A and thus cAMP is preferentially released from the active site before PPi (Tesmer et al., 1999).

Divalent cations are not only vital for reaction progression, they also impart an element of regulation. For example, as age increases in rats so does the need for a Mg^{2+} co-factor (Pignatti et al., 1993), potentially altering signalling dynamics over time. Furthermore, increases in Mg^{2+} concentration favour different signalling pathways through the AC, particularly through activation of the GTP regulatory site of the AC activating G-protein Gα_s (Alvarez & Bruno, 1977) and by promoting the formation of functional complexes between Gα_s and AC (Pignatti et al., 1993). Hormones increase the affinity of tmACs to Mg^{2+} (Alvarez & Bruno, 1977), whilst the cation also improves tmAC affinity for forskolin by favouring activation of Gα_s, as mentioned (Pignatti et al., 1993).

1.3.5 AC and cAMP Signalling Pathway

Generally mammalian tmACs work as part of a signalling pathway in response to a hormonal stimulus. The classic example of this is activation of the β-adrenergic receptor by adrenaline or, as relevant to this work, parathyroid hormone (PTH) activation of the PTH receptor (Section 1.7.3). Hormones bind to hepta-helical seven-transmembrane receptors (7-TM) at the plasma-membrane which transduce the signal into the cell. With receptor activation, hetero-trimeric G-proteins attached to the receptor intracellular domain are activated (Figure 4). Hetero-trimeric G-proteins consist of distinct α, β and γ subunits, the α-subunit of which is activated when bound to GTP. When stimulated by a ligand the 7-TM receptor acts as a guanine nucleotide exchange factor (GEF) exchanging GDP for GTP on the Gα subunit, thus activating it (Kimata et al., 2012). This α subunit

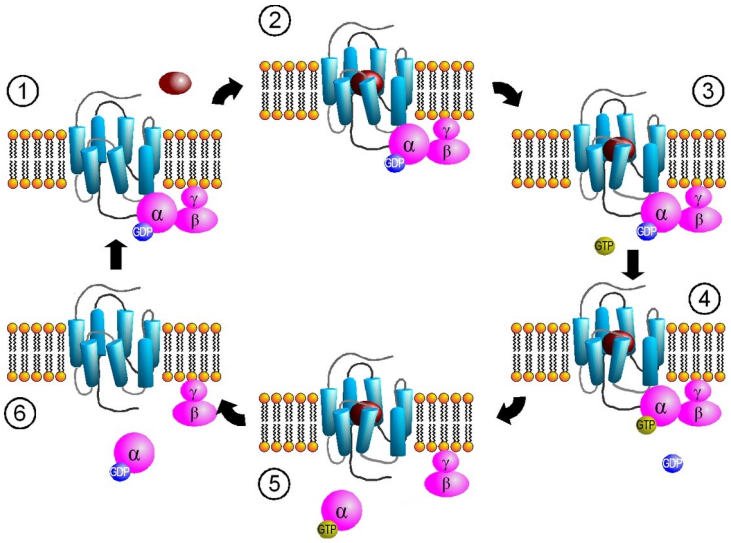

Figure 4: G-protein coupled receptor activation cycle. When a ligand activates the G-protein-coupled receptor (1-2), it induces a conformational change in the receptor that allows the receptor to function as a guanine nucleotide exchange factor (GEF) that exchanges GDP for GTP on the Gα subunit (3-4). This exchange triggers the dissociation of the active GTP-bound Gα subunit from the G$\beta\gamma$ dimer and the receptor (5). Following GTP hydrolysis Gα reassociates with G$\beta\gamma$, terminating the signal (6). Figure adapted from *Jähnichen et al.* (Jähnichen, 2006).

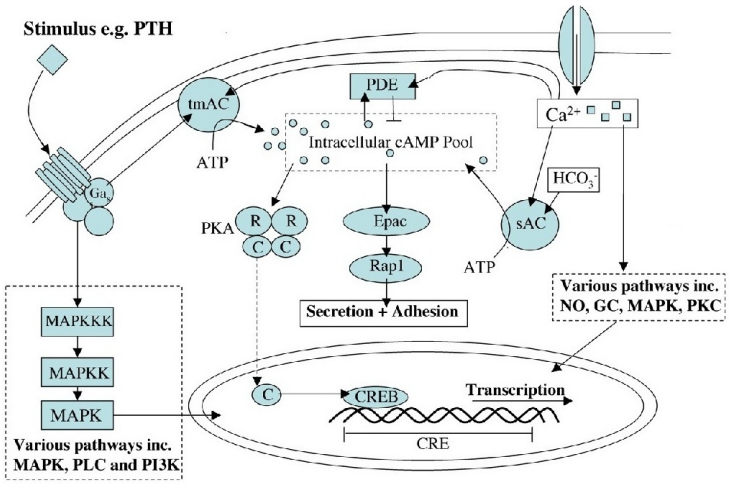

Figure 5: Adenylyl cyclase activated pathway. Abbreviations used: CRE, cAMP Response Element; CREB, CRE Binding protein; Epac, Exchange proteins activated by cAMP; GC, Guanylyl Cyclase; MAPK, Mitogen Activated Protein Kinase; NO, Nitric Oxide; PI3K, Phospho-tri-inositol Kinase; PKA, Phospho-Kinase A; PKC, Phospho-Kinase C; sAC, soluble Adenylyl Cyclase; tmAC, transmembrane Adenylyl Cyclase.

is then released from the receptor and the β-γ dimer complex, allowing it to diffuse within the cell and influence downstream ACs accordingly, binding directly with the AC catalytic core (Sunahara et al., 1997; Dessauer et al., 1997). The Gα subunit also contains an intrinsic GTPase activity which hydrolyses the bound GTP to GDP and inorganic phosphate. Following GTP hydrolysis Gα then reassociates with G$\beta\gamma$ and the receptor, terminating the signal.

There are numerous Gα moieties, although particularly relevant to AC signalling are the stimulatory Gα_s and inhibitory Gα_i forms (Nowak & Zawilska, 1999; Cooper, 2003), as mentioned in Section 1.3.2. Although the α subunit appears to be most important to AC regulation, the β-γ dimer can also have a regulatory effect on AC. This can either occur directly, with AC1 inhibited and both ACs 2 and 7 activated by the β-γ dimer, or indirecty through β-γ chelation of G-protein α-subunits (Cooper, 2003). Both the activation of the G-proteins and their interaction with the allosteric site on the AC catalytic moiety is dependent on the availability of Mg^{2+} ions (Pignatti et al., 1993), which is also the co-factor required for tmAC catalysis, as mentioned. As Gα_s has lower affinity for Mg^{2+} compared to Gα_i, increased Mg^{2+} concentration leads to a higher proportion of active Gα_s and therefore AC, increasing basal cAMP production (Pignatti et al., 1993). Of course, this G-protein activation is not the case for sAC, which instead is activated by HCO_3^- and Ca^{2+} ions (Sections 1.3.3 and 1.3.6).

The AC product, cAMP, is an important signalling molecule and second messenger, providing a diffusible signal able to activate effector proteins. In the case of cAMP these effector proteins are: protein kinase A (PKA), whose catalytic domains separate from the regulatory domains and move to the nucleus (Meinkoth et al., 1993) to activate transcirption factor CREB (cAMP response element-binding protien); exchange proteins activated by cAMP (Epacs); phopsho-diesterase GAF domains; and cyclic nucleotide-gated ion channels CNGs and HCNs (Kamenetsky et al., 2006). A diagrammatic representation of this pathway is presented in Figure 5.

As with all signalling molecules, the degradation and removal of the signal is as important as its generation. For cAMP this is achieved through hydrolysis of its 3′-phosphate bond, yielding 5′-AMP (Johnson et al., 1994). Although this reaction is exergonic, a high activation energy prevents spontaneous degradation which makes cAMP relatively stable in the cell (Hancock, 2005). To overcome this, cAMP breakdown is catalysed by phosphodiesterases (PDEs). These enzymes comprise of homologous catalytic domains fused to varying N-terminal regulatory domains, making them differently sensitive to regulation by a number of small molecules, including calmodulin/Ca^{2+} and cNMPs (Omori & Kotera, 2007). Within the mammalian PDEs there are eleven families which

are further divided by a multitude of splice variants. These exhibit unique tissue expression patterns, gene regulation, substrate specificities, kinetic properties, enzymatic regulation by phosphorylation and regulatory proteins, subcellular localisation and interaction with association proteins but all have high affinities for cAMP and/or cGMP (Omori & Kotera, 2007). PDEs often located with ACs and downstream protein kinase A (PKA), especially as both are known to attach to scaffold proteins (Omori & Kotera, 2007; Stefan et al., 2007). These associations create signalling microdomains which are able to respond to stimuli rapidly and reversibly, thereby integrating and spatially restricting their cellular effects in both time and space (Di Benedetto et al., 2008; Mongillo et al., 2004; Houslay et al., 2007). An example of this involves muscle-specific A-kinase anchoring protein (mAKAP) which is located at the perinucleus in striated muscle (Dodge-Kafka et al., 2005). This AKAP binds to PDE4A, PDE4D3, PKA and Epac1, localising a compartmentalised signalling network to the nucleus (Dodge-Kafka et al., 2005). In this system activated PKA both stimulates PDE4D3 to reduce local cAMP concentrations (Dodge-Kafka et al., 2005) and phosphorylates the PDE at Ser-13, enhancing its affinity to mAKAP further and allowing for quicker signal termination (Carlisle Michel et al., 2004). Furthermore, PDE4D3 functions as an adaptor protein that recruits Epac1, maintaining the signalling pathway (Dodge-Kafka et al., 2005).

1.3.6 Involvement of Carbon Dioxide in Adenylyl Cyclase Regulation

There has been extensive research into the control of ACs by inorganic carbon following the discovery that sperm development, hypermotility, capacitation and the acrosome reaction in some organisms (Hyne & Garbers, 1979; Beltran et al., 2007; Xie et al., 2006) is initiated by the bicarbonate sensitive sAC (Esposito et al., 2004; Xie et al., 2006). This sAC isoform is first expressed during the late stages of spermatogenesis (Sinclair et al., 2000; Xie & Conti, 2004) and, therefore, is a key molecule in fertility, with sperm from $sAC^{-/-}$ mice unable to fertilise oocytes *in vitro* (Esposito et al., 2004; Hess et al., 2005). sAC is not activated by G-proteins (Braun & Dods, 1975) like most other known ACs, but is synergistically activated by calcium and bicarbonate ions (Garbers et al., 1982; Litvin et al., 2003). Importantly, this bicarbonate activation was pH independent both *in vivo* and *in vitro* (Chen et al., 2000). Since then, sAC has been found expressed in somatic cells from most parts of the body (Sinclair et al., 2000) and has been shown to be involved in processes ranging from the regulation of the cystic fibrosis trans-membrane conductance regulator (CFTR) in both airway (Wang et al., 2005) and corneal endothelial cells (Li et al., 2008; Sun et al., 2003); maintenance of pH by V-ATPases in both the male reproductive tract (Pastor-Soler et al., 2003) and kidney (Paunescu

et al., 2008); airway cilia beat frequency (Schmid et al., 2007); and nerve growth factor mediated neuronal differentiation (Stessin et al., 2006).

It is now known that a sAC is not the only AC activated by inorganic carbon. In prokaryotes numerous examples have been reported, indicating that the response is highly conserved (Esposito et al., 2004). Examples are mostly class III ACs and include isoforms from *Spirulina (Arthrospira) platensis* (Chen et al., 2000), *Stigmatella aurantiaca* (Cann et al., 2003), *Anabaena* (Cann et al., 2003; Hammer et al., 2006), and *Synechocystis* (Hammer et al., 2006). In mammals, there is even conclusive evidence that while sAC alone is responsive to both HCO_3^- and CO_2, all other class III trans-membrane ACs (types I-IX) are responsive to CO_2 (Townsend et al., 2009).

Understanding of the mechanism behind this inorganic carbon activation of ACs first began in 2003 when *Litvin et al.* published a paper examining the kinetic properties of sAC. Here, bicarbonate stimulation resulted in an increase in V_{max} with little effect on K_M (Litvin et al., 2003). These results were similar to observations for rat olfactory neuron GC-D where bicarbonate caused pH independent activation (Guo et al., 2009) and for *Anabaena* cyaB1 (Cann et al., 2003). It appeared that inorganic carbon acts directly at the active site (Jaiswal & Conti, 2001; Chen et al., 2000), coordinated by a lysine residue (Cann et al., 2003; Hall et al., 2010) in conjunction with an aspartate to threonine polymorphism conserved in class III adenylyl cyclases from diverse eukaryotes and prokaryotes (Cann et al., 2003; Kobayashi et al., 2004; Hall et al., 2010). Using recombinant proteins *Cann et al.* demonstrated that adenylyl cyclases that contain this active site threonine such as cyaB of *Stigmatella aurantiaca* and Rv1319c of *Mycobacterium tuberculosis* are bicarbonate-responsive, whereas adenylyl cyclases with a corresponding aspartate such as Rv1264 of *Mycobacterium* are bicarbonate-insensitive (Cann et al., 2003).

The effect of the bicarbonate ion on AC appears to involve both the promotion of active site closure in addition to its ability to aid the recruitment of one of the two metal ions essential for catalysis (Steegborn et al., 2005). The involvement of the metal co-factor in the mechanism by which bicarbonate stimulates ACs was futher supported in a report on human sAC (Geng et al., 2005). This sAC isoform only exhibits minimal response to bicarbonate in the absence of divalent cations, but bicarbonate divergently stimulates the Mg^{2+} bound form and inhibits the Mn^{2+} bound form in dose dependent manner. Furthermore, *Townsend et al.* have shown that inorganic carbon, here in the form of CO_2, interacts directly with the apoenzyme prior to any metal recruitment with the knock-on effect of increasing k_{cat} (Townsend et al., 2009).

1.4 Calcium Signalling

In addition to cAMP there is another second messenger of note: calcium. Unlike many other intracellular signals which can be generated and destroyed, Ca^{2+} ions can neither be made nor destroyed; it is the concentration ($[Ca^{2+}]$) at subcellular locations that constitutes a signal. Calcium release can have a range of downstream effects depending on the cell type and signalling mechanism. These range from cell division to apoptosis and include: secretion, muscle contraction and neuronal excitation. Its use as a signalling molecule is ubiquitous across all kingdoms of life from simple bacteria to plants and mammals (Hancock, 2005).

Rapid changes in intracellular calcium affect a range of downstream signalling pathways. As a result cells have tight control over their cytosolic levels, maintaining resting cytoplasmic concentrations at less than 1 μM (Streb et al., 1983; Zacchetti et al., 1991). If cells are activated cytosolic Ca^{2+} may reach 10 μM (Zacchetti et al., 1991). Control is managed both through the continuous action of ATP powered calcium pumps across the plasma membrane and by storage of Ca^{2+} ions in subcellular organelles, including the endoplasmic reticulum (Section 1.4.1), mitochondria (Section 1.4.2) and acidic endosomal organelles such as lysosomes (Section 1.4.3). Calcium signalling is complicated to study, due to the number of calcium stores within the cell and the diverse signals involved in its release and response (Figure 6).

In the cell calcium is maintained in its ionic form Ca^{2+} or bound to specific molecules. These binding molecules have two roles: to remove free active calcium from solution and/or to provide a mechanism to propagate the calcium signal (Hancock, 2005). Proteins which bind to calcium typically do so via the oxygen molecules of glutamate or aspartate residues which are normally charged at physiological pH (Hancock, 2005; Musgaard et al., 2011). There are two main calcium binding motifs: EF hands or C2 domains.

EF-hands consist of two α-helices positioned roughly perpendicular to one another and connected by a short loop that provides the calcium binding domain (Figure 7A). This loop is typically 12 residues in length, containing 7 oxygen atoms from the amino acid side-chain carboxyl or hydroxyl groups and a main chain carbonyl group (Zhou et al., 2009). This provides a binding pocket for a Ca^{2+} ion which has pentagonal bi-pyramidal geometry (Zhou et al., 2009) in which the Ca^{2+} ion can bind to both the peptide backbone and the side-chains via charge interactions (Zhou et al., 2009). The rest of the amino acids in the calcium binding loop tend to be hydrophobic, stabilising the two helices (Lewit-Bentley & Réty, 2000). Proteins containing this structural EF-hand domain include parvalbumin,

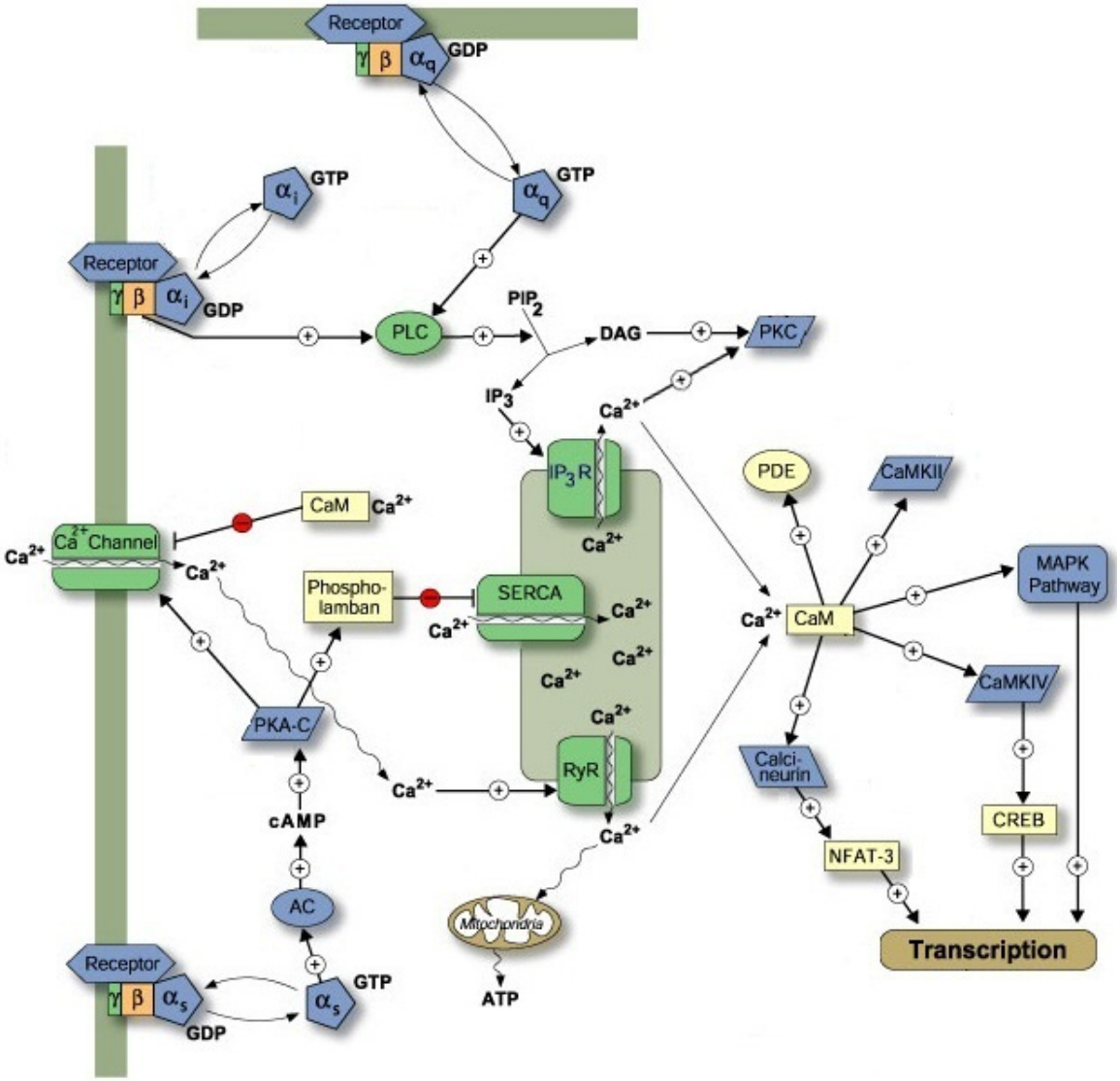

Figure 6: Calcium signalling pathway: overview of the signalling networks involving Ca^{2+} ions. Abbreviations used: CREB, cAMP Response Element Binding protein; CaM, Calmodulin; CaMK, CaM Kinase; DAG diacylglycerol; IP_3, Inositol Triphosphate; IP_3R, IP_3 Receptor; MAPK, Mitogen Activated Protein Kinase; NFAT-3, Nuclear Factor of Activated T cells-3 (transcription factor); PDE, Phosphodiesterase; PIP2, Phosphatidylinositol 4,5-bisphosphate; PKA/C, Phospho-Kinase A/C; PLC, Phospho-Lipase C; PI3K, Phospho-tri-inositol Kinase; RyR, Ryanodine Receptor; SERCA, Sarcoplasmic/Endoplasmic Reticulum Ca^{2+}-ATPases. Figure adapted from *Berridge et al.* (Berridge et al., 2012).

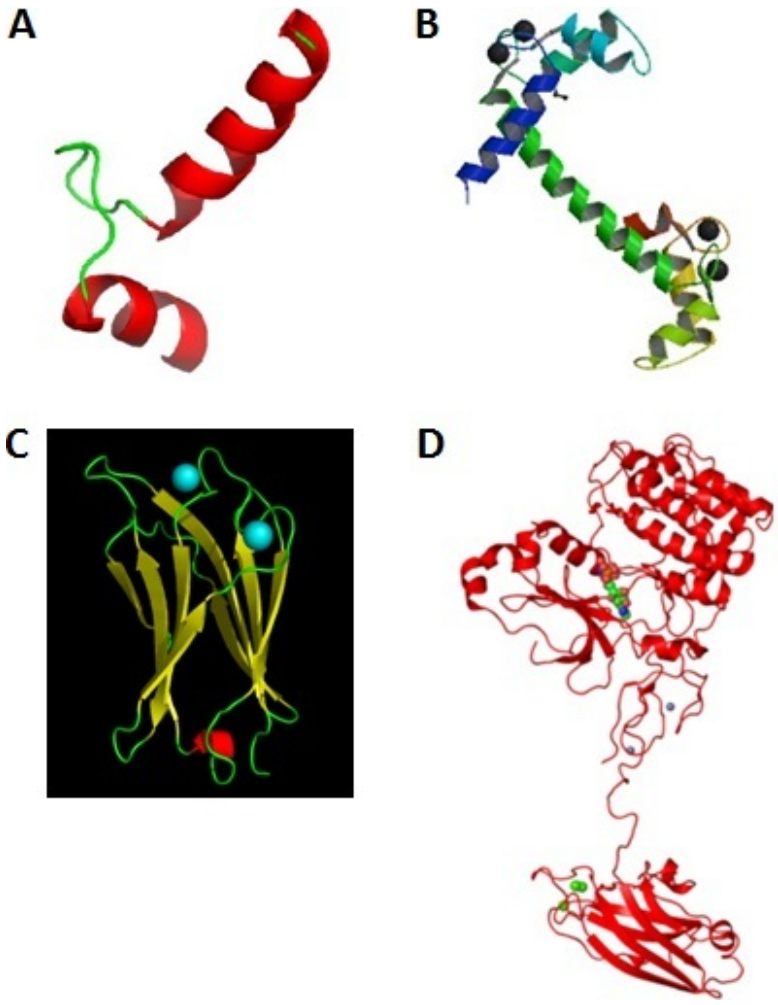

Figure 7: Calcium binding proteins - EF and C2 calcium binding domains.

A. EF-hand domain showing the two perpendicular α-helices in red and the calcium binding loop in green. Figure adapted from webpage (Maine-University, 2011).

B. Calmodulin from *Homo sapiens* with two globular Ca^{2+} ion binding regions connected by a long α-helix. Ca^{2+} ions are shown in black and bound by two sets of adjacent EF-hands at each end of the molecule, allowing calmodulin to bind a total of four Ca^{2+} ions. Figure adapted from Chattopadhyaya et al. (Chattopadhyaya et al., 1992).

C. C2 domains from *Clostridium absonum* α-toxin phospholipase C. Calcium ions shown in cyan, coordinated within the cavity provided by the N- and C-terminal loops. Anti-parallel β-sandwich shown in yellow. Figure adapted from Clark et al. (Clark et al., 2003)

D. Structure of *Rattus norvegicus* protein kinase C βII containing both the regulatory and catalytic domains tethered by a hinge region. Enzyme regulatory Ca^{2+} binding C2 domain evident as the bottom globular region, with the Ca^{2+} ions in this domain shown in green. Figure adapted from Leonard et al. (Leonard et al., 2011).

calmodulin (calcium modulated protein, CaM), S100 proteins and calcineurin (Yáñez et al., 2012). Of these, the most notable for this report is the ubiquitously expressed protein calmodulin, which is involved in the mediation of the Ca^{2+} signal in a large number of regulatory pathways. These include the regulation of metabolic activity, gene expression and control of other signalling pathways (Hancock, 2005). One example of its importance is in the regulation of cAMP signalling where it is able to activate both AC isoforms and Ca^{2+}/CaM-dependent phosphodiesterases (Section 1.5). CaM is a small, acidic protein able to bind four molecules of calcium with an affinity for the ion between the levels typical for a resting and activated system (Hancock, 2005). CaM's shape resembles a dumb-bell with two globular regions connected by a long, flexible, mobile α-helix (Figure 7B). Each lobe contains three α-helices and two Ca^{2+} binding EF-hand loops with a short anti-parallel β-sheet between the adjacent EF-hands (Chattopadhyaya et al., 1992). Binding Ca^{2+} causes major conformational changes to the molecule, revealing two hydrophobic patches which can then interact with other molecules (Hancock, 2005), propagating the Ca^{2+} signal.

C2 domains consist of a β-sandwich composed of 8 antiparallel β-strands that co-ordinate two or three Ca^{2+} ions (Figure 7C). The N- and C-terminal loops of the domain come together to form a cavity on the membrane binding face where the Ca^{2+} ions can bind (Nalefski & Falke, 1996). This domain has also been shown to be involved in membrane binding, particularly involving phospholipids, phosphatidylserine and phosphatidylcholine, as well as mediating protein-protein interactions and small molecule binding (Nalefski & Falke, 1996). The C2 domain is most frequently found coupled to enzymatic domains, in particular in protein kinase C (Figure 7D), phospholipases A_2, C, D (Section 1.4.1) and phospho-inositol 3 kinase (Nalefski & Falke, 1996).

Ca^{2+} may also be stored bound to non-protein molecules. In bones and teeth enamel Ca^{2+} ions are attached to phosphate molecules to form rigid hydroxyapaptite ($Ca_{10}(PO_4)_6(OH)_2$), a triangular structure made up of a central $Ca(OH)_2$ and three surrounding $Ca_3(PO_4)_3$ groups (Gutowska et al., 2005). Hydroxyapatite provides a high density store of minerals which is tightly controlled and can be readily accessed to provide calcium exchange with the extracellular matrix (Section 1.7.3).

1.4.1 Calcium Storage and Release: Endoplasmic Reticulum

Crucial aspects of calcium signalling are the maintenance of low cytoplasmic calcium concentrations and the ability to allow this to rise rapidly and reversibly. These aspects are controlled through the use of intracellular stores in which Ca^{2+} ions can be sequestered. For example, in metazoans cytosolic

calcium is maintained at nanomolar concentrations whilst within the endoplasmic reticulum (ER), where the majority of intracellular calcium is stored, these concentrations are in the millimolar range (Christensen et al., 2002; Zacchetti et al., 1991). Here, calcium ions are bound to specific protein molecules, rendering the Ca^{2+} ions inactive. In the ER these proteins are most commonly chaperones, such as calreticulin, and to a lesser degree, calnexin. In the sarcoplasmic reticulum (SR) of muscle cells calsequestrin is employed to maintain high SR concentrations following muscle contraction (Beard et al., 2004).

Despite the presence of these calcium-sequestering proteins, the ER is a dynamic Ca^{2+} store from which calcium can be released when appropriate. In order to maintain this store and replenish its contents after activation, protein pumps transport Ca^{2+} ions from the cytoplasm into the organelle. These proteins are called sarco/endoplasmic reticulum Ca^{2+}-ATPases (SERCA) and actively pump Ca^{2+} ions against the electrochemical gradient using the energy derived from ATP hydrolysis. This is achieved through the action of a phosphoryl intermediate generated through the ATP hydrolysis reaction; this causes a conformational change in the SERCA protein which results in Ca^{2+} ion movement across the membrane. Through this process two Ca^{2+} ions can be transported and two/three protons counter-transported for every ATP molecule hydrolysed (Musgaard et al., 2011). The activity of SERCA is not entirely continuous and mechanisms are present to control this Ca^{2+} transport. An example of this is in muscle cells where phospholamban inhibits SERCA activity unless phosphorylated by PKA (Vandecaetsbeek et al., 2011).

There are a number of mechanisms through which calcium can be released from the ER; via inositol triphosphate (IP_3) receptors, ryanodine receptors, and calcium-induced calcium release (CICR). These signalling pathways are covered in the following subsections with particular reference to the IP_3 receptor as the most relevant to the results in this thesis.

Inositol Triphosphate

As shown in Figure 6, IP_3 is generated by the enzyme phospholipase C (PLC). The signalling pathway responsible is similar to the AC activating mechanism described in Section 1.3.5. When a hormone binds to a G-protein coupled receptor (GPCR) it activates certain G-protein isoforms attached to the receptor's intracellular domain, which then diffuse through the cytoplasm to activate PLC. In the case of PLC these activating G proteins are $G\alpha_q$ (Cockcroft & Stutchfield, 1988) and the $G\beta\gamma$ subunits of Gi/Go (Klein et al., 2011). Activated PLC hydrolyses the phospho-ester bonds in

phoshatidylinositol-4,5 bisphosphate (PIP2), a reversibly phosphorylated phospholipid which always faces the cytosol. This hydrolysis generates two second messengers; membrane bound diacylglycerol (DAG), which activates protein kinase C (PKC); and the diffusible signal inositol triphosphate (IP_3) (Streb et al., 1983). IP_3 is thus available to open ligand-gated channels (Sugawara et al., 1997) in the ER membrane, allowing calcium efflux from the store (Streb et al., 1983). This triggers the downstream signalling cascades, most notably via PKC. PKC, which is activated through the combined stimulation of DAG and Ca^{2+}, is implicated in stimulating cytoplasmic Ca^{2+} removal by activating Ca^{2+}-transport ATPases and Na^{+}/Ca^{2+} exchangers (Section 1.4.4), as well as mediating IP_3 levels by blocking receptor mediated hydrolysis of inositol phospholipids by PLC (Nalefski & Falke, 1996).

IP_3 receptors are regulated by IP_3 and Ca^{2+}, as well as being modulated by many other signals, including Mg^{2+} ions, ATP (Section 1.4.2), and via phosphorylation (for example by cAMP dependent protein kinase (Hancock, 2005; Taylor et al., 2009)). These properties allow IP_3 receptors to initiate and regeneratively propagate Ca^{2+} signals. There are three mammalian isoforms of IP_3 receptors present in cells derived from three distinct genes and each with different sensitivities to IP_3 (Sugawara et al., 1997). All three isoforms have high levels of amino acid homology with Types 2 and 3 respectively 69% and 63% similar to Type 1 (Sugawara et al., 1997). All IP_3 receptor gene products have a common overall structure with an amino-terminal arginine- and lysine-rich cytoplasmic IP_3 binding domain, a carboxy-terminal membrane-spanning region comprising six transmembrane domains, and an inter-linking regulatory domain (Sugawara et al., 1997; Mignery et al., 1990; Miyawaki et al., 1991; Seo et al., 2012). Each protein forms a subunit which needs to form a tetramer to create a functional calcium channel. The last pair of transmembrane domains and the linking luminal loop from each of the four subunits form the channel pore (Taylor et al., 2009). The channel domain alone is sufficient to enable formation of the tetramer (Mignery et al., 1990; Miyawaki et al., 1991). As this domain is highly conserved across isoforms it has been suggested that both homotetramers and heterotetramers may exist between the gene products and their many splice variants (Monkawa et al., 1995).

IP_3 acts as a ligand and binding to the receptor N-terminal domain causes partial closure of a 'clam-like' IP_3 binding core. This initiates conformational changes which in turn lead to gating of the pore (Seo et al., 2012). Whilst it is known that IP_3 must bind to several of the four IP_3 binding sites, it is unclear whether binding to all four is required to activate the channel (Meyer et al., 1988; Marchant & Taylor, 1997; Boehning & Joseph, 2000). Once open, the receptor activity

is not controlled by IP_3, but instead by the passage of Ca^{2+} ions and in this respect Ca^{2+} is often referred to as a co-agonist. All IP_3 receptors are biphasically regulated by cytosolic calcium with Ca^{2+} ions rapidly stimulating and more slowly inhibiting the receptors (Taylor & Laude, 2002). This biphasic response requires Ca^{2+} binding to one of two locations on the cytosolic portion of the protein. Whilst activation involves direct Ca^{2+} ion binding, inhibition probably requires an accessory protein, which has not yet been unequivocally identified, but is likely to be calmodulin (Taylor & Laude, 2002). This biphasic stimulation is important in both propagating Ca^{2+} signals from other sources (see below) and moderating the magnitude of Ca^{2+} signals through IP_3 receptor inhibition at high Ca^{2+} concentrations.

Ca^{2+} ion signals generated from IP_3 receptors can have varying magnitudes, providing either local or global signals and thereby increasing the versitility of intracellular Ca^{2+} signals. Local signals usually derive from different IP_3 concentrations. Small concentrations cause 'Ca^{2+} blips', spatially restricted events lasting no more than 130 ms which increase cytosolic Ca^{2+} to 40 nM (Taylor et al., 2009). Higher IP_3 concentrations of 50-600 nM cause more long-lasting events of approximately 1 s known as 'Ca^{2+} puffs', which spread no more that a few micrometers and are thought to result from several closely spaced IP_3 receptors opening synchronously (Marchant et al., 1999; Shuai et al., 2006; Taylor et al., 2009). With further increases in IP_3 concentrations, 'puffs' become more frequent and Ca^{2+} diffusing from one receptor can activate another, regeneratively propagating the Ca^{2+} signal (Marchant et al., 1999). These effects are augmented by the phenomenon of IP_3 receptor clustering, whereby low concentrations of IP_3, lower than that required for channel gating, cause the receptors to rapidly and reversibly cluster into groups of approximately four (Shuai & Jung, 2003; Shuai et al., 2006; Taylor et al., 2009). Furthermore, these IP_3 receptor derived Ca^{2+} ions may then also activate other Ca^{2+} sensitive signalling machinery to further propagate the signal, for example ryanodine receptors. These signal propagations across receptors and in some cases organelles, are known as Ca^{2+} induced Ca^{2+} release (CICR).

Ryanodine Receptors

In addition to IP_3 receptor mediated calcium release, the ER also contains ryanodine receptors (RyRs), which are also sensitive Ca^{2+} ions. They are named due to their sensitivity to ryanodine, an alkaloid from the plant *Ryania speciosa* which opens the channel at low concentrations and closes them when higher (Fill & Copello, 2002). RyRs are encoded by three genes in vertebrates, demonstrating different expression patterns across the body; type 1 is predominantly found in the skeletal muscle, type 2 in cardiac muscle and type 3 in smooth muscle (Querfurth et al., 1998). Like

IP_3 receptors, RyRs are tetrameric Ca^{2+} channels with a carboxyl-terminal calcium pore formed by between four and ten transmembrane domains and are regulated by signals detected by their large N-terminal cytosolic domains (Seo et al., 2012).

Like IP_3 receptors, RyRs also exhibit biphasic activation by Ca^{2+} ions, with low concentrations of 10-100 μM maximally opening the channel and higher concentrations of 1-10 mM closing them (Fill & Copello, 2002; Diaz-Sylvester et al., 2011). This suggests the existence of two different types of cytosolic Ca^{2+} binding sites: activating sites with high affinity and inhibitory sites with low affinity (Coronado et al., 1994). They are, however, more sensitive than IP_3 receptors to Ca^{2+} and their main function is to propagate Ca^{2+} signals from other stores through CICR. Spatiotemporally-restricted Ca^{2+} ion release events from RyRs are known as 'calcium sparks'. As the receptors tend to cluster, these 'sparks' often lead to activation of surrounding RyRs, leading to augmentation of the signal.

RyRs do not have a second messenger that activates all isoforms in the same way as IP_3 activates IP_3 receptors. However RyR2 and 3 (Mészáros et al., 1993) have been shown to be activated by cyclic-ADP ribose, cADPR (Clapper et al., 1987; Lee et al., 1989). Pyridine nucleotide-derived cADPR is synthesised in cells by ADP ribosyl cyclase (Genazzani & Galione, 1997) in response to signals from cell surface receptors such as cholechystokinin receptors. RyRs can also be controlled by adenine and ATP (Anderson et al., 1989; Chen et al., 1992), Mg^{2+} ions (Anderson et al., 1989; Chen et al., 1992; Diaz-Sylvester et al., 2011), CaM (Meissner, 1986), phosphorylation (Seiler et al., 1984; Takasago et al., 1991), thiol oxidation/reduction, nitrosylation and possibly reactive oxygen species (Coronado et al., 1994; Fill & Copello, 2002; Meissner, 2004). Furthermore, activation of either RyRs or IP_3 receptors can affect one another and both receptors can either use the same (Zacchetti et al., 1991) or segregated ER calcium stores (Volpe et al., 1991; Kijima et al., 1993).

1.4.2 Calcium Storage and Release: Mitochondria

Mitochondria can also act as a calcium source, with Ca^{2+} concentrations within these organelles reaching 500 nM, although their contribution to the wide range of calcium signalling events has yet to be fully understood (Walsh et al., 2009). Whilst mitochondria are able to produce a calcium signal, they mostly act as a calcium sink, blocking local and global calcium oscillations. Mitochondria can directly influence the calcium concentration in the cytosol of the cell by importing Ca^{2+} into the organelle via a relatively fast, energy consuming, Ca^{2+} sensitive Ca^{2+} uniporter, which uses mitochondrial membrane potential as a driving force (Selwyn et al., 1970; Scarpa & Azzone, 1970;

Rottenberg & Scarpa, 1974). They are also able to slowly release Ca^{2+} ions from the interior of the organelle to the cytosol by means of Na^{+}/Ca^{2+} or H^{+}/Ca^{2+} exchangers (Carafoli et al., 1974; Crompton et al., 1978; Fiskum & Lehninger, 1979), for example during programmed cell death (Walsh et al., 2009).

Mitochondria can also influence Ca^{2+} signalling indirectly by altering the intracellular concentrations of ATP, NAD(P)H, pyruvate and reactive oxygen species. These molecules can in turn modulate components of the Ca^{2+} signalling machinery either by buffering or stimulating ion release from internal stores, influx from the extracellular solution, uptake into cellular organelles, or extrusion by plasma membrane Ca^{2+} pumps (Walsh et al., 2009). The best examples of how these molecules modulate Ca^{2+} signalling is from the ER. Mitochondria and the ER form close links (Rizzuto et al., 1998) which result in local regulation of ER mediated Ca^{2+} release. Local modulation can be due to the fast uptake of Ca^{2+} by mitochondria, which has been shown to affect IP_3 receptors in close mitochondrial proximity, lowering their sensitivity to IP_3 (Hajnóczky et al., 1999), or as a result of mitochondrial respiratory products. ATP and other adenine nucleotides bind to IP_3 receptors (Maeda et al., 1991) causing an increase in the frequency and average duration of the receptor opening event (Bezprozvanny & Ehrlich, 1993), particularly through potentiating the binding of IP_3 (Spät et al., 1992) and Ca^{2+} (Mak et al., 1999). Similar effects of ATP on RyRs have been observed with ATP increasing the open probability of channels and decreasing the Ca^{2+} activating threshold (Bull et al., 2007). Another mitochondrial product, NADH, is also known to interact with RyRs; decreasing the receptors' open probability (Zima et al., 2004). Furthermore, ATP can both regulate a passive ER Ca^{2+} leak, with a reduction in ATP supressing this leak, and inhibiting store-operated Ca^{2+} entry (Section 1.4.4). The ability of mitochondria to influence the calcium signalling events of other organelles has important implications as the location of the organelle can thus alter local signals and arrest global Ca^{2+} oscillations (Walsh et al., 2009). In addition to this, Ca^{2+} temporarily accumulated in the mitochondria following ER release can be an effective method for reloading the ER or preventing further Ca^{2+} release from this organelle (Walsh et al., 2009).

1.4.3 Calcium Storage and Release: NAADP Store

In addition to the ER and mitochondria, there an is additional calcium store located in acidic vaculolar endosomal compartments such as lysosomes (Christensen et al., 2002). Here the Ca^{2+} concentration is kept high with the average free Ca^{2+} available in macrophage lysosomes being 400-600 μM, less than half the extracellular concentration, but much higher than that of the cytosol

(Christensen et al., 2002). Despite these organelles' ER origins, Ca^{2+} ions found within these stores are not released via IP_3Rs, RyRs or via cADPR, but can be influenced by endocytosis (Christensen et al., 2002), lysosomal pH (Christensen et al., 2002) and the second messenger, nicotinic acid adenine dinucleotide phosphate, NAADP (Clapper et al., 1987; Lee et al., 1997; Cancela et al., 2000; Yamasaki et al., 2004; Churchill et al., 2002). NAADP is a pyridine nucleotide metabolite which is produced by the same enzyme family as cADPR; the ADP-ribosyl cyclases (Genazzani & Galione, 1997). Like IP_3 and cADPR, it can be produced by cell surface agonists via cholechystokinin receptors (Yamasaki et al., 2004). NAADP activates Ca^{2+} ion release through two-pore channels, TPCs (Ruas et al., 2010; Zhu et al., 2010; Tugba Durlu-Kandilci et al., 2010; Dionisio et al., 2011; Lin-Moshier et al., 2012). However, it is currently unknown how NAADP activates these channels at the structural level (Lin-Moshier et al., 2012). Although more potent than either IP_3 and cADPR (Galione, 2006), NAADP only produces calcium gradients across the cell rather than propagated waves (Section 1.4.5) due to the TPC's inability to respond to Ca^{2+} themselves to support CICR (Galione, 2006; Churchill & Galione, 2000). However, Ca^{2+} ions released from this store may interact with the other stores and Ca^{2+} signalling machinery in the cell to result in a more global calcium signal (Galione, 2006).

Calcium concentrations within these endosomal organelles are maintained by the activity of Ca^{2+}/H^+ exchangers across the membrane. Due to the proton requirement of this exchanger the vacuolar pH acts as a driving force for Ca^{2+} ion uptake. Thus, vacuolar H^+-ATPase, the enzyme responsible for maintaining the proton gradient, is critical in maintaining lysosomal Ca^{2+} uptake (Christensen et al., 2002).

1.4.4 Calcium Storage and Release: The Extracellular Environment

The extracellular matrix (ECM) has a high level of stored calcium and entry into cells is tightly controlled. Access to this extracellular store, however, is required under certain conditions and is most notable with store operated calcium entry (SOCE) and cell depolarisation. SOCE is a method by which the ER calcium store is replenished using calcium derived from outside the cell, across the plasma membrane (Rosado, 2006). Small molecules of stromal interaction molecule 1 (STIM1) located in the ER lumen, detect calcium concentrations via ER lumen EF-hand domains (Liou et al., 2005). In response to a depletion in ER Ca^{2+} concentration, dimeric STIM1 molecules cluster and relocate near to the plasma membrane (Liou et al., 2005; Stathopulos et al., 2006; Park et al., 2009). Here the collected cytoplasmic STIM C-termini associate with phosphatidylinositol 4,5-

bisphosphate in the plasma membrane to directly activate a subunit of the calcium release-activated calcium channel protein 1 (CRAC1/Orai1) via protein-protein interaction (Feske et al., 2006; Wu et al., 2007; Park et al., 2009). This interaction then simulates Ca^{2+} entry via Orai1 enabling store replenishment and maintenance of Ca^{2+} signals when they are required over a prolonged periods, such as during cell proliferation (Berridge, 2002).

Another calcium entry route into cells is via voltage-dependent calcium channels (VDCCs), which are a critical entry pathway in many cells (Zong et al., 1995). These channels are classified into E-, L-, P/Q-, N-, R- and T-type subtypes by their pharmacological and electrophysical properties (Hayashi et al., 2007). Of most relevance to this thesis are the L-type channels which are not only regulated by cAMP (Zong et al., 1995), but also show substantial distribution throughout renal vascular and tubular tissue (Hayashi et al., 2007). However, being voltage-gated, these channels are activated with membrane depolarisation and, therefore, are most active in nerve and muscle cells. At resting membrane potential, VDCCs are normally closed. They are opened by membrane depolarising potentials and then allow Ca^{2+} to enter the cell. They may also form close relationships with other elements of a cell's signalling machinery, an example of this being between L-type channels and ryanodine receptors. In skeletal muscle L-type voltage-gated channels are in direct contact with RyR1 and membrane depolarisation causes a conformational change in the channel opening RyR1 through direct protein-protein interaction (Berridge, 2002). In cardiac muscle this interaction is more indirect as the two channels are not directly linked. Instead, membrane depolarisation causes a small Ca^{2+} influx through the L-type channel which then activates RyR2 to release Ca^{2+} ions from the ER (Fill & Copello, 2002).

Proteins in the plasma membrane do not only regulate calcium entry. Being under constant pressure to maintain low intracellular calcium concentrations, cells have developed a sophisticated system for the elimination of Ca^{2+} ions from the cytoplasm after a signal has developed. This system not only includes calcium uptake into stores, but also Ca^{2+} extrusion into the extracellular space by an ATP-driven plasma membrane Ca^{2+} ATPase pump (PMCA) and a Na^{+}/Ca^{2+} exchanger. PMCA (Schatzmann, 1966) serves as a high-affinity system (K_M of 100 to 200 nM), ejecting Ca^{2+} ions against the electrochemical gradient (Strehler & Zacharias, 2001). Similar to SERCA in the ER, this Ca^{2+} ion extrusion is powered by the energy derived from ATP hydrolysis with a stoichiometry of one Ca^{2+} ion extrusion for each molecule of ATP hydrolysed (Strehler & Zacharias, 2001; Leva Di et al., 2008). PMCA is controlled by cytoplasmic Ca^{2+} and a number of regulators, including CaM. Cytoplasmic Ca^{2+} activates the pump, whilst CaM increases its affinity and maximal transport rate

(Leva Di et al., 2008). Na^+/Ca^{2+} exchange works against the Ca^{2+} gradient by using the high Na^+ electrochemical gradient, allowing Na^+ ions to flow down their gradient into the cell. By this mechanism a single calcium ion can be extruded for every three sodium ions imported (Yu & Choi, 1997). Whilst PMCA has a higher affinity for Ca^{2+}, the Na^+/Ca^{2+} exchanger can pump Ca^{2+} at a higher rate. Thus, following a calcium signal it is the Na^+/Ca^{2+} exchanger which rapidly returns the cytoplasm to near normal concentrations whilst PMCA then further lowers intracellular concentrations from this point (Carafoli, 1991).

1.4.5 Calcium-Induced Calcium Release, Waves and Oscillations

Most proteins involved in Ca^{2+} signalling respond to the Ca^{2+} ion signal itself. In this way Ca^{2+} signals can be propagated and controlled. An example of this is when Ca^{2+} release from one store initiates the efflux of Ca^{2+} ions from another via CICR. It is these interactions between receptors, stores and signalling pathways that shapes the resultant Ca^{2+} signal, affecting its outcome. Due to these interactions, local and global signalling events can take the shape of gradients, waves or oscillations.

Ca^{2+} ions released from a single point migrate for approximately 50 μs, covering only 0.1-0.5 μm. If they are recognised by other Ca^{2+} responsive molecules within this distance, signal propagation will occur. This creates a calcium gradient that can reach up to 1-10 μm, but which lasts less that a millisecond (Hancock, 2005). Gradients are important in cell migration, exocytosis, ion transport and gap junction regulation (Hancock, 2005). If these gradients become established a Ca^{2+} wave or a more global oscillation may be generated. These signalling events are initiated when one store is emptied to the point where the resultant high cytosolic Ca^{2+} concentrations inhibit further release. Whilst Ca^{2+} ions from this site may go on to stimulate neighbouring receptors propagating the signal, at this first location the cytosolic Ca^{2+} concentration drops. This is due to both an absence of further Ca^{2+} release and activation of Ca-ATPases, which return the Ca^{2+} ions into the store once more. The spatial differences in Ca^{2+} release and re-absorption thus creates a signalling wave. Such waves can move through the cytosol at speeds of 5-100 μm/s and can even travel between cells via gap junctions (Marchant & Taylor, 1997).

Calcium oscillations not only involve CICR and store regulated Ca^{2+} ion release, but also receptor activation at the plasma membrane (Berridge et al., 1988; Cancela et al., 2000). One example model of calcium oscillation involves IP_3 generation. In this model activation of a plasma membrane receptor stimulates PLC, which in turn generates IP_3 and results in Ca^{2+} ion release via IP_3 receptors. The released Ca^{2+} ions then diffuse through the cytoplasm to once more stimulate PLC, producing further IP_3 molecules and setting up an oscillation. As IP_3 receptors are inhibited at high Ca^{2+} concentration, these oscillations finally desist as these channels become closed and Ca^{2+} is returned to the ER once more. With lower cytosolic Ca^{2+} concentrations, PLC activity also drops, terminating the signal. Similar alternate models exist which highlight the interactions between the second messengers IP_3, cADPR, and NAADP and their activation of common oscillator units, including IP_3 and ryanodine receptors (Cancela et al., 2000). As a result of these waves and

oscillations, the calcium signal is often made up of the ion concentration in addition to the wave amplitude or frequency (Taylor et al., 2009).

1.5 Calcium Interaction with the AC and cAMP pathway

The Ca^{2+} and cAMP pathways are highly interlinked, both up and downstream of the second messengers as well as directly at the point of generation.

1.5.1 Direct Interaction - Ca^{2+}/CaM regulation of ACs and cAMP modulation of IP_3 receptors

Whilst all tmAC isoforms are inhibited by high (∼100 μM) concentrations of calcium due to competition between these divalent ions and the Mg^{2+} co-factor (Guillou et al., 1999), certain tmAC isoforms are dynamically regulated at lower Ca^{2+} concentrations with isoforms I, III and VIII activated by Ca^{2+}/Ca^{2+} bound calmodulin (Bakalyar & Reed, 1990; Cali et al., 1994; Fagan et al., 1996), and isoforms V and VI inhibited (Ishikawa et al., 1992; Yoshimura & Cooper, 1992; Guillou et al., 1999). While the Ca^{2+} concentrations required to activate AC I are in the normal physiological range (0.1-1 μM) the levels required for type III are supra-normal (Cooper et al., 1995). Furthermore, as previously mentioned, Ca^{2+} ions also activate sAC, by replacing the Mg^{2+} ions in the active site, increasing the enzyme's affinity for ATP and thus its K_M (Litvin et al., 2003). In fact, sAC activity is highest with a magnesium as ion A and a calcium as ion B in the active site (Kamenetsky et al., 2006). The source of this regulatory calcium appears to be predominantly from capacitative Ca^{2+} entry/SOCE (Cooper et al., 1994; Sunahara & Taussig, 2002; Willoughby et al., 2005). AC VIII, for example, has been unequivocally demonstrated to only respond to only STIM1-Orai1 mediated SOCE Ca^{2+} ions whilst being unaffected by Ca^{2+} released from intracellular stores, agonist induced cellular influx, or increases in Ca^{2+} concentration by the ionophone ionomycin (Fagan et al., 1996; Martin et al., 2009).

AC isoforms can also be regulated by other elements of the calcium signalling machinery. ACs II, IV and VII are stimulated by PKC (Cooper, 2003; Linder & Schultz, 2003) with isoform II less susceptive to $G\alpha_s$ activation in the presence of PKC and VII more so (Cooper et al., 1995). AC VI is inhibited by PKC through phosphorylation of the enzyme's N-terminus and ACs I and III are inhibited by CaM kinases and AC IX by calcineurin (Cooper, 2003; Kamenetsky et al., 2006).

Cyclic-AMP has also been shown regulate the formation and phosphorylation of IP_3, the activities of Ca^{2+} channels and pumps and the formation of other Ca^{2+} mobilising messengers (Tovey et al., 2008). The best characterised interaction is the sensitisation of IP_3 receptors to IP_3 by cAMP.

In 2008 *Tovey et al.* demonstrated that in human embryonic kidney cells intracellular signalling after stimulation by parathyroid hormone (Section 1.7.3) involved 'cAMP junctions'. In these 'cAMP junctions' AC VI and IP_3 receptor 2 were selectively coupled, allowing local delivery of supramaximal concentrations of cAMP to the IP_3 receptor. This cAMP delivery then directly increased the receptor's sensitivity to IP_3 (Tovey et al., 2008). Following on from this, in 2010 the group published another paper demonstrating that all IP_3 receptor isoforms were similarly sensitised by cAMP through binding to a novel site (Tovey et al., 2010). The effect of cAMP on IP_3 receptors alone has no effect on Ca^{2+} release and does not mediate an increase in IP_3 affinity but instead increases the effectiveness with which IP_3 binding is coupled to channel opening (Tovey et al., 2010).

All three IP_3 receptors can also be phosphorylated at multiple sites by PKA. This phosphorylation in turn increases receptor activity, for example PKA phosphorylation of IP_3 receptor 1 increases the receptor's IP_3 sensitivity around 2-fold (Wojcikiewicz & Luo, 1998; Dyer et al., 2003; Tovey et al., 2010). Similarly, PKA can phosphorylate RyRs releasing bound inhibitory proteins such as FKBP12.6 and calstabin-2, release of which results in a Ca^{2+} ion leak from these receptors (Marx et al., 2000; Wehrens et al., 2006). Furthermore, cAMP can activate cyclic nucleotide-gated ion channels, allowing Ca^{2+} ions from outside the cell to permeate the cell (Kamenetsky et al., 2006).

1.5.2 Upstream of Second Messenger Generation - Plasma Membrane Receptors and G-proteins

Both cAMP and Ca^{2+} signals can be generated by GPCRs and regulated by G proteins. This can lead to a multiplicity of signalling interactions due to interplay between the G protein Gα and G$\beta\gamma$ subunits, PLC, and differentially regulated AC isoforms. Some receptors are reported to negatively couple to AC whilst at the same time positivity coupling to PLC. Examples include adenosine A1, muscarinic m4, somatostatin and the α-2-adrenegic receptor (Bugrim, 1999). On the other hand, other receptors are able to activate both PLC and AC enzymes such as the α-1-adrenegric and receptors for growth factors, endothelin-1, vasopressin, and lutinizing hormone (Bugrim, 1999). These mulitple combinations of simultaneous regulation between pathways are due to the ability of one GPCR to produce both Gα and G$\beta\gamma$ G-proteins. On occasions where Gα_s or Gα_i subunits are mobilised AC isoforms may be respectively activated or inhibited while the simultaneously released G$\beta\gamma$ subunits activate PLC isoforms β1, β2 and η2 (Blank et al., 1992; Boyer et al., 1992; Camps et al., 1992; Zhou et al., 2008) and increase IP_3 production (Figure 8A). On the other hand, if

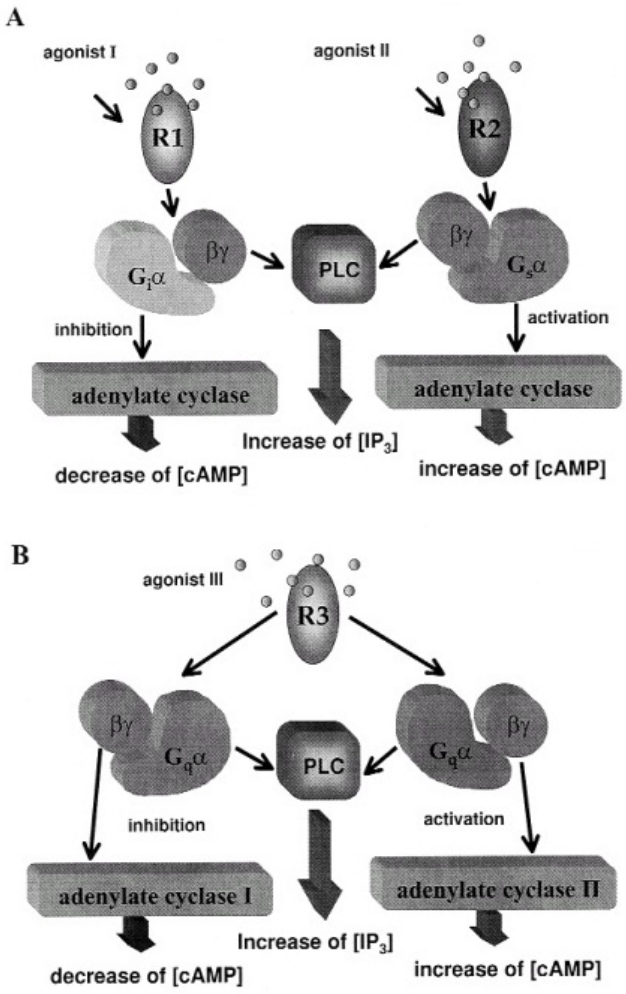

Figure 8: G protein regulation of AC and PLC. Figure taken from *Bugrim et al.* (Bugrim, 1999). **A.** Receptors coupled to either $G\alpha_s$ or $G\alpha_i$. AC is either activated or inhibited by the G protein α subunit while at the same time $G\beta\gamma$ activates PLC. **B.** Receptor coupled to $G\alpha_q$. PLC is activated by $G\alpha_q$ while different isoforms of AC are either activated or inhibited by the $G\beta\gamma$ subunits.

G_q is involved, PLC is activated via the $G\alpha_q$ subunit and the $G\beta\gamma$ can activate or inhibit AC, depending on the AC isoform present (Figure 8B). To complicate matters further some receptors can also signal to multiple G-protein subtypes. An example is the calcium-sensing receptor CaR which responds to changes in extracellular calcium by inducing intracellular signalling and can modulate cellular function to cause parathyroid hormone secretion from the parathyroid glands or calcium reabsorption in the kidneys (Section 1.7.3). This GPCR couples to both $G\alpha_q$ and $G\alpha_i$ to both mobilise intracellular calcium through the activation of phospholipases and suppress cAMP formation (Ward, 2004).

1.5.3 Signal Termination - Ca^{2+}/CaM Regulated PDEs and cNMP Senstitive Ca^{2+}-ATPases

Interactions between the two signalling pathways can also occur at the signal termination step. In the same way that cAMP generation by individual AC isoforms can be regulated by Ca^{2+} ions, so can its degradation by PDEs. Ca^{2+}/CaM activates PDE1 whilst PDE2 can be activated by Ca^{2+} activated PKC (Geoffroy et al., 1999; Omori & Kotera, 2007). In PDE1 this regulation is provided through a methionine rich, hydrophobic Ca^{2+}/CaM binding site at the N-terminus. Ca^{2+}/CaM binding to this site causes a conformational change which prevents the N-terminal region from obstructing the active site, thus activating the enzyme and stimulating cAMP hydrolysis (Omori & Kotera, 2007).

Cyclic-nucleotides can also play a part in the termination of a Ca^{2+} signal through regulation of Ca^{2+}-ATPases. An example of this is from cardiac cells where phospholamban regulates the activity of Ca-ATPases in SR membranes in a manner dependent on cAMP-dependent protein kinase (Tada & Toyofuku, 1998), which is in turn activated by cAMP. Closely related cyclic nucleotide cGMP has also been demonstrated to enhance SR sequestration of Ca^{2+} ions in smooth muscle, purportedly through activation of Ca^{2+}-ATPases (Twort & van Breemen, 1988).

1.6 Role of Carbon Dioxide *in vivo*

1.6.1 Environmental Carbon Dioxide

Carbon dioxide is currently maintained at an atmospheric level of 370-90 μmol/mol, 0.0387% (Hetherington & Raven, 2005; Taylor & Cummins, 2011), although it is proposed that this is steadily increasing due to anthropomorphic production, including the burning of fossil fuels and deforestation (Watson et al., 2011). Naturally, carbon dioxide levels are generally maintained at a controlled level, with the gases in the atmosphere constantly equilibrating with dissolved gas in the oceans. Long-term regulation is provided over millions of years via the rock cycle, with volcanic activity providing a source and sedimentation and subduction sequestering the gas (Hetherington & Raven, 2005).

Carbon dioxide is critical for life on Earth, particularly as a substrate for ribulose-1, 5-bisphosphate carboxylase-oxygenase (Rubisco); an essential step in the Calvin cycle of photosynthesis enabling the synthesis of sugars. This enzyme forms the most abundant protein on Earth in terms of mass (Hetherington & Raven, 2005) and catalyses two major reactions. These reactions include a carboxylase reaction whereby a carbon dioxide molecule is added to an organic molecule and an oxygenase reaction adding an oxygen molecule to this same organic compound (Andersson, 2008). Carbon dioxide is also a key by-product in the catabolism of sugars, lipids and proteins via various biochemical pathways, in particular glycolysis and the Krebs cycle, and is therefore produced constantly by the aerobically respiring cell. The biosphere regulates atmospheric levels of CO_2, with fluxes in respiration and gross photosynthesis in the region of 150 Pg (petagrams, x 10^{15}) of carbon per annum (Hetherington & Raven, 2005). Historically these fluxes have been responsible for the largest changes in atmospheric composition. The best example of this is the evolution of photosynthetic organisms, debatably as far back as 3.45-3.80 billion years ago (Hetherington & Raven, 2005), which caused a downward shift in the amount of free CO_2 and increased atmospheric oxygen levels. Reciprocally, these changes in atmospheric concentrations affected life itself. As an example, it is proposed that as Rubisco must have evolved before global oxygenation, its oxygenase activity may not have appeared until later (Hetherington & Raven, 2005). Another example is that many contemporary photosynthetic and aquatic organisms have 'inorganic carbon concentrating mechanisms' and micro-compartments known as carboxysomes where CO_2 is elevated around the active site of Rubisco and prevented from escape by a diffusion barrier such as a protein shell (Badger et al., 2006). These mechanisms were evolutionary adaptations in response to different atmospheric conditions (Badger et al., 2006) to overcome the problems associated with low atmospheric carbon

dioxide levels, such as the kinetic limitations of Rubisco (Hetherington & Raven, 2005; Badger et al., 2006; Andersson, 2008).

Temporal changes in environmental carbon dioxide concentration are not only restricted to the millienia time-frame. For example, estuarine systems are characterised by large seasonal and diurnal fluctuations in CO_2 and pH (Section 1.6.2). In esturine sytems, these fluctuations are due to variations in freshwater influx, soil drainage, biota composition and activity and gas exchange rates with the atmosphere and ocean waters (Tomanek et al., 2011). Furthermore, naturally occuring niche habitats with variations in CO_2 can be spatial, for example in the case of burrowing animals where gas exchange to the atmosphere is restricted (Lechner, 1976).

1.6.2 Carbon Dioxide Equilibrium in Solution and *in vivo* Chemistry

Carbon dioxide is not an inert gas and in solution reacts with water molecules to produce carbonic acid and ultimately bicarbonate ions and protons (Figure 9) until equilibrium is established. As a result any increase in carbon dioxide increases solution acidity through the production of protons and visa versa. As this reaction has a pKa of 6.2, which is close the physiological pH of 7.2 (Bonar & Casey, 2008) CO_2, HCO_3^- and pH are inextricably linked in biological system. Acid-base homeostasis is crucial to sustain CO_2 production and respiration especially as cellular enzymes and chemical reactions are sensitive to pH (Tresguerres et al., 2010) and large alterations to pH can be deleterious to an organism (Richerson, 2004). In contrast, it is also important to note that due to the nature of this equilibrium, CO_2/HCO_3^- are also important in buffering intra- and extra-cellular physiological fluid pH (Tresguerres et al., 2010).

$$CO_2 + H_2O \overset{1}{\leftrightarrow} H_2CO_3 \overset{2}{\leftrightarrow} HCO_3^- + H^+$$

Figure 9: Carbon dioxide in solution

The reaction illustrated in Figure 9 can be split into steps (1) and (2). Whilst (2) occurs naturally at a very fast rate, step (1) is a slower and becomes rate limiting (Boron, 2006). To address this, organisms contain the ubiquitous enzyme carbonic anhydrase (CA), which is able to catalyse the whole reaction. CA is one of the fastest enzymes known with CAII having a maximum turnover

rate of the CO_2 hydration step of more than 1 x 10^6 s^{-1}, close to the limit of diffusion (Sly & Hu, 1995; Christianson & Cox, 1999). Catalysis proceeds via nucleophilic attack on carbon dioxide by conserved threonine and glutamine acid residues in CA active site. These amino acid residues contribute to a hydrogen bonded network with the enzyme's zinc co-factor, holding the active site in the right orientation for nucleophilic attack at low entropy (Sly & Hu, 1995; Christianson & Cox, 1999). High turnover is achieved through the use of a histidine mediated proton shuttle to regenerate amino acid charges in the active site (Sly & Hu, 1995; Christianson & Cox, 1999).

Carbon dioxide can also react with amino acids to form carbamates. Carbamates form as a result of the nucleophilic attack of uncharged amines upon CO_2 (Figure 10).Under physiological conditions only the N-terminal α and ϵ-amino groups of lysine residues are suitably dissociated to react with CO_2 in this way although, with the correct surrounding amino acids, other amine groups are possible targets (Lorimer, 1983). Carbamate formation is exothermic and readily reversible, thus providing a useful feature for biological regulation. As the formation of a carbamate converts a neutral or cationic group to an anionic one, this newly formed species is often stabilised by electrostatic interactions with surrounding amino acids (Lorimer, 1983). Examples of naturally occuring carbamates include haemoglobin in metazoans and Rubisco in plants. In haemoglobin the N-terminal α and ϵ-amino groups in the α- and β-chains can react to form carbamates (Kilmarti et al., 1973; Gros et al., 1981). These modifications help stabilise the protein when it becomes deoxyhaemoglobin and increases the likelihood of the release of remaining oxygen molecules bound to the protein (Lorimer, 1983). In the Rubisco active site a Mg^{2+} ion is bound to glutamate and aspartate residues, as well as a lysine carbamate. This carbamate is formed from a reaction between the lysine and the air in the rate-determining step and renders the amino acid charged and, therefore, able to bind the enzyme's Mg^{2+} co-factor to facilitate catalysis (Lorimer, 1983; Lundqvist & Schneider, 1991).

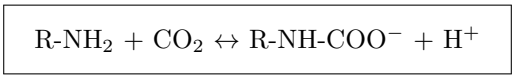

Figure 10: Formation of carbamates: carbon dioxide reacts with the N-terminal amino groups

1.6.3 Inorganic Carbon Entry into Cell

When considering inorganic carbon in the physiological environment both CO_2 and HCO_3^- species must be considered (Section 1.6.2). Both species can cross biological membranes with their movement typically faciliated by proteinaceous transporters. However, whilst CO_2 transport by aquaporins and Rhesus channels has been demonstrated there is also contrasting evidence suggesting that CO_2 diffuses freely across membranes, with little contribution from protein transporters. Both of these theories are presented below.

Carbon Dioxide Transport

Until recently it had been a general consensus that gases can pass through biological membranes by virtue of their high diffusibility through the lipid phase (Endeward et al., 2008). However, membranes exhibit different levels of permeability, which can not be accounted for by this simple diffusion principle. For example, some apical epithelial membranes appear to have poor permeability to CO_2 (Waisbren et al., 1994; Endeward & Gros, 2005; Azzam et al., 2010) whilst others, such as the membrane of red blood cells, exhibit extremely high permeability. The high CO_2 permeability of red blood cells has been attributed to the presence of two proteins: aquaporin 1 (Endeward et al., 2006) and Rhesus complex RhAG (Endeward et al., 2008).

Aquaporins (AQPs) refer to a family of 13 isoforms of channel with tissue specific expression (Herrera & Garvin, 2011). AQP channels are involved in the passive transport of water molecules across membranes but AQP1 (and to some degree 4 and 5) has also been demonstrated to transport CO_2 (Herrera & Garvin, 2011; Musa-Aziz et al., 2009). Individual subunits of AQP1 are 28 kDa and are made of six bilayer spanning domains which form a functional water pore (Herrera & Garvin, 2011). These subunits associate with one another to form a homotetramer, the generation of which leaves a fifth pore of hydrophobic amino acids at the centre of the four monomers. This fifth pore forms a path for non-polar molecules such as CO_2 (Endeward et al., 2006; Herrera & Garvin, 2011; Wang et al., 2007), whilst the four aquapores have been shown to have limited CO_2 permeability (Wang et al., 2007). AQP1 is highly expressed in cells requiring gas transport including pulmonary capillaries, epithelial cells and vascular smooth muscle (Herrera & Garvin, 2011) in addition to red blood cells where AQP1 has been demonstrated to be responsible for $\sim$60% of the cells' CO_2 permeability (Endeward et al., 2006). AQP1 is also abundantly expressed in the renal proximal tubule where it has a role in facilitating bicarbonate reabsorption from the glomerular filtrate (Section 1.7.3).

Rhesus channels are predominantly ammonia channels (Ripoche et al., 2004; Li et al., 2006b; Endeward et al., 2008), encoded in humans by the erythroid RHAG and the non-erythroid RHBG and RHCG genes (Winkler, 2006). Rhesus proteins comprise of 11 conserved transmembrane helices which hetero-trimerise to form a pore lined by hydrophobic side chains, through which ammonia can travel in the RhAG isoform (Li et al., 2006b; Winkler, 2006). *Endeward et al.* demonstrated that these channels are not selective for one gas but also allow the passage of CO_2 as well as NH_3 and thus contribute to the high CO_2 permeability of red blood cell membranes (Endeward et al., 2008). This is due to the fact that the molecular diameter of CO_2 (2.9 to 3.3 Å) is quite similar to that of NH_3 (3.0 to 3.15 Å), allowing either to pass through the hydrophobic environment of the channel (Endeward et al., 2008).

The AQP and RhAG channel routes for CO_2 entry into cells, however, is only one paradigm. *Missner et al.* published a paper in 2008 demonstrating that inorganic carbon movement across a membrane is via passive diffusion of CO_2 (Missner et al., 2008), instead of facilitated passage through channels. The authors demonstrate that at physiological pH, movement of inorganic carbon across a membrane is restricted by the near-membrane unstirred layer which acts as a diffusional barrier to the membrane. Here, carbonic anhydrases convert any HCO_3^- ions from the extracellular bulk to CO_2 allowing diffusion across to the intracellular comparment where the reverse can occur enabling both CO_2 and HCO_3^- to exist within the cell (Missner et al., 2008). Based on this principle, the entry pathways into any protein channels extend beyond the unstirred layer and thus be an unlikely route for the gas to cross the membrane. The authors substantiate this theory further by demonstrating that CO_2 fluxes across AQP1 expressing cells and non-expressing cells are identical.

Recently a correspondence was published by *Boron et al.* to discuss these two contrasting theories (Boron et al., 2011). This publication suggests that the two contrasting paradigms may be a result of differences in experimental design, particularly the use of artificially generated membranes compared to *in vivo* extracts. The authors suggest that whilst the effects observed by *Missner et al.* may be true in a pure membrane preparation, the presence of membrane-spanning proteins within the membrane could potentially decrease the efficiency by which CO_2 moves from aqueous to lipid phase and back. An example of this may include red blood cells where integral membranes make up more than 50% of the cell surface membrane, thus requiring the presence of specialised proteins to facilitate CO_2 transport (Boron et al., 2011). As such, gas conduction through AQP1 and the RhAG complex may only be physiologically relevant in either membranes of low gas permeability, or in cells where a major fraction of the cellular membrane is occupied by the channels (Wang et al., 2007).

Bicarbonate Ion Transport

Being charged, HCO_3^- ions are not able to diffuse through the lipid membrane and need specialised transport proteins to facilitate transmembrane bicarbonate flux. These bicarbonate transporters fall into one of two families: SLC4 or SLC26 (Sterling & Casey, 2002). Differences in the tissue distribution, electrogenicity, and regulation of each of these anion exchanger proteins allows for precise regulation of HCO_3^- transport throughout the human body (Bonar & Casey, 2008).

The SLC4 family consists of ten genes, of which eight of the encoded proteins transport HCO_3^- ions. Functionally, these eight proteins fall into two major groups: three Cl^--HCO_3^- anion exchangers (AE1-3) and five Na^+ dependent HCO_3^- transporters (NBCe1, NBCe2, NBCn1, NDCBE, NCBE) (Romero et al., 2004). Anion exchangers perform reversible electroneutral exchange of Cl^- for HCO_3^- ions across a membrane, driven simply by concentration gradient. For most cells the inward Cl^- chemical gradient dominates, driving the exchange of extracellular Cl^- for intracellular HCO_3^- (Romero et al., 2004). The three isoforms share a common structure with cytosolic N- and C-terminal domains flanking a central transmembrane domain, which exhibits 80% sequence homology between isoforms (Bonar & Casey, 2008). The isoforms do, however, exhibit differences in tissue distribution, apical or basolateral epithelial expression, electrogenicity, regulation and physiological roles (Bonar & Casey, 2008).

NBC proteins exhibit similar structures to the AEs, but use the transmembrane Na^+ electro-chemical gradient to support transport. NBCe1 and NBCe2 are electrogenic Na^+-HCO_3^- co-transporters which move these ions in the same direction with a stoichiometry of 1:2 or 1:3 (Romero et al., 2004). Being electrogenic, one complete cycle of transport activity results in the net movement of charge across the membrane, carrying electrical current and shifting membrane potential. NBCn1 works in the same way as NBCe1 and NBCe2, co-transporting Na^+ and HCO_3^- ions, but is electroneutral with a stoichiometry of 1:1 and thus transport carries no electrical charge. NDCBE and NCBE transport HCO_3^- differently, being electroneutral sodium-driven Cl^--HCO_3^- exchangers. NDCBE is a hybrid co-transporter/exchanger that co-transports one Na^+ and two HCO_3^- ions into the cell in exchange for a single Cl^- (Grichtchenko et al., 2001; Romero et al., 2004). Whilst NCBE was originally described as a sodium-driven Cl^--HCO_3^- exchanger, the involvement of Cl^- ions is inconclusive and further work is required to establish its mode of activity (Romero et al., 2004).

The C-terminal cytoplasmic domain of all the SLC4A anion exchangers contains a ∼40 residue acidic motif involved in interactions with carbonic anhydrases, providing the exchangers with HCO_3^- and

increasing the ion flux through the transporter by about 40% (Sterling & Casey, 2002). This CA activity is of particular note with AE1 (Vince & Reithmeier, 1998) which plays a key role in inorganic carbon homeostasis, both in erythrocytes carrying CO_2 from systemic tissues to the lungs and in HCO_3^- reabsorption from the lumen of the renal collecting duct (Section 1.7).

The human SLC26 family consists of ten genes encoding anion exchangers capable of transporting a wide variety of monovalent and divalent anions through their hydrophobic transmembrane core (Mount & Romero, 2004). Of these SLC26A3, SLC26A4, SLC26A6 and possibly SLC26A7, SLC26A8 and SLC26A9 transport HCO_3^- ions (Mount & Romero, 2004; Bonar & Casey, 2008), usually with the counter exchange of Cl^- ions. Between isoforms, however, the stochiometry of Cl^--HCO_3^- exchange differs, with SLC26A3 transporting ≥ 2 Cl^- per HCO_3^- ion and SLC26A6 ≥ 2 HCO_3^- ions per Cl^- (Mount & Romero, 2004).

1.6.4 Sensing Inorganic Carbon

Whilst inorganic carbon is involved in the regulation of certain elements of cell signalling such as ACs (Section 1.3.6), it also has a signalling role itself. In plants, Rubisco acts as a primary CO_2 sensor. As this photosynthetic enzyme is rate-limited by the availabilty of CO_2, it is therefore a vital step in controlling flux through the plant's metabolism. CO_2 also competitively inhibits the Rubisco oxygenation reaction, which produces glycolate leading to photorespiration (Long et al., 2004) and thus CO_2 levels control rates of biomass production. Sensation of differing atmospheric CO_2 concentrations also controls transpiration rates through the regulation of stomatal opening (Long et al., 2004; Messinger et al., 2006; Mott, 1988) and expression. Stomatal pore number in *Arabidopsis thaliana* is controlled by the gene HIC (high for carbon dioxide) which encodes a negative regulator of stomatal development that responds to CO_2 concentration (Gray et al., 2000). This gene encodes a putative 3-keto acyl coenzyme-A synthase, an enzyme involved in the synthesis of long-chain fatty acids (Gray et al., 2000) typically found in the cuticle of leaves (Woodward, 2002). These fatty acids have been postulated to provide short-distance cell-to-cell signalling, which is then translated into a more systemic signal involving abscisic acid, ethylene and jasmonates. This enables CO_2 detection in mature leaves to control stomatal development in immature leaves (Woodward, 2002).

At the whole organism scale CO_2 can have profound effects. In both the plant fungal pathogen *Mucor racemosus* and the mammalian pathogen *Candida albicans* exposure to elevated CO_2 induces

morphogensis from spherical, budding yeast-like cells to a virulent hyphae/mycelium morphology (Larsen & Sypherd, 1974). In *Candida*, this change in morphology is regulated by the HCO_3^- responsive AC Cyr1p (Sheth et al., 2008) and elevated CO_2 leads to the downregulation of heat shock protein HSP12. Thus CO_2 may play a role in biofilm formation (Sheth et al., 2008), potentially improving the virulence of the pathogen.

Just as CO_2 can enable an organism to adapt its growth and undergo morphological change, other organisms adapt their behaviour in response to the gas. Organisms respond in different ways, either eliciting attraction or avoidance. In female blood-feeding mosquitos from species *Anopheles gambiae, Culex quinquefasciatus* and *Anopheles aegypti*, this signal is perceived as an attractant to their blood food source (Dekker et al., 2005; Turner et al., 2011). In these insects CO_2 is detected by heteromeric receptor proteins similar to those in *Drosophila* (see below), activating the cpA neuron (Turner et al., 2011). CO_2 can also act as an attractive cue for many insects that seek plants as food sources and oviposition sites. An example of this is the moth *Manduca sexta*, which uses labial pit organs whose receptor neurons project afferents to the antennal lobe to sense CO_2 released from its preferred host, *Datura wrightii* flowers (Guerenstein et al., 2004; Thom et al., 2004; Goyret et al., 2008). Some insects even use the CO_2 signal generated from plant wounds or rotting meat as an attractant. The Queensland fruit fly *Bactrocera tryoni*, for example, uses this signal as a strong oviposition cue (Stange, 1999).

Avoidance is also a common behavioural response and can be observed in both the fruit fly *Drosophila melanogaster* and the nematode *Caenorhabditis elegans*. *Drosophila* have CO_2 responsive neurons, able to sense the gas through 7TM receptors Gr21a and Gr63a, which are co-expressed in antennal olfactory sensory ab1C neurons (Jones et al., 2007; Kwon et al., 2007). The intracellular signalling network is at present unknown, although the G-proteins $G\alpha_q$ and $G\gamma_{30A}$ have been postulated (Yao & Carlson, 2010). CO_2 avoidance occurs at levels as low as 0.1% (Suh et al., 2004) and is proposed as an alarm response (stressed flies release 3- to 4-fold more CO_2 than unstressed flies (Suh et al., 2004)) and as CO_2 has profound deleterious effects. In *Drosophila* elevated CO_2 causes defects in egg laying, hatching and embryonic development (Helenius et al., 2009). Furthermore, elevated CO_2 can also disrupt the fly's immune response by repressing expression of antimicrobial peptides regulated by Relish (Helenius et al., 2009). This in turn can lead to increased *Drosophila* morbidity due to infection by a number of bacterial species, including *Enterococcus faecalis*, *Agrobacterium tumefaciens* and *Staphylococcus aureus* (Helenius et al., 2009). These long term deleterious effects are not unique to *Drosophila*. Long-term exposure to CO_2 at levels exceeding 9% causes aberrant

motility, age-dependent deterioration of body muscle organisation, slowed development, and reduced fertility and brood size in *Caenorhabditis elegans* (Sharabi et al., 2009). *C. elegans* also exhibit avoidance behaviour of CO_2 levels 0.5% and above, characterised by the cessation of forward movement and the rapid initiation of backward movement (Hallem & Sternberg, 2008). CO_2 detection occurs via two sets of neurons located in the head: the BAG O_2 sensors and the AFD thermosensors (Bretscher et al., 2011). Here CO_2 activates the cGMP signaling pathway via the ETS-5 transcription factor which controls the expression of a single target gene encoding receptor-type guanylate cyclase GCY-9 (Brandt et al., 2012). This signalling pathway also includes cGMP-gated heteromeric channel TAX-2/TAX-4 (Hallem & Sternberg, 2008; Hallem et al., 2011) and atypical soluble guanylate cyclases (sGCs) GCY-31 and GCY-33 to evoke Ca^{2+} signals and neuron activity (Bretscher et al., 2011). Downstream of this initial detection step CO_2 avoidance is modulated by multiple signaling molecules, including the neuropeptide Y receptor NPR-1 and the calcineurin subunits TAX-6 and CNB-1 (Hallem & Sternberg, 2008).

The involvement of GC and cGMP signalling in CO_2 detection has also been demonstrated in mice. Mice can smell CO_2 in the air at concentrations as low as 0.066% using specialised olfactory neurons that express the GC isoform GC-D (Hu et al., 2007). Detection involves CA-II mediated catalysis of CO_2 to HCO_3^- (Hu et al., 2007; Sun et al., 2009) which stimulates GC-D directly at the intracellular cyclase domain (Sun et al., 2009; Guo et al., 2009). This HCO_3^- interaction with GC-D has been demonstrated in the rat isoform to increase enzyme V_{max} whilst unaffecting the K_M for GTP (Guo et al., 2009), similar to the observations for sAC (Section 1.3.6). Activated GC-D then produces cGMP which opens CNG channels, stimulating the neuron to depolarise (Hu et al., 2007).

In humans, however, GC-D is a pseudogene and thus we are unable to detect CO_2 through our olfactory organs (Young et al., 2007), although detection is possible via the sour-sensing taste cells on the tongue, which exhibit direct responses to both dissolved and gaseous CO_2. However, as this mechanism acts through CA IV activation and the 'sour-sensing' ion channel PKD2L1, the true signal may instead be the CA generated protons (Chandrashekar et al., 2009). In addition to gustation, there are a number internal systemic locations able to sense changes in inorganic carbon, predominantly chemoreceptors in the carotid body and medulla oblongata. Chemoreception at these locations is involved in regulating body gases and systemic pH levels through control of breathing rate and kidney function. These topics will be covered in depth in Section 1.7, including descriptions of associated clinical problems when these homeostatic processes go awry.

1.7 Hyper/Hypocapnia: Control and Clinical Relevance

Control of systemic inorganic carbon is important as, when left unregulated, it can lead to toxic changes in body fluid pH and death (Richerson, 2004). Homeostasis is, therefore, required to avoid cellular damage as a result of abnormal levels of inorganic carbon, anoxia, and pH change. Whilst various serum constituents, particularly amino acids, are able to innately buffer small changes in pH, homeostasis is mainly controlled via pulmonary (Section 1.7.1), renal and hepatic responses (Section 1.7.3). Futher homeostasis is also provided by the natural buffering capacity of bone (Section 1.7.3) and the alterations made to blood volume and pressure in order to dilute the effects on bodily fluids (Marshall & Bangert, 2008).

These homeostatic mechanisms work well under normal conditions to maintain appropriate inorganic carbon and pH levels, but when an underlying disease presents this can lead to a pathological acid-base disorder. There are several categories of disorder (Figure 11), depending on the direction of pH change away from the norm, the system compromised, and the systemic levels of CO_2, HCO_3^- and various other ions, including chloride, phosphorus, sodium, potassium, calcium, and magnesium (Atkins, 1969). An excess of acid is termed an acidosis and an excess in bases an alkalosis. These disorders are often associated with alterations to the equilibrium of inorganic carbon in solution (Section 1.6.2), with hypercapnia referring to an elevation of CO_2 and hypocapnia, a decrease. Due to the effects of CO_2 in solution, hypercapnia is often associated with an increase in blood H^+ ions, a drop in pH and thus an acidosis. Classification of the processes that cause the imbalance is based on the etiology of the disturbance, either respiratory or metabolic, and the time-frame of the event: acute or chronic. Thus, acute respiratory acidosis may occur following choking, where systemic CO_2 levels rise rapidly and pH drops (Siggaard-Andersen, 2005), whilst chronic metabolic alkalosis may occur over an extended period following a kidney malfunction that prevents or interupts bicarbonaturia (Marshall & Bangert, 2008). Each differentiated disorder is characterised by pH, pCO_2 and $[HCO_3^-]$ deviations from the norm (Figure 12).

On detection of an acid-base disorder (Section 1.7.1), the mechanisms that maintain acid-base homeostasis may alter their function to compensate (Table 3). Most commonly, this involves alteration of breathing rate to combat metabolic acidosis/alkalosis and modification of renal excretion rates for respiratory disorders. A good example of this is in individuals suffering ketoacidosis as a result of diabetes mellitus. These individuals have an inability to completely metabolise triacylglycerols from adipose tissue, which results in a build-up of ketoacids in the body. This

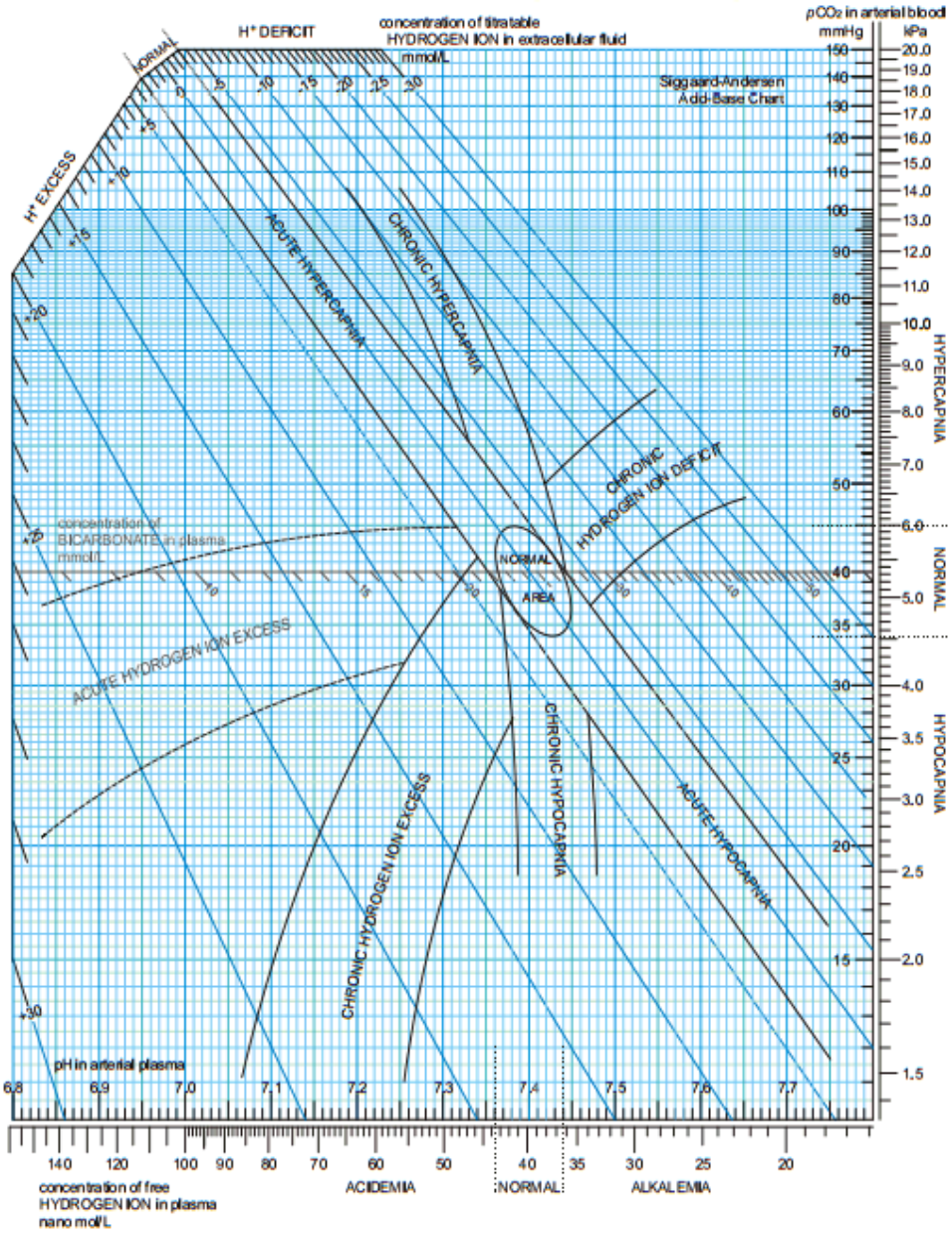

Figure 11: The Siggaard-Andersen acid-base chart used by medical professionals to diagnose acid-base disorders. Under normal conditions the systemic acid-base balance maintains a pH around 7.4 in the extracellular fluid by excreting CO_2 in the lungs and HCO_3^- ions from the kidneys. However, when this control is disrupted an acid-base disorder may present, characterised by changes in arterial blood pH, carbon dioxide tension (pCO_2) and concentration of titratable hydrogen ions (H^+). As shown, a pH, log pCO_2 chart can be used to illustrate these conditions as shown. The chart displays normal values, as well as those expected in typical acid-base disturbances, including acute and chronic respiratory acidosis and alkalosis, and acute and chronic metabolic acidosis and alkalosis. Figure adapted from *Siggaard-Anderson* (Siggaard-Andersen, 2005).

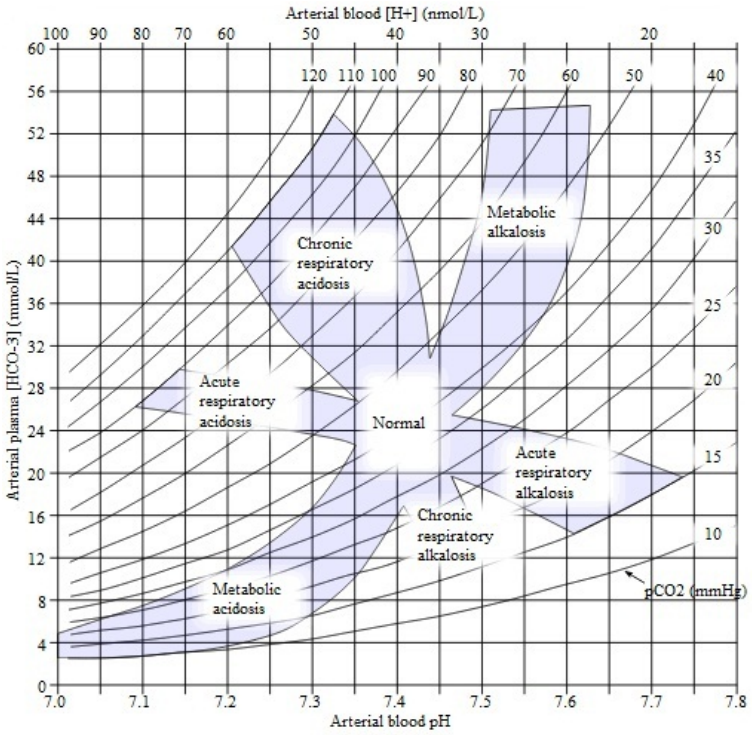

Figure 12: Acid-base disorders and the pH, pCO_2 and $[HCO_3^-]$ associated. Acid-base disorders are characterised by their onset time-frame (acute or chronic), etiology (respiratory or metabolic) and their pH deviation from the norm (acidosis or alkalosis). Due to the nature of dissolved CO_2, these disorders are accompanied by alterations in systemic pH, pCO_2 and $[HCO_3^-]$, measurement of which forms a diagnostic tool. Figure adapted from *Huckfinne* (Huckfinne, 2010).

Process	**pH**	**Ci Levels**	**Compensatory Mechanism**	**Compensatory Effect**
Metabolic Acidosis	Down	CO_2 normal/decreasing HCO_3^- down	Respiratory	CO_2 down
Respiratory Acidosis	Down	CO_2 up HCO_3^- normal/increasing	Renal	HCO_3^- up
Metabolic Alkalosis	Up	CO_2 normal/increasing HCO_3^- up	Respiratory	CO_2 up
Respiratory Alkalosis	Up	CO_2 down HCO_3^- normal/decreasing	Renal	HCO_3^- down

Table 3: Compensatory mechanisms activated by acid-base disorders and their effects.

manifests as a metabolic acidosis and, in order to compensate, individuals experience excessive urine production in order to remove ketoacids and re-absorb bicarbonate ions. In severe, acute cases, however, individuals experience heavy, laboured gasping, known as 'Kussmaul breathing', as the body tries to expel as much CO_2 as possible in an attempt to increase blood pH once more (Marshall & Bangert, 2008).

This report is primarily concerned with how inorganic carbon concentrations can affect cellular and systemic biochemistry and physiology. Under normal conditions tissues are maintained at pH 7.4 and a pCO_2 of 40 ± 5 mmHg, which equates to about 5.3% (Azzam et al., 2010; Briva et al., 2010). Hypercapnia occurs when this pCO_2 rises above 45 mmHg and is generally caused by hypoventilation, lung disease, or diminished consciousness. Hypercapnia is common in patients with diseases such as chronic obstructive pulmonary disease (COPD), cystic fibrosis (CF), bronchopulmonary dysplasia (BPD) and muscular dystrophies (Li et al., 2006a; Vohwinkel et al., 2011). In COPD patients it is not unusual for pCO_2 to reach 60-80 mmHg in the arterial blood (Connors et al., 1996) and levels as high as 250 mmHg have been described in individuals with uncontrolled asthma (Mutlu et al., 2002). Patients with hypercapnia generally have a worse prognosis (Belkin et al., 2006; Kessler et al., 1999), associated with a decrease in wound repair (Doerr et al., 2005). At the cellular level, cells grown in the presence of high CO_2 have been shown to have reduced proliferation, independent of extracellular pH and osmolarity (Vohwinkel et al., 2011), as well as depressed glycolysis rates (De Zengotita et al., 2002). In the context of disease, these effects on proliferation may prove detrimental to recovery. Elevated CO_2 can also cause oxidative stress and injury (Doerr et al., 2005) and inhibit alveolar fluid reabsorption (Briva et al., 2007; Vadász et al., 2008a), potentially impairing gas exchange, and increasing the likelihood of infection and pulmonary oedema (Vadász et al., 2008a). Furthermore, hypercapnia and the often concomitant acidosis may have deleterious effects on vascular and cardiac tissues. In accordance with this, the leading cause of hospitalisation and morbidity among COPD patients is cardiovascular events (Sin & Man, 2005). *Azzam et al.* suggests that as chronic hypercapnia is known to cause permanent damage to muscle cells in *C.elegans* (Sharabi et al., 2009), a similar mechanism might explain the cardiovascular complications (Sin & Man, 2005) and reductions in muscle mass observed with COPD patients (Maltais & Debigaré, 2003).

At the other extreme, hypocapnia is characterised by pCO_2 levels less that 35 mmHg and usually results from chronic hyperventilation. Hypocapnia can occur as a complication of pathophysiological situations, including high-altitude hypoxemia, pulmonary disorders such as asthma and acute lung

injury (Laffey & Kavanagh, 2002), central nervous system diseases, anxiety-hyperventilation, hepatic failure, chronic vomiting, sepsis and salicylate intoxication (Adrogue & Madias, 1998). With these pathologies patients initially experience a moderate acute decrease in HCO_3^- occurs due to tissue buffering and Cl^- ion release from cells (Laffey & Kavanagh, 2002). This is followed by the progression of chronic hypocapnia as a result of renal homeostatic mechanisms, which may require up to 2-3 days to be established (Adrogue & Madias, 1998; Laffey & Kavanagh, 2002). One of the most common causes of hypocapnia is pregnancy, where the arterial pCO_2 is maintained approximately 10 mmHg lower than normal by the high circulating levels of the hormone progesterone (Laffey & Kavanagh, 2002).

1.7.1 Chemoreceptors and Control of Respiration

Changes to systemic carbon dioxide are monitored throughout the body at peripheral chemoreceptors, but most importantly at those located within the aortic and carotid bodies. Chemoreceptors in the carotid body are also able to detect changes in pH, often related to the level of CO_2 (Section 1.6.2). These sensors are proposed to be regulated by HCO_3^- sensitive sAC and the output signal is cAMP dependent (Nunes et al., 2009). Further monitoring occurs within the brain at central chemoreceptors located on the highly vascularised ventro-lateral surface of the medulla oblongata, which is capable of detecting changes in the pH and pCO_2 of cerebrospinal fluid (Eldridge et al., 1985; Shams, 1985).

These chemoreceptors are able to send nervous signals within the body in order to compensate for any acid-base alterations. The fastest compensation mechanism initiated is via alteration of breathing rate and, therefore, the amount of exhaled CO_2. An increase in pCO_2 of just 1 mmHg causes a 20-30% increase in ventilation (Feldman et al., 2003), a change primarily instigated by the central chemoreceptors of the brain on the respiratory centre of the medulla oblongata (Laffey & Kavanagh, 1999). Here, CO_2 sensitive connexin-26 hemichannels, located on astrocytes, open to release ATP which increases respiration rate through excitation of respiratory neurons (Gourine et al., 2005; Huckstepp et al., 2010a,b; Wenker et al., 2012). Respiratory neurons in turn send impulses to the intercostal muscles and diaphragm via the intercostal and phrenic nerves respectively, altering breathing rate (Laffey & Kavanagh, 1999). Peripheral chemoreceptors are also involved, although these chemoreceptors are not able to sense CO_2, only pH. Under normal conditions these chemoreceptors send a continual signal to the brainstem via cranial nerves IX and X, but when a drop in plasma pH is detected this signal intensifies and results in an increase in ventilation rate

(Buckler et al., 1991; Huckstepp & Dale, 2011).

The ability to monitor blood pH and gases and control breathing rate is of paramount importance in acid-base homeostasis. As covered in Section 1.7, the inability to maintain this balance can lead to a multitude of pathological states. Due to the accessible nature of the ventilatory system, alteration of the gas content of inspired air can also be used medically to manipulate systemic acid-base levels. An example of this is the use of depressed mechanical ventilation to induce permissive hypercapnia. In contrast to the paradigm that the effects of hypercapnia are potentially damaging (Section 1.7), the use of permissive hypercapnia is of increasing interest as a treatment for a range of pathological disorders, including acute lung injury, ischaemia-reperfusion injury, and acute respiratory distress syndrome. Clinical treatment of these disorders involves decreasing the tidal volume and inspiratory pressures of artificial ventilation and thus allowing pCO_2 to increase, often as high as 100 mmHg (Laffey et al., 2004; Ismaiel & Henzler, 2011; Oliver et al., 2012). This practice limits the amount of potential damage caused by overstretching lungs with compromised compliance (Broccard et al., 2001; Sinclair et al., 2002; Amato et al., 1998), for example in patients with acute respiratory distress syndrome (Amato et al., 1998), and allows permissive hypercapnia to develop (Sinclair et al., 2002). The protective effects of permissive hypercapnia have been attributed to the effect of CO_2 on the haemoglobin oxygen dissociation curve, which shifts to improve arterial oxygenation (Azzam et al., 2010). Additional protection is provided by the concomitant acidosis which decreases cardiac contractility and increases cardiac output and the often simultaneous effects of hypoxia on pulmonary vasoconstriction which increases oxygen delivery to the alveoli (Laffey & Kavanagh, 1999). Together, these effects result in a net increase in pO_2, furthered by an increase in regional blood flow (Laffey & Kavanagh, 1999). There is also a well-documented anti-inflammatory influence of CO_2 which may provide further benefits to using permissive hypercapnia in a clinical setting (Section 1.7.2). Furthermore, hypocapnia is known to cause bronchospasm, hyperventilation (Laffey & Kavanagh, 2002) and increased production of dysfunctional surfactants. This could worsen lung compliance and further damage the affected tissue and consequently should be avoided (Laffey & Kavanagh, 2002).

In contrast, in patients administered near pure oxygen, this respiratory stimulant can cause hyperventilation and thus lead to hypocapnia (Iscoe & Fisher, 2005). This is due to the Haldane effect, which describes that oxygenated haemoglobin binds to less CO_2 and so systemic inorganic carbon transport can only occur via dissolved gas/ions. This dissolved gas leads to increased local tissue pCO_2, particularly at the central chemoreceptors, driving inspiration and leading to hyperventilation

(Iscoe & Fisher, 2005). The basis for giving patients O_2 gas is to increase blood pO_2 and thus increase delivery to the tissues. However, this has a counter-productive two-fold effect: firstly the induced hypocapnia and resultant metabolic alkalemia causes vasoconstriction of CO_2 responsive vascular beds, reducing O_2 delivery. Secondly, it also increases the haemoglobin affinity for O_2, further reducing off-loading into tissues (Iscoe & Fisher, 2005; Adrogue & Madias, 1998; Laffey & Kavanagh, 2002). Hypocapnia can also increase the metabolic demand of a tissue through cellular excitation or contraction (Laffey & Kavanagh, 2002), further augmenting the requirement for oxygen. Thus, this misinformed delivery of O_2 and the resultant metabolic alkalemia can lead to a number of clinical oversights. Common examples include a decline in fetal pO_2 during labour, worsening fetal outcome (Iscoe & Fisher, 2005), and a counter-productive decrease in cerebral and myocardial blood flow (Iscoe & Fisher, 2005; Adrogue & Madias, 1998) in stroke and myocardial ischaemia patients respectively (Iscoe & Fisher, 2005). This latter example occurs as a result of arteriolar constriction (Adrogue & Madias, 1998) and reduced oxygen delivery (Laffey & Kavanagh, 2002). The concomitant alkalemia can also have deleterious effects on the recovery rate of these patients as it increases neuron excitability which results in deleterious seizures (Laffey & Kavanagh, 2002) or ventricular arrhythmias (Adrogue & Madias, 1998) in cerebral and cardiac patients respectively.

Whilst long durations of hypocapnia can adversely affect patient outcome, transient clinical induction can be advantageous. This can be the case in patients with severely augmented intracranial pressure as a result of head trauma or brain tumour (Neumann et al., 2008), neonatal pulmonary-artery hypertension and alongside general anesthesia to minimise the spontaneous respiratory effort (Laffey & Kavanagh, 2002). The majority of the positive effects of this short term hypocapnia are associated with the vasoconstriction caused by the often concomitant alkalosis (Laffey & Kavanagh, 2002).

1.7.2 Systemic Effects of Hyper/Hypocapnia on the Immune System

Sections 1.7 and 1.7.1 present somewhat contrasting consequences of hyper- and hypocapnia in a clinical setting. Whilst the extent of the advantages and disadvantages may depend on the pathological condition presenting, a large part has been attributed to the effects of CO_2 on the immune system. Acidosis has been known to attenuate a range of inflammatory processes including: neuronal apoptosis, phospholipase A_2 activity, neutrophil Na^+/H^+ exchange (Laffey & Kavanagh, 1999), pro-inflammatory cytokine production, and neutrophil recruitment (Laffey et al., 2004). There is now evidence that some of these inflammatory alterations are caused by CO_2 and not the associated acidosis. *Cummins et al.* demonstrated a pH independent attenuation of the NF-κB

pathway with elevated CO_2. Under these conditions NF-κB regulatory protein IKKα is reversibly translocated to the nucleus, where it is able to alter gene expression (Cummins et al., 2010) and repress NF-κB activity (Lawrence et al., 2005). In addition the same group have also shown that the anti-inflammatory NF-κB family member RelB is also cleaved and translocated to the nucleus where it can suppress cytokine-stimulated inflammatory gene expression (Oliver et al., 2012). The NF-κB pathway is a major regulator of inate immune and inflammatory gene expression and the effects of CO_2 can be demonstrated to inhibit bacterial lipopolysaccharide induced gene expression (Takeshita, 2003; Cummins et al., 2010). These effects may underlie the therapeutic benefits of permissive hypercapnia observed in conditions where infection or wounding is present (Hanly et al., 2006; Costello et al., 2009; Nichol et al., 2009). This is of paramount importance when considering that the most common predisposing cause of acute respiratory distress is infection (Nichol et al., 2009). However, it is also worth noting that, in the wrong setting, this attenuation of the immune response may prove counter-productive and thus harmful to recovery (Doerr et al., 2005; O'Croinin et al., 2008; O'Toole et al., 2009).

The effects of CO_2 on the immune system may also have a prophylactic as well as therapeutic use. This is not only evident in cases of acute endotoxin-induced lung injury (Laffey et al., 2004), but also with trigeminal neuron activated migraine and seasonal allergic rhinitis (Casale et al., 2008). With the latter examples, prophylaxis has been demonstrated using non-physiological concentrations of CO_2 of 100%. *Casale et al.* showed that two intra-nasal one minute applications of 100% CO_2 provided both rapid (ten minutes) and sustained (twenty-four hours) relief from allergic rhinitis symptoms including congestion, rhinorrhea, itching and sneezing (Casale et al., 2008). This relief was provided through the prevention of mast cell agonist induced Ca^{2+} ion release and cell degranulation (Strider et al., 2011).

Further effects of hypercapnia and the often concomitant acidosis include the attenuation of reactive oxygen species (ROS) production, including repressed leukocyte superoxide formation and lipid peroxidation (Laffey & Kavanagh, 1999), as well as xanthine oxidase inhibition (Shibata et al., 1998). These alterations to ROS can have profound effects particularly as oxygen-derived free radicals are central to the pathogenesis of acute lung injury and ischaemia reperfusion injury (Laffey & Kavanagh, 1999). In the case of reperfusion injury, the return of blood to an ischaemic area often causes inflammation and oxidative damage which may lead to the production of free radicals from membrane breakdown. These free radicals cause cytochrome c release and caspase-9/-3 cleavage, leading to DNA fragmentation and apoptosis (Chen et al., 2012). Thus, in this setting, use of

permissive hypercapnia may have clinical precedent. Demonstrations of this have been shown in rats where hypercapnic acidosis is shown to protect rats against heart ischaemia, brain ischaemic stroke, and lung ischaemic reperfusion injury (Laffey & Kavanagh, 1999).

Elevated CO_2 is also an important consideration in growing tumours as prior to vascularisation pCO_2 levels can increase within the cellular mass. Previous studies have shown that in experimental animal systems pCO_2 levels of 70-80 mmHg can be observed within tumours, compared to 40 mmHg in the blood (Gullino et al., 1965). Before sufficient angiogenesis can occur and vasculature develop, spheroids of cancer cells exhibit difficulties in maintaining pH and rely on inorganic carbon to provide an extracellular mobile pH buffer to chaperone protons away from cells (Hulikova et al., 2011). Due to this poor pH homeostatic mechanism, acidic pH has become a hall-mark of cancer, further augmented by the characteristic elevated metabolism of cancer cells, and has been suggested to exert selection pressure over normal cells to promote tumour invasiveness. Nevertheless, when acid extrusion and removal is compromised in experimental spheroids, they become highly uniform and inadequate at the core (Hulikova et al., 2011). This artificial disruption of acid extrusion can also be mimicked in the absence of CO_2/HCO_3^- or with CA inhibition, thus highlighting the importance of the Ci buffer (Hulikova et al., 2011).

CO_2 levels can also have another effect on tumour growth through the aforementioned alteration of immune response gene expression. As an example of this, *Samspon and Chaplin* demonstrated that increasing pCO_2 concentrations from 5% to 7% decreased the amount of phorbol 12-myristate 13-acetate induced production of the potent cytotoxic cytokine TNFα (tumour necrosis factor α) from the monocyte cell line U937 (Sampson & Chaplin, 1996). This suppression of TNFα by elevated CO_2 has since been further demonstrated in human alveolar A549 cells (Oliver et al., 2012). In a tumorgenic system, this cytokine acts as an important angiogenic factor and, therefore, the effect of CO_2 on its release requires further study. (Sampson & Chaplin, 1996).

1.7.3 Control of Hyper/Hypocapnia - Kidney Function

Whilst alteration of respiratory rate is a quick and effective method to control physiological pCO_2 and pH, chronic alterations or respiratory derived acid-base disorders require different mechanisms to return to normal. In these cases compensation is provided both through hepatic and renal responses. The liver is able to dispose of a small amount of CO_2 through the anaplerotic carboxylation of pyruvate to form oxaloacetate, but the majority of regulation is provided by the kidneys where

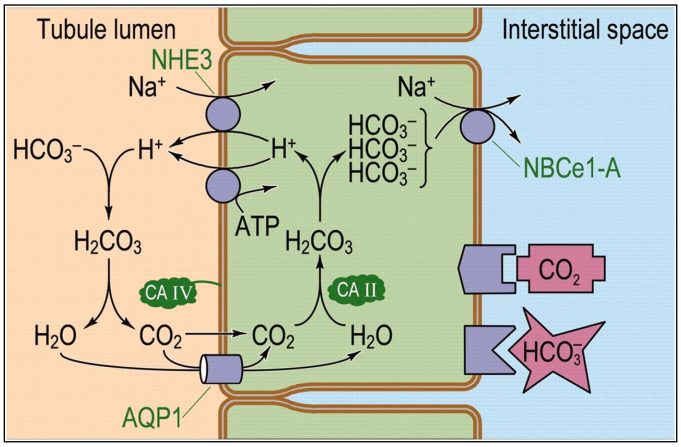

Figure 13: Diagram illustrating acid-base transport in renal proximal tubules.

The proximal tubule reabsorbs HCO_3^- by using active transport processes to secrete H^+ into the tubule lumen. This causes lumen HCO_3^- to form CO_2 and H_2O under the influence of CA VI. The lumenal CO_2 and H_2O can then enter the cells via AQP1, where HCO_3^- ions are again formed through the action of CAII. Once inside the cell, HCO_3^- exits across the basolateral membane via NBCe1. This process is controlled internally through CO_2 and HCO_3^- sensors in the cells' basolateral membrane and by systemic signals, such as parathyroid hormone.

Abbreviations used: NHE3, Na^+-H^+ exchanger 3; AQP1, aquaporin 1; CA II and CA IV, carbonic anhydrases II and IV; NBCe1-A, electrogenic Na^+/HCO_3^- co-transporter 1, splice variant A.

Figure adapted from *Boron* (Boron, 2006).

HCO_3^- ions are excreted via the urine (Marshall & Bangert, 2008). An example of this is during respiratory acidosis, which is characterised by in increase in blood pCO_2 that causes a decrease in blood pH and an increase in $[HCO_3^-]$; and this raises the re-absorption of HCO_3^- from the urine to buffer the blood pH (Bouyer et al., 2003). There are several mechanisms to control this loss of HCO_3^- through the kidneys, 80% of which takes place in the proximal tubules (Wang & Deen, 1980; Chen & Boron, 1995a), 10% in the thick ascending limb and 10% in the distal nephron (Boron, 2006). The proximal tubule (PT) is located within the renal cortex and is a unique region containing morphologically specialised epithelial cells with numerous apical brush border microvilli and basal interdigitating folds (Shlatz et al., 1975). Its key function is to re-absorb nutrients and ions downstream from the glomerular filtrate, according to the body's current needs.

Whenever blood pH levels drop due to increased systemic CO_2, HCO_3^- reabsorption from the PT increases, independent of any changes to pH at the basolateral membrane (Bouyer et al., 2003). A diagrammatic representation of the process is presented in Figure 13. HCO_3^- reabsorption is initiated through the active secretion of protons into the tubule lumen by Na^+/H^+ anti-porters (Boron & Boulpaep, 1983; Murer et al., 1976) and V-type H^+ pumps (Boron, 2006; Paunescu et al., 2008). Most of the protons secreted by the PT cells titrate the filtered HCO_3^- to form CO_2 and H_2O. This reaction is catalysised by CA IV, which is tethered to the apical membrane (Sly & Hu, 1995). CO_2 and H_2O are then able to enter the PT cells via AQP1 channels (Section 1.6.3) in the apical membrane (Boron, 2006; Missner et al., 2008). In the lumen, 'new HCO_3^- ' is also created to neutralise the volatile mineral acids generated by metabolism (Boron, 2006; Bouyer et al., 2003). Any protons remaining are buffered by creatine and ammonium and dihydrogen phosphate ions (Bouyer et al., 2003; Boron, 2006; Marshall & Bangert, 2008).

Reabsorbed Ci from this process does not remain in the cell, but instead is transported across the basolateral membrane into the interstitial fluid and eventually to the blood. This is achieved through the conversion of CO_2 to HCO_3^- ions by cytoplasmic CA II (Sly & Hu, 1995). HCO_3^- can then be basolaterally transported out of the cell through the activity of electro-neutral Na^+/HCO_3^- co-transporters 1.6.3, namely NBCe1-A (Boron & Boulpaep, 1983; Seki et al., 1996; Boron, 2006). NBCe1 is the predominant basolateral pathway in the S1 and S2 segments of the PT, where the majority of the HCO_3^- reabsorption occurs, but a basolateral Cl^--HCO_3^- is also important in the S3 segment (Kondo & Frömter, 1987; Seki & Frömter, 1990).

Proximal tubule cells have been postulated to have either CO_2 or HCO_3^- sensors on their basolateral membrane, able to detect hyper- or hypocapnic concentrations of Ci and resultantly stimulate apical

Na^+/H^+ anti-porters to respond accordingly (Chen & Boron, 1995a,b). However, the overall level of HCO_3^- reabsorbed is controlled by parathyroid hormone, PTH, an important homeostatic hormone involved in HCO_3^-, Ca^{2+}, and phosphate homeostasis (Agus et al., 1973).

Parathyroid Hormone

PTH is an 84-amino acid polypeptide hormone (Azarani et al., 1995) secreted continuously from the chief cells of the parathyroid gland under the fine and precise control of blood calcium (Sherwood et al., 1966). Hormone release is stimulated in response to systemic decreases in serum Ca^{2+} levels (Sherwood et al., 1966). This Ca^{2+} decrease is detected via a 7-TM Ca^{2+} sensitive receptor coupled to PLC (Darè et al., 1998), in addition to a further level of control by intracellular Ca^{2+} and cAMP (Willgoss et al., 1980). However, PTH is not exclusively involved in Ca^{2+} homeostasis, but also has important roles in the regulation of systemic phosphate, HCO_3^- and, therefore, pH. The complementary 7-TM G-protein coupled PTH receptor (Short & Taylor, 2000) is found predominantly in the target cells of osteo-blasts (see below) and renal proximal tubule cells (Aurbach & Potts, 1964; Melson et al., 1970; Shlatz et al., 1975).

Bone is an important PTH responsive organ, where osteoblasts (fully differentiated bone cells embedded in the extra-cellular matrix) react to the hormone through a variety of different mechanisms, including the production of cAMP (Chase & Aurbach, 1970). Most notably at this location, PTH acts to increase the calcium concentration of the blood by activating the release of Ca^{2+} from bones (Raisz, 1965), predominantly through the destruction and re-absorption of osteoblasts (Forrest et al., 1985; Raisz, 1965). Osteoblast breakdown is carried out by a normal, non-pathological mechanism carried out by another bone cell type: osteoclasts, themselves indirectly stimulated by PTH (McSheehy & Chambers, 1986). This same mechanism is also important in increasing serum phosphate levels (Doyle & Jan de Beur, 2008). Furthermore, bone cells have a role in acid-base homeostasis as any decreases in proton levels, as typical with metabolic acidosis, have been shown to stimulate osteoclast and inhibit osteoblast activity (Goldhaber & Rabadjija, 1987; Krieger et al., 1992). Systemic pH decrease thus results in marked effluxes of sodium and potassium ions, as well as depletion of mineral carbonates (Bushinsky et al., 2002). This provides an ionic flux capable of buffering some of the available protons, often with sodium and potassium ions exchanging for hydrogen and the carbonate binding protons to produce HCO_3^-, which results in significant neutralisation of the increased acidity (Bushinsky et al., 2002). In fact, by this mechanism, for each millimole of calcium released from the bone, approximately 12 mmol of protons are neutralised (Bushinsky et al., 2002). Unlike in renal cells, however, these effects do not appear to be PTH

controlled and are instead mediated by physio-chemical bone mineral dissolution and additional osteoclast activity (Bushinsky et al., 2002). These effects on acid-base homeostasis are particularly relevant as bone contains approximately 80% of the body's stored Ci, including carbonate, HCO_3^- and CO_2 (Bushinsky et al., 2002). Two thirds of this is in the form of carbonate complexed with hydrogen, calcium, potassium, sodium and other cations, located in the lattice of the bone crystals where it is relatively inaccessible to systemic circulations. The other third is located in the hydration shell of hydroxyapatite (Section 1.4) where it is readily accessible to the systemic circulation (Bushinsky et al., 2002).

In the renal PT, PTH acts to increase calcium (Agus et al., 1973) and decrease HCO_3^- and phosphate re-absorption from the urine (see below), in addition to decreasing volume re-absorption as a knock-on effect of regulating HCO_3^- (Pollock et al., 1986). PTH also has a number of other effects on these cells, including stimulation of gluconeogenesis and the inhibition of Na^+/K^+-ATPases (Friedlander & Amiel, 1994). As first suggested by *Chase and Aurbach*, intracellular transduction of the PTH signal is predominantly via AC (Chase & Aurbach, 1967; Agus et al., 1971), which results in an increase in nephrogenous (Broadus et al., 1977) and urinary excreted cAMP (Chase & Aurbach, 1967). However, it is now known that signalling can also occur from the same receptor (Abou-Samra et al., 1992) via a G protein - PLC - Ca^{2+} - PKC route, coupled to discrete high affinity receptors (Cole et al., 1987; Hruska et al., 1987; Azarani et al., 1995). These two pathways are purported to be spatially separated, with the AC coupled pathway predominantly located at the basolateral membrane (Shlatz et al., 1975) and the PLC pathway potentially apical (Cole et al., 1987). In addition, each signalling route is coupled to a downstream receptor with different affinities; AC coupled receptors being of low affinity in comparison (Cole et al., 1987). This information has led to the suggestion that PTH transduction under normal conditions is PKC mediated, as a response to PTH can be seen as low as picomolar concentrations (Pollock et al., 1986), whilst PKA activation may be tumorigenic in nature (Azarani et al., 1995). However, discovery of 'cAMP junctions' between AC VI and IP_3 receptors may affect this paradigm as they enable the delivery of super-maximal concentrations of cAMP directly to the target enzyme at distances impenetrable to PDEs (Tovey et al., 2008). It may also be worth noting that both the PLC/PKC and cAMP/PKA pathways converge on MAPK-kinase and it has been suggested that this downstream signalling molecule may serve to transduce both signals (Cole, 1999; Bacic et al., 2003). Demonstration of this can be provided using MAPK-kinase antagonists which prevent PTH stimulated NaPi-IIa internalisation (Bacic et al., 2003; Cole, 1999) and regulation of Na^+/H^+ exchange (Bacic et al., 2003). Nevertheless, AC and cAMP is widely accepted as the mediator of the majority of PTH's hormonal effects on both bone and kidney.

Results to illustrate this include the ability of the AC agonist forskolin to reproduce PTH mediated changes in luminal pH, as a result of alterations in downstream Na^+/H^+ transporter activity (Pollock et al., 1986), as well as the ability of PKA inhibitors to attenuate these effects (Nogueira et al., 2008). Furthermore, *Martin et al.* found that inhibition of PLC did not affect PTH regulation of phosphate transport and the authors note that the evidence to support the PKC route is mainly based on the use of PKC inhibitors, which are often not specific for PKC and also inhibit PKA (Martin et al., 1994).

As the PTH response is involved in the systemic regulation of inorganic carbon, it would be interesting to establish whether there is also a further intracellular level of control via AC. This is of particular interest, both due to the multitude of interactions currently established between AC isoforms and Ci (Section 1.3.6), as well as the contradicting deleterious and benefical effects of hypercapnia and permissive hypercapnia (Sections 1.7, 1.7.1 and 1.7.2). Work carried out by *Rodriguez et al.* with parathyroidectomised rats (therefore unable to produce PTH) demonstrated that administration of acetazolamine, a carbonic anhydrase inhibitor, decreased cAMP in their urine, independent of any changes in pH. In fact, acetazolamine was shown to have a dose-dependent effect on AC activity (Rodriguez et al., 1974); perhaps an indication that it was not the inhibitor itself acting on the enzyme, but rather the changes in Ci brought about by alterations in the CA activity. This hypothesis of Ci directly influencing the intracellular signalling is further supported by the observation that respiratory alkalosis results in a resistance to the phosphaturic effect of PTH and cAMP, an effect shown to be a result of the decrease in pCO_2, not the concomitant pH change (Hoppe et al., 1988). Experimental demonstration of a decrease in PTH induced cAMP accumulation at elevated pCO_2 is provided in Chapters 3 and 4, with the physiological effects on the downstream Na^+/H^+ exchanger and NaPi-IIa provided in Chapter 5.

Regulation of HCO_3^- Excretion and Na^+/H^+ Exchanger Activity

In the kidney, the PTH response constitutes a fundamental step in the regulation of HCO_3^- re-absorption via the inhibition of apical membrane (Friedlander & Amiel, 1994) Na^+/H^+ anti-porters NHE (Murer et al., 1976; Schwartz, 1981; Pollock et al., 1986). As explained above, by acidifying the PT lumen, HCO_3^- ions in the glomerular filtrate can be converted to CO_2 and reabsorbed into the cell. There are nine isoforms of mammalian NHE distinguished by their kinetic characteristics, drug sensitivity, modulation by protein kinases, response to external stimuli, and tissue and cellular distribution (Tse et al., 1992). Pharmacological (Wu et al., 1996), genetic (Schultheis et al., 1998), and immunohistochemical (Biemesderfer et al., 1993, 1999) data indicate that the NHE3 isoform is

predominantly responsible for this activity. NHE3 is specific to the intestine and kidney (Tse et al., 1992; Schultheis et al., 1998) and its C-terminus contains a regulatory domain (Tse et al., 1992), which is targeted by AC/PKA (Nogueira et al., 2008). Phosphorylation at this site inhibits the anti-porter (Fan et al., 1999) and in the long term PKA activity decreases transcription and thus expression through interactions with the NHE3 promotor region -152 to +55 (Nogueira et al., 2008).

PTH also causes a redistribution of NHE3 from the apical microvilli to the base of the intermicrovillar cleft (Fan et al., 1999; Leong et al., 2004), where endocytosis from the apical to subapical region occurs (Nogueira et al., 2008). This redistribution is associated with the activity of two adaptor proteins: NHE-regulatory factors NHERF-1 and -2. These proteins are known to assemble macromolecular complexes and determine the localisation, trafficking and signalling of select GPCRs (Ardura et al., 2011). They share a common structure, including two tandem PDZ (Post-synaptic Density-95, discs large, Zonula occludens-1) protein interaction domains and a C-terminal MERM (Erzin-Radixin-Moesin-Merlin) binding domain and are both able to self-associate and heterodimerise (Cunningham et al., 2004). Under basal conditions, NHE3 and NHERF-2 closely associate, but within one minute of intracellular Ca^{2+} elevation NHERF-2 releases the exchanger. NHE3 is then mobile and able to redistribute from the brush border into the intervilli clefts where ion transport may be compromised (Cha et al., 2010), in addition to the transporter being susceptible to endocytosis (Zhu et al., 2011).

NHERFs also have an additional role in PTH signalling at the hormone receptor level. NHERF-1 interacts with PTH receptor 1, PTHR1 (Mahon et al., 2003a), to attenuate PTH induced cAMP synthesis (Karim et al., 2008). Under basal conditions, NHERF-1 binds to PTHR1 via its PDZ binding motif and this interaction tethers the receptor to the actin cytoskeleton and plasma membrane (Ardura et al., 2011). NHE3 can also bind directly to NHERF-1 and actin via erzin and thus may form a signalling microdomain with the PTH receptor. Upon PTH stimulation NHERF-1 dissociates from PTHR1, which is then trafficked to clathrin-coated pits for internalisation. Recruitment of β-arrestins is delayed until NHERF-1 dissociates, but when detached, the receptor is endocytosed and eventually recycled to the membrane or targeted for degradation (Ardura et al., 2011).

Further regulation of NHE activity occurs via IRBIT (IP_3 receptor binding protein released with IP_3). At the IP_3 receptor phosphorylated IRBIT competitively binds to the IP_3 binding site, inhibiting receptor activity and preventing Ca^{2+} ion leakage (Ando et al., 2006). With NHE3, phosphorylated IRBIT binds the C-terminal domain to provide Ca^{2+} dependent stimulation via CaM and CaMKII (He et al., 2008). This interaction initiates exocytotic insertion of the NHE3-

IRBIT complex into the plasma membrane. Whilst this interaction does not occur as a result of PTH signalling, it is worth noting as the response is involved in fluid reabsorption via similar mechanisms as HCO_3^-. An example of this is after stimulation by angiotensin II, which acts by decreasing cAMP and increasing Ca^{2+} to activate downstream IRBIT (He et al., 2010). IRBIT is also able to activate NBCe1 via its N-terminus and the combined effects on both NHE3 and NBCe1 may, therefore, increase transcellular HCO_3^- transport (Yang et al., 2011). Kinetically, most Na^+/H^+ exchangers also have an internal H^+-modifier site to regulate transport activity in response to an acid load (Tse et al., 1992; Fan et al., 1999). The overall effect of this is to decrease HCO_3^- re-absorption and thus allow excess Ci to be excreted.

Regulation of Phosphate Excretion and NaPi-IIa Activity

Phosphate is predominantly stored in the body as the ion $PO_4{}^{2-}$ with 85% of systemic phosphate found in bone and teeth as a component of the crystal hydroxyapatite (Hammerman, 1986). The principal organs involved in excretion and absorption are the kidneys and intestine respectively, both through the use of sodium-phosphate co-transporters. In the kidney, phosphate excretion is regulated by PTH, which stimulates cAMP production (Chase & Aurbach, 1967; Agus et al., 1971). This cAMP decreases the activity of apical membrane (Friedlander & Amiel, 1994) Na^+/PO_4^- co-transporters involved in the reabsorption of PO_4^{3-} ions from the glomerular filtrate, resulting in increased phosphaturia (Agus et al., 1973; Caverzasio et al., 1986). PTH signalling has an inhibitory effect on both type II and III phosphate transporters, but most regulation is via the NaPi-IIa co-transporter. In fact, in mice lacking the NaPi-IIa co-transporter, PTH injections do not cause phosphaturia, emphasising its importance in phosphate homeostasis (Zhao & Tenenhouse, 2000). PTH signalling decreases NaPi-IIa expression (Kempson et al., 1995; Picard et al., 2010), in addition to causing transporter internalisation (Malmstrom & Murer, 1986) and targeting to lysosomes for degradation (Keusch et al., 1998; Pfister et al., 1998; Picard et al., 2010). NaPi-IIa forms part of a multiprotein complex, interacting via its PDZ-binding motif with the scaffolding proteins NHERF-1 and actin, which hold it in place at the apical membrane. NHERF1 is phosphorylated as a result of PTH signalling, leading to dissociation of the NaPi-IIa-NHERF1 complex. This dissociation allows NaPi-IIa to be routed via clathrin coated pits to be degraded by lysosomes (Picard et al., 2010).

2 Chapter 2: Materials and Methods

2.1 Chemicals, Reagents and Equipment

All consumable plasticware was purchased through Thermo-Fisher Scientific®, STARLAB® and Starstedt® with the exception of Poly-prep chromatography columns (Bio-Rad - 731-1550). Cell cultures were received from various sources as detailed in Section 2.3.1. All other chemicals used are listed in the table below.

Chemicals	**Company**	**Code**
Acetazolamine	Sigma	A6011
Acetic acid	Sigma	242853
Acetonitrile	Sigma	34967
Acrylamide	Sigma	A9926
2, 8-[^{3}H] Adenine	Perkin Elmer	NET063005MC
Adenosine	Sigma	A9251
Adenosine 3, 5 cyclic mono-phosphate (cAMP)	Sigma	A9501
Adenosine diphosphate (ADP)	Sigma	A2754
Adenosine monophosphate (AMP)	Sigma	A1752
Aluminium oxide (Activity Grade 1, WN-3: neutral)	Sigma	A9003
Ammonium persulphate	Sigma	A3678
2-Aminoethyl diphenylborinate (2-APB)	Ascent Scientific	Asc-124
Autocamtide II	Calbiochem	189475
Bafilomycin A1	Enzo Life Sciences	BML-CM110-0100
1, 2-bis (o-Aminophenoxy) ethane-N, N, N', N'-tetraacetic Acid Tetra (-acetoxymethyl) ester (BAPTA-AM)	Calbiochem	196419
2', 7'-bis (Carboxyethyl)-5(6)-Carboxyfluorescein (-acetoxymethyl) ester (BCECF-AM)	Sigma	C3411
Bovine serum albumin (BSA)	Sigma	A7906
Bradford Reagent	Biorad	500-0006
Bromophenol Blue	Sigma	B0126
Calcium chloride	Sigma	C1016
Carbon dioxide (2.5, 5, 10% [v/v] in air)	BOC	Special order
Carbon dioxide mix (5% CO_2, 18% O_2, 77% N_2 [v/v])	BOC	Special order
cAMP Biotrak EnzymeImmunoAssay Kit	GE Healthcare	RPN2251
Chicken serum	Biosera	CH-515

Chemicals	**Company**	**Code**
3-[(3-Cholamidopropyl) dimethylammonio] -1-propanesulfonate hydrate (CHAPS)	Sigma	C9426
Choline chloride	Sigma	C7017
Collagen	Sigma	C8919
Coomassie G-250	Sigma	201391
Dantrolene (sodium salt)	Sigma	9175
5-(N,N-Dimethyl)-amiloride (DMA)	Sigma	A5462
Dimethyl sulfoxide (DMSO)	Sigma	D2650
Dithiothreitol (DTT)	Simga	43817
Dulbecco's Modified Eagle Medium	Sigma	D1152
DMEM/F12 (1:1)	Sigma	D8900
Dowex AG 50W-X4 resin	Biorad	142-1341
EcoScint XR	National Diagnostics	LS-272
Ethylenediaminetetraacetic acid (EDTA)	Sigma	E6758
Ethylene glycol-bis (2-aminoethylether)-N, N, N′, N′ -tetraacetic acid (EGTA)	Sigma	E0396
Ethanol	Dept. Stores	-
Fibrinogen	Sigma	F1141
Fetal Bovine Serum	Sigma	F6178
Forskolin	Sigma	F6886
Fura-2 Calcium Imaging Calibration Kit	Molecular Probes®	F-6774
Fura-2 pentakis(acetoxymethyl) ester (Fura 2-AM)	Sigma	F0888
Glucose	Sigma	158968
L-Glutamine	Sigma	G6392
Glycerol	Sigma	G5516
Glycine	Sigma	241261
Gö6983	Calbiochem	365251
G-418	Sigma	A1720
4-(2-hydroxyethyl)-1-piperazineethanesulfonic acid (HEPES)	Sigma	H3375
Hydrochloric acid	Sigma	H1758
H89	Sigma	B1427
Imidazole	Sigma	I5513
Instant Blue	Triple Red	-
Isobutylmethylxanthine (IBMX)	Sigma	I5879
Isopropanol	Dept. Stores	-
Isopropyl β-D-thiogalactoside (IPTG)	Sigma	I5502

Chemicals	**Company**	**Code**
iTRAQ Reagent	Applied Biosystems	-
KH7	Enamine Ltd.	Special order
Lithium chloride	Sigma	L4408
Magnesium chloride	Sigma	M8266
Manganese chloride	Sigma	244589
Methyl methanethiosulfonate	Sigma	64306
^{32}P-Monopotassium phosphate	Perkin Elmer	NEX 060002MC
β-mercaptoethanol	Sigma	M6250
Methanol	Sigma	M1775
Nifedipene	Sigma	N7634
Nigericin	Sigma	N7143
N-Methyl-D-glucamine	Sigma	66930
Non-Essential Amino Acids (NEAA)	Sigma	M7145
OptiPhase HiSafe 2	Perkin Elmer	1200-436
Pageruler^{TM}pre-stained protein ladder	Fermentas	SM0671
Parathyroid Hormone Fragment (bovine, 1-34)	Sigma	P3671
Penicillin/Streptomycin	Sigma	P0781
Phenol Red	Sigma	P3532
Phosphate buffered saline	Sigma	79382
Phosphoric acid	Sigma	P5811
Poly-D-Lysine	Sigma	P6407
Potassium bicarbonate	Sigma	P9144
Potassium chloride	Sigma	P9333
Potassium phosphate monobasic	Sigma	60221
Propanoic acid	Sigma	402907
Rotenone	Sigma	R8875
RPM1 1640 Media	Biosera	LM-R1641
Ryanodine Inhibitor	Ascent Scientific	Asc-083
Skimmed Milk Powder	Co-op	-
Ski/ROMe (sphingosine kinase antagonists)	Kind gift from Prof. Nigel Pyne, University of Strathclyde	
Sodium bicarbonate	Sigma	S6297
Sodium chloride	Sigma	S7653
Sodium dodecyl sulphate (SDS)	Sigma	L3771
Sodium hydroxide	Sigma	221465
Sodium phosphate dibasic dihydrate	Sigma	71643
SQ 22536	Calbiochem	568500
Staurosporine	Calbiochem	569397

Chemicals	**Company**	**Code**
STO-609	Enzo Life Sciences	BML-EI389-0001
Tetramethylethylenediamine (TEMED)	Sigma	T9281
Thapsigargin	Sigma	T9033
Thiourea	Sigma	88810
Trichloroacetic acid (TCA)	Sigma	T9159
Triethylammonium bicarbonate	Sigma	T7408
Tris-HCl	Sigma	93363
Tris(2-carboxyethyl)phosphine	Sigma	C4706
Triton X-100	Sigma	T8787
Trizma Base	Sigma	T4661
Trypsin-EDTA	Sigma	594180
Urea	Sigma	U5378
U-73122	Enzo Life Sciences	BML-ST391-0005
Xestospongin C	Enzo Life Sciences	BML-CA409-0050

Table 4: List of reagents used and purchasing details

2.2 Computer Software and Statistical Analysis

The text for presentation of this thesis was written and formatted in LaTeX using TeXnicCenter or TeXworks and viewed via Adobe Reader®. Numerical manipulations were carried out in either Microsoft Excel™ or GraphPad Prism 4®, the latter also used to produce all graphical representations and statistical analysis of data. All error bars included in the thesis are the standard error of the mean.

BCECF fluorescence measurements for intracellular pH were measured via a Life Sciences® microspectrofluorimeter system and computer software PhoCAL PRO 1.6b. Fura-2 measurements for intracellular Ca^{2+} were measured via a Perkin Elmer® LS-55 Luminescence Spectrometer and computer software Perkin Elmer® FL Winlab. Measurement of cAMP accumulation data was carried out via a Perkin Elmer® Liquid Scintillation Analyser Tri-Carb 2900TR and program QuantSmart™. Proteomics iTRAQ™ data was identified and quantitated using Applied Biosystems™ ProteinPilot™ 2.0.1 and the analysis program displayed in Section 8.3.1 was written using Python™ and displayed using TextWrangler™.

2.3 Mammalian Cell Culture

2.3.1 General Cell Culture

All cells were cultured at 37 °C and 5% (v/v) CO_2 in air with media changes every two to three days. With adherant cell lines, sub-culturing was carried out at 80 - 100% confluence, with three PBS washes preceding the addition of 1 mL of 0.1% (v/v) aqueous trypsin. Cells were incubated with trypsin until cells were visibly lifting from the surface and the enzyme arrested by dilution with 10 mL of required media. A centrifugation step at 160 x g for 3 minutes was employed to remove any residual enzyme from the cell suspension. Alterations to the culturing method and details of media required for each cell type are listed in the subsections below.

Suspension cell lines were maintained at cell concentrations between 2 x 10^5 mL^{-1} and 4 x 10^6 mL^{-1}, as measured using a haemocytometer. Passage was carried out at 2 x 10^6 mL^{-1} cells and required centrifugation of cells, at 160 x g for 3 minutes, aspiration of old media, and re-suspension in the required volume of fresh, pre-warmed media.

A549 cells (Human carcinomic alveolar basal epithelial cells)

Obtained from Dr. Paul Yeo, Biophysical Sciences Institute, Durham University

Media consisted of Dulbecco's Modified Eagle's Medium/Ham's Nutrient Mixture F12 (1:1 volume) containing 15 mM HEPES (Sigma® D8900) and 14 mM sodium bicarbonate, supplemented with 10% (v/v) fetal bovine serum, 1% (v/v) antibiotic penicillin-streptomycin, 2% (v/v) non-essential amino acids, pH 7.4. Sub-culturing was carried out between 1:2 and 1:6 dilutions.

DT40 (*Gallus gallus*, avian leukosis virus induced B lymphoblasts)

Obtained from Prof. Colin Taylor, Pharmacology Department, University of Cambridge

Two DT40 cell lines were used, both stabily transfected and therefore requiring the same media constituents. Strains used were either referred to as 'DT40-K/O' for cells where both alleles of all three genes for the IP_3 receptor have been disrupted (Sugawara et al., 1997), or 'DT40-IP_3R1' where the gene for IP_3 receptor 1 has been re-introduced by transfection (Laude et al., 2005). DT40

cells were cultured in accordance to published work (Tovey et al., 2006) in RPMI 1640 medium supplemented with 10% (v/v) fetal bovine serum, 1% (v/v) heat-inactivated chicken serum, 1% (v/v) antibiotic penicillin-streptomycin, 2 mM glutamine and 50 μM 2-mercaptoethanol. 15 mM HEPES and 14 mM sodium bicarbonate were also added for assay medium. Passaging was carried out as detailed above.

HEK 293 (Human Embryonic Kidney) cells

Obtained from Dr. Michael Gray, Institute for Cell and Molecular Biosciences, University of Newcastle

HEK293 cells, immortalised through transformation with sheared fragments of adenovirus type 5 DNA (Graham et al., 1977), were cultured in Dulbecco's Modified Eagle's Medium (Sigma® D777), supplemented with 10% (v/v) newborn calf serum, 1% (v/v) antibiotic penicillin-streptomycin, 2% (v/v) non-essential amino acids, pH 7.4. Sub-culturing was carried out between 1:3 and 1:6.

HEKPR1 cells

Obtained from Prof. Colin Taylor, Pharmacology Department, University of Cambridge

HEKPR1 (HEK 293 cells stably expressing human parathyroid hormone receptor 1 (Short & Taylor, 2000)) were cultured in Dulbecco's Modified Eagle's Medium/Ham's Nutrient Mixture F12 (1:1 volume) containing 15 mM HEPES (Sigma® D8900) and 14 mM sodium bicarbonate supplemented with 10% (v/v) fetal bovine serum, 1% (v/v) antibiotic penicillin-streptomycin, 2% (v/v) non-essential amino acids, 1% (v/v) L-glutamine, 500 μg mL^{-1} G418 (to retain transfected phenotype), pH 7.4. Sub-culturing was carried out at 1:3 or 1:6.

OK (*Didelphis virginiana*, Opossum Kidney) cells

Three independent lines were obtained from: Dr. Michael Gray, Institute for Cell and Molecular Biosciences, University of Newcastle; LGC/ATCC®; and Dr. H Murer, Institute of Physiology and Zurich Center for Integrative Human Physiology, University of Zurich

Media consisted of Dulbecco's Modified Eagle's Medium/Ham's Nutrient Mixture F12 (1:1 volume)

containing 15 mM HEPES (Sigma® D8900) and 14 mM sodium bicarbonate, supplemented with 10% (v/v) fetal bovine serum, 1% (v/v) antibiotic penicillin-streptomycin, 2% (v/v) non-essential amino acids, 1% (v/v) L-glutamine, pH 7.4. OK cells were sub-cultured at one day post-confluence and required frequent media change; every 24 hours where possible (Koyama et al., 1978). Sub-culturing was between 1:2 and 1:6 dilutions and trypsinisation often involved a 5 minute incubation step at 37°C to encourage cells to detach from one another (Koyama et al., 1978).

UMR-106 (*Rattus norvegicus*, ^{32}P induced osteosarcoma) cells

Obtained from Prof. J.A. Gallagher, Department of Human Anatomy and Cell Biology, University of Liverpool

Cells were cultured in Dulbecco's Modified Eagle's Medium (Sigma® D777) supplemented to contain 15 mM HEPES, 14 mM sodium bicarbonate, 10% (v/v) fetal bovine serum, 1% (v/v) antibiotic penicillin-streptomycin, 2% (v/v) non-essential amino acids, 1% (v/v) L-glutamine, pH 7.4. Sub-culture was carried out between 1:2 and 1:6.

2.3.2 Preparation of -140 °C Freezer Stocks

To produce a permanent cell stock, cryo-vials of cells were frozen and stored at -140 °C. To prepare for freezing, cells were centrifuged after trypsining and re-suspended in 0.5 mL normal media, to which 0.5 mL media with 20% DMSO (v/v) was added drop-wise, with constant but gentle agitation. Cell suspensions were then transferred to appropriate cryo-vials and cooled slowly for 2 to 3 hours at -20 °C and overnight at -70 °C before transfer to -140 °C.

When reviving cells from frozen, cells were thawed as quickly as possible, using a pre-heated water-bath at 37°C. DMSO was removed through a wash in pre-warmed media with centrifugation at 160 x g for 3 minutes prior to transfer to a flask for growth. Whenever cells were in or had been recently in media containing DMSO care was taken when pipetting to reduce damage and cell lysis as a result of sheer stresses.

2.3.3 Coating Tissue Culture Plates with Poly-D-Lysine

To improve HEKPR1 cell adherence to tissue culture plastic sterile 5 mg/ml poly-D-lysine solution was added to cover the base of well and incubated for 10 minutes at room temperature, with constant agitation. The poly-D-lysine solution was then aspirated off, wells washed with sterile water and plates left to dry for either 1 hour in the microbiological safety hood or overnight in the incubator before use.

2.4 *In cellulo* Biochemical Assays

2.4.1 Measurement of Intracellular pH

Cells were grown to confluence on 25 mm diameter glass coverslips, with HEKPR1 coverslips pre-coated with 5 mg/mL poly-D-lysine (as in Section 2.3.3), and serum starved overnight in the presence of 0.2% (w/v) bovine serum albumin (BSA) prior to assay. 5 μM of the pH sensitive fluorescent dye 2',7'-bis(carboxyethyl)-5(6)-carboxyfluorescein (BCECF) was added in pre-warmed and gassed phosphate buffered solution (PBS) supplemented with 25 mM glucose and 14 mM sodium bicarbonate and incubated for 20 minutes at 37°C, 5% (v/v) CO_2 in air. Loading of this dye was via its non-fluorescent membrane permeable acetoxymethyl ester (-AM) derivative enabling better cell penetration. The -AM group is removed within the cell through cleavage of its adjoining ester bond by endogenous non-specific esterases to give the active, hydrophilic compound (Thomas et al., 1979; Hegyi et al., 2004). BCECF-AM (Rink et al., 1982) is a highly useful dye not only due the aforementioned qualities but also has a pK_a of pH 7.0, well within the normal cytoplasmic range and at these pH values, once cleaved from its -AM group, it leaks out from cells far more slowly than the parent compound, using key negative charges to aid cell retention (Invitrogen, 2006).

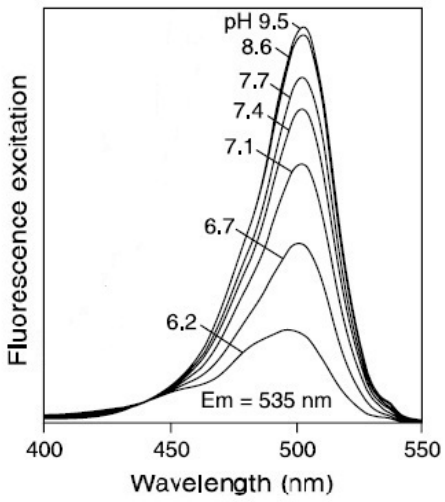

Figure 14: The pH-dependent fluorescence excitation spectra of BCECF (Invitrogen, 2006)

Coverslips were mounted in a perfusion chamber suspended over an inverted microscope, attached to a photomultiplier tube enabling intracellular pH to be measured by exciting the cells at both 490 and 440 nm, whilst measuring emission at 535 nm. This enabled ratiometric monitoring of BCECF

excitation and pHi to be measured due to the pH-dependent fluorescence spectra of this dye (Figure 14), where lowering the pH decreases the absorbance at 490 nm (Thomas et al., 1979) therefore decreasing the ratio (Hegyi et al., 2004). Using a ratio instead of absolute values also eliminates a number of potential artifacts: photobleaching, excessive dye leakage, non-uniform cell loading, cell thickness and instrument stability (Invitrogen, 2006). Solution change and CO_2 concentration was altered through a heated microperfusion system, enabling the flow of 37°C pre-gassed cell media across cells at a variable rate (most commonly at 3 mL/min). Media used for perfusion was identical to the cell growth media but lacking serum (for details see Section 2.3.1). Where propanoic acid concentrations were required these were added after medium constitution and pH normalisation. Intracellular pH calibration was carried out using potassium nigericin solutions (130 mM KCl, 25 mM Glucose, 20 mM HEPES, 14 mM $NaHCO_3$, 1 mM $CaCl_2$, 1 mM $MgSO_4$ and 10 μg/mL nigericin) at a range of pH values. Through this method nigericin, a K^+/H^+ antiporter, equilibrates the intracellular pH to that of the surrounding solution due to the high K^+ of this solution (Thomas et al., 1979; Hegyi et al., 2004). Specific detail into this calibration method is provided in Appendix 7.1. Compensation for 'drift', the continuous and unavoidable leakage of dye, shown by a steady decrease in emission intensity, was calculated using the method outlined by Hegyi et al. (Hegyi et al., 2004) (see Appendix 7.1 for more detail). An identical method was used with OK cells with the exception that loading used 7.5 μM BCECF-AM for 30 minutes.

2.4.2 Measurement of Intracellular Ca^{2+}

DT40 cells were grown to a concentration of 2 x 10^6 mL^{-1} and the required volume loaded with 10 μM of the Ca^{2+} sensitive fluorescent dye Fura-2 pentakis(acetoxymethyl) ester (Fura 2-AM) in serum free media and incubated for 30 minutes at 37°C, 5% (v/v) CO_2 in air. As a lipid-soluble acetoxymethyl ester (-AM) derivative, loading of this dye is similar to the BCECF-AM outlined in Section 2.4.1. To enable complete cleavage of the ester, cells were then centrifuged at 160 x g for 3 minutes and re-suspended in pre-warmed Krebs-Ringer-HEPES solution (130 mM NaCl, 25 mM glucose, 20 mM HEPES, 14 mM $NaHCO_3$, 5 mM KCl, 1 mM $CaCl_2$ and 1 mM $MgSO_4$, pH 7.4) for 30 minutes at 37°C, 5% (v/v) CO_2. Where required, antagonists were added at this stage and maintained in the media for the duration of the experiment. Cells were then transferred to fresh Krebs-Ringer-HEPES pre-gassed with the desired CO_2 concentration and allowed to equilibrate, with gassing, prior to experimentation. Where required, 2 mM propanoic acid was added at this

stage. For repeats within experiments cells were labelled with dye *en mass* and separated to take readings.

Measurement of dye emission was carried out using 1 mL of cells transferred to a quartz cuvette within a spectrofluorometer able to excite the cells at 340 and 380 nm, whilst measuring emission at 510 nm. As Fura 2-AM emits with excitation at 340 when bound to Ca^{2+} ions and 380 nm in their absence (Figure 15), these measurements enable a ratio to be calculated, giving comparative concentrations of the intracellular Ca^{2+} available. Similar to BCECF-AM, generation of such a ratio removes certain aspects of data variability, such as the effects of photobleaching, leakage, dye concentration and cell thickness (Hayashi & Miyata, 1994; Invitrogen, 2012). Using this ratio, the intracellular Ca^{2+} concentration can be calculated using the calibration methods outlined by *Bouyer et al.* (Bouyer et al., 2003) and *Grynkiewicz et al.* (Grynkiewicz et al., 1985), as detailed in Appendix 7.3.

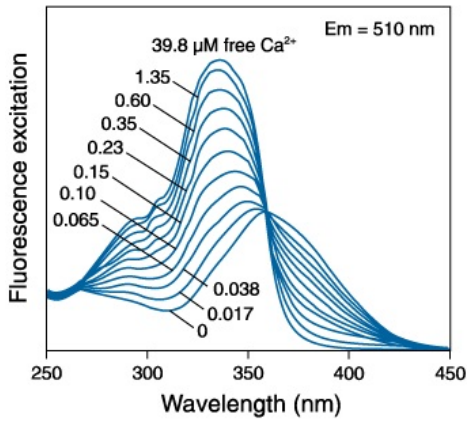

Figure 15: The Ca^{2+}-dependent fluorescence excitation spectra of Fura-2 (Invitrogen, 2012)

2.4.3 Cellular Equilibration with CO_2, Pharmacological Inhibitors and Agonists

For adherant cell lines (A549, HEK 293, HEKPR1, OK and UMR-106), cells were cultured in 12 well plates and were allowed to reach 90% confluence over 3-4 days (OK cell assays grown to 1 day post-confluence) and then serum starved overnight in the presence of 0.2% (w/v) BSA in serum free media (Section 2.3.1). Cells were then washed 3 times with PBS, pre-warmed in a water bath to 37°C, and incubated for 30 minutes at 37°C at the desired CO_2 concentration in 990 μL pre-incubation medium using a , environment-controlled Galaxy 14S incubator. This pre-incubation media contained: DMEM/F12 1:1 or DMEM depending on cell type, 15 mM HEPES, 1% (v/v) penicillin-streptomycin, 1 mM IBMX and, where required, 2 mM propanoic acid and was pre-gassed

for 20 minutes with the desired CO_2 concentration and the pH adjusted accordingly prior to addition to cells. Assays were initiated by the addition of 10 μL agonist or H_2O/DMSO control. Lysis buffers and conditions were dependant on the experiment performed and are detailed in the appropriate sections.

Experimentation in DT40 suspension cell lines followed a similar protocol, with minor adjustments. Cells were allowed to grow to a concentration of 2 x 10^6 mL^{-1} for assay. PBS washes and addition of pre-incubation medium were identical except that centrifugation steps at 160 x g for 3 minutes and resuspension pipetting were employed with each medium change. After pre-incubation medium was added, the cells were separated into 990 μL volumes in open eppendorf tubes and returned to the appropriate incubator. Lysis also followed a similar centrifugation and aspiration step.

2.4.4 *In cellulo* cAMP Accumulation

Cells were prepared as detailed in Section 2.4.3 except that prior to PBS washing cells were labelled for at least 2 hours with 0.75 μCi mL^{-1} (37 kBq) [^{3}H]-adenine, allowing it to be incorporated into the intracellular ATP pool for subsequent use by adenylyl cyclases (Alvarez & Daniels, 1992). After incubation with agonist for 10 minutes at 37°C, media was aspirated from wells and 1 mL ice cold 5% (w/v) trichloroacetic acid (TCA) containing 1 mM ATP and 1 mM cAMP added and cells left to lyse at 4 °C for at least an hour before a twin column chromatography step (Section 2.4.6). An acid such as TCA is preferable to stop the AC reaction and lyse cells as it has been shown that cAMP can be made non-enzymmatically under alkaline conditions (Johnson et al., 1994), and also avoids false results due to alkaline proton exchange from tritium labelled nucleotides to water (Johnson et al., 1994). Additionally, a low pH promotes increased cAMP binding to the alumina for subsequent chromatography (Johnson et al., 1994) and the additional ATP and cAMP limits sample loss on irreversible binding sites on this alumina column.

2.4.5 Antagonist Assays

Cells were prepared as detailed in Sections 2.4.3 and 2.4.4 with the required antagonist added as part of the pre-incubation medium. Cells were therefore exposed to the antagonist for 30 minutes prior to agonist addition, with the exception of Ski/ROMe, which were added to the starvation media

Inhibitor	Details	Conc. Used
Acetozolamide	Carbonic anhydrase inhibitor	100 μM
2-APB	Modulator of IP_3-induced calcium release	100 μM
Autocamtide II	CamKII inhibitor	100 nM
Bafilomycin A1	Inhibits vacuolar H^+ATPases	100 nM
BAPTA-AM	Intra-cellular Ca^{2+} chelator	1 mM
Dantrolene	Inhibitor of ryanodine receptors	10 μM
EGTA	Inter-cellular Ca^{2+} chelator	1 mM
Gö6983	PKC inhibitor	1 mM
H89	PKA inhibitor	10 μM
IBMX	PDE inhibitor	1 mM
KH7	Non-competitive sAC inhibitor	10 μM
Nifedipene	L-type calcium channel blocker	100 μM
Rotenone	Inhibitor of mitochondrial electron transport	5 μM
Ryanodine	Modulator of ryanodine receptors	5/100 μM
SKi/ROMe	Sphingosine kinase inhibitors	10/10 μM
SQ 22,536	Adenylyl cyclase inhibitor	200 μM
Staurosporine	Non-specific kinase inhibitor (PKA/C/G, CamK, MLCK)	1 μM
Sto-609	Calmodulin-dependent protein kinase kinase inhibitor	5 μM
Thapsigargin	IP_3 independent intracellular calcium releaser	10 μM
U-73122	Phospholipase C inhibitor	5 μM
Xestospongin C	Inhibitor of IP_3 receptor	500 nM

Table 5: List of inhibitors and concentrations used

and thus exposed to cells overnight. Concentrations of each inhibitor used are detailed in Table 5. Wherever possible the antagonist was dissolved into aqueous solution, with DMSO employed if not.

2.4.6 Radio-labelled cAMP Measurement

Cell lysates obtained by method 2.4.4 were quantified via modification of a twin column chromatography approach (Salomon et al., 1974; Wincek & Sweat, 1975; Johnson et al., 1994). This method works on the basis that negatively charged ions, such as nucleotides, can be easily separated from solutions through the use of strong anionic-exchange resins (Kaczorowski et al., 1994). 1 mL TCA samples were added directly to poly-prep (Bio-Rad®) columns containing 1 g of pre-acidified AG 50W-X4 Dowex (Salomon et al., 1974; Wincek & Sweat, 1975) cation exchange resin and washed through with 2 mL water into scintillation vials positioned beneath. The Dowex elutions contained [^{3}H]-adenosine and [^{3}H]-AMP/ADP/ATP but limited amount of [^{3}H]-cAMP (Johnson et al., 1994), and were defined as total adenine nucleotide values. These were used later to normalise data as an indication of total cell adenine pool labelling. Dowex columns were then placed over a second set of columns containing 1 g of neutral aluminium oxide (alumina - Activity grade 1, Type WN-3 (White & Zenser, 1971; Salomon et al., 1974; Johnson et al., 1994)) and contents washed through

using 5 mL of water (Wincek & Sweat, 1975). As this eluate is slightly acidic, cAMP becomes adsorbed onto the alumina (Alvarez & Daniels, 1992; Johnson et al., 1994), requiring an increase in pH and ionic strength for elution (Johnson et al., 1994). Two elutions of 3 mL (White & Zenser, 1971) 100 mM Tris-HCl, pH 7.5, followed (White & Zenser, 1971; Salomon et al., 1974; Wincek & Sweat, 1975; Alvarez & Daniels, 1992; Johnson et al., 1994) to remove this cAMP and were collected in scintillation vials as before. Using this method cAMP can be separated from other polyvalent nucleotides (AMP/ATP etc), which are retained on the alumina (White & Zenser, 1971; Alvarez & Daniels, 1992) due to their anionic character at this pH (White & Zenser, 1971). All elutions had 2.5 mL of scintillation fluid (EcoScint XR or Optiphase HiSafe 2 depending on availability) added and tritium disintergrations-per-minute measured via scintillation counter; Perkin Elmer® Liquid Scintillation Analyzer Tri-Carb 2900TR. This liquid scintillation process is based on the conversion of the energy of a radioactive decay event to a release of light from the scintillant, which can be recorded. In order to compare results from different sample sets, values were normalised to produce the following ratio:

Ratio = [Alumina elution counts / Dowex flow-through counts] = [^{3}H]-cAMP/ Total [^{3}H] nucleotides

Chromatography columns were retained and regenerated between experiments (Johnson et al., 1994) using 2 sets of alternating 5 mL washes of 1 M hydrochloric acid and de-ionised water for Dowex columns (Salomon et al., 1974) and 10 mL 100 mM Tris-HCl at pH 7.5 for the alumina. This was often carried out prior to experimentation as columns performed better when moist.

2.4.7 Amersham Biotrak cAMP EnzymeImmunoAssay (EIA) System

For some experiments a greater level of sensitivity for cAMP was required than could be provided by the the radio-labelled method outlined in Sections 2.4.4 and 2.4.6. To achieve this an ELISA assay was employed (GE Healthcare®, RPN2251). Cells were assayed as detailed in Section 2.4.3 and after incubation with agonist for 10 minutes at 37°C media was aspirated from wells and 200 (adherant cell lines)/300 (suspension cells) μL of lysis buffer 1B, provided with the kit, was added. Cells were then left on a shaker for at least 30 minutes to ensure complete lysis. In most cases, 10 μL of this lysate was further diluted to 100 μL with lysis buffer 1B for use in the ELISA itself. After this stage, experimentation followed manufacturer's recommendations where results are measured quantitatively via a change in optical density and compared to a simultaneously produced cAMP

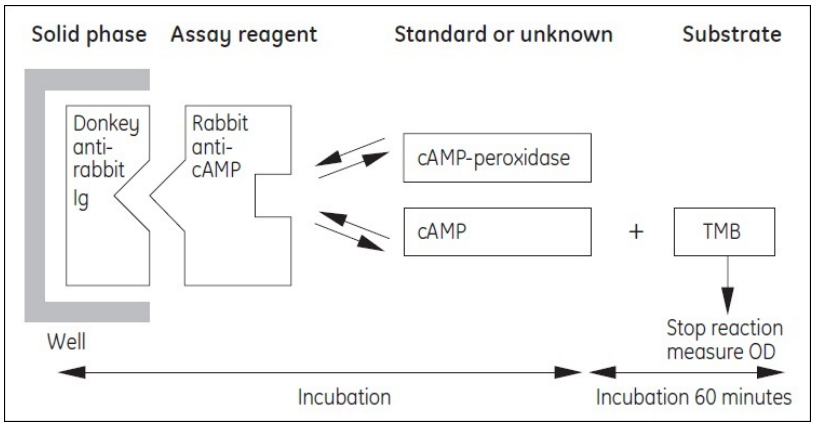

Figure 16: Biotrak cAMP enzyme-linked immunosorbent assay (ELISA) principle. Adapted from manufacturer's product booklet (Healthcare, 2007)

standard curve. Briefly, the ELISA is based on competition between unlabelled sample derived cAMP and a fixed quantity of peroxidase-labelled cAMP conjugate; for a limited number of binding sites on a cAMP specific antibody added directly to the sample prior to the conjugate. A visual representation of how the ELISA works is shown in Figure 16.

As DT40 samples may have contained cAMP from marginally different numbers of cells, ELISA evaluated cAMP concentrations were normalised to sample protein content. Protein concentration was calculated through use of a Bradford assay, as detailed in Section 2.6.2. Further information on this method is appended in Section 7.2.

2.5 Physiology Methodology

2.5.1 Sodium-Phosphate Co-transporter Radioassay

Sodium-phosphate co-transporter activity was monitored by measuring the uptake of ^{32}P-labelled phosphate into cells from a surrounding solution. The method used was developed from protocols published by *Cole et al.* (Cole et al., 1989), and *Mahon et al.* (Mahon et al., 2003b). OK cells were grown to 100% confluence in a 12 well plate and serum starved overnight in the presence of 0.2% (w/v) BSA in serum free media (Section 2.3.1). Similar to the cAMP accumulation assay detailed in Section 2.4.4, cells were washed once with pre-warmed PBS and then 990 μL of a pre-warmed, gassed and pH normalised pre-incubation media added (DMEM/F12 1:1, 100 mM HEPES, 1% (v/v) penicillin-streptomycin and appropriate inhibitors at concentrations shown in Table 5). After 30 minutes incubation at 37°C and the desired CO_2 concentration, assays were initiated by the addition of 10 μL agonist or H_2O/DMSO control.

After further incubation under the same conditions for 4 hours, ample time for cells to reach maximal phosphate transport (Cole et al., 1989), cells were washed twice in pre-warmed and gassed phosphate uptake solution (150 mM NaCl, 20 mM glucose, 10 mM HEPES pH 7.4, 1.8 mM $MgSO_4$, 1 mM $CaCl_2$) followed by incubated treatment with 500 μL phosphate uptake buffer containing 1 μCi mL^{-1} $KH^{32}PO_4$. A 5 minute incubation period was chosen in accordance with previous publications to represent an estimation of the initial rate of phosphate transport (Cole et al., 1989). Phosphate uptake was then stopped by washing with 3 x 1 mL volumes of ice-cold stop solution (150 mM choline chloride, 20 mM glucose, 10 mM HEPES pH 7.4, 1.8 mM $MgSO_4$ and 1 mM $CaCl_2$) and cells lysed using 1 mL 1% (v/v) Triton X-100 solution. Samples were transfered to scintillation vials, 2.5 mL of scintillation fluid (EcoScint XR or Optiphase HiSafe 2 depending on availability) added and ^{32}P disintergrations-per-minute measured via scintillation counter; Perkin Elmer® Liquid Scintillation Analyzer Tri-Carb 2900TR.

2.5.2 Ammonium Chloride Pulse pH Recoveries - NHE3 Activity

Sodium-proton exchange was monitored by measuring the intracellular pH recovery after an NH_4Cl pulse, using the pH sensitive fluorescent dye BCECF-AM and a microspectrofluorometer. The method used was developed from protocols published by *Cunningham et al.* (Cunningham et al., 2004), and *Hegyi et al.* 2004 (Hegyi et al., 2004). OK cells were grown to 100% confluence on 25

mm diameter glass coverslips in a 6 well plate and serum starved overnight in the presence of 0.2% (w/v) BSA in serum free media (Section 2.3.1). Following a similar methodology as outlined in Section 2.4.1, cells were loaded with 7.5 μM BCECF-AM for 30 minutes at 37°C and 5% (v/v) CO_2, using pre-warmed and gassed Krebs-Ringer-HEPES solution (130 mM NaCl, 25 mM Glucose, 20 mM HEPES, 14 mM $NaHCO_3$, 5 mM KCl, 1 mM $CaCl_2$ and 1 mM $MgSO_4$, pH 7.4). Coverslips were mounted on a microspectrofluorometric system and dye emission collected at 535 nm when excited at 440 nm and 490 nm. Cells were perfused during experiments with Krebs-Ringer-HEPES solutions bubbled to the desired CO_2 concentration and containing any agonists and/or inhibitors (concentrations provided in Table 5). NH_4Cl pulses (110 mM NaCl, 25 mM Glucose, 20 mM NH_4Cl, 20 mM HEPES, 14 mM $NaHCO_3$, 5 mM KCl, 1 mM $CaCl_2$, mM $MgSO_4$, pH 7.4) were for 3 minutes and were followed by at least 5 minutes perfused exposure to Krebs-Ringer-HEPES solution. When recovery in the absence of sodium was required, N-methyl-D-glucamine was used to replace the NaCl in the Krebs-Ringer-HEPES solution without affecting solution osmolarity. In order to follow sodium-free recovery, NH_4Cl pulses were carried out as per norm and cells returned directly to an N-methyl-D-glucamine solution and recovery monitored prior to return to normal Krebs-Ringer-HEPES.

pH calibration was performed using high potassium nigericin solutions as published (Thomas et al., 1979; Hegyi et al., 2004) and compensation for 'drift' calculated using the method outlined by *Hegyi et al.* (Hegyi et al., 2004). Post NH_4Cl pulse recoveries were calculated by either linear regressions over 45 second periods immediately when pHi began to recover, or by direct comparison of change in pHi (ΔpHi) between treatments over the same timeframes, represented as ΔpHi/s. Further information on these methods are provided in Appendix 7.4.

2.6 Molecular Biology and Proteomics

2.6.1 Generation of iTRAQ Proteomics Samples

HEK 293 cells were grown to 90-100% confluence in 10 cm diameter tissue culture petri dishes. Cells were then washed with pre-warmed PBS and incubated for 30 minutes at 37°C at the desired CO_2 concentration in 10 mL of pre-incubation medium (DMEM, 100 mM HEPES, 1% (v/v) penicillin-streptomycin and, where required, 1 mM BAPTA-AM or 2 mM propanoic acid). Assays were initiated by the addition of 10 μM forskolin agonist or the equivalent volume of negative control; agonist solvent DMSO. These cells were then incubated at 37°C and the desired CO_2 concentration for 8 hours, sufficient time for translation to occur. To lyse cells, media was aspirated and 500 μL urea lysis buffer (9 M urea, 2 M thiourea, 4% (w/v) CHAPS) added and cells collected from the plasticware using a cell scraper. The protein concentration of these samples was then calculated through the use of a Bradford assay (Section 2.6.2) and once checked for equal loading by SDS-PAGE (Section 2.6.3) these were then acetone precipitated (Section 2.6.4) and prepared for iTRAQ labelling (Section 2.6.5).

2.6.2 Bradford Assay

Bradford reagent is a dye which binds to protein and changes colour according to the amount of protein available. For DT40 ELISA samples (Section 2.4.7), 1 mL solutions were made up with 200 μL Bradford Reagent (Biorad® - 500-0006), 790 μL deionised water and 10 μL ELISA sample, left to stand at room temperature for 10-15 minutes and the optical density measured at 595 nm. The resultant value was then compared to a standard curve, created using known concentrations of BSA. Slight modifications were made to measure samples for iTRAQ (carried out in collaboration with Joanne Robson, Proteomics Facility, Biological and Biomedical Sciences, Durham University), using a mix of 900 μL, 98 μL H_2O and 2 μL sample and compared to a modified standard curve, made to the specifications presented in Table 6:

Standards	**0**	**1**	**2**	**5**	**10**	**15**	**20**
1mg/ml BSA (μL)	0	1	2	5	10	15	20
0.1mM HCl (μL)	10	10	10	10	10	10	10
Urea Lysis Buffer (μL)	2	2	2	2	2	2	2
H_2O (μL)	88	87	86	83	78	73	68
Bradford Reagent 20% (μL)	900	900	900	900	900	900	900

Table 6: Modified Bradford standard curve - for samples in urea lysis buffer

2.6.3 Sodium Dodecyl Sulphate Poly-Acrylamide Gel Electrophoresis (SDS-PAGE)

0.75 mm thick gels were used, varying the resolving gel acrylamide content to best resolve the desired protein (Table 7), with 375 mM Tris-HCl pH 8.8, 0.1% SDS (w/v), 0.1% (w/v) APS and 0.1% (v/v) TEMED. Stacking gels were made to a standard of 5% (v/v) acrylamide with 130 mM Tris-HCl pH 6.8, 0.1% SDS (w/v), 0.1% (w/v) APS and 0.1% (v/v) TEMED. For whole cell lysates 12% (v/v) resolving acrylamide gels were used.

Samples were mixed for loading 1:1 with SDS loading buffer (50 mM Tris-HCl pH 6.8, 2 % (w/v) SDS, 0.1 % (w/v) bromophenol blue, 10 % (w/v) glycerol, 100 mM DTT) to a maximum volume of 20 μL and incubated for 3 minutes at 95 °C to enable complete protein denaturation. Gels were then loaded (usually with 10-15 μL sample/buffer per well), along with 10 μL protein ladder (Pageruler^{TM} pre- stained protein ladder - Fermentas SM0671) in order to monitor gel progress and enable estimation of protein size. Gels were run in running buffer (25mM Tris-HCl pH 7.5, 192 mM glycine, 0.1 % (w/v) SDS) at 150-200 V for approximately 50 minutes or until the loading dye had reached the bottom of the gel. Gels were then stained overnight in Coomassie dye (0.1% (w/v) Coomassie G-250 dye, 10% (v/v) acetic acid, 50% (v/v) methanol) and de-stained in 10% (v/v) acetic acid, 50% (v/v) methanol.

Acrylamide Percentage of Gel	Protein Size
4%	100-400 kDa
6%	60-300 kDa
8%	40-250 kDa
10%	30-200 kDa
12%	15-120 kDa
14%	6-80 kDa
16%	5-60 kDa
18%	2-50 kDa

Table 7: SDS-PAGE resolving gel acrylamide concentrations

2.6.4 Acetone Precipitation

Undertaken in collaboration with Miss Joanne Robson, Proteomics Facility, School of Biological and Biomedical Sciences, Durham University

Using samples generated for iTRAQ (Section 2.6.1), 250 μg of each sample (as calculated using a modified Bradford; Section 2.6.2, and checked using SDS-PAGE; Section 2.6.3) were acetone

precipitated to remove non-protein contaminating molecules, such as salts, lipids and nucleic acids. The relevant volume of protein for 250 μg was placed in an acetone-compatible tube with 4 sample volumes of acetone at -20 °C, vortexed and incubated at -20 °C for at least 60 minutes. These tubes were then centrifuged (15,000 x g, 10 minutes), the supernatant removed and the residual acetone allowed to evaporate by incubating uncapped tubes for 30 minutes at room temperature. Precipitated protein was then resuspended in 10 μl of 2% (w/v) SDS and incubated at 60 °C for approximately 1 hour, sonicated 2-3 times for 5 minutes and subsequently 90 μL of dissolution buffer (500 mM triethylammonium bicarbonate) was added. These protein samples were then in the correct buffer for trypsin digest and preparation of labelling with iTRAQ reagents (Section 2.6.5).

2.6.5 Trypsin Digests and Preparation of Samples for iTRAQ

Undertaken in collaboration with Dr. William Simon and Miss Joanne Robson, Proteomics Facility, School of Biological and Biomedical Sciences, Durham University

Using samples generated by previous steps (Sections 2.6.1), 2.6.2 and 2.6.4, a second precautionary Bradford assay (Section 2.6.2) and SDS-PAGE gel (Section 2.6.3) were run and once satisified that all samples had the same protein concentration, trypsin digests were carried out on 50 μg of each sample, using 5 μg of trypsin in each. In order to trypsin digest, samples were incubated with 2 μL of the reducing reagent tris(2-carboxyethyl)phosphine for 1 hour at 60°C, 10 minutes at room temperature with the addition of 1 μL cysteine blocking reagent methyl methanethiosulfonate and 50 μL of 10 mM calcium chloride, followed by the trypsin. Digests were incubated at 37 °C overnight and then vacuum centrifuged until dry.

Samples were then ready for iTRAQ labelling, through the direct addition of the relevant iTRAQ reagent resuspended in 50 μL isopropanol. Labelling then proceeded via a 2 hour incubation step at room temperature with occasional vortexing. Once fully labelled, samples were pooled together and vacuum dried.

Pooled iTRAQ labelled protein samples were resuspended in 1 mL of 'cation exchange buffer A' (10mM KH_2PO_4, 25% acetonitrile (v/v)) and the pH adjusted to between 2.8 and 3.0 using 1 M phosphoric acid. This solution could then be injected directly onto GE Healthcare® Ettan™ Micro Liquid Chromatography HPLC system for cation exchange fractionation producing 40 fractions before passing into the Dionex Ultimate® 3000 RSLC nano system for further fractionation and

finally into the Applied Biosystems^{TM} API QSTAR^{TM} Pulsar I LC/MS/MS system. Once data was generated, using the Applied Biosystems^{TM} ProteinPilot^{TM} Software 2.0.1, the peptide sequences were searched against the NCBI library for *Homo sapiens* to give the data presented in Appendix 8.4.

3 Chapter 3: *In cellulo* cAMP Accumulation Under Different Capnic States

3.1 Introduction

The study of ACs and their regulation by inorganic carbon is a developing field. Whilst *in vitro* assays have identified that CO_2 interacts with the AC apo-protein to increase metal co-factor affinity (Townsend et al., 2009), *in cellulo* evidence is limited. Townsend et al. demonstrated in HEK 293 cells stimulated by isoproterenol that CO_2 activates AC at 5% (v/v) compared to ambient CO_2 (v/v). This chapter aims to investigate this *in cellulo* CO_2 activation of AC further at the pathophysiological CO_2 concentrations of 2.5% and 10% (v/v) representing hypo- and hypercapnia respectively.

To establish this aim, cell lines responsive to the hormone PTH were chosen. This hormonal response not only acts through AC and cAMP (Agus et al., 1971, 1973) but is a particularly useful model as is physiologically involved in systemic inorganic carbon homeostasis (Section 1.7.3). As PTH has its most notable effect at the kidney and bone, two renal derived cell lines OK and HEKPR1, in addition to the osteoblast UMR-106 cell line, have been utilised to identify patterns in cAMP accumulation across hypo-, normo- and hypercapnic CO_2 concentrations (2.5%, 5% and 10% [v/v] respectively). Additionally, pHi measurements and the use of the weak acid propanoic acid to mimic CO_2 induced pHi changes have been utilised to ensure that any CO_2 effects on cAMP are pH independent.

This chapter presents evidence for a hypercapnic reduction in cAMP levels that is independent of activating stimulus, cell line, partial hypoxia, and both extra- and intracellular pH.

3.2 Cell Lines Used in Experimentation

Three different cell lines were used to measure PTH activated cAMP production under different capnic conditions: OK (Opossum Kidney), HEKPR1 (Human Embryonic Kidney cells expressing human Parathyroid hormone Receptor one) and UMR-106 (rat osteoblast cells). These lines will form the focus of this chapter and are decribed in the following sections.

3.2.1 OK cells

The response to PTH is well documented in OK cells after its first description by *Teitelbaum and Strewler* in 1984 (Teitelbaum & Strewler, 1984). First established in 1978 by *Koyama et al.* (Koyama et al., 1978), these cells exhibit numerous renal epithelial properties, including polarised distribution of plasma membrane proteins, expression of apical microvilli, and active renal transport systems characteristic of the proximal tubule (Cole et al., 1989), especially endogenous expression of high affinity PTH receptors (numbering some 300,000 per cell (Teitelbaum & Strewler, 1984)) coupled to both AC activation (Teitelbaum & Strewler, 1984; Malmstrom & Murer, 1986; Caverzasio et al., 1986; Cole et al., 1987), NHE3 inhibition, and sodium dependent phosphate transport (Cole et al., 1989). This PTH response is stable for 35 passages and the receptor affinity is similar to that found in renal plasma membranes (Teitelbaum & Strewler, 1984). As the only renal epithelial cell line to reliably respond to PTH (Cole et al., 1989) and with the complete signalling machinery for this response intact, these cells provide a useful system to test the CO_2 effect on cAMP accumulation, providing a physiologically relevant model.

Optimisation of cAMP Accumulation Assay Using OK Cells

In total three independent sources of OK cells (Section 2.3.1) were tested in order to detect a cAMP response to PTH. This response could not be detected in commercially available cells or those sent from one collaborator but was finally demonstrated using cells received from another collaborator.

As experiments with HEKPR1 cells under identical conditions demonstrated a response to PTH (Figure 18), the problem lay with the OK cells themselves, not the assay conditions. It is possible that if the cells obtained from the first collaborator (passage number unknown) were cultured for a long period of time without PTH challenge that they no longer expressed the PTH receptor or

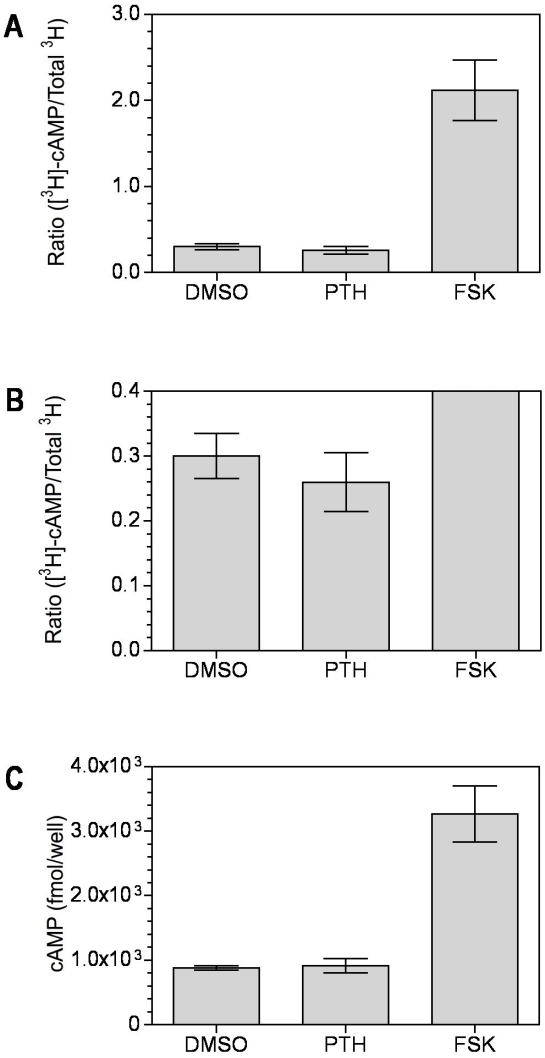

Figure 17: Failure to obtain parathyroid hormone response.

Cells assayed at one day post-confluence after overnight starvation (in absence of BSA, unlike most experimentation) and two hour labelling with 1.5 μCi (55.5 kBq) [^{3}H]-adenine per well. Agonist concentrations used were 100 nM PTH and 1 μM forskolin.

A Pooled results, $n = 3$. T-test p-values compared to DMSO control: PTH 7.88 x 10^{-2}, FSK 3.22 x 10^{-3}

B Same results as A with y-axis altered to draw attention to PTH results; having a similar level of cAMP accumulation as DMSO (basal cellular cAMP), $n = 24$

C cAMP measurement using an enzyme immunoassay (ELISA) kit to ensure results were independent of method of cAMP measurement used, $n = 4$. T-test p-values compared to DMSO control: PTH 3.40 x 10^{-1}, FSK 9.92 x 10^{-4}

an unknown part of signalling machinery. This is in accordance with previous papers which have shown that these cells required additions to the culture media in order to maintain OK cell hormone sensitivity (Armston & Wood, 1994). Further negative results with cells bought from ATCC® are less easy to explain. One possibility is that trypsinising cells between passages may have damaged the hormone receptor, although this is unlikely as HEKPR1 PTH receptors would be expected to be similarly affected. A repeated assay was carried out on cells reaching confluence in 7 days opposed to 3-4 to increase cell recovery and mirror the growth times documented in several papers (Pollock et al., 1986; Caverzasio et al., 1986; Cole et al., 1987, 1989; Armston & Wood, 1994). Results from this were again negative, with no cAMP accumulated in response to PTH, as were results using the increased sensitivity provided by the Biotrak ELISA and from samples of the media itself, ruling out the possibility that these cells were secreting any cAMP produced.

Further experimentation to establish why these cells did not respond to PTH could have included immunofluorescence or western blots to establish whether the PTH receptor was being expressed in each batch of cells, but with no downstream appearance of cAMP this was deemed too time consuming. It is possible that cells from each source exhibited different sensitivities to the hormone or that the PTH receptor was being internalised via receptor-mediated endocytosis (Teitelbaum & Strewler, 1984). It has previously been shown by *Cole et al.* that OK cell subline populations can exhibit different PTH and forskolin effects on phosphate transport, with the OK cell line 'morphologically and functionally heterogeneous' (Cole et al., 1989). In fact, within the same *Cole et al.* paper ^{125}I-PTH receptor binding experiments show non-uniform receptor affinity across these different clonal lines. In further agreement, *Armston and Wood* also had difficulty maintaining the OK cell PTH response, which they claim to be 'variable' from batch to batch, despite attempts to control it through constant feeding, sub-culturing, seeding cells at a constant density and altering growth media constituents (Armston & Wood, 1994). The long term nature of the OK cell culture is likely to be responsible for some of the heterogeneity due to the accumulation of spontaneous transformants (Cole et al., 1989), particularly as it has been noted that 'the inablility to maintain hormone-sensitive trans-epithelial transport activity in cultured cells is the major obstacle to the detailed analysis of epithelial transport function *in vitro*' (Valentich, 1986). Despite these initial obstacles, once a PTH responsive cell line was obtained, these cells provided a useful physiological model for the desired thesis aims.

Experimental repetition proved useful in determining optimal assay conditions. OK cells produce optimal cAMP responses at one-day post confluence and after overnight starvation in the presence of serum-free media supplemented with 0.2% BSA. This starvation step alone lead to a 35% increase in total cell adenine labelling. Through numerous experiments, radio-labelling conditions were set to contain 0.75 μCi (27.75 kBq) [^{3}H]-adenine per well, with 2 hours labelling time, in preference to longer exposure or higher tritium concentrations. Labelling also required the use of serum free media to both enable media gassing without excess bubble formation and to prevent serum inhibition of the PTH response as noted by *Goldring et al.* (Goldring et al., 1978). In addition, 10 minute agonist exposure proved best, opposed to longer assay incubations, a time-frame that matches the amount of time for cAMP levels to increase in rat urine following PTH injection (Chase & Aurbach, 1967) and follows observations by *Teitelbaum et al.* and *Malmstrom et al.* that intracelluar cAMP reached maximum 2-5 minutes after agonist addition, (Teitelbaum & Strewler, 1984; Malmstrom & Murer, 1986) and remained elevated as long as PTH was in contact with cells (Malmstrom & Murer, 1986). Finally, care was further taken to optimise the pre-incubation step for these assays, which was set to 30 minutes allowing both inhibitor penetration and transient pHi change and recovery to occur, in accordance with results presented in Section 3.3.

3.2.2 HEKPR1 cells

Both OK and HEK 293 renal cell lines are purportedly derived from the proximal tubule of the kidney; the area naturally responsive to PTH, and were therefore used in combination to demonstrate that any findings were not species specific. According to most publications (except *Jobert et al.* (Jobert et al., 1997)) parent HEK 293 cells have lost their natural ability to respond to PTH resulting from their time in culture. This is due to an absence of the PTH receptor (Behar et al., 1996; Jobert et al., 1997). Wild type HEK 293 were thus transfected to contain the complete coding sequence for human parathyroid hormone receptor one (-PR1) using expression vector pRezex-2, enabling the desired hormonal response to PTH for at least 40 passages (Short & Taylor, 2000). However, due to this transfection requirement, although useful as a comparision, HEKPR1 cells could not be used to produce physiologically relevant data. In addition to this, the HEKPR1 parent line, HEK 293, is now under increasing scrutiny as to its true origin, especially as it is has proven difficult to characterise these cells post adenovirus transformation (Graham et al., 1977). This difficulty occurs not only as a result of viral transformation itself (Graham et al., 1977), but also due to the developing embryonic

nature of the tissue originally sampled, which would have contained cells of numerous lineages, as well as the variable polypeptide expression already noted in the original paper creating the line (Graham et al., 1977). In addition, due to the segmental heterogeneity of the kidney, isolating cells and creating any renal cell line of a specific lineage at all is a major problem in the field (Armston & Wood, 1994). In fact, there is convincing evidence to suggest that HEK 293 cells are of neuronal origin, expressing a number of neuronal specific mRNA and gene products (Shaw et al., 2002); further reason for repetition of results in OK cells.

3.2.3 UMR-106 cells

To provide confirmation of a general CO_2 elicited response, UMR-106 cells (Partridge et al., 1980), also responsive to PTH, were used to show that results were neither species nor tissue specific, as UMR-106 are of osteoblast lineage opposed to kidney. Bone is an important PTH responsive organ, where osteoblasts (fully differentiated bone cells embedded in the extra-cellular matrix) react to the hormone through a variety of different mechanisms. These include cAMP production (Chase & Aurbach, 1970) which results in the release of minerals from the bone, causing another bone cell type, osteoclasts, to be indirectly stimulated to destroy and re-absorb osteoblasts (Forrest et al., 1985). UMR-106 cells (Partridge et al., 1980) are rat derived osteosarcoma cells which have been repeatedly proven as valuable model systems for studying the effects of PTH on bone cells (Forrest et al., 1985) via ACs and cAMP (Partridge et al., 1981, 1980) and therefore provide a useful comparative tool.

3.2.4 cAMP Agonist Responses in Experimental Cell Lines

A primary objective was to ensure that all cell lines were responsive to the agonists PTH and FSK. Figure 18 displays cAMP accumulation in response to negative control DMSO, PTH, and a FSK positive control in OK, HEKPR1 and UMR-106 cells. Data is presented as normalised values of [^{3}H]-cAMP compared to total cell labelling, as explained in Section 2.4.6.

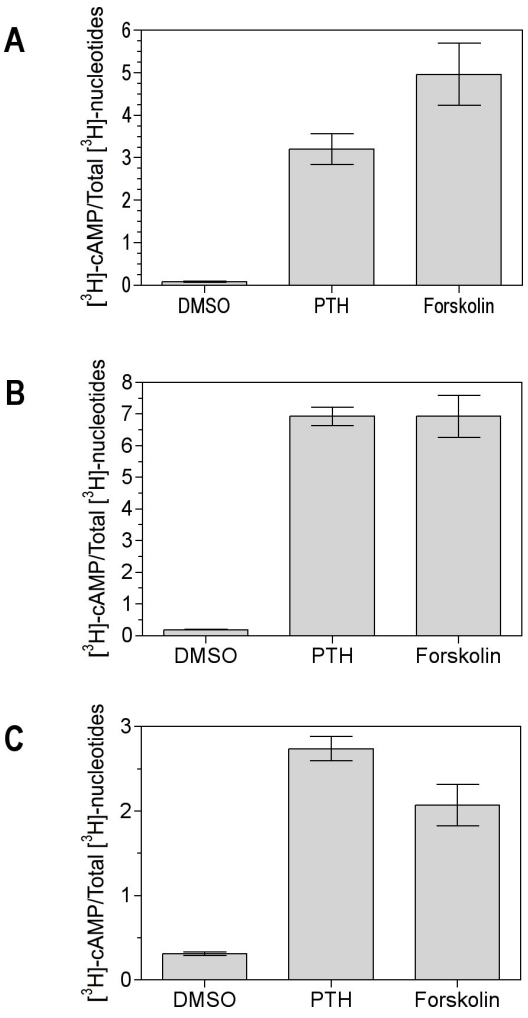

Figure 18: cAMP accumulation agonist responses in OK, HEKPR1 and UMR-106 cell lines.

Agonist response at 5% CO_2 (v/v), pH 7.0, concentrations of agonist used were 100 nM PTH and 10 μM FSK. DMSO used as a negative control.

A: OK cells, $n = 8$, T-test p-values: 1.33 x 10^{-10} and 1.37 x 10^{-6} for PTH and FSK compared to the control respectively;

B: HEKPR1 cells, $n = 8$, T-test p-values: 1.31 x 10^{-8} and 6.43 x 10^{-5} for PTH and FSK compared to the control respectively;

C: UMR-106 cells, $n = 4$, T-test p-values: 4.76 x 10^{-7} and 5.61 x 10^{-5} for PTH and FSK compared to the control respectively;

3.3 Intracellular pH Control Experiments

3.3.1 Transient Intracellular pH Changes with Different Capnic States

Prior to any cAMP accumulation assays with varying CO_2, it was important to ensure that assaying cells in the presence of different CO_2 concentrations had an effect on solely the intracellular pCO_2 and not pH. This is particularly important as pH has a pronounced effect on adenylyl cyclase activity (Hammes & Rodbell, 1976) and therefore, if not tightly controlled, could lead to erroneous results. Previously published data by *Townsend et al.* showed that HEK 293 cells undergo a transient pHi change on exposure to different CO_2 concentrations. To establish whether OK and HEKPR1 cells would respond similarly, a microspectrofluorometric device was employed to measure pHi with alteration of pCO_2 in a perfused media. The premise of this experiment is that if pHi were to recover from a change in pCO_2 within a suitable time-frame, any cAMP measurements taken after this period could be inferred to be influenced solely by the CO_2 and not pH.

Intracellular pH measurement followed the method in Section 2.4.1, after optimisation. Each cell line required different labelling conditions, 7.5 μM BCECF-AM (Rink et al., 1982) for OK cells and 5 μM for HEKPR1. Also, to enable cells to adequately recover from the different CO_2 concentrations, loading required the use of a pre-warmed, pre-gassed solution maintained at 37 °C and 5% CO_2 (v/v). If cells were left to load on the bench CO_2 was lost from the loading medium and thus its pH allowed to increase, the cells ability to recover from further changes was compromised. As a result of this observation, the initial loading solution of PBS and glucose was supplemented with 14 mM $NaHCO_3$ to facilitate solution gassing. Through these experiments and frequent measurements of the bubbled perfusate, it was deemed that concentrations of 14 mM $NaHCO_3$ and 15 mM HEPES were sufficient to buffer the media for these periods of CO_2 gassing, although an increase to 20 mM HEPES was implemented in the Krebs-Ringer-HEPES solutions used in ammonium pulse experiments detailed in Chapter 5 due to the extended time period of experimentation.

Both cell lines experience transient pHi changes on exposure to different CO_2 concentrations, with an acidification occuring as CO_2 is increased, as shown in Figure 19. These graphs demonstrate that cells recover to a resting pH of 7.05 for OK cells and 7.21 for HEKPR1 cells, as calculated by nigericin calibration (Appendix 7.1). For example, with HEKPR1 cells when moving from a normocapnic (5% CO_2 [v/v]) to a hypercapnic (10% CO_2 [v/v]) solution at time point 3583 s an initial acidification event of 0.25 pH units occurs which recovers in under 10 minutes (here around 8 minutes 40 seconds). Recovery time, on average, is around 10 minutes for both cell lines, with a maximum recovery period

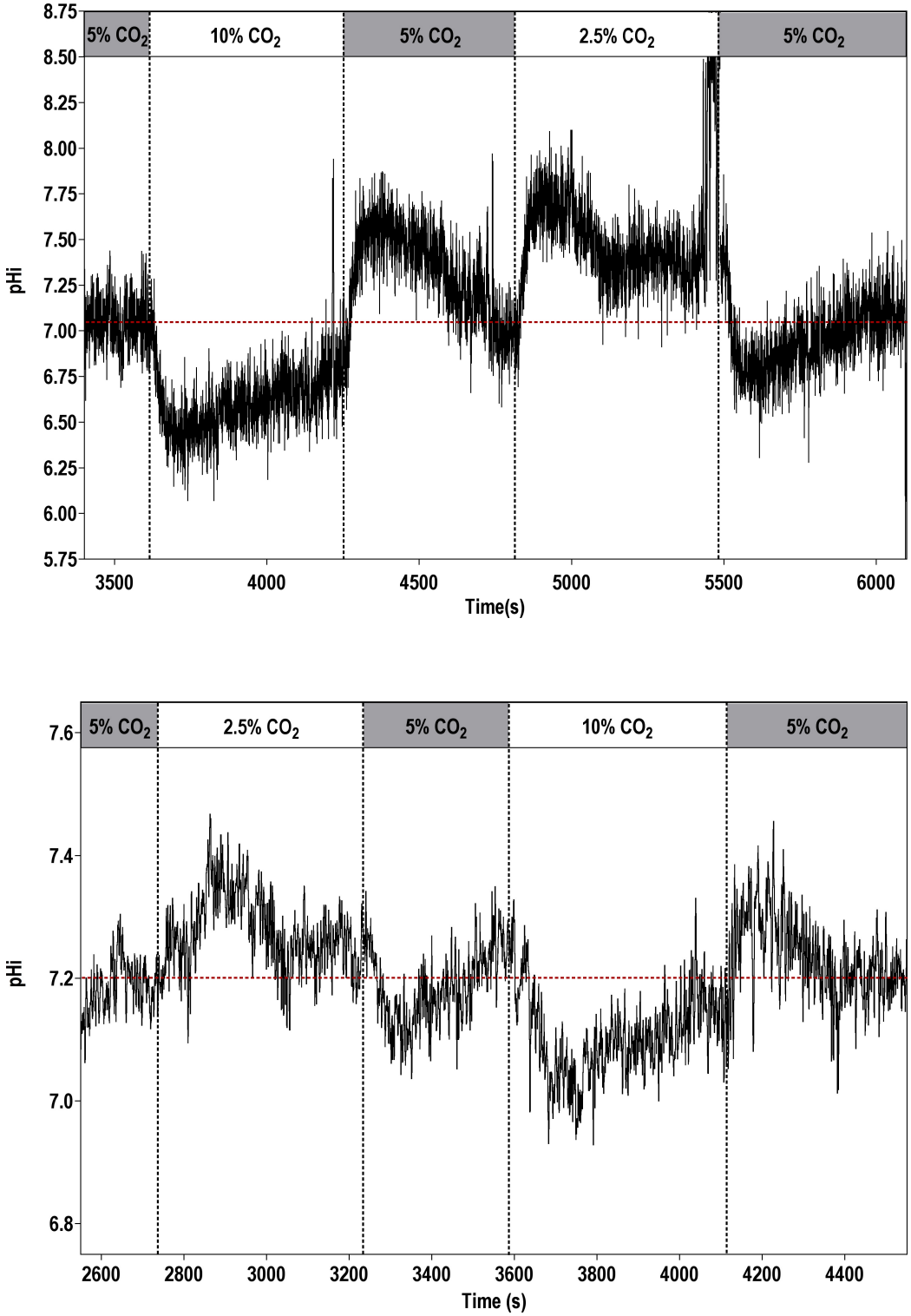

Figure 19: Intracellular pH in response to different CO_2 concentrations. Experimentation using PBS solution at pH 7.35 and DMEM CO_2 containing solutions adjusted to pH 7.0 Dashed vertical lines represent solution changes. Top: OK cells; Bottom: HEKPR1 cells.

of 15 minutes. This fact was implemented when designing cAMP accumulation assays where a pre-incubation step of 30 minutes was employed, allowing cells to respond to the influx of CO_2 and recover their pH before agonist addition, in addition to facilitating inhibitor cell permeation.

3.3.2 Mimicking CO_2 Induced pHi Changes with Propanoic Acid

As shown in Section 3.3.1 both cell lines recover from a change in pCO_2, with average recovery around 10 minutes. However, their pHi does change, with average ΔpHi values of 0.65 $\pm$ 3.50 x10^{-2} and 0.28 $\pm$ 4.79 x10^{-2} for OK and HEKPR1 cells respectively when considering the 5% to 10% CO_2 (v/v) shift. Although this change recovers in a matter of minutes, in the physiological time-frame this could still be long enough for the cells, or a cellular constituent, to respond. In order to eliminate pH as a experimental factor, the weak acid propanoic acid (PA) was implemented to mimic the transient pHi acid change experienced from 5% to 10% CO_2 (v/v), without altering CO_2 in any way, as previously published by *Willoughby et al.* (Willoughby et al., 2005).

In order to calculate the correct concentration of PA to use, cells were perfused (and then left to recover) with normal 5% CO_2 media containing different PA concentrations, ranging from 1 mM to 10 mM, as shown in Figure 20. From these experiments 2 mM was chosen as the correct PA concentration to mimic both cell lines 5% to 10% (v/v) CO_2 induced pHi change, giving average ΔpHi values of 0.64 $\pm$ 2.42 x10^{-2} and 0.36 $\pm$ 3.29 x10^{-2} OK and HEKPR1 cells respectively. Representative graphs of these pHi changes for both the CO_2 and PA experiments are presented in Figure 21.

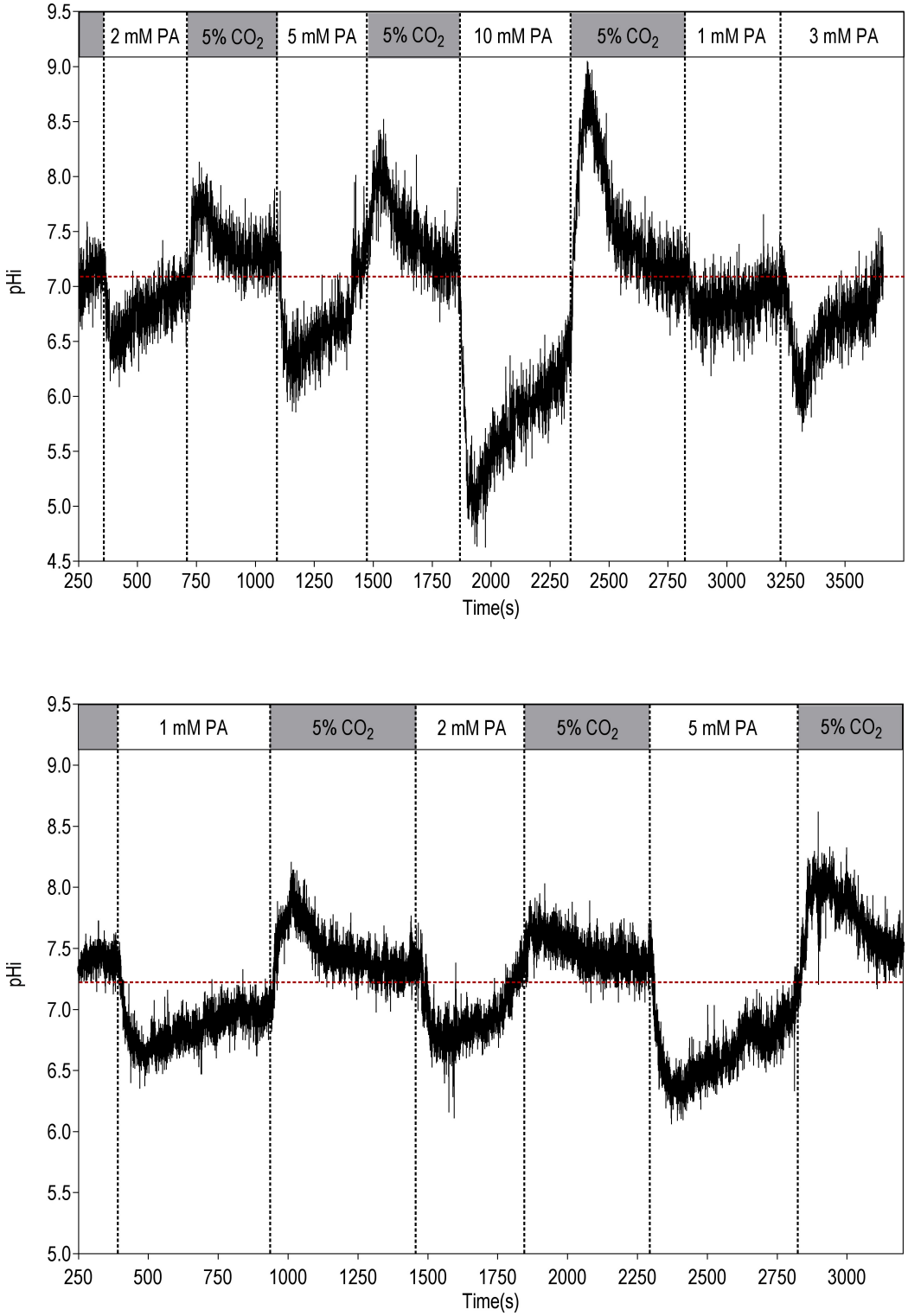

Figure 20: Intracellular pH in response to propanoic acid concentrations. Experimentation using DMEM CO_2 containing solutions adjusted to pH 7.4. Dashed vertical lines represent solution changes. Top: OK cells; Bottom: HEKPR1 cells.

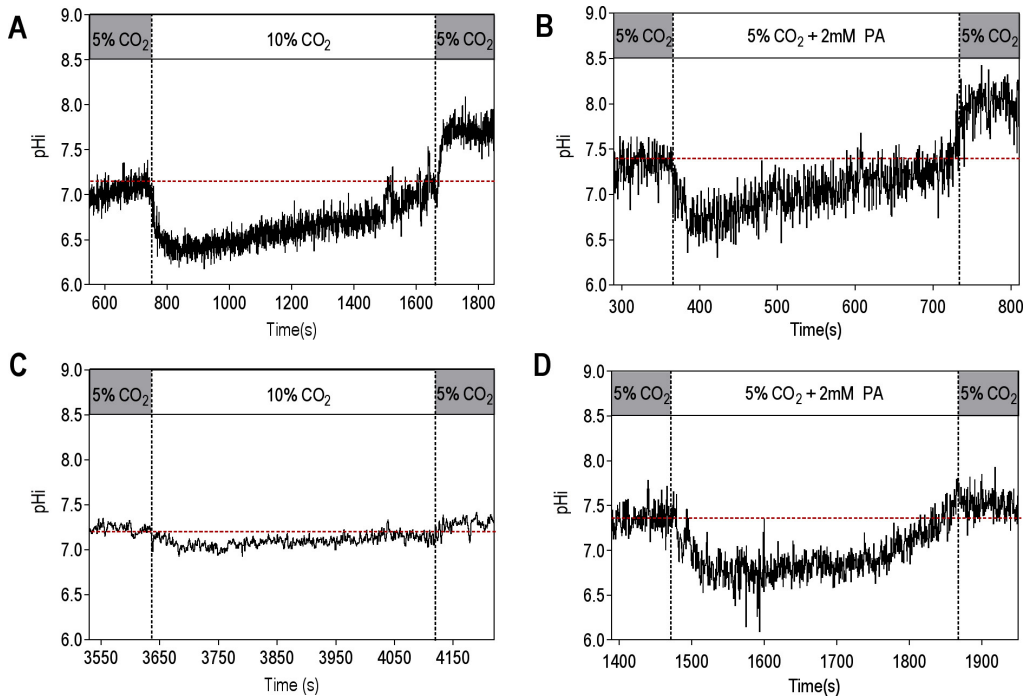

Figure 21: Transient pHi changes relevant for future experimentation. **A**: OK cells, 5% (v/v) to 10% (v/v) CO_2 **B**: OK cells, 5% (v/v) CO_2 to 5% (v/v) CO_2 and 2 mM PA. **C**: HEKPR1 cells, 5% (v/v) to 10% (v/v) CO_2 **D**: HEKPR1 cells, 5% (v/v) CO_2 to 5% (v/v) CO_2 and 2 mM PA

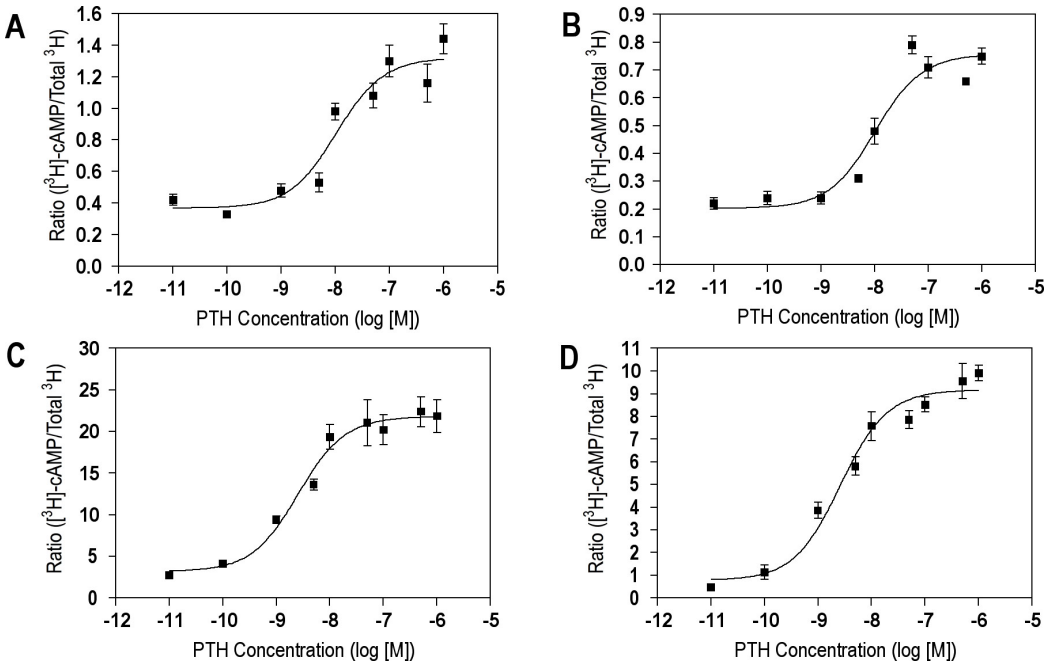

Figure 22: OK and HEKPR1 cells PTH dose responses. PTH sigmoidal dose-response at 5% CO_2 and defined pH, PTH in aqueous solution. **A**: OK cells, pH 7.0 (physiological acidosis), $n = 7/8$, $EC_{50} = 1.09 \times 10^{-8}$, R^2 value = 0.7498 **B**: OK cells, pH 7.5 (physiological alkalosis), $n = 7/8$, $EC_{50} = 9.83 \times 10^{-9}$, R^2 value = 0.8205 **C**: HEKPR1 cells, pH 7.0, $n = 7/8$, $EC_{50} = 2.55 \times 10^{-9}$, R^2 value = 0.7537 **D**: HEKPR1 cells, pH 7.5, $n = 7/8$, $EC_{50} = 2.60 \times 10^{-9}$, R^2 value = 0.8785

3.4 PTH Dose-Response at pH levels 7.0 and 7.5

Dose responses for PTH stimulated cAMP production were characterised at both pH 7.0 and 7.5 to model the physiological acidotic and alkalotic conditions typical of systemic hyper- and hypocapnia respectively (Marshall & Bangert, 2008), to determine whether pH had an effect of the efficacy of the hormone (Figure 22). PTH concentrations between 10 pM and 1 μM were implemented with the lowest recordable response at 100 pM. Although these values are higher than the circulating serum concentration of 1 pM (Chambers et al., 1978; Allgrove et al., 1983) the dose responses for OK cells match those published (Teitelbaum & Strewler, 1984; Malmstrom & Murer, 1986; Armston & Wood, 1994) and this repeatable difference between experimentally determined EC_{50} values and the much lower serum concentrations has been noted previously by *Cole et al.* (Cole et al., 1987).

Within each cell line there were no significant EC_{50} differences between the two pH values. Extracellular pH therefore does not have an effect on PTH efficacy and downstream AC activation and cAMP production. As CO_2 concentration and pH are intrinsically linked this result demonstrates that any alterations in PTH stimulated cAMP production with varied CO_2 will not result from any pH fluctuations on the PTH signalling response. From the dose responses it was decided to use 5 nM PTH in future cAMP accumulation experiments for both cell lines. This concentration was deemed appropriate as it should give a clear and measurable result with lower cAMP concentrations still detectable, whilst still allowing the system to be stimulated further if required.

3.5 cAMP Accumulation with Differing CO_2 Concentrations

Accumulated cAMP levels were measured in cells exposed to different capnic conditions using 2.5%, 5% and 10% (v/v) CO_2 in air to model hypo-, normo- and hypercapnia respectively (Marshall & Bangert, 2008). Methodology was altered accordingly to ensure that any pHi changes induced in cells with exposure to a different level of CO_2 to that of their culture (5% [v/v] CO_2) would experience the transient pHi change shown in Section 3.3.1 and recover before cAMP levels were measured. Experiments used both the agonists PTH and FSK to answer whether the method of AC stimulation affected the result. In addition, both extracellular pH values of 7.0 and 7.5 were tested, to mimic the typical pH levels experienced by the cells during acidosis or alkalosis respectively and repeated across both OK and HEKPR1 cells.

As can be seen in Figures 23 and 24 for both PTH and FSK, 2.5% and 5% (v/v) CO_2 solutions elicit similar responses, whilst there is a drop in cAMP production at 10% (v/v) CO_2. For comparison between data sets tritiated adenine derived ratios ([^{3}H]-cAMP/ Total [^{3}H] adenine nucleotides) are displayed as percentages of the normocapnic (5%) agonist induced value. Negative control data has also been included for comparison, using the agonist solvents H_2O or DMSO for PTH and FSK respectively. Table 8 displays statistical two-way ANOVA (with post hoc Bonferroni) testing of these data sets to show that this trend is statistically significant. Tabulated results are calculated as a percentage of the normocapnic (5%) agonist induced values to match graphically presented data. Similar statistical analysis for raw data also show the same trend (not shown). Importantly, negative control data does not follow this trend, implying the effect of CO_2 is solely on the agonist activated AC, although it is possible that the experimental method employed was not sensitive enough to distinguish between these basal cAMP levels.

This trend is independent of the mode of AC activation with both PTH and FSK giving identical results, suggesting that the CO_2 sensor is either directly at the AC or interacting closely with the enzyme and is not part of the upstream signalling pathway from the PTH receptor. Additionally, it is not species/cell line specific as appears across OK and HEKPR1 cell lines and, crucially, is pH independent. This latter conclusion is drawn from that fact that changing the extracellular pH from pH 7.0 to 7.5 maintained the drop in cAMP levels at 10% (v/v) CO_2, in conjunction with the established fact that these cell lines will experience a transient pH change with exposure to the different CO_2 levels which quickly recovers before the time at which cAMP measurements are made. Nevertheless, as mentioned in Section 3.3.2, despite this speedy recovery it is possible that

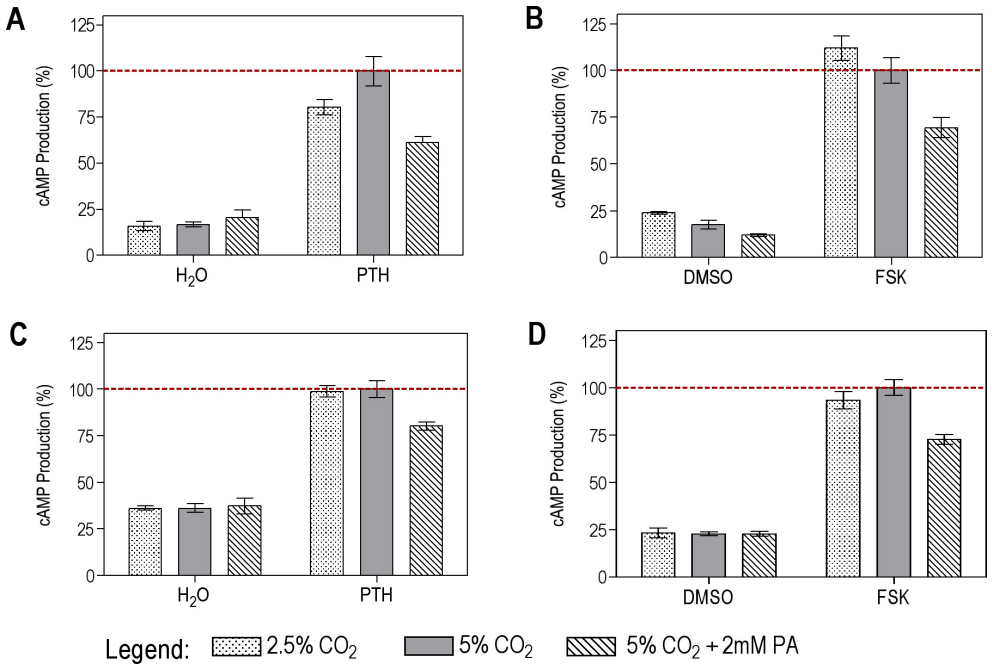

Figure 23: OK PTH and FSK responses at 2.5%, 5% and 10% (v/v) CO_2. Agonist concentrations of 5 nM PTH and 10 μM FSK, agonist solvents H_2O and DMSO respectively as negative controls. Results shown as a percentage of the 5% CO_2 value. **A**: PTH activation at pH 7.0, $n = 8$ **B**: FSK activation at pH 7.0, $n = 8$ **C**: PTH at pH 7.5, $n = 8$ **D**: FSK at pH 7.5, $n = 8$

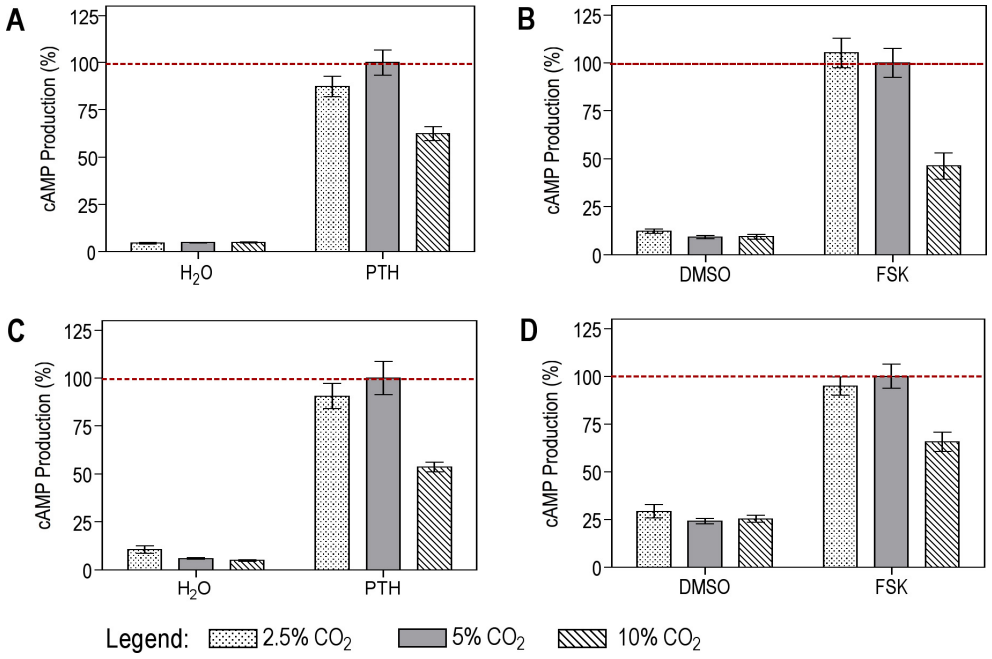

Figure 24: HEKPR1 PTH and FSK responses at 2.5%, 5% and 10% (v/v) CO_2. Agonist concentrations of 5 nM PTH and 10 μM FSK, agonist solvents H_2O and DMSO respectively as negative controls. Results shown as a percentage of the 5% CO_2 value. **A**: PTH activation at pH 7.0, $n = 5/6$ **B**: FSK activation at pH 7.0, $n = 6$ **C**: PTH at pH 7.5, $n = 5/6$ **D**: FSK at pH 7.5, $n = 6$

Comparison	Negative Control (H_2O/DMSO)		Agonist(PTH/FSK)	
	Difference	**P value**	**Difference**	**P value**
OK pH 7.0 PTH				
2.5% vs 5%	0.978	$P \geq 0.05$	19.56	$P \leq 0.05$
2.5% vs 10%	4.645	$P \geq 0.05$	-19.32	$P \leq 0.05$
5% vs 10%	3.667	$P \geq 0.05$	-38.88	$P \leq 0.001$
OK pH 7.0 FSK				
2.5% vs 5%	-6.218	$P \geq 0.05$	-11.92	$P \geq 0.05$
2.5% vs 10%	-11.92	$P \geq 0.05$	-42.29	$P \leq 0.001$
5% vs 10%	-5.699	$P \geq 0.05$	-30.57	$P \leq 0.001$
OK pH 7.5 PTH				
2.5% vs 5%	0.054	$P \geq 0.05$	1.163	$P \geq 0.05$
2.5% vs 10%	1.163	$P \geq 0.05$	-18.60	$P \leq 0.001$
5% vs 10%	1.109	$P \geq 0.05$	-19.77	$P \leq 0.001$
OK pH 7.5 FSK				
2.5% vs 5%	-0.4566	$P \geq 0.05$	6.589	$P \geq 0.05$
2.5% vs 10%	-0.4500	$P \geq 0.05$	-20.81	$P \leq 0.001$
5% vs 10%	0.0066	$P \geq 0.05$	-27.40	$P \leq 0.001$
HEKPR1 pH 7.0 PTH				
2.5% vs 5%	0.3636	$P \geq 0.05$	12.55	$P \geq 0.05$
2.5% vs 10%	0.3546	$P \geq 0.05$	-25.09	$P \leq 0.001$
5% vs 10%	-0.0121	$P \geq 0.05$	-37.64	$P \leq 0.001$
HEKPR1 pH 7.0 FSK				
2.5% vs 5%	-2.946	$P \geq 0.05$	-5.260	$P \geq 0.05$
2.5% vs 10%	2.820	$P \geq 0.05$	-58.99	$P \leq 0.001$
5% vs 10%	0.1260	$P \geq 0.05$	-53.73	$P \leq 0.001$
HEKPR1 pH 7.5 PTH				
2.5% vs 5%	-4.768	$P \geq 0.05$	9.407	$P \geq 0.05$
2.5% vs 10%	-5.799	$P \geq 0.05$	-36.98	$P \leq 0.001$
5% vs 10%	-1.031	$P \geq 0.05$	-46.39	$P \leq 0.001$
HEKPR1 pH 7.5 FSK				
2.5% vs 5%	-5.195	$P \geq 0.05$	5.195	$P \geq 0.05$
2.5% vs 10%	-3.896	$P \geq 0.05$	-29.22	$P \leq 0.001$
5% vs 10%	1.299	$P \geq 0.05$	-34.42	$P \leq 0.001$

Table 8: Statistical analysis of cAMP capnic response: Two-way ANOVA analysis with post hoc Boniferroni testing

this change in pH may have been long enough for the cells, or a cellular constituent, to respond in some way. This problem is addressed in Section 3.7.

3.6 UMR-106 Cell cAMP Accumulation at Differing CO_2 Concentrations

Section 3.5 demonstrated an *in cellulo* inhibitory effect of hypercapnia (modelled using 10% (v/v) CO_2) on cAMP accumulation, unreliant on species origin, method of AC activation or extracellular pH. Whilst the data presented using OK and HEKPR1 cells suggests that the effect is true for both *Didelphis virginiana* and *Homo sapiens*, both cell lines are of renal origin. PTH is not only active in the kidney; it also causes bone breakdown and re-absorption to release stored calcium and phosphate ions (Forrest et al., 1985). This section demonstrates the inhibiton of cAMP accumulation at elevated CO_2 in another species (*Rattus norvegicus*) using UMR-106 cells (Partridge et al., 1980), a rat osteosarcoma cell line known to respond to PTH through the production of cAMP (Partridge et al., 1980, 1981) and thus demonstrates similar responses across both organ lineages. As shown in Figure 25 hypo- and normocapnic levels of CO_2 (2.5% (v/v) and 5% (v/v)) exhibit similar cAMP levels with a decrease across the board at hypercapnic 10% (v/v) CO_2. Again this trend is present for both extracellular media pH levels of 7.0 and 7.5, indicating that extracelluar pH is not a determining factor, and independent of mode of AC stimulation with identical trends with both PTH and FSK. Statistical ANOVA evidence is presented in Table 9, again showing that only the agonist activated AC is affected by CO_2, as noted in Section 3.5.

Comparison	**Negative Control (H_2O/DMSO)**		**Agonist(PTH/FSK)**	
	Difference	**P value**	**Difference**	**P value**
UMR-106 pH 7.0 PTH				
2.5% vs 5%	0.1104	$P \geq 0.05$	-9.713	$P \geq 0.05$
2.5% vs 10%	1.656	$P \geq 0.05$	-61.26	$P \leq 0.001$
5% vs 10%	1.545	$P \geq 0.05$	-51.55	$P \leq 0.001$
UMR-106 pH 7.0 FSK				
2.5% vs 5%	-3.430	$P \geq 0.05$	-9.675	$P \geq 0.05$
2.5% vs 10%	-3.782	$P \geq 0.05$	-54.62	$P \leq 0.001$
5% vs 10%	-0.351	$P \geq 0.05$	-44.94	$P \leq 0.001$
UMR-106 pH 7.5 PTH				
2.5% vs 5%	-1.846	$P \geq 0.05$	8.795	$P \geq 0.05$
2.5% vs 10%	-5.103	$P \geq 0.05$	-37.68	$P \leq 0.001$
5% vs 10%	-3.257	$P \geq 0.05$	-46.47	$P \leq 0.001$
UMR-106 pH 7.5 FSK				
2.5% vs 5%	-0.1992	$P \geq 0.05$	-16.33	$P \leq 0.05$
2.5% vs 10%	-0.3984	$P \geq 0.05$	-55.68	$P \leq 0.001$
5% vs 10%	-0.1992	$P \geq 0.05$	-39.34	$P \leq 0.001$

Table 9: Statistical analysis of UMR-106 cAMP capnic response: ANOVA analysis with post hoc Bonferroni testing

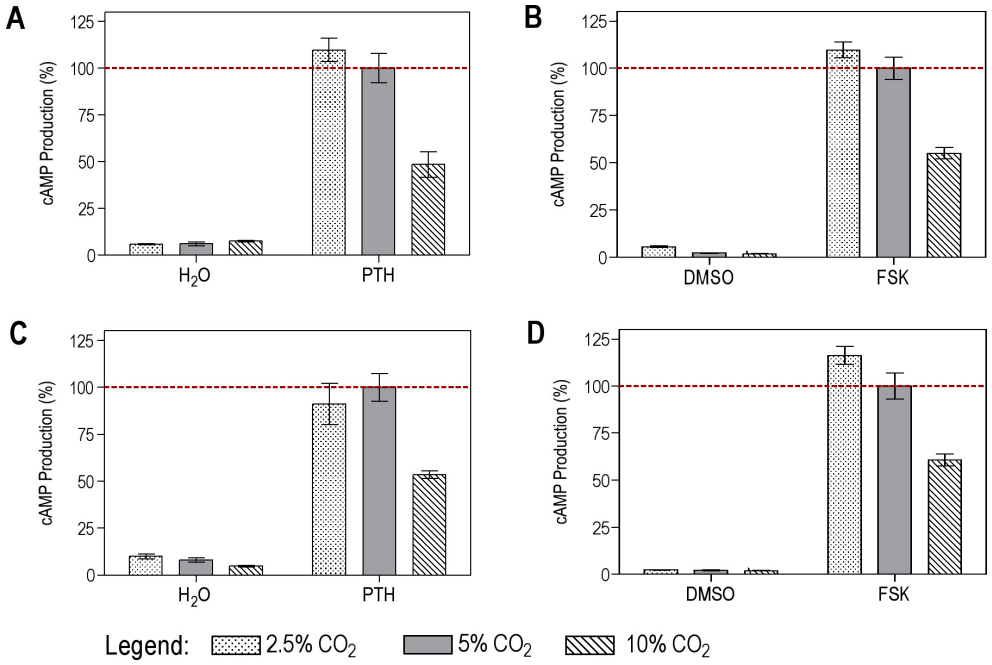

Figure 25: UMR-106 PTH and FSK responses at 2.5%, 5% and 10% (v/v) CO_2. Agonist concentrations of 5 nM PTH and 10 μM FSK, agonist solvents H_2O and DMSO respectively as negative controls. Results shown as a percentage of the 5% (v/v) CO_2 value. **A**: PTH activation at pH 7.0, $n = 8$ **B**: FSK activation at pH 7.0, $n = 8$ **C**: PTH at pH 7.5, $n = 8$ **D**: FSK at pH 7.5, $n = 8$

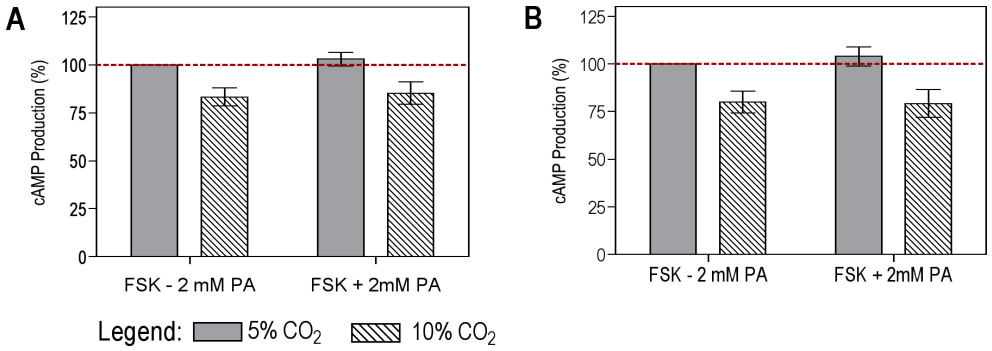

Figure 26: Effect of acidosis on cAMP accumulation. 10 μM FSK agonist with 2 mM propanoic acid (PA) used to mimic the transient pH change associated with 10% (v/v) CO_2. Results shown as a percentage of the 5% (v/v) CO_2 FSK value, with error bars generated from across individual experimental replicates. **A**: OK cells, pH 7.5, $n = 6$ **B**: HEKPR1 cells, pH 7.5, $n = 7$

3.7 pH Independent Effect of Hypercapnia on cAMP Accumulation

Sections 3.5 and 3.6 demonstrate that hypercapnia induces a potentially pH-independent inhibition in cAMP accumulation, based on the fact that alteration of extracellular pH from 7.0 to 7.5 had no effect on the observed reduction in cAMP levels at 10% (v/v) CO_2, and that increased CO_2 administration causes only a transient intracellular pH change which should recover before cAMP accumulation measurements are made (Section 3.3). In order to eliminate pH completely, the pHi change associated with 5% (v/v) CO_2 was mimicked using 2 mM propanoic acid (Section 3.3.2). Propanoic acid was also introduced to cells at 10% (v/v) CO_2 to establish whether the propanoate ion or its related intracellular pH change, in addition to that ellicited by the higher concentration of CO_2, would affect the observed hypercapnic effect on cAMP accumulation. As extracellular pH had no effect on previous cAMP accumulation experiments, these experiments were carried out at pH 7.5.

It should be noted that a similar weak base was not introduced to mimic the pHi change experienced with 2.5% (v/v) CO_2 as this hypocapnic CO_2 concentration was dropped from later experiments in order to focus on the effects on cAMP accumulation observed at 10% (v/v) CO_2. Hypercapnic acidosis is of arguably greater clinical interest, having contrasting positive and negative implications on pathophysiological prognosis (Section 1.7), further justifying this focus.

Results displayed in Figure 26 show that 5% (v/v) CO_2 with 2 mM propanoic acid did not cause the drop in cAMP associated with 10% (v/v) CO_2, with no statistical difference between 5% (v/v) CO_2 and 5% with the acid (Table 10). This was found for both renal cell lines, HEKPR1 and OK, and the inhibition of cAMP accumulation with hypercapnia can therefore be viewed reliably as a pH independent phenomena. In addition to this, it is also worth noting that it has previously been demonstrated that G-protein regulated ACs are offered some protection from changes in pHi through the action of Na^+/H^+ antiporters (Willoughby et al., 2005), further justifying this conclusion. The introduction of PA to cells at 10% (v/v) CO_2 also had no statistical effect on the observed decrease in cAMP levels, further validating the usage of this acid as a control (Figure 26 and Table 10).

Comparison	FSK Agonist	
	Difference	P value
OK pH 7.5		
5% vs 5% + 2mM PA	3.078	$P \geq 0.05$
5% vs 10%	-16.77	$P \leq 0.05$
5% + 2 mM PA vs 10% + 2mM PA	-17.75	$P \leq 0.05$
10% vs 10% + 2mM PA	2.097	$P \geq 0.05$
HEKPR1 pH 7.5		
5% vs 5% + 2mM PA	3.952	$P \geq 0.05$
5% vs 10%	-19.91	$P \leq 0.05$
5% + 2 mM PA vs 10% + 2mM PA	-24.70	$P \leq 0.01$
10% vs 10% + 2mM PA	-0.831	$P \geq 0.05$

Table 10: Statistical analysis of the effect of PA: ANOVA analysis with post hoc Bonferroni testing. CO_2 percentages presented as v/v.

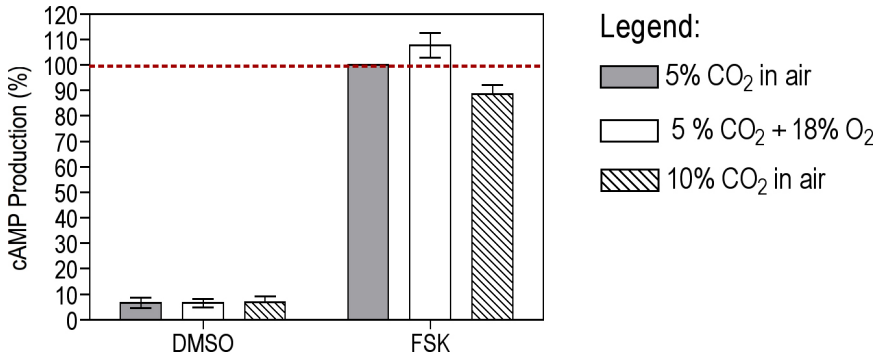

Figure 27: Effect of O_2 on cAMP accumulation in HEKPR1 cells at pH 7.5. 10 μM FSK used with FSK solvent DMSO used as a negative control. 5% CO_2, 18% O_2, 77% N_2 (v/v) used to mimic the alteration of O_2 experienced by cells exposed to 10% compared to 5% (v/v) CO_2 in air. Results shown as a percentage of the 5% CO_2 value, with error bars generated from across individual experimental replicates, n =4

Comparison	Negative Control - DMSO		FSK Agonist	
	Difference	P value	Difference	P value
HEKPR1 pH 7.5				
5% CO_2 vs 5% CO_2, 18% O_2, 77% N_2	0.005	$P \geq 0.05$	7.733	$P \geq 0.05$
5% CO_2 vs 10% CO_2	0.4225	$P \geq 0.05$	-11.340	$P \leq 0.05$
5% CO_2, 18% O_2, 77% N_2 vs 10% CO_2	0.417	$P \geq 0.05$	-19.07	$P \leq 0.001$

Table 11: Statistical analysis of the effect of O_2: ANOVA analysis with post hoc Bonferroni testing. CO_2 percentages presented as v/v.

3.8 Hypercapnic Effect on cAMP Accumulation Independent of Hypoxia

In order to expose cells to different capnic conditions, solutions have been gased using mixtures of CO_2 in air (2.5, 5, 10% (v/v)). As the percentage of CO_2 is altered between mixtures, so too must be the relative percentage of air present and thus the oxygen content. Therefore, based on the premise that air contains 20.95% (v/v) O_2, under these conditions cells at 5% (v/v) CO_2 will experience 19.90% (v/v) O_2 and cells at 10% (v/v) CO_2, 18.85% (v/v) O_2. This discrepancy, although minor, could explain the observed differences between 5% and 10% CO_2 (v/v), especially due to evidence in the literature that down-regulation of the cAMP signalling systems may be a mechanism by which cells adapt to long-term hypoxia (Beitner-Johnson et al., 1998). To test for this, HEKPR1 cells were exposed to a gaseous mixture of 5% CO_2, 18% O_2, 77% N_2 (v/v) and compared to cells exposed to 5% and 10% CO_2 (v/v) in air. The results displayed in Figure 27 and Table 11 demonstrate that under these conditions, whilst the expected drop in cAMP accumulation from 5% to 10% CO_2 in air is present, this phenomenon does not occur with the 5% CO_2, 18% O_2, 77% N_2 (v/v) mixture. Thus it can be inferred that the effect of 10% (v/v) CO_2 on cAMP accumulation occurs as a result of CO_2 and not O_2.

3.9 Chapter Conclusions

This chapter provides evidence for a pH independent inhibition of cAMP production by AC during hypercapnia (Figure 28). Alteration of extracellular pH had no effect on this blunted response or on normocapnic PTH induced cAMP production, with no change in EC_{50} values. Thus, any potential media pH changes associated with altering the CO_2 concentration are not responsible for the observed trends. In addition, transient pHi changes experienced by cells with exposure to elevated CO_2 were measured and mimicked using weak acid 2 mM propanoic acid. Use of this acid in the absence of simultaneously elevated CO_2 had no effect on cAMP production, suggesting that the blunted cAMP levels observed are due to CO_2 and not any changes in pHi. Together these results infer a pH independent effect on AC mediated cAMP production.

This inhibition of AC with elevated CO_2 was also true regardless of the agonist employed, with the same trend present for both PTH and FSK, indicating that the inhibitory effect of CO_2 does not occur upstream of AC and is independent of the AC isoform (PTH couples specifically to AC VI in HEKPR1 cells (Tovey et al., 2008) whilst FSK activates all tmAC isoforms (Zhang et al., 1997)). Results displayed include evidence from three cell lines: HEKPR1, OK and UMR-106; suggesting a species and tissue independent effect.

Hypocapnia, modelled by 2.5% (v/v) CO_2 in air, did not inhibit AC and cAMP production but instead resulted in cAMP levels statistically similar to that of normocapnia (5% (v/v) CO_2 in air). This hypocapnic CO_2 concentration has been henceforth abandoned in order to focus on the effects of elevated CO_2, which both gave a clear effect on cAMP accumulation and is of arguably more clinical interest, having contrasting postive and negative implications on pathophysiological prognosis (Section 1.7). The benefits of therapeutically administed permissive hypercapnia have in part been attributed to inhibition of alveolar fluid reabsorption via a cAMP mediated mechanism (Vadász et al., 2008b). Thus, the hypercapnic attenuation of cAMP signalling demonstrated in this chapter could provide a link to the physiological effects observed with elevated CO_2. Further work to delinearise the contributing signalling pathways in this hypercapnic effect on AC, as well as evidence for its physiological implications, are presented in the following chapters.

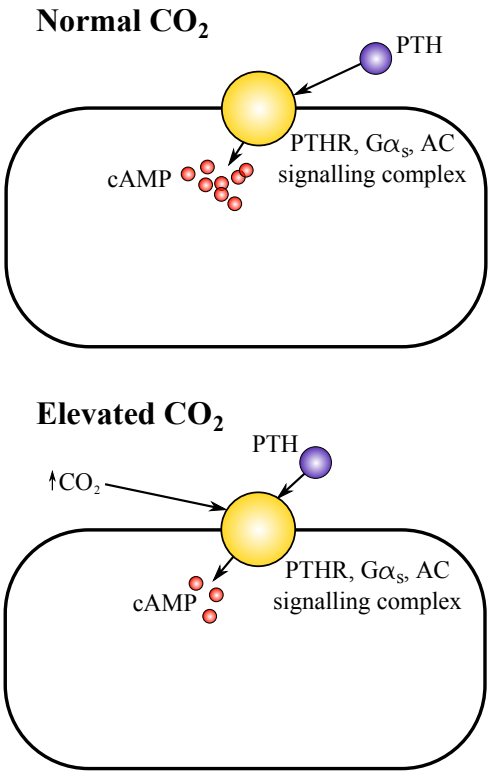

Figure 28: Chapter 3 overview of signalling events at normal and elevated CO_2. Normal CO_2: PTH activation of the AC signalling complex increases cAMP levels. Elevated CO_2: CO_2 blunts the PTH activation of AC leading to a reduction in cAMP production.

4 Chapter 4: Ca^{2+} Ion Requirement in the Inhibition of cAMP Production at Elevated CO_2

4.1 Introduction

Chapter 3 presented evidence for a pH independent inhibition of cAMP production under hypercapnic conditions. This trend is true for multiple cell lines (HEKPR1, OK and UMR-106), making it potentially common across species and tissue types, and is independent of the mechanism of AC activation: present with both PTH and FSK agonists. This latter fact not only suggests that the hypercapnic mechanism is independent of the AC isoform (PTH couples specifically to AC VI in HEKPR1 cells (Tovey et al., 2008) whilst FSK activates all tmAC isoforms (Zhang et al., 1997)), but also that CO_2 is not interacting with a protein upstream from the AC.

This chapter is concerned with investigating the hypercapnic phenomena in more depth, elucidating whether any of the known AC interacting signalling pathways are involved in generating the observed inhibition of cAMP generation. To do this, cAMP accumulation assays were repeated with a range of pharmacological antagonists (including inhibitors and chelators) to eliminate possible intervening pathways. Verification of a component's involvement was based on the assumption that its inhibition would remove the CO_2 constraint on AC, i.e. giving similar cAMP levels at 10% CO_2 (v/v) to that at 5% CO_2 (v/v). As will be shown in Section 4.3, this assumption held true for BAPTA-AM, implying that intracellular calcium ions are required to inhibit AC at elevated CO_2.

Futher antagonist assays led to the conclusion that these calcium ions were released from the ER via the IP_3 receptor. Due to the relative non-specificity of pharmacological antagonists, this conclusion was further examined using a genetic approach with two DT40 cell lines (chicken B lymphoblasts). These cells were also used to demonstrate CO_2 dependent Ca^{2+} release, independent of intracellular pH. Together these results demonstrate a blunted cAMP response to agonist activation at elevated CO_2, which is both pH independent and reliant on Ca^{2+} release from IP_3 receptors.

4.2 Cell Lines Used in Experimentation

Throughout this chapter the renal derived lines OK and HEKPR1 (Section 3.2) are primarily used. Three further lines are implemented, A549 (human alveolar epithelial cells (Giard et al., 1973)) and two DT40 lineages: DT40-K/O (Sugawara et al., 1997) and DT40-IP_3 R1 (Laude et al., 2005). Descriptions of these cells and information regarding their usage can be found in the following sections.

4.2.1 A549 cells

The A549 cell line (Giard et al., 1973) was initiated from a human alveolar adenocarcinoma and has been identified as a type II alveolar epithelial cell line (Lieber et al., 1976). Culture of these cells is straightforward and their growth rate high, therefore they were implemented as a useful non-PTH sensitive cell to confirm the capnic effect on AC/cAMP and its requirement for Ca^{2+} ions. The data from these cells infers the presence of a more general hypercapnic trend across cell lineages, independent of the PTH signalling pathway.

4.2.2 DT40 cells

DT40 cells are B lymphoblasts harvested from a Hyline SC chicken bursal lymphoma induced by the avian leukosis virus (Baba et al., 1985). These cells were used to provide genetic evidence for a role for calcium release from IP_3 receptors in the AC response to elevated CO_2 (Section 4.6). Two lineages were used: DT40-K/O (Sugawara et al., 1997) and DT40-IP_3R1 (Laude et al., 2005), both cell lines manipulated with respect to their IP_3 receptors. DT40-K/O cells have both alleles for all three of the IP_3 receptor genes disrupted by sequential homologous recombination within the region that encodes the transmembrane domain and thus produce no detectable transcripts or translation products from the IP_3R genes, nor do they exhibit any IP_3 sensitive stores (Sugawara et al., 1997). Using these cells to investigate a contribition of Ca^{2+} ions from an IP_3 receptor controlled store is particularly useful as the absence of any IP_3R genes provides a null background for IP_3 production (Tovey et al., 2006). DT40-IP_3R1 cells are DT40-K/O cells with the rat gene for IP_3 receptor 1 re-introduced by transfection (Laude et al., 2005). Due to the functional redundancy of the IP_3 receptor isoforms, even if only one isoform is present the cells behave as normal with all IP_3 related signalling events returning (Sugawara et al., 1997), thus giving these cells their value. As will be

explained in Section 4.6, CO_2 induced inhibition of cAMP production was abolished with DT40-K/O cells and returned with DT40-IP_3R1 cells. This result provides genetic proof for the requirement of IP_3R derived Ca^{2+} ions in this phenomenon.

4.2.3 cAMP Agonist Responses in A549 and DT40 Cell Lines

All cell lines were tested for a cAMP response to agonist. As all of these lines are insensitive to PTH, only 10 μM FSK was implemented. Figure 29 displays cAMP accumulation in each line in response to both a DMSO negative control and FSK. Data for A549 cells is presented as normalised values of [^{3}H]-cAMP compared to total cell labelling (Section 2.4.6). DT40 cells required use of an ELISA due to complications with suspension cells clogging the chromatography columns usually used. Thus, values are presented as the sample cAMP concentration normalised to protein content (as calculated through use of a Bradford assay, see Section 2.6.2 and Appendix 7.2). P-values were calculated via a two-sample T-test. All three cell lines respond to FSK and therefore are suitable for use in further experiments.

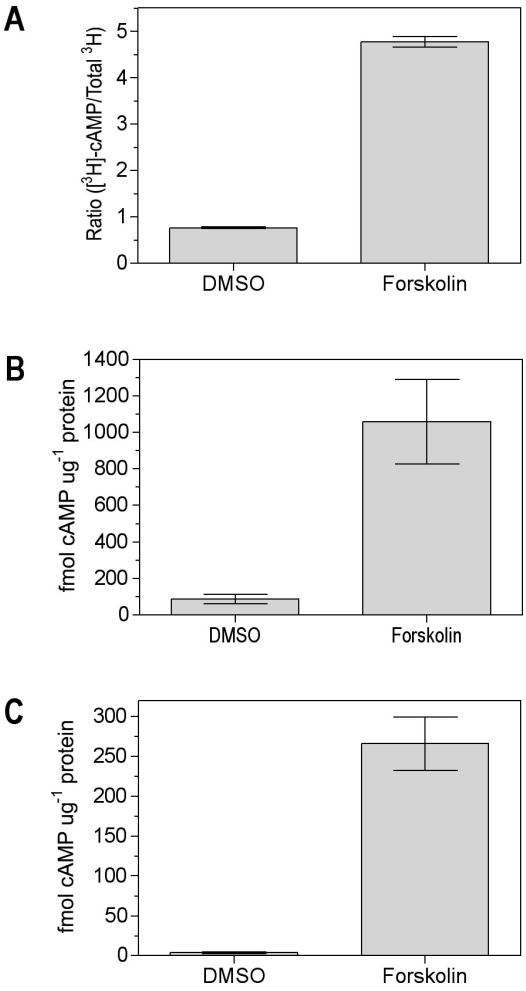

Figure 29: cAMP accumulation agonist responses in A549, DT40-K/O and DT40-IP_3R1 cell lines.

Agonist response at 5% CO_2 (v/v) and pH 7.5. Agonist concentration of 10 μM FSK with DMSO negative control.

A: A549 cells, $n = 4/8$, P-value 3.19 x 10^{-9}

B: DT40-K/O, $n = 6$, P-value 1.09 x 10^{-2}

C: DT40-IP_3 R1, $n = 6$, P-value 3.19 x 10^{-5}

4.3 The Role of Ca^{2+} Ions in AC Inhibition at Elevated CO_2

4.3.1 HEKPR1 cells

In order to characterise the capnic response, it is important to ascertain whether AC is the site of CO_2 action. Through cAMP accumulation experiments in the presence of various antagonists, other signalling pathways can be ruled out based on the assumption that if the same trends are found whist a pathway is inhibited (i.e. a significant reduction in cAMP at 10% [v/v] CO_2) then it is unlikely to be involved. Conversely, production of cAMP levels with 10% (v/v) CO_2 similar to the normocapnic values, would implicate the disrupted cell signalling pathway.

Section 3.5 demonstrated that the mechanism of AC stimulation, by PTH or FSK, made no difference to the resultant trend. Therefore, all inhibitor assays used 10 μM FSK. This decision simplified the assayed system as FSK activates the AC enzyme directly, binding via hydrophobic pockets on its second catalytic domain (Zhang et al., 1997). Use of PTH, known to also stimulate IP_3 generation leading to Ca^{2+} release (Hruska et al., 1987; Pines et al., 1996) would potentially offer more complicated results. Similarly, as extracellular pH was also unimportant, all experiments were carried out at pH 7.5. HEKPR1 cells were uniformly used, taking advantage of their fast growth cycle.

Results for a range of antagonists with HEKPR1 cells are shown in Figure 30 with statistical ANOVA analysis presented in Table 12. All data is presented as a percentage of the normocapnic (5% [v/v] CO_2) value for each inhibitor. Negative control data, using DMSO addition instead of agonist, has been omitted for clarity.

Through the retained hypercapnic trends displayed, it can be concluded that the effect of elevated CO_2 on cAMP does not require the activity of cAMP phosphodiesterases (IBMX (Beavo et al., 1970)), soluble adenylyl cyclase (KH7 (Hess et al., 2005)), cAMP dependent protein kinase A (H-89 (Chijiwa et al., 1990)), carbonic anhydrase (acetazolamide (Maren, 1952)), sphingosine kinases 1 and 2 (SKi (French et al., 2003, 2006)/ROMe (Lim et al., 2011) respectively), calmodulin-dependent protein kinase II (autocamtide-II (Hanson et al., 1989)) or protein kinase C (staurosporine (Omura et al., 1977; Tamaoki et al., 1986)/Gö6983 (Gschwendt et al., 1996)). Finally, through the relative non-specificity of staurosporine, other kinases might potentially be ruled out, including protein kinase G, CaM kinase, CDK2-5, GSK-3β, Pim-1 kinase and MLCK (Enzo-Life-Sciences, 2010; Gani & Engh, 2010) but further experiments would be needed to confirm this.

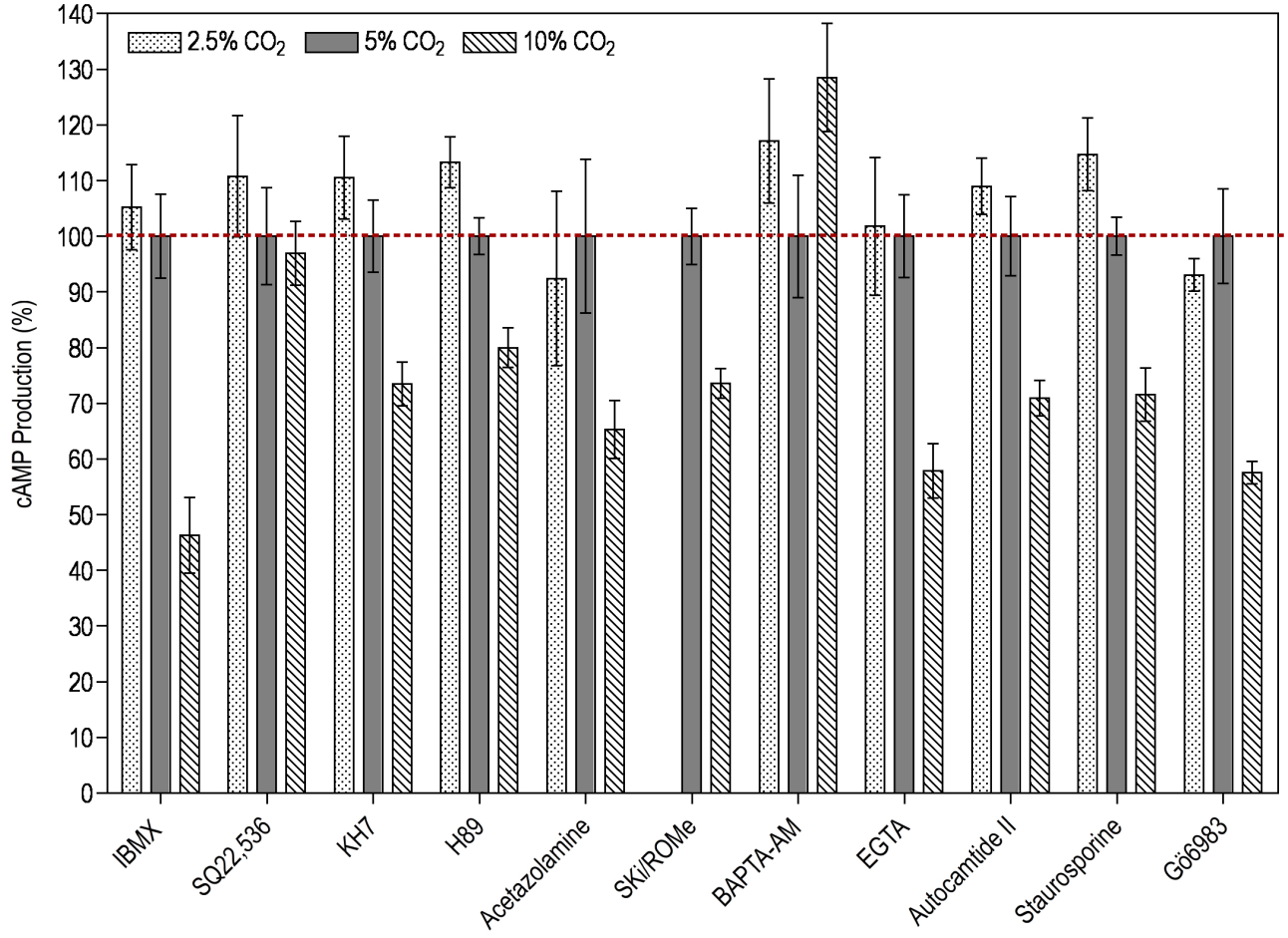

Figure 30: HEKPR1 cell inhibitor assays at 2.5% (v/v), 5% (v/v) and 10% (v/v) CO_2 where avaliable. Agonist concentration of 10 μM FSK, pH 7.5, n $\geq$ 4. Results shown as a percentage of the 5% (v/v) CO_2 value for each inhibitor.

Comparison	Agonist(PTH/FSK)	
	Difference	P value
IBMX		
2.5% vs 5%	-5.260	$P \geq 0.05$
2.5% vs 10%	-58.99	$P \leq 0.001$
5% vs 10%	-53.73	$P \leq 0.001$
SQ 22, 536		
2.5% vs 5%	-10.77	$P \geq 0.05$
2.5% vs 10%	-13.85	$P \geq 0.05$
5% vs 10%	-3.077	$P \geq 0.05$
KH7		
2.5% vs 5%	–10.50	$P \geq 0.05$
2.5% vs 10%	-37.02	$P \leq 0.01$
5% vs 10%	-26.52	$P \leq 0.05$
H89		
2.5% vs 5%	-12.81	$P \geq 0.05$
2.5% vs 10%	-33.28	$P \leq 0.01$
5% vs 10%	-20.00	$P \leq 0.05$
Acetazolamide		
2.5% vs 5%	7.570	$P \geq 0.05$
2.5% vs 10%	-39.81	$P \leq 0.001$
5% vs 10%	-27.00	$P \leq 0.05$
SKi/ROMe		
2.5% vs 5%	-	-
2.5% vs 10%	-	-
5% vs 10%	-25.14	$P \leq 0.01$

Comparison	Agonist(PTH/FSK)	
	Difference	P value
BAPTA-AM		
2.5% vs 5%	-17.10	$P \geq 0.05$
2.5% vs 10%	11.40	$P \geq 0.05$
5% vs 10%	28.50	$P \leq 0.05$
EGTA		
2.5% vs 5%	-1.794	$P \geq 0.05$
2.5% vs 10%	-43.95	$P \leq 0.001$
5% vs 10%	-42.15	$P \leq 0.001$
Autocamtide II		
2.5% vs 5%	-8.995	$P \geq 0.05$
2.5% vs 10%	-38.10	$P \leq 0.01$
5% vs 10%	-29.10	$P \leq 0.01$
Staurosporine		
2.5% vs 5%	-14.72	$P \geq 0.05$
2.5% vs 10%	-43.19	$P \leq 0.001$
5% vs 10%	-28.47	$P \leq 0.05$
Gö6983		
2.5% vs 5%	6.962	$P \geq 0.05$
2.5% vs 10%	-35.44	$P \leq 0.01$
5% vs 10%	-42.41	$P \leq 0.001$

Table 12: Statistical analysis of HEKPR1 inhibitor data: two-way ANOVA analysis with post hoc Boniferroni testing. Percentages of CO_2 concentration given as v/v.

Within these conclusions, there are some interesting points to note. First, despite overwhelming evidence in the literature for Ci stimulation of sAC, this AC isoform did not appear to contribute to the hypercapnic inhibition observed, whilst the lack of CO_2 effect with tmAC inhibitor SQ 22, 536 (Harris et al., 1979) demonstrated the requirement for G-protein activated tmAC. This reflects growing evidence towards a regulatory role for Ci with tmACs. Use of SQ 22, 536 reduced cAMP levels, as expected, though this result is deceptive when viewed as a percentage of the 5% (v/v) CO_2 value as presented in Figure 30 and can be seen clearly in Figure 31 where each value is normalised to a 5% (v/v) CO_2 IBMX containing control, run simultaneously. SQ 22, 536 addition halved the level of cAMP accumulated across all CO_2 concentrations but did not completely ablate cAMP production due to incomplete inhibition by the antagonist.

Second, the carbonic anhydrase inhibitor acetazolamide had no effect, demonstrating that there is no requirement for the CO_2 present in the media to be converted to HCO_3^- to inhibit the AC (Guo et al., 2009; Huckstepp et al., 2010a).

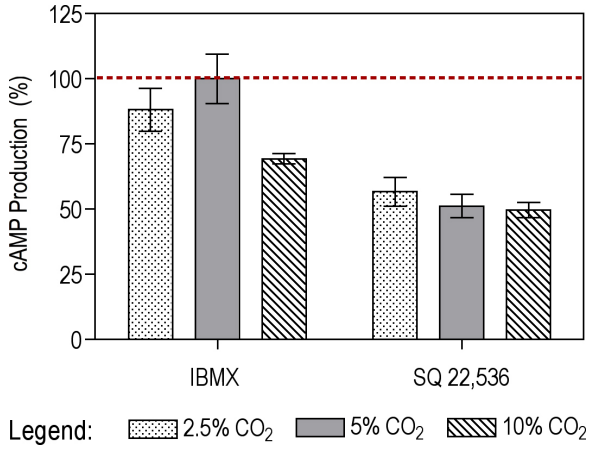

Figure 31: True values for SQ 22, 536 assay. Agonist concentration of 10 μM FSK, pH 7.5, $n = 8$. Results shown as a percentage of the 5% (v/v) CO_2 IBMX containing sample.

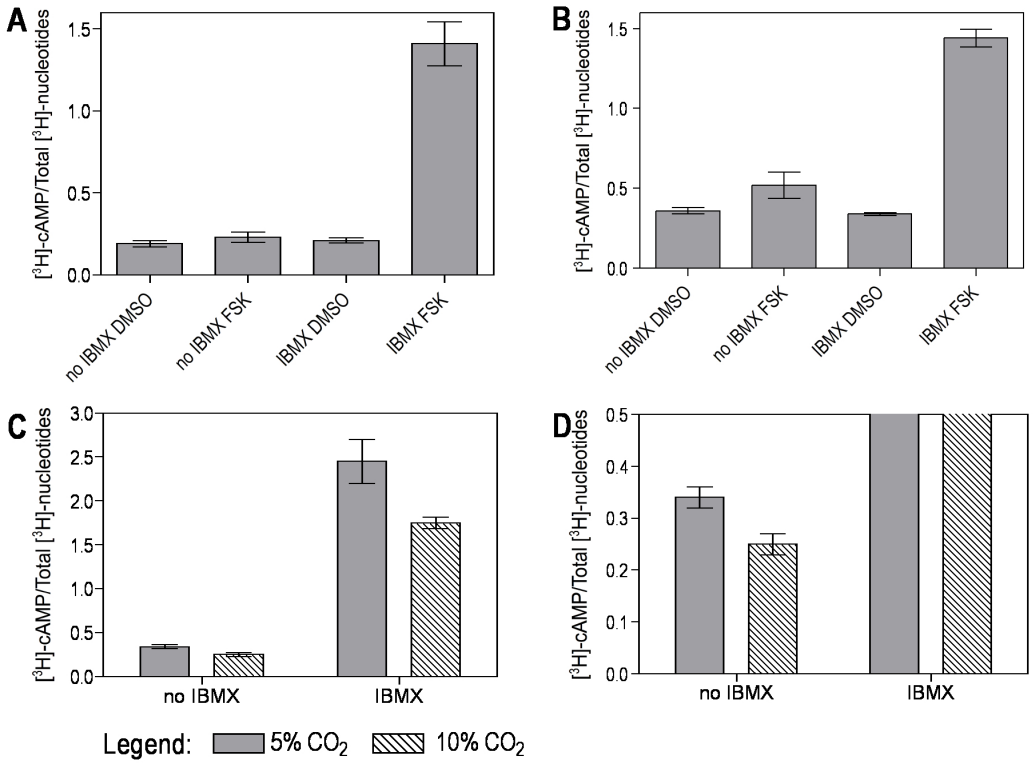

Figure 32: Usage of PDE inhibitor IBMX. Agonist concentration of 10 μM FSK with DMSO negative control, pH 7.5. **A**: OK cells, $n = 6$, **B**: HEKPR1 cells, $n = 6$, **C**: HEKPR1 cells exposed to 5% and 10% (v/v) CO_2 in the presence or absence of IBMX, $n = 6$. T-tests for cAMP accumulation in response to different capnic states: No IBMX = 0.0221, IBMX = 0.0385, **D**: Data presented in C with y-axis enlarged to highlight cAMP levels in the absence of IBMX.

Of note are the data from the two Ca^{2+} chelators EGTA and BAPTA-AM. Whilst the extracellular calcium chelator EGTA (Christian et al., 1965) had no effect on the cAMP trend, it was abolished by the membrane permeable intracellular calcium chelator BAPTA-AM (Lew et al., 1982). Although statistical analysis comparing 5% and 10% (v/v) CO_2 for BAPTA-AM showed a significant difference this represented an increase in cAMP accumulation at elevated CO_2 opposed to the expected decrease. Therefore, the CO_2 dependent inhibition of cAMP production is reliant on calcium ions that are provided from an intracellular source. It is important to note that chelator affinity for Ca^{2+} is often altered by pH (Christensen et al., 2002), although both EGTA and BAPTA-AM maintain suitable affinities within the pH range required: the calcium affinity of BAPTA-AM has been shown to remain relatively constant between pH levels of 6.0 and 7.5 (Tsien, 1980). Chelators of this type will also bind other divalent cations such as Mg^{2+} which, as the co-factor metal required by AC, could inhibit cAMP production. However, this is unlikely to be a problem as BAPTA-AM has a selectivity for Ca^{2+} of more than 10^5 higher than that for Mg^{2+}, giving a Ca^{2+} dissociation constant of 1.1 x 10^{-7} M (Tsien, 1980).

As noted in Chapter 3, the hypocapnic CO_2 concentration of 2.5% (v/v) was abandoned in later experimentation, however, this pCO_2 was included in these experiments (with the exception of SKi/ROMe) to identify whether any of the interacting signalling pathways could alter cAMP accumulation at this concentration. As all values were statistically similar to 5% (v/v) CO_2, none of the tested signalling components had an impact on cAMP levels at reduced CO_2.

All cAMP accumulation assays are carried out in the presence of the non-selective phosphodiesterase antagonist IBMX (Acin-Perez et al., 2011). Inhibition of these enzymes is necessary to enable comparision of cAMP levels under different conditions and without it the cAMP turnover is too high and resultant levels too low to measure accurately by this method (Figure 32). Figure 32 also demonstrates blunted cAMP levels at 10% (v/v) CO_2 in both the presence and absence of IBMX, suggesting that this antagonist is not the causitive agent of this hypercapnic effect. Use of this antagonist is accepted widely as cAMP levels are not easily measured without it, due to the aforementioned high phosphodiesterase turnover (Caverzasio et al., 1986).

4.3.2 OK cells

Section 4.3.1 demonstrated that the reduction in cAMP levels with elevated CO_2 required an availability of intracellular calcium in HEKPR1 cells. This conclusion was drawn from the observation that intracellular calcium chelator BAPTA-AM removed the cAMP decrease at 10% (v/v) CO_2, whilst extracellular chelator EGTA did not. Further cAMP accumulation assays with both EGTA and BAPTA-AM were then repeated using OK cells. Experiments were carried out under identical conditions to HEKPR1 cells for comparison and only 5% (v/v) and 10% (v/v) CO_2 concentrations were employed. Results are presented in Figure 33 as percentages of the normocapnic value for each inhibitor. DMSO negative controls have been omitted for clarity. Statistical analysis was via a two sample t-test with values presented in the figure caption.

These results confirm conclusions drawn from HEKPR1 data, that the reduction in cAMP levels at elevated CO_2 requires intracellular calcium. This conclusion can be drawn from the evidence that both control IBMX and EGTA values have statistically different cAMP production at 5% (v/v) compared to 10% (v/v) CO_2, with both p-values below 0.05. Inclusion of intracellular calcium chelator BAPTA-AM, however, resulted in statistically similar cAMP production at both CO_2 concentrations, with a p-value of 0.097. This indicates that Ca^{2+} release from an intracellular source is required for elevated CO_2 to blunt the production of cAMP and that this Ca^{2+} requirement is neither cell line nor species specific.

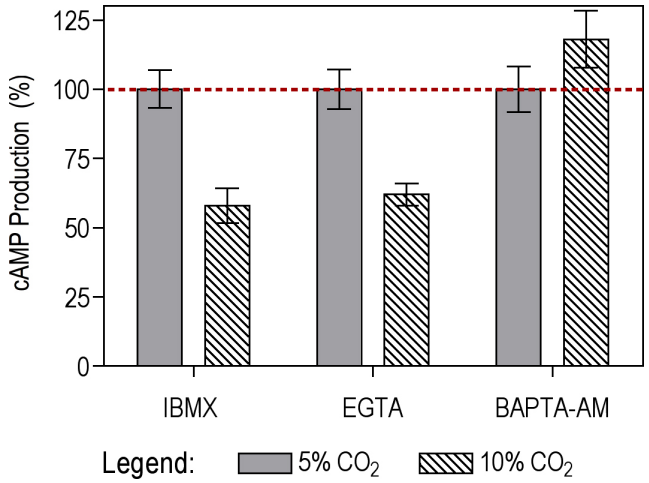

Figure 33: OK cell inhibitor assays at 5% and 10% (v/v) CO_2. Agonist concentration of 10 μM FSK, pH 7.5, n $\geq$ 4. Results shown as a percentage of the 5% (v/v) CO_2 value. T-test p-values as follows: IBMX, 8.75 x 10^{-3}; EGTA, 1.00 x 10^{-3}; BAPTA-AM, 9.70 x 10^{-2}

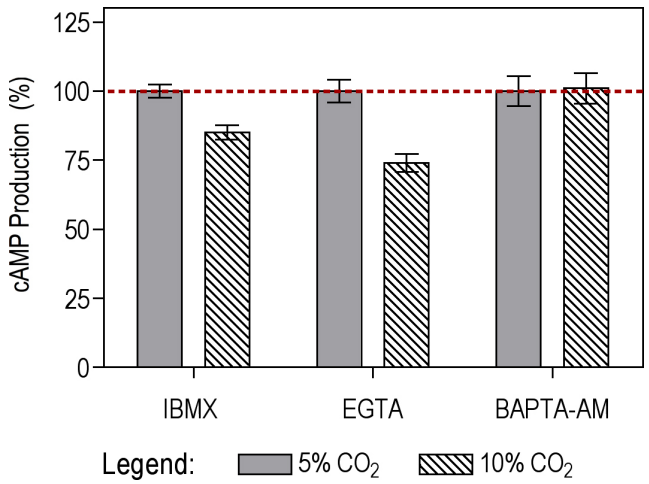

Figure 34: A549 inhibitor assay. Agonist concentration of 10 μM FSK, pH 7.5, n $\leq$ 7. Results shown as a percentage of the 5% (v/v) CO_2 value. T-test p-values as follows: IBMX, 1.37 x 10^{-3} ; EGTA, 2.15 x 10^{-4}; BAPTA-AM, 7.97 x 10^{-1}.

4.3.3 A549 cells

Experiments so far have taken place in cell lines responsive to PTH and containing at least part of the signalling machinery to sense this hormone and bring about the correct physiological outcome. Results presented in this chapter suggest the possibility that the effects of elevated CO_2 on cAMP and Ca^{2+} signalling might be a general effect, especially as results from Chapter 3 demonstrated that the mechanism of AC activation did not alter the outcome. To test this hypothesis, key inhibitor assays were repeated using A549 cells (Giard et al., 1973), an alveolar epithelial cell line unresponsive to PTH. Figure 34 displays these results with values shown as percentages of the normocapnic cAMP level and DMSO negative control data has been omitted for clarity.

These data sets confirm the trends shown previously, that 10% (v/v) CO_2 causes a reduction in cAMP compared to 5% (v/v), a trend unaffected by chelation of extracellular calcium by EGTA, but abolished by intracellular calcium chelator BAPTA-AM, which gave a p-value of 0.797. This result suggests that the effect of hypercapnia on the cell is a general cellular phenomenon, although it must be noted that all of the cell lines tested are of epithelial nature and lineage.

4.4 CO_2 Sensitive Calcium Store Identified as the ER

As shown in Section 4.3, the CO_2 induced decrease in cAMP levels is dependent on intracellular calcium as the cell permeable calcium chelator BAPTA-AM ablated the expected inhibition of AC activity. As an important signalling molecule in its own right, Ca^{2+} levels are tightly controlled throughout the cell. In metazoans cytosolic calcium is maintained at nanomolar concentrations, with the bulk of the Ca^{2+} ions stored in discrete subcellular organelles, in addition to being available from outside the cells where the concentrations are in the millimolar range (Christensen et al., 2002). More detail on this storage and release of Ca^{2+} can be found in Section 1.4.

In order to establish which source was providing these calcium ions, pharmacological antagonists were used to inhibit calcium release from each intracellular compartment: bafiliomycin A1 (Werner et al., 1984) inhibiting release from NAADP sensitive lysosomal granules (Christensen et al., 2002), thapsigargin (Rasmussen et al., 1978) for the ER, nifedipene (Fleckenstein et al., 1972; Vater et al., 1972) inhibiting L-type calcium channels in the plasma membrane, and rotenone (Geoffroy, 1895) for the mitochondria. These experiments were repeated for both HEKPR1 and OK cells and results are presented in Figures 35 and 36. Data is displayed as a percentage comparison of the normocapnic 5% (v/v) CO_2 value with negative control DMSO values omitted for clarity. Statistical analysis was by two sample t-tests and values are presented within the figure captions. Bafilomycin A1 results are only presented for OK cells.

Based on the assumption that inhibition of a source required to provide the calcium ions would remove the expected drop in cAMP production at 10% (v/v) CO_2, these data sets indicate that the calcium ions are likely to be released from the ER, as thapsigargin abolishes this trend in both cell lines (in fact significantly reversing it in OK cells). Thapsigargin is an antagonist of sarcoplasmic/endoplasmic reticulum Ca^{2+}-ATPases (SERCAs) (Thastrup et al., 1990; Lytton et al., 1991), disruption of which unmasks a constitutive leak of Ca^{2+} from the ER by blocking calcium uptake (Mason et al., 1991; Thastrup et al., 1990). Thus, the ER store is emptied of Ca^{2+} and cannot be rejuvenated, rendering it unable to respond to any further stimulus for the controlled release of Ca^{2+} ions. Based on this, abolition of the cAMP inhibition by CO_2 can be reasonably inferred to require ER derived calcium ions.

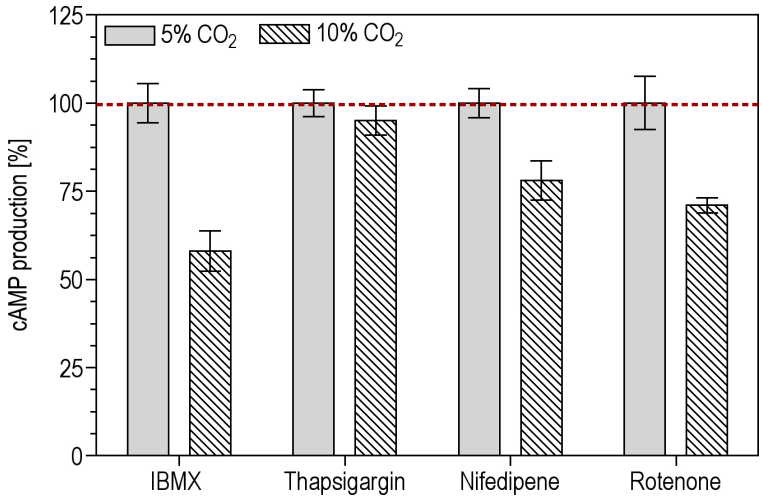

Figure 35: HEKPR1 cell calcium store inhibitor assays. Agonist concentration of 10 μM FSK, pH 7.5, n $\geq$ 8. Results shown as a percentage of the 5% (v/v) CO_2 value for each inhibitor. T-test p-values as follows: IBMX, 2.01 x 10^{-3} ; Thapsigargin, 0.36; Nifedipene, 7.10 x 10^{-3}, Rotenone, 1.93 x 10^{-3}

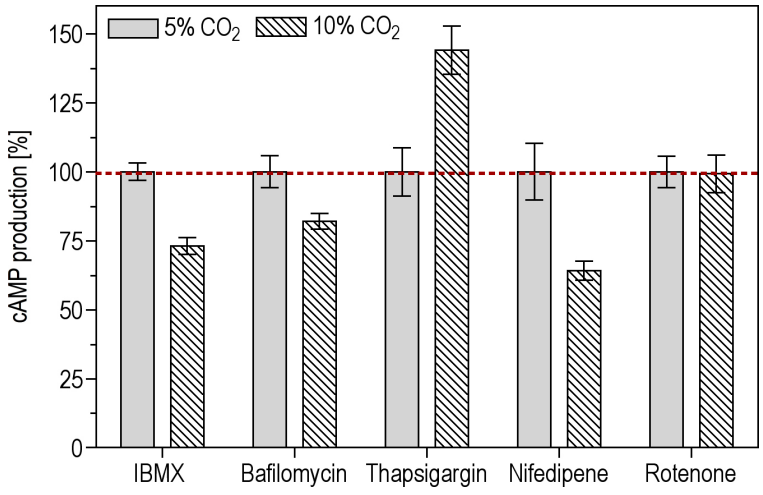

Figure 36: OK cell calcium store inhibitor assays. Agonist concentration of 10 μM FSK, pH 7.5, n $\geq$ 6. Results shown as a percentage of the 5% (v/v) CO_2 value for each inhibitor. T-test p-values as follows: IBMX, 1.54 x 10^{-4} ; Bafilomycin A1, 2.28 x 10^{-2} ; Thapsigargin, 5.012.28 x 10^{-3}; Nifedipene, 1.27 x 10^{-2}, Rotenone, 9.20 x 10^{-3}

The use of nifedipene, a dihydropyridine antagonist exclusive to L-type calcium channels (Hayashi et al., 2007) in these cells is controversial in that their expression in HEK 293 parent cells is dubious due to the fact that the calcium channels present cannot be attributed to any particular class (Berjukow et al., 1996). Although most of the calcium channels show more similarities to the low-voltage activated E- and T-type channels (Berjukow et al., 1996), an endogenous L-type signal can be detected (Zong et al., 1995), especially if the cells have been serum starved prior to experimentation, which leads to an increase in endogenous calcium channel density (Berjukow et al., 1996). As these cAMP accumulation experiments occur after a similar overnight starvation, this detail may be relevant. In fact, the α subunit of L-type channels has been detected all over the rat kidney, including cells of the proximal tubules (Zhao et al., 2002), where both HEKPR1 and OK cells are purported to originate. Therefore, use of nifedipene is a valid experiment, especially as antisense oligonucleotides to the α_{1D} subunit inhibit PTH induced calcium influx (Barry et al., 1998) and PTH stimulated cAMP can phosphorylate the α_{1C} receptor subunit enhancing channel opening (Zhao et al., 2002). As presented in Figures 35 and 36, L-type channels are not the source of Ca^{2+} ions required to inhibit cAMP production with elevated CO_2, a result further supported by trends gained using the non membrane permeable calcium chelator EGTA as both antagonists imply that an extracellular source of Ca^{2+} ions is not required.

Most results presented so far have been confirmed through the usage of two cell lines. Here, however, there is discrepancy between the rotenone results for HEKPR1 and OK cells. Whilst the results from OK cells implicate mitochondrial calcium in the CO_2 effect, HEKPR1 cell results do not. Calcium is stored in the mitochondria and whilst the organelle does have Na^+/Ca^{2+} or H^+/Ca^{2+} exchangers for the release of Ca^{2+} ions into the cytosol, it predominantly acts as a calcium sink via its Ca^{2+} uniporter (Walsh et al., 2009). In fact, as described in Section 1.4, mitochondria have more of an indirect influence on Ca^{2+} signalling through changing the cellular concentrations of ATP, NAD(P)H, pyruvate and reactive oxygen species (Walsh et al., 2009). Therefore rotenone, which primarily disrupts the electron transport chain, is a useful antagonist, shown previously to abolish calcium signals and cellular oscillations in many cell types (Walsh et al., 2009). However, as rotenone primarily interferes with the electron transport chain preventing ATP formation coupled to respiration, it will have multiple effects on the cell, thus leading to this discrepancy between results. Nevertheless, based on this knowledge and the HEKPR1 pattern, it is unlikely that mitochondrial calcium is involved in the cAMP capnic effect or at most it is a minor contributor compared to the ER.

Finally, ER calcium store depletion is known to trigger Ca^{2+} influx through the plasma membrane via 'capacitative Ca^{2+} entry' (Putney, 1986; Kwan et al., 1990), noted previously with use of thapsigargin (Gouy et al., 1990; Takemura et al., 1989; Mason et al., 1991). Although this Ca^{2+} entry may be being inhibited with the concentration of thapsigargin implemented (Mason et al., 1991), capacitative entry may still be occuring. To eliminate the possibility that this source of Ca^{2+} ions were activating the AC at elevated CO_2 with thapsigargin, leading to erroneous conclusions, an additional set of experiments was undertaken with OK cells, using thapsigargin in combination with intracellular calcium chelator BAPTA-AM. The premise of these experiments was that BAPTA-AM should chelate any Ca^{2+} ions which enter the cell via this method. This data, provided as a percentage of the 5% control (Figure 37), shows a lack of cAMP reduction at 10% (v/v) CO_2, implying that Ca^{2+} activation from this source is not required. In addition, this result also proves that the transient efflux of Ca^{2+} from the ER with application of thapsigargin is also not stimulating any AC isoforms.

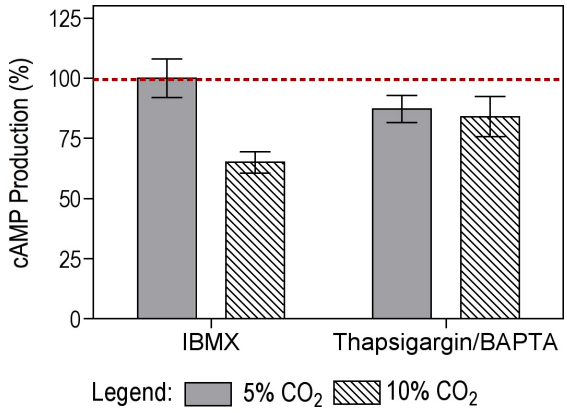

Figure 37: Thapsigargin and BAPTA-AM assay. Agonist concentration of 10 μM FSK, pH 7.5, $n = 9$. Results shown as a percentage of the 5% (v/v) CO_2 value for each inhibitor. T-test p-values as follows: IBMX, 1.53 x 10^{-3}; Thapsigargin/BAPTA-AM, 8.30 x 10^{-1}

Together the results displayed in Figures 35, 36 and 37 give evidence that the capnic effect of inhibiting cAMP production requires Ca^{2+} release from the endoplasmic reticulum in both OK and HEKPR1 cell lines.

4.5 Pharmacological Determination of the ER Calcium Source

Sections 4.3 and 4.4 display evidence that the blunted cAMP production at elevated CO_2 levels required intracellular Ca^{2+} ion release from the ER, based upon cAMP accumulation assays in the presence of BAPTA-AM and thapsigargin. The ER, being the principal cellular calcium store, provides Ca^{2+} ion release via a number of mechanisms, namely via IP_3 receptors (Ross et al., 1989) or ryanodine receptors, RyRs (Pessah et al., 1985). By emptying this store of calcium using thapsigarin, these routes will both be abolished (Galione, 2006), necessitating further experiments to determine which route was involved in the capnic response. To achieve this, further pharmacological antagonists were implemented in cAMP accumulation assays. In addition to the IP_3 receptor inhibitors 2-APB (Maruyama et al., 1997) and Xestospongin C (Gafni et al., 1997) and the RyR inhibitor dantrolene (Snyder et al., 1967), two further inhibitors U-73122 (Bleasdale et al., 1989) and Sto-609 (Tokumitsu et al., 2002) were also used. These chemicals inhibit phospholipase (PLC) and Ca^{2+}/calmodulin-dependent protein kinase kinase (CaM-KK) respectively, enzymes of potential interest. PLC catalyses an important Ca^{2+} signalling reaction, the production of IP_3 and DAG from PIP_2 (Section 1.4) and CaM-KK has recently been implicated in the transduction of a CO_2 induced Ca^{2+} ion release in alveolar epithelial cells to Na^+/K^+-ATPase, causing endocytosis of this pump and thus impaired alveolar fluid reabsorption (Vadász et al., 2008b). While the most obvious regulator of RyRs is the plant alkaloid ryanodine itself, this chemical has a biphasic effect. Ryanodine activates the channel at low concentrations ($\leq$ 10 μM) by stabilising it in a subconductance state, and an inhibits only at higher levels ($\geq$ 100 μM) by locking the channel closed (Querfurth et al., 1998). Use of this regulator could potentially lead to erroneous conclusions due to its biphasic effect. Dantrolene was therefore employed, which is known to inhibit both RyRs and their effects on Ca^{2+} induced Ca^{2+} release (Ohta et al., 1990).

As prior conclusions have been found to be true for both HEKPR1 and OK cell lines, here assays only used OK cells, as the most physiologically relevant line. Data collected from these experiments is presented in Figure 38. Results are presented as percentages of the 5% (v/v) value for each antagonist, with DMSO negative controls omitted for clarity. Two sample T-test p-values are presented in the figure caption.

From these data sets, it can be concluded that RyRs, CaMKK-α, CaMKK-β and PLC activity are not required to inhibit AC at elevated CO_2. The latter two inferences are significant as they imply that the effect of elevated CO_2 on cells is not via the same CaMKK-β dependent route identified

recently by *Vadasz et al.* (Vadász et al., 2008b) and also that any potential Ca^{2+} release from IP_3 receptors is unlikely to be a result of PLC derived IP_3 production, the most likely route. However, the efficacy of U-73122 has since been questioned by *Klein et al.* who have demonstrated both inhibition and activation of PLC isoforms by the chemical, as well as a host of other unspecific interactions with signalling molecules (Klein et al., 2011), thus further experimentation into the contribution from this signalling component may be of interest.

Results using IP_3 receptor antagonists are a little more complex. When normalised across experiments, 2-APB implicated IP_3 receptor mediated Ca^{2+} release in the cAMP drop at 10% (v/v) CO_2 whilst Xestospongin C did not. 2-APB occasionally caused cells to lift from the plasticware and it is possible that this may altered results, but as [^{3}H]-cAMP level are normalised to total cell [^{3}H]-adenine nucleotide labelling this variable should not have altered the final values. Despite repetition, this discrepancy between antagonists could not be remedied, nor could a definitive trend be established using Xestospongin C in A549 cells. Therefore, although these data sets do potentially implicate Ca^{2+} release from IP_3 receptors causing the reduction in cAMP production at elevated CO_2, this interpretation could not be unambiguously proven. Further experiments were designed to test this hypothesis, using DT40 cells lines (Section 4.6).

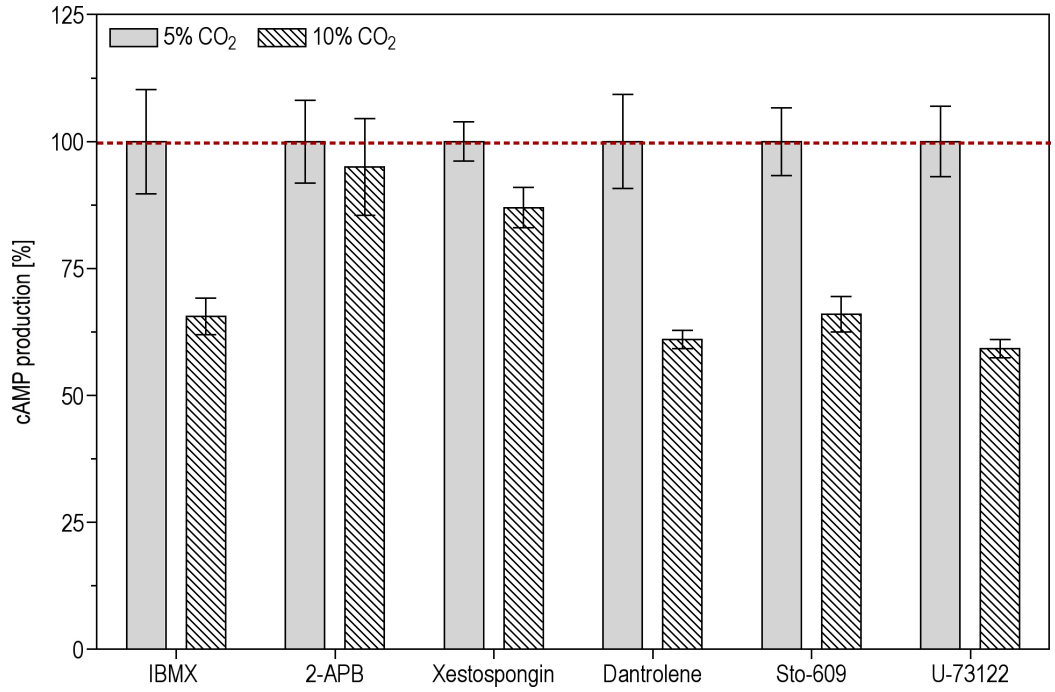

Figure 38: OK cell determination of the ER sensitive store. Agonist concentration of 10 μM FSK, pH 7.5, n $\leq$ 6. Results shown as a percentage of the 5% (v/v) CO_2 value for each inhibitor. T-test p-values as follows: IBMX, 1.01 x 10^{-2} ; 2-APB, 0.81 ; Xestospongin C, 4.37 x 10^{-3}; Dantrolene, 3.38 x 10^{-4}; Sto-609, 1.25 x 10^{-3}; U-73122, 1.95 x 10^{-4}

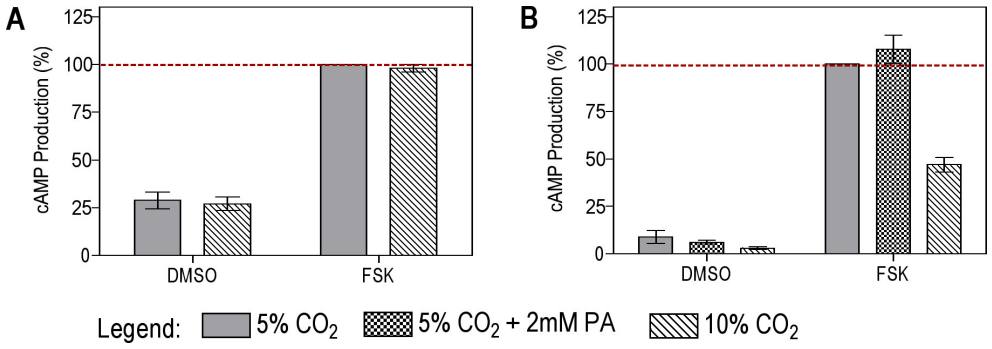

Figure 39: DT40 IP_3 receptor assays. Agonist concentration of 10 μM FSK, DMSO negative control, pH 7.5. Results shown as a percentage of the 5% (v/v) CO_2 value, with error bars generated from across individual experimental replicates. **A**: DT40 K/O, $n = 4$, **B**: DT40 IP3R1, $n = 6$

4.6 Genetic Proof of IP_3R Involvement using DT40 cell line

As presented in Section 4.5, results from pharmacological antagonists in OK cells implied that the hypercapnic effect on cAMP required calcium release via IP_3 receptors in the ER. However, this was not entirely conclusive, due not only to the contradictions presented using the two IP_3R inhibitors 2-APB and Xestospongin C, but also to the inherent fallibility of pharmacological antagonists. To catagorically prove this hypothesis, a genetic approach was employed. Using DT40 cell lines (Section 4.2.2), cAMP accumulation assays were carried out at varying CO_2 concentrations in a cellular environment where IP_3 receptor expression was controlled. Two DT40 cell lines were used: 'DT40-K/O', where both alleles of all three genes for the IP_3 receptor had been disrupted (Sugawara et al., 1997), and 'DT40-IP_3 $_3$R1', which have the rat gene for IP_3 receptor 1 reintroduced by transfection (Laude et al., 2005).

In contrast to all other cell lines used in this thesis, DT40 cells are not an adherant line and instead grow in suspension. Despite effort to adhere these cells to the plasticware for use in cAMP accumulation assays, mimimal adherance was acheived. This was attempted using 5 mg/ml poly-D-lysine similar to the protocol used for HEKPR1 cells (Section 2.3.3) and the published DT40 methodology by *Tovey et al.* (Tovey et al., 2006). In addition, fibronectin (25 μg/ml) and collagen (100 μg/ml) were also tested, although due to the lymphocyte origin of these cells again limited adherance was observed. Therefore, substantial changes to methodology were required for cAMP accumulation assays as detailed in Sections 2.4.3 and 2.6.2, especially as DT40 cAMP levels in response to 10 μM FSK were too low to measure using tritium-labelled methods. DT40 assays instead employed use of an ELISA and cAMP concentrations were normalised to Bradford determined sample protein content.

Results are displayed in Figure 39 and Table 13. Data is presented as a percentage of the 5% (v/v) CO_2 normocapnic cAMP level and statistical analysis was via an ANOVA with post-hoc Boniferroni testing, as displayed in the table.

Comparison	Negative Control - DMSO		FSK Agonist	
	Difference	**P value**	**Difference**	**P value**
DT40-K/O				
5% vs 10%	1.996	$P \geq 0.05$	9.894	$P \geq 0.05$
DT40-IP_3 R1				
5% vs 5% + 2mM PA	-2.742	$P \geq 0.05$	7.712	$P \geq 0.05$
5% vs 10%	-5.877	$P \geq 0.05$	-53.02	$P \leq 0.001$

Table 13: Statistical analysis of DT40 assays: ANOVA analysis with post hoc Bonferroni testing

These results categorically show that Ca^{2+} release from IP_3 receptors is required to blunt the AC response to FSK at elevated CO_2 concentrations. In the absence of any IP_3 receptors, this effect of CO_2 on cAMP was removed (DT40-K/O), whilst re-introduction of an isoform of this receptor restored this response (DT40-IP_3R1). Importantly, use of 5% (v/v) CO_2 with 2 mM PA in DT40-IP_3R1 cells did not ellicit the same response as 10% (v/v) CO_2 and instead gave high cAMP levels similar to that at 5% (v/v), proving this CO_2 effect to be pH-independent. This latter conclusion agrees with the data presented in Chapter 3 for OK, HEKPR1 and UMR-106 cells. Overall these data provide proof of a pH-independent inhibition of cAMP accumulation at elevated CO_2 which requires the release of Ca^{2+} ions from an IP_3 sensitive store.

4.7 Intracellular Ca^{2+} Measurement using Fura 2-AM

The results from the above sections led to the inference that the blunted cAMP response observed at 10% (v/v) CO_2 compared to 5% (v/v) requires the release of Ca^{2+} ions from an intracellular source (BAPTA-AM result from Section 4.3), in particular via IP_3 receptors in the ER (Sections 4.4, 4.5 and 4.6). To test for this CO_2 induced Ca^{2+} release, DT40 cell Ca^{2+} levels were measured under different conditions, using the ratiometric calcium dye Fura 2-AM. Introduced by Roger Tsien in 1985 (Grynkiewicz et al., 1985), Fura 2 combines the tetracarboylate pattern of liganding groups characterisic of Ca^{2+} specific chelators such as EGTA and BAPTA to enhance Ca^{2+} selectivity, a bright stilbene flurophore and a cleavable membrane permeable acetoxymethyl ester group for biological application (Grynkiewicz et al., 1985). This dye exhibits minimal compartmentalism (Paredes et al., 2008), leakage or bleaching (Invitrogen, 2012) during the time-frame of these experiments and the ratiometric element of its measurements limits data variability from the effects of photobleaching, leakage, dye concentration and cell thickness (Hayashi & Miyata, 1994; Invitrogen, 2012). Further advantages of this dye include the fact that it is bright enough to enable measurements of intracellular Ca^{2+} using concentrations unlikely to cause significant Ca^{2+} buffering or damping of Ca^{2+} transients (Invitrogen, 2012), in addition to being relatively unaffected by pH changes within the physiological range (Grynkiewicz et al., 1985), ideal where CO_2 is acting as a variable.

4.7.1 Release of Calcium by Thapsigargin

Prior to exposure to CO_2 concentrations both DT40 cell lines (DT40-IP_3R1 and DT40-K/O) were loaded with Fura-2 AM and intracellular calcium release induced using SERCA antagonist thapsigargin to prove that the instrumentation employed worked correctly and that dye loading conditions were sufficient. Figure 40 provides sample data for thapsigargin responses in both cell lines, proving that experimentation could proceed.

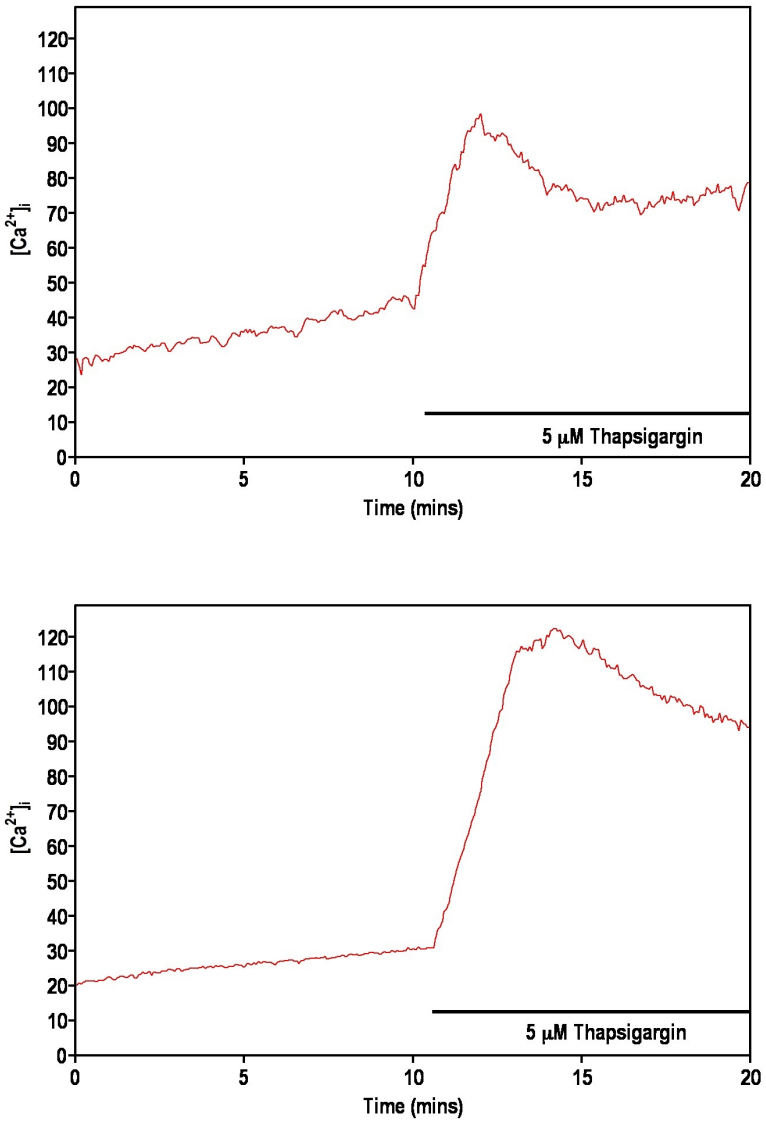

Figure 40: DT40 thapsigargin induced Ca^{2+} release. Agonist concentration of 5μM thapsigargin, pH 7.5. **A**: DT40 K/O, **B** DT40 IP3R1

4.7.2 Release of Calcium by Elevated CO_2

DT40-IP_3R1 and DT40-K/O cells were exposed to 5% (v/v) and 10% (v/v) CO_2 in combination with a number of antagonists of the elements of the Ca^{2+} signalling pathway (Figures 42, 41 and Table 14). Elevated CO_2 induced an increase in intracellular Ca^{2+} concentration in DT4-IP_3R1 cells, on average 116.63% ± 6.81 that of the resting 5% (v/v) CO_2 level. As mentioned previously (Sections 3.3 and 3.8) use of this elevated CO_2 concentration may lead to changes in pHi or pO_2. These variables were eliminated using propanoic acid and gas mix 5% CO_2, 18% O_2, 77 % N_2 (v/v) repectively, both of which failed to increase [Ca^{2+}].

Importantly this Ca^{2+} release appears to be generated via IP_3 receptors as both disruption of IP_3R activity via antagonists 2-APB and Xestospongin C and genetic ablation (DT40-K/O) removed the observed elevation in Ca^{2+} levels at 10% (v/v) CO_2. This result agrees with the inferences made previously in this chapter based on cAMP accummulation data (Sections 4.5 and 4.6).

Interestingly inhibition of PLC by U-73122 also removed the effect of CO_2 on Ca^{2+} release. As PLC cleaves phosphatidylinositol 4,5-bisphosphate to yield diacylglycerol and IP_3, the latter product likely to then activate Ca^{2+} release from IP_3 receptors, this result suggests that the CO_2 sensor is located within or upstream of this pathway. However, when U73-122 was used in cAMP accumulation experiments (Section 4.5) there was no demonstrable effect. This discrepancy may be due to the questionable effects of U73-122 on PLC as evidence in the literature suggests both inhibition and activation of PLC isoforms by the chemical, as well as a host of other unspecific interactions with signalling molecules (Klein et al., 2011). It is also possible that DT40s contain different PLC isoforms to the OK cells employed for cAMP accumulation, with different sensitivities to U73-122 and/or CO_2.

Finally, when extracellular calcium was chelated by EGTA, although the overall effect of CO_2 on Ca^{2+} release was unaffected, the magnitude of this response decreased. Under control conditions with DT40-IP_3R1 cells the percentage increase in Ca^{2+} at 10% (v/v) CO_2 was 116.63% ± 6.81 that of the resting 5% CO_2 level, whilst with EGTA this value was 109.29% ± 2.81. This may suggest that whilst the Ca^{2+} release is from an intracellular source, replenishment of this store from outside the cell is required to maintain signalling while pCO_2 levels are elevated. Such interactions between the ER and extracellular stores of Ca^{2+} are well recognised, supporting this inference (Rosado, 2006; Kwan et al., 1990; Wu et al., 2007)

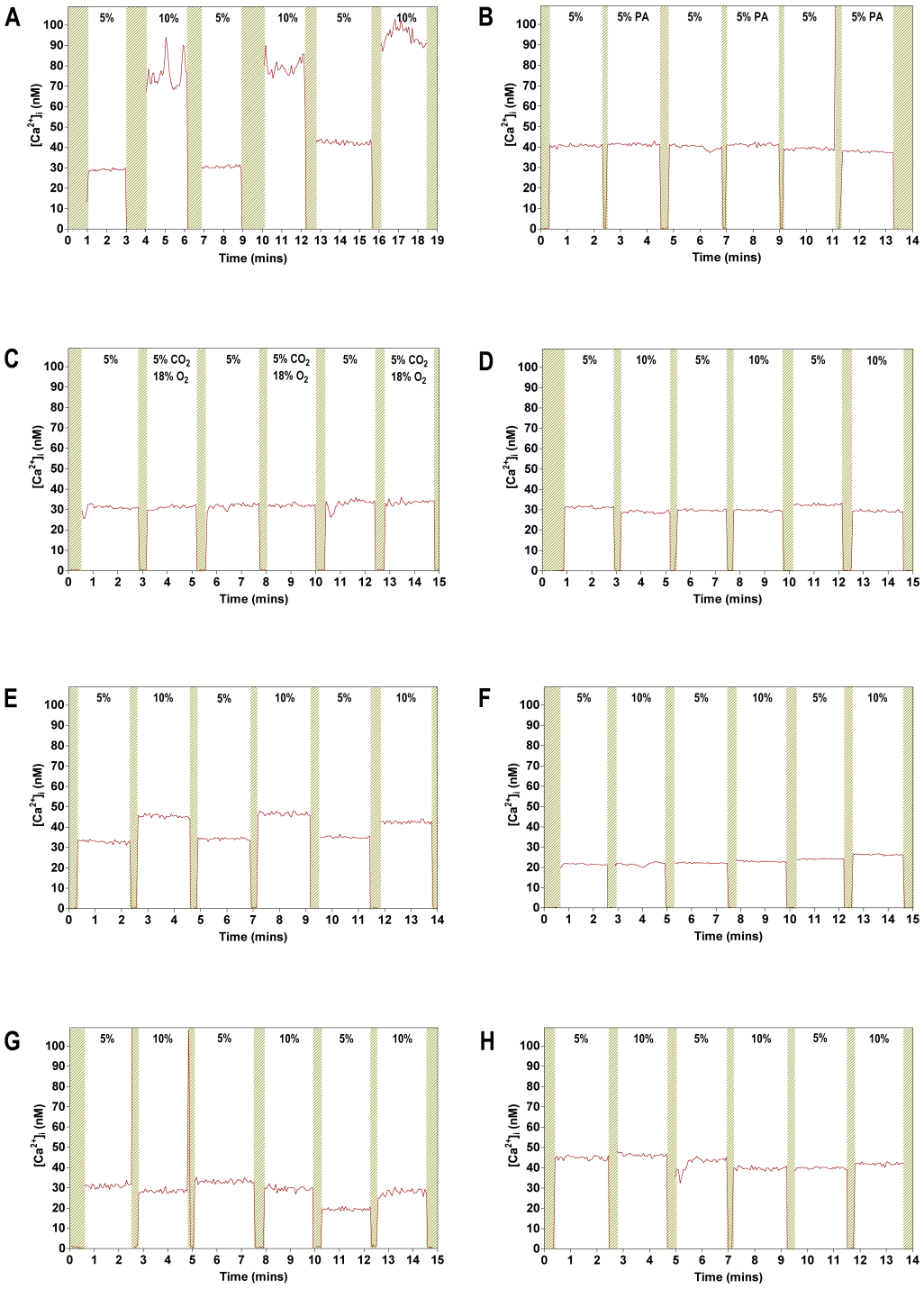

Figure 41: DT40 Ca^{2+} imaging sample graphs, pH 7.5. **A**: DT40 IP_3R1 5 - 10% (v/v) CO_2, Ttest: 1.79 x 10^{-5} **B**: DT40 IP_3R1 5 - 5% (v/v) CO_2 + 2 mM PA, Ttest: 0.844 **C**: DT40 IP_3R1 5 % CO_2 - 5% CO_2, 18% O_2, 77 % N_2 (v/v), Ttest: 0.882 **D**: DT40 K/O 5 - 10% (v/v) CO_2, Ttest: 0.565 **E**: DT40 IP_3R1 no Ca^{2+} and 500 μM EGTA; 5 -10% (v/v) CO_2, Ttest: 1.19 x 10^{-3} **F**: DT40 IP_3R1 5 μM U73-122; 5 - 10% (v/v) CO_2, Ttest: 0.120 **G**: DT40 IP_3R1 100 μM 2-APB; 5 - 10% (v/v) CO_2, Ttest: 0.354 **H**: DT40 IP_3R1 500 nM Xestospongin C; 5 - 10% (v/v) CO_2, Ttest: 0.948

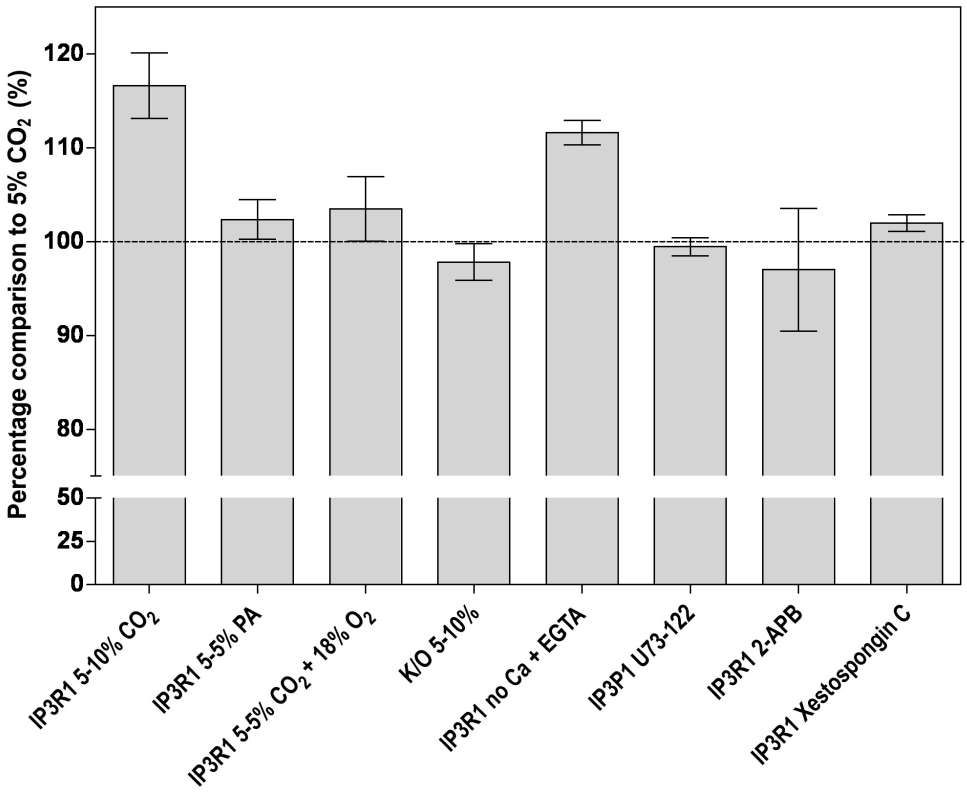

Figure 42: Percentage comparison of Ca^{2+} released at 10% (v/v) CO_2 compared to 5% (v/v) in DT40 cells. Where relevant: 100 μM 2-APB, 500 μM EGTA, 5 μM U73-122, 500 nM Xestospongin C. pH 7.5, $n \geq 4$

Comparison	**Difference**	**P value**
IP3R1 5-10% CO2 vs IP3R1 5-5% PA	14.27	$P \leq 0.05$
IP3R1 5-10% CO2 vs IP3R1 5-5% CO_2 + 18% O_2	13.13	$P \geq 0.05$
IP3R1 5-10% CO2 vs K/O 5-10%	18.8	$P \leq 0.001$
IP3R1 5-10% CO2 vs IP3R1 no Ca + EGTA	5.01	$P \geq 0.05$
IP3R1 5-10% CO2 vs IP3P1 U73-122	17.18	$P \leq 0.05$
IP3R1 5-10% CO2 vs IP3R1 2-APB	19.62	$P \leq 0.001$
IP3R1 5-10% CO2 vs IP3R1 Xestospongin C	14.65	$P \geq 0.05$
IP3R1 5-5% CO2 + 18% O2 vs IP3R1 5-5% PA	1.146	$P \geq 0.05$
IP3R1 2-APB vs IP3R1 Xestospongin C	-4.973	$P \geq 0.05$

Table 14: Statistical analysis of DT40 calcium data presented in Figure 41: Two-way ANOVA analysis with post hoc Boniferroni testing

4.8 Chapter Conclusions

This chapter provides evidence that the inhibition of cAMP accumulation at 10% (v/v) CO_2 compared to 5% (v/v) is controlled by Ca^{2+} ions released from IP_3 receptors in the ER. Proof is provided through use of both pharmacological and genetic approaches. Abolition of the CO_2 induced constraint on cAMP accumulation with the chelator BAPTA-AM and antagonists thapsigargin and 2-APB led to the conclusion that in HEKPR1 cells Ca^{2+} ion release was required to inhibit AC and that the source of this calcium was the ER, specifically via IP_3 receptors. This requirement for calcium is true for HEKPR1, OK and A549 cells and is, therefore, not specific to cell line or species. Further evidence is provided through the use of DT40 cells which have been genetically ablated for IP_3 receptors (DT40-K/O). In these cells the inhibition of AC at 10% (v/v) CO_2 was ablated with the re-introduction of IP_3 receptors (DT40-IP_3R1) which again resulted in a blunted cAMP response. This latter result forms genetic evidence for an IP_3 receptor mediated release of Ca^{2+} ions interacting with cAMP signalling. Furthermore, using DT40 cells, intracellular Ca^{2+} concentrations were shown to increase with elevated CO_2, independent of pHi or hypoxia. This increase in Ca^{2+} was demonstrated to proceed via an IP_3 dependent mechanism, established by pharmacological and genetic methods. A pictorial representation of this hypothesised signalling pathway at normal and elevated CO_2 is displayed in Figure 43.

These findings are of particular interest in the clinical treatment of a number of pathological conditions. Hypercapnia can occur as a complication of numerous disease states, with elevated CO_2 often associated with a worse prognosis and elevated morbidity (Section 1.7). Inconsistent with this detrimental effect of CO_2, permissive hypercapnia is often used as a treatment, particularly when mechanical ventilation is required to support patients with respiratory complications, and this use of CO_2 is here related to an improved outcome. Whilst this protective effect has been largely attributed to the anti-inflammatory influence of CO_2, futher understanding into the mechanisms involved in these hypercapnic effects is required. The effects of CO_2 on both cAMP and Ca^{2+} signalling pathways presented in this chapter may provide further insight into understanding the clinical effects of hypercapnia and aid clinicians' attempts to better patient prognosis. Further work is required, however, to prove that these biochemical phenomena presented have physiologically relevant outcomes and this will be provided in Chapter 5.

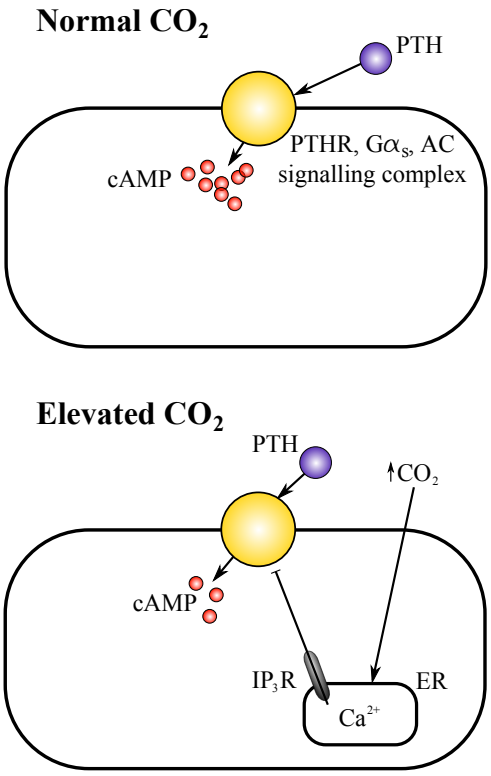

Figure 43: Chapter 4 overview of signalling events at normal and elevated CO_2. Normal CO_2: PTH activation of the AC signalling complex increases cAMP levels. Elevated CO_2: CO_2 induces a Ca^{2+} ion release from the ER via the IP_3 receptor, blunting AC's response to PTH resulting in reduced cAMP production.

5 Chapter 5: Physiological Experiments to Determine the Effect of Hypercapnia on Renal Cell Function

5.1 Introduction

Chapter 3 presented evidence for a pH independent inhibition of cAMP production with elevated CO_2 (from normocapnic 5% [v/v] to hypercapnic 10% [v/v]) that is true for multiple cell lines and independent of the mechanism of AC activation. This signalling phenomenon was demonstrated in Chapter 4 to require the release of Ca^{2+} ions from IP_3 receptors in the ER. This finding was confirmed using both pharmacological and genetic methods.

The majority of data presented so far has involved biochemical analysis of cAMP levels under different experimental conditions. This chapter focuses on whether the observed alterations to the cell signalling patterns have a physiological outcome. To achieve this the activity of two luminal membrane transporters was investigated; the sodium-phosphate co-transporter NaPi-IIa and sodium-hydrogen exchanger 3 (NHE3). Both these transporters are downstream of AC and are inhibited in response to PTH in order to control the levels of phosphaturia and bicarbonaturia respectively (Section 1.7.3). To monitor the activity of NaPi-IIa, cellular re-absorption of radio-labelled phosphate was measured (Section 5.2), whilst measurement of NHE3 activity employed measurement of pHi in response to an ammonium chloride pulse (Section 5.3). For all physiological experiments OK cells were used as a representative model of a proximal tubule cell responsive to PTH, in which the complete signalling machinery is present to regulate the desired transporters (Cole et al., 1989). Numerous publications exist supporting use of these cells for these physiological experiments, studying both phosphate (Caverzasio et al., 1986; Malmstrom & Murer, 1986; Cole et al., 1987; Jehle et al., 1999) and NHE activity (Pollock et al., 1986; Azarani et al., 1995).

This chapter demonstrates that the effects of elevated CO_2 and IP_3 receptor mediated Ca^{2+} release have downstream physiological implications, particularly on the activity of NHE3 and its ability to rescue pHi after an ammonium chloride pulse. The effects on phosphate transport with CO_2 are more complicated and no definitive effect of CO_2 was identified.

5.2 Activation of Downstream Sodium-Phosphate Co-transporters

PTH causes marked phosphaturia *in vivo* (Chase & Aurbach, 1967), an effect mediated by cAMP (Chase & Aurbach, 1967; Agus et al., 1971). This cAMP causes both inactivating phosphorylation of the sodium-dependent phosphate co-transporter NaPi-IIa in addition to a decrease in its number at the plasma membrane (Malmstrom & Murer, 1986) due to both decreased expression (Kempson et al., 1995; Picard et al., 2010) and targetted internalisation for lysosomal degradation (Keusch et al., 1998; Pfister et al., 1998; Picard et al., 2010). Together these effects decrease phosphate re-absorption in the renal proximal tubule (Agus et al., 1971, 1973) thus leading to the observed phosphaturia (Section 1.7.3). As a physiologically relevant process downstream of cAMP accumulation, this system was used to demonstrate whether the observed effects of elevated CO_2 on *in cellulo* cAMP levels could have a physiological outcome.

Several published works have shown that PTH causes time and concentration dependent decreases in sodium-dependent phosphate transport in OK cells (Cole et al., 1987; Malmstrom & Murer, 1986; Caverzasio et al., 1986) with significant inhibition in phosphate transport at PTH concentrations stimulating relatively low concentrations of cAMP (Caverzasio et al., 1986). In fact, *Malmstrom et al.* commented that in all the renal cell lines studied by the authors, including porcine LLC-PK_1 (Hull et al., 1976) and monkey derived JTC-12.P3 (Katsuta et al., 1960) cells, OK cell lines are the only line to retain the complete phosphate transport regulatory cascade (Malmstrom & Murer, 1986). OK cells were thus deemed a reliable model for further experimental purposes.

Experiments detailed in the sections below monitored the re-absorption of radio-labelled phosphate molecules under a variety of conditions. These assays were used to assess whether elevated CO_2, demonstrated to influence cAMP levels in Chapters 3 and 4, would have an effect on phosphate transport across the apical membrane.

5.2.1 Optimisation of Phosphate Transport Assay

The methodology used for the phosphate transport assays (Section 2.5.1) required a 4 hour incubation step at the appropriate pCO_2 and agonist/antagonist concentration. This step was required to allow cells to reach maximal phosphate transport levels (Cole et al., 1989), taking into account the time required for initial alterations to cAMP signalling (Caverzasio et al., 1986; Malmstrom & Murer, 1986) followed by their effects on NaPi-IIa expression (Kempson et al., 1995; Picard et al., 2010),

internalisation and degradation (Keusch et al., 1998; Pfister et al., 1998; Picard et al., 2010). The efficacy of this extended incubation period was demonstrated using PTH activation in OK cells, where phosphate transport was observed to decrease progressively over time with a 30% reduction of phosphate transport after 1 hour and 60% after 4 hours (Malmstrom & Murer, 1986).

This incubation period was significantly longer than cAMP accumulation assays, which required only 30 minutes. As CO_2 decreases the pH of solutions, preliminary experiments were carried out to monitor extracellular pH over the whole 4 hour period in an attempt to keep medium pH as controlled as possible between experiments requiring different CO_2 concentrations to eliminate pH as a determining factor. With cAMP and pHi measurements (Chapters 3 and 4), 15 mM HEPES was used to effectively buffer any CO_2 changes; therefore, different concentrations of this buffer were tested to establish optimal assay conditions.

Incubation experiments were carried out with cells with a starting pre-gassed medium pH of 7.5. Assays were performed by taking 500 μL samples of each medium every hour and measuring pH using a Hamilton Biotrode pH probe, specially designed to measure pH of small volumes, requiring only a 7 mm immersion depth (Hamilton, 2011). These samples were then returned to their respective bulk medium and the process repeated to cover the whole 4 hour period. Through repetition with different HEPES concentrations it was possible to identify optimal experimental conditions; foremostly maintaining similar pH levels for the longest period in those experiments with different CO_2 exposure levels, thereby eliminating pH as a variable as far as possible (Figure 44A). Phosphate uptake assays under basal conditions (no PTH or FSK agonists) using each HEPES concentration were also performed to establish the effect this buffer would have on phosphate uptake (Figure 44B).

From these experiments 100 mM HEPES was chosen for use in future experiments as use of this concentration resulted in minimal pH changes between samples exposed to each CO_2 concentration. However, this increased HEPES concentration increased phosphate uptake (Figure 44B). It is probable that this observed effect of HEPES was due to the fact that this buffer was applied to the media as a sodium-salt. As phosphate transport requires the activity of a $Na^+/PO_4{}^{3-}$ co-transporter, this process must be sodium dependent (Baumann et al., 1975) and thus application of Na-HEPES in this way could have partially altered transport dynamics. As all experiments were carried out under the same conditions and the cAMP activated system of interest causes inhibition of phosphate transport with no requirement for further activation of the transporter, this HEPES concentration was deemed acceptable for use.

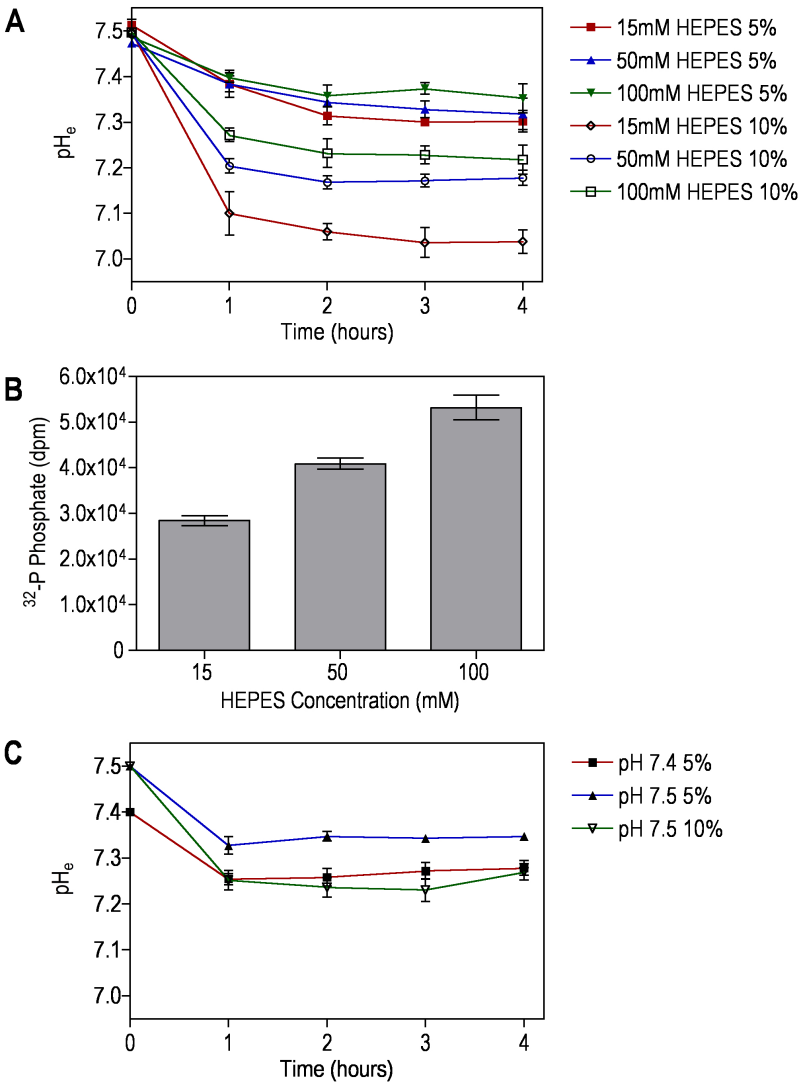

Figure 44: pH optimisation of phosphate transport assay across independent repetitions, pCO_2 percentage concentrations presented as v/v. **A**: Effect of HEPES concentration on cell medium pH at each pCO_2, all experiments started at pH 7.5, $n = 5$ **B**: Effect of HEPES on basal (no agonist) phosphate uptake, pH 7.5, $n = 4$ **C**: Medium pH changes with each pCO_2 and different starting pH values (detailed in the legend), 100mM HEPES

With 100 mM HEPES the pH difference between samples exposed to 5% (v/v) CO_2 and 10% (v/v) was 0.34 ± 0.07 pH units after 4 hours. It was also observed that the pH of the medium dropped rapidly within the first hour and then remained relatively constant. Data presented in Figure 44A was from experiments with the same starting pH. To maintain extracellular pH as close as possible across experiments with different CO_2 concentrations, the effect of different starting pH levels was tested. Figure 44C shows that with 100 mM HEPES, implementation of a starting pH of 7.5 for 10% (v/v) CO_2 and 7.4 for 5% (v/v) allowed the medium to remain at similar pH values for the greatest portion of the incubation period. Use of these conditions resulted in a pH value difference between samples from each CO_2 concentration of only 0.01 ± 0.04 pH units after 4 hours.

Assays to test whether the PDE antagonist IBMX should be included in the incubation media were also performed. IBMX had no effect on phosphate uptake at normocapnic 5% CO_2 in the absence of any agonist (Figure 45). Evidence in the literature, however, noted that IBMX greatly increased the observed agonist inhibition of phosphate transport (Caverzasio et al., 1986) while under basal conditions OK cells with 4 hours of 1 mM IBMX experienced a 50% reduction in phosphate transport (Malmstrom & Murer, 1986), indicating that basal AC activity was enough to inhibit NaPi-IIa if cAMP was not broken down by PDEs. It was decided not to include this PDE inhibitor so that the effects of cAMP turnover would also impact on the resultant phosphate uptake trends and the effects of endogenous basal AC activity would not lead to erroneous conclusions.

5.2.2 Phosphate Uptake In Response to PTH and FSK Agonists

A primary objective was to ensure that OK cells were responsive to the agonists PTH and FSK, causing measurable inhibition of phosphate uptake. FSK has been shown to mimic PTH inhibition of phosphate transport in OK cells (Caverzasio et al., 1986; Malmstrom & Murer, 1986) and should, therefore, have a similar effect. Results presented in Figure 46A demonstrate that in these OK cells both PTH and FSK inhibit phosphate uptake, most likely via their ability to generate cAMP. Inclusion of the PKA inhibitor H89 abolished this inhibition, giving phosphate uptake values statistically similar to the basal value (Figure 46B) . This demonstrated that both PTH and FSK inhibition of phosphate transport is via cAMP responsive PKA. Based on these results, these cells and this method can be used to monitor phosphate uptake in response to agonist with elevated CO_2.

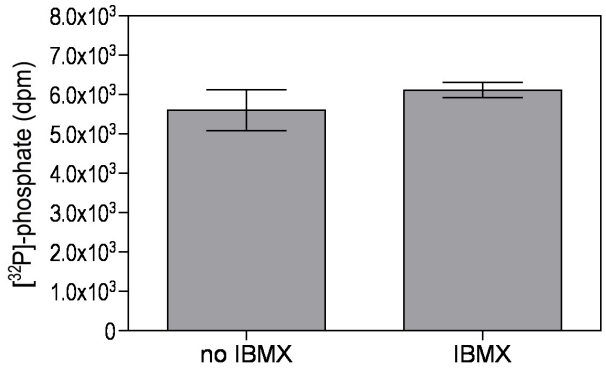

Figure 45: Effect of IBMX on phosphate uptake. Experimental conditions were 5% (v/v) CO_2, pH 7.5, 1mM IBMX added as indicated. T-test compared to control: 3.42 x 10^{-1}, $n = 4$

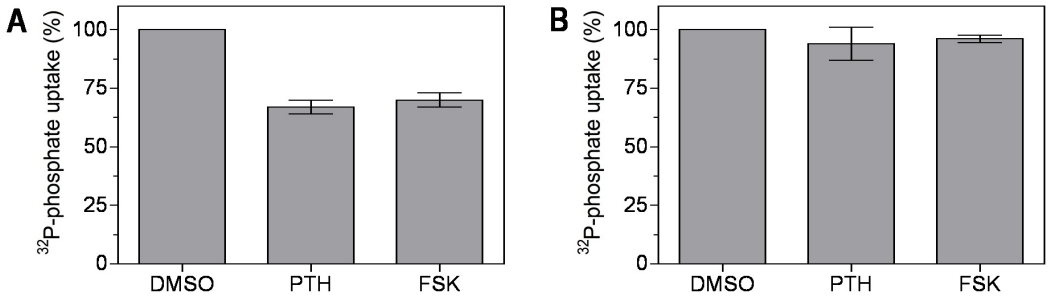

Figure 46: Phosphate uptake positive agonist responses. Agonist concentrations of 100 nM PTH and 10 μM forskolin with agonist solvent DMSO used as a negative control. Experimental conditions were 5% (v/v) CO_2, pH 7.5, antagonist added as indicated. Bar chart results shown as a percentage of phosphate uptake of the DMSO control averaged across independent experiments. **A**: $n = 4$, T-test compared to control: PTH, 2.91 x 10^{-5}; FSK, 7.37 x 10^{-5} **B**: H89, $n = 4$, T-test compared to control: PTH, 5.00 x 10^{-1}; FSK, 7.70 x 10^{-2}

5.2.3 Phosphate Uptake at Different Capnic Conditions

Section 5.2.2 demonstrated that PTH and FSK cause inhibition of phosphate uptake reliant on PKA activation in OK cells. These cells could thus be employed to monitor whether elevated CO_2 had an effect on this transport mechanism and if the effects of CO_2 on decreased cAMP accumulation would have a physiological effect. Figure 47 presents data from across independently performed experiments, with results presented as a percentage of phosphate uptake at 5% CO_2 with the DMSO control.

These results demonstrate an inhibition in total phosphate uptake with both PTH and FSK agonists as expected (Section 5.2.2), although the difference in their efficacy can only be explained as a consequence of the concentrations used. Regarding the effect of CO_2, however, these results do not match those found previously with cAMP accumulation. The decrease in cAMP observed with elevated CO_2 would be expected to relieve agonist induced inhibition of phosphate transport at this CO_2 concentration, demonstrable by an increase in phosphate uptake compared to the values at normocapnic 5% (v/v) CO_2. Instead there is a marked decrease in phosphate uptake. This observation is true for both control DMSO samples and agonist induced phosphate uptake. This inhibition of phosphate uptake at elevated CO_2 can not be attributed to cAMP and PKA activity as explained. The reduction in phosphate reabsorption with hypercapnia has been demonstrated previously in the literature (Lotspeich & Malvin, 1956; Webb et al., 1977; Haramati & Nienhuis, 1984; Guntupalli et al., 1987; Krapf et al., 1992; Jehle et al., 1999) and may be attributable to Ca^{2+} release at elevated CO_2 (Section 4.7.2) inhibiting phosphate uptake via PKC (Malmstrom & Murer, 1986; Cole et al., 1987; Martin et al., 1994).

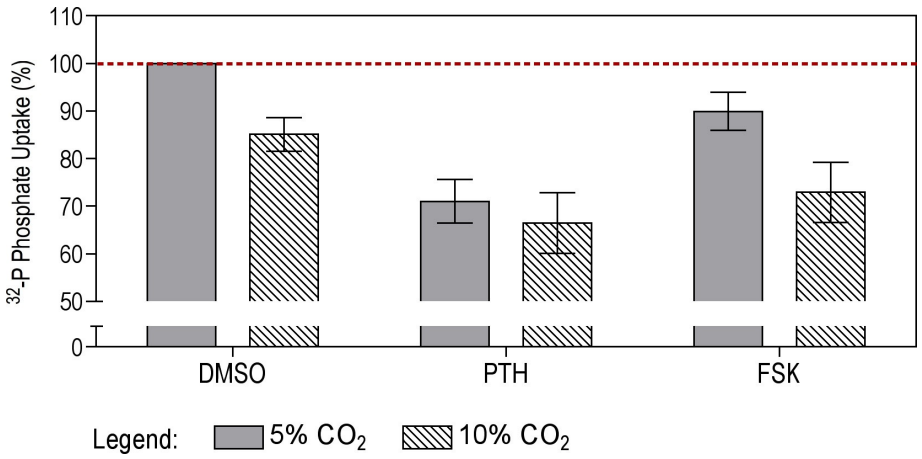

Figure 47: Phosphate uptake at 5% (v/v) and 10% (v/v) CO_2. Agonist concentrations of 100 nM PTH and 10 μM forskolin with agonist solvent DMSO used as a negative control. Bar chart results shown as a percentage of phosphate uptake of the 5% CO_2 DMSO control averaged across independent experiments, $n = 7$. T-test between CO_2 concentrations: DMSO, 9.96 x 10^{-5}; PTH, 6.16 x 10^{-1}; FSK, 3.08 x 10^{-1}

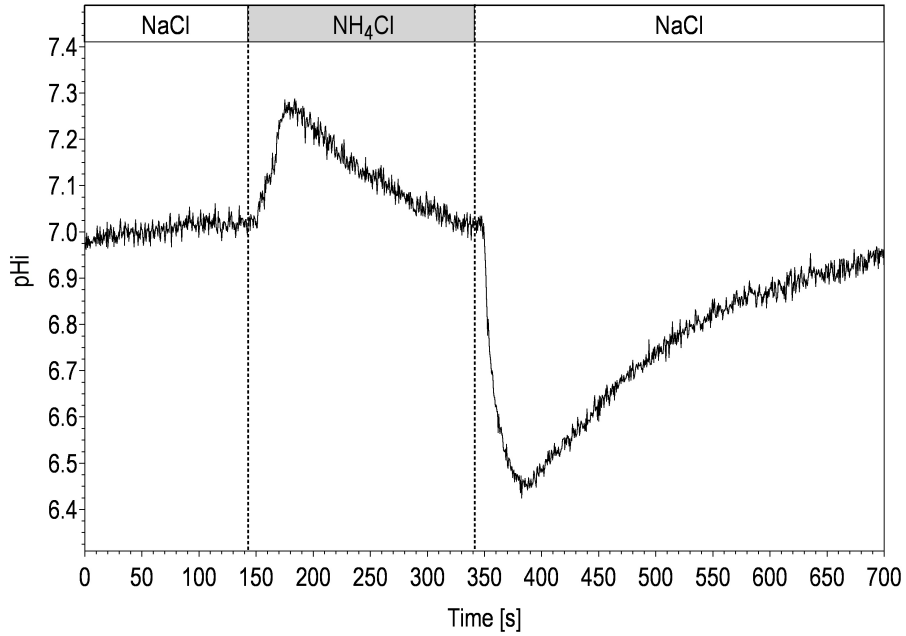

Figure 48: Typical ammonium chloride pulse: 'NaCl' refers to a Krebs-Ringer-HEPES solution (130mM NaCl, 25mM Glucose, 20mM HEPES, 14mM $NaHCO_3$, 5mM KCl, 1mM $CaCl_2$ and 1mM $MgSO_4$, pH 7.4, 5% [v/v] CO_2) and 'NH_4Cl' to the ammonium chloride pulse solution (110mM NaCl, 25mM Glucose, 20mM NH_4Cl, 20mM HEPES, 14mM $NaHCO_3$, 5mM KCl, 1mM $CaCl_2$ and 1mM $MgSO_4$, pH 7.4, 5% [v/v] CO_2). Cells are typically exposed to the NH_4Cl pulse solution for 3 minutes before return to Krebs-Ringer-HEPES.

5.3 Sodium-Hydrogen Exchangers and Intracellular pH recovery

Section 5.2 demonstrated that whilst agonist inhibition of phosphate uptake could be measured, a definitive effect linking elevated CO_2 and cAMP levels in this system could not be identified. It is possible that the effects of CO_2 are relatively short lived and thus, instead of concentrating on a chronic effect such as phosphate re-absorption, experiments were carried out on the more acute physiological effect provided by the regulation of sodium-proton exchangers, principally NHE3 (Tse et al., 1992). Here the inhibitory effects of PTH on Na^+-H^+ transport in OK cells can be observed after 2 minutes and are maximal after 4 minutes (Pollock et al., 1986). As a physiologically relevant acute response downstream of cAMP accumulation, this system was used to demonstrate whether the observed effects of elevated CO_2 on *in cellulo* cAMP levels could have a physiological outcome. This system is particularly relevant as NHE activity is involved in controlling PTH induced bicarbonaturia via cAMP inhibition of the exchanger (Section 1.7). OK cells have been used in numerous studies to investigate the effect of PTH on NHE3 activity (Pollock et al., 1986; Azarani et al., 1995) and therefore provide a useful model system on which to study the effects of CO_2 on NHE3 activity, particularly as they are noted to have a PTH NHE3 response similar to that recorded in isolated renal proximal tubules (Pollock et al., 1986).

In order to monitor the activity of NHE3, OK cells equilibrated at the desired CO_2 level and agonist/antagonist concentration were exposed to an ammonium chloride pulse. A typical pHi trace is presented as Figure 48. NH_4Cl causes an alkalinisation of pHi due to the rapid influx of NH_3 into cells which buffers intracellular protons (Boyarsky et al., 1988; Hegyi et al., 2004). This rapid alkalisation is then followed by a slower 'plateau-phase' acidification caused by the slower entry of NH_4^+ which is dissociated to NH_3 and H^+ (Boyarsky et al., 1988; Weintraub & Machen, 1989). When NH_4Cl is washed off the cells the reverse occurs, with efflux of NH_3 from the cells leaving behind a large number of trapped H^+ ions, which causes a rapid decrease in pHi (Boyarsky et al., 1988). These changes in pHi activate sodium-proton exchangers, particularly NHE3, which pump protons across the plasma membrane to return the cell to its resting pHi. It is this latter recovery step after the NH_4Cl pulse which is of most interest here. Comparsion of the rate at which this recovery occurs under different conditions allows the effect on NHE3 to be measured. A number of different methods of measuring this recovery have been used (Appendix 7.4). The initial recovery rate is most relevant as is representative of the activity of NHEs prior to any buffering of protons by cellular constituents. The majority of graphs presented display this period with the lowest measured pHi point set as time 0 and change in pH units (ΔpH) from this point displayed. In addition to

this, recovery rates have been calculated either by measuring this ΔpHi or by performing a linear regression on the first 45 seconds of recovery.

5.3.1 Sodium Dependent pHi Recovery

Pollock et al. demonstrated that in OK cells, PTH induced pHi changes were due to an amiloride-sensitive Na^+-H^+ antiporter and a cAMP response to the hormone (Pollock et al., 1986). The authors also noted that in the absence of sodium in the media or use of amiloride to inhibit Na^+-H^+ exchange via NHE3 there was a resultant decrease in pHi demonstrating an impairment in proton extrusion (Boyarsky et al., 1988) in addition to abolishing the PTH effect on this system (Pollock et al., 1986). To establish whether the pHi recoveries measured in response to NH_4Cl pulse involved this NHE3 dependent pHi recovery mechanism, experiments were performed using both a sodium-free solution and the Na^+-H^+ exchange inhibitor 5'-(N,N-dimethyl)-amiloride, DMA (Vigne et al., 1984; Kleyman & Cragoe, 1988). For sodium-free experiments, N-methyl-D-glucamine was used to replace the sodium chloride in the Krebs-Ringer-HEPES solution without affecting solution osmolarity. Potassium cations were not implemented as a substitute for sodium, even though the NHE family are known to not be able to use this ion (Beltrán et al., 2008), as they may have had electrogenic effects on the cell or modulate HCO_3^- uptake (Rakonczay et al., 2006). Thus, sodium-free recoveries were performed using an ammonium chloride pulse and cells were then returned to the N-methyl-D-glucamine solution for monitored recovery prior to return to normal Krebs-Ringer-HEPES.

Figure 49 demonstrates that in the presence of both the sodium-free Krebs-Ringer-HEPES and DMA containing solutions pHi recovery was compromised, giving initial recovery rates of 1.10 x 10^{-5} ± 2.69 x 10^{-5} pH units s^{-1} and 7.34 x 10^{-4} ± 4.41 x 10^{-5} pH units s^{-1} for the two conditions respectively, compared to the control sodium containing recovery of 1.58 x 10^{-3} ± 7.96 x 10^{-5} pH units s^{-1}. When t-tested against the control, sodium-free conditions gave a value of 3.46 x 10^{-3} and DMA; 3.58 x 10^{-3}, providing statistical support for this blunted ability to recover. These results indicate that under these experimental conditions the OK cells exhibit pHi recovery which is chiefly dependent on NHE activity, agreeing with evidence from the literature (Pollock et al., 1986). The results presented in Figure 49B demonstrate an inhibition in pHi recovery when cells were exposed to 10 μM FSK, covered further in Section 5.3.3. Of note here, FSK inhibition of pHi recovery does not reduce the rate to the same low levels as the exchanger inhibitor DMA, which indicates that at this concentration of agonist the pHi recovery rate can still be both activated and inhibited further.

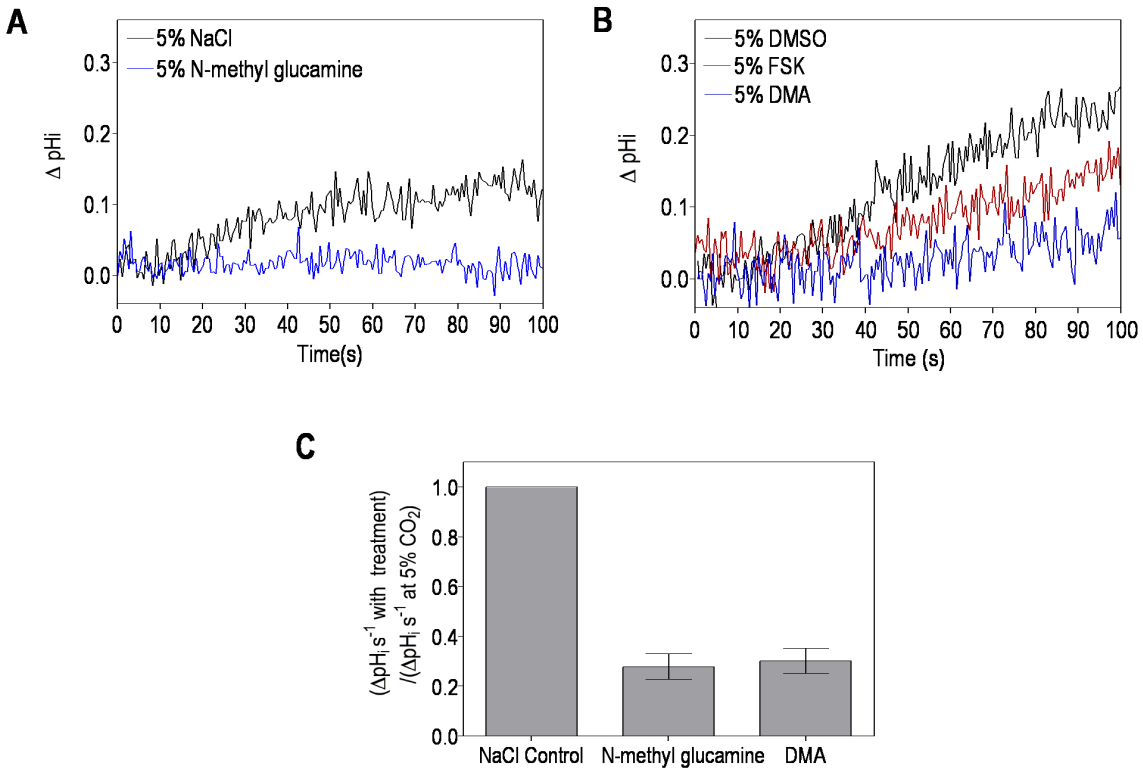

Figure 49: Control experiments to monitor pHi recovery when NHE is compromised. **A**: Rate of pHi recovery after NH_4Cl pulse with and without Na^+ (N-methyl-D-glucamine substitute), pH 7.4, **B**: Rate of pHi recovery after NH_4Cl pulse with DMSO control, 10 μM FSK and 100 μM DMA, pH 7.4, **C**: Bar chart of pHi recovery rates when NHE is compromised compared to control, 100 μM DMA, pH 7.4, $n = 7$.

5.3.2 DMSO Control with Different Capnic Conditions

Having established that in OK cells pHi recovery in response to NH_4Cl pulse occurs via the activity of Na^+-H^+ antiporters (Section 5.3.1), pHi recovery was monitored in the presence of different concentrations of CO_2. As presented in Figures 50 and 51, under control conditions the rate of pHi recovery after NH_4Cl pulse was decreased in the presence of 10% (v/v) CO_2 compared to 5% (v/v), resulting in a slower return to resting pHi. Estimates of the initial rate of pHi recovery were then calculated by applying linear regression to data points generated within the first 45 seconds of recovery. Using these values, the mean pHi recovery at 10% (v/v) CO_2 was calculated as 58.36% $\pm$ 5.57 of the rate at 5% (v/v). Possible explanations for this difference in pHi recovery rate are covered in Section 5.3.5, which may implicate the involvement of CO_2 induced Ca^{2+} ions and subsequently activated PKC modulation of NHE3 activity. At this stage it is sufficient to note the difference in recovery found between conditions as a comparison point for future experiments.

As the majority of agonists and antagonists required for experimentation (Sections 5.3.3, 5.3.4 and 5.3.5) were dissolved as stock solutions in DMSO, equivalent concentrations of this solvent were added to control experiments to determine whether it would have any effect on the observed trends in pHi recovery. Figure 51 presents evidence that the inclusion of DMSO had no effect on the rates of pHi recovery, displaying the same 5-10% trend established above. To remove this potential variable further, all comparisons from this point were thus compared to control experiments containing DMSO.

5.3.3 pHi Recovery with Agonist Activation at Different Capnic Levels

As outlined above, the principal aim of this Chapter was to identify whether the diminished cAMP response to agonist at 10% (v/v) CO_2 compared to 5% (v/v) presented in Chapters 3 and 4 could have a physiological outcome. As cAMP and downstream PKA activation inhibit the Na^+/H^+ antiporter NHE3 (Tse et al., 1992) via phosphorylation (Fan et al., 1999) and eventually decreased expression rate (Nogueira et al., 2008), monitoring pHi recovery after an NH_4Cl pulse provided a useful system in which to test for any physiological effect. This signalling network is predominantly used in the context of a PTH response, with the whole pathway previously demonstrated in OK cells (Pollock et al., 1986; Nogueira et al., 2008). *Pollock et al.* also demonstrated that direct activation of ACs by FSK could reproduce the PTH inhibition on NHE activity in OK cells via the same signalling mechanism, causing a decrease in $^{22}Na^+$ uptake by up to 64% (Pollock et al., 1986).

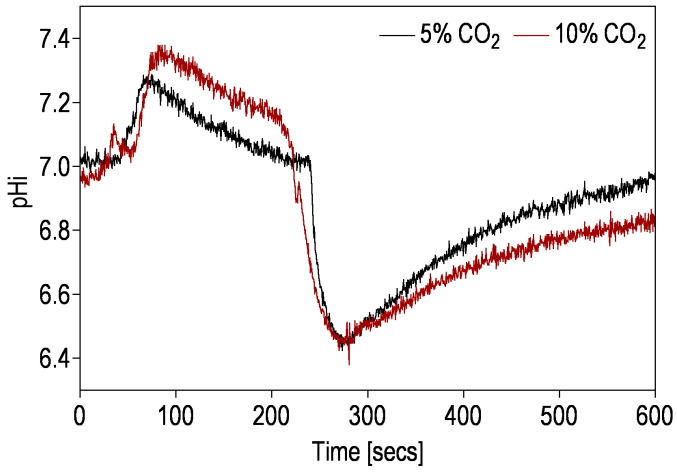

Figure 50: Control NHE experiment at different CO_2 concentrations, overlay of NH_4Cl pulses. CO_2 percentages given as v/v in air.

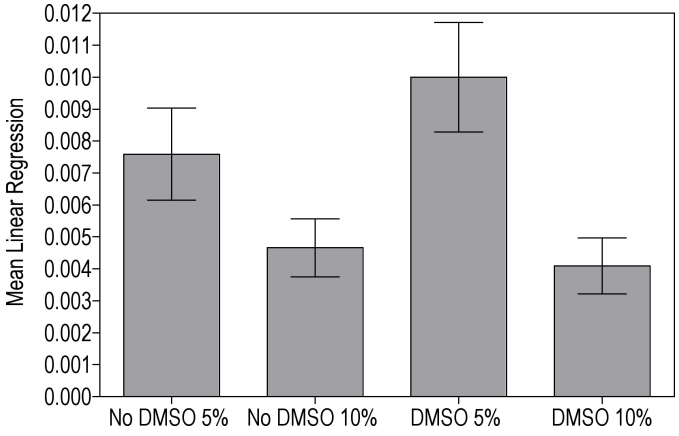

Figure 51: Effect of DMSO on pHi recovery after NH_4Cl pulse at different CO_2 concentrations. Percentages refer to CO_2 concentration in air, given as v/v. Linear regression values calculated from the first 45 seconds of recovery following NH_4Cl pulse, $n = 4$.

Thus, pHi recovery was measured after activation by both PTH and FSK agonists.

As shown in Figures 52B, 52C and 53 both agonists result in a decrease in pHi recovery rate. Therefore, cAMP production initiated by both agonists is able to inhibit NHE3 activity, as demonstrated by this alteration in pHi recovery. This inhibition is reduced in the presence of PKA inhibitor H89 (Figures 52D, 52E and 53), suggesting that PTH and FSK are both acting on NHE3 via PKA, in accordance with the literature (Nogueira et al., 2008).

These results also demonstrate an effect of the CO_2 concentration. Comparing panel A with B and C in Figure 52, the 5-10% (v/v) CO_2 trend is reversed in the presence of both agonists compared to the control, with pHi recovery rate at 10% (v/v) CO_2 faster than 5% (v/v). This result is seen clearly in Figure 53 where mean linear regression values are presented as a percentage ratio of the recovery rates between CO_2 concentrations, with associated statistical ANOVA data displayed as Table 15. As an increase in CO_2 brings about a decrease in cAMP production in the presence of agonist (Chapters 3 and 4), at 10% (v/v) CO_2 NHE3 would be expected to experience less inhibition and therefore be more active compared to normocapnic conditions. Thus, as observed, the pHi recovery rate following an NH_4Cl pulse would be expected to be greater, removing the constraint on recovery observed at 10% (v/v) CO_2 compared to 5% (v/v) under control conditions. This effect is not observed in the presence of H89 with either agonist, further suggesting involvement of a PKA mediated mechanism. In a physiological context this would mean that with hypercapnia bicarbonaturia would be expected to increase. These results match those found in normal, PTH responsive men with increased CO_2 inhalation where a decrease in bicarbonaturia was observed (Barker et al., 1957).

5.3.4 Physiological Evidence for the Requirement of IP_3R Generated Ca^{2+} Ions in the Response to Elevated CO_2

Section 5.3.3 demonstrated a CO_2 dependent effect on NHE3 mediated pHi recovery in response to AC agonists PTH and FSK, which was abolished in the presence of PKA inhibitor H89. This response correlated with data generated in Chapters 3 and 4 whereby CO_2 blunted the cAMP response to agonist (Section 5.3.3). Results from both antagonist application to cAMP accumulation assays in renal derived cells and cAMP measurements in genetically manipulated chicken lymphoblasts provided evidence for an involvement of Ca^{2+} ion release from the ER via IP_3 receptors in mediating this cAMP effect (Chapter 4). It was, therefore, of interest to establish whether this Ca^{2+} ion release was involved in the CO_2 mediated cAMP effect on NHE3 demonstrated in the previous section.

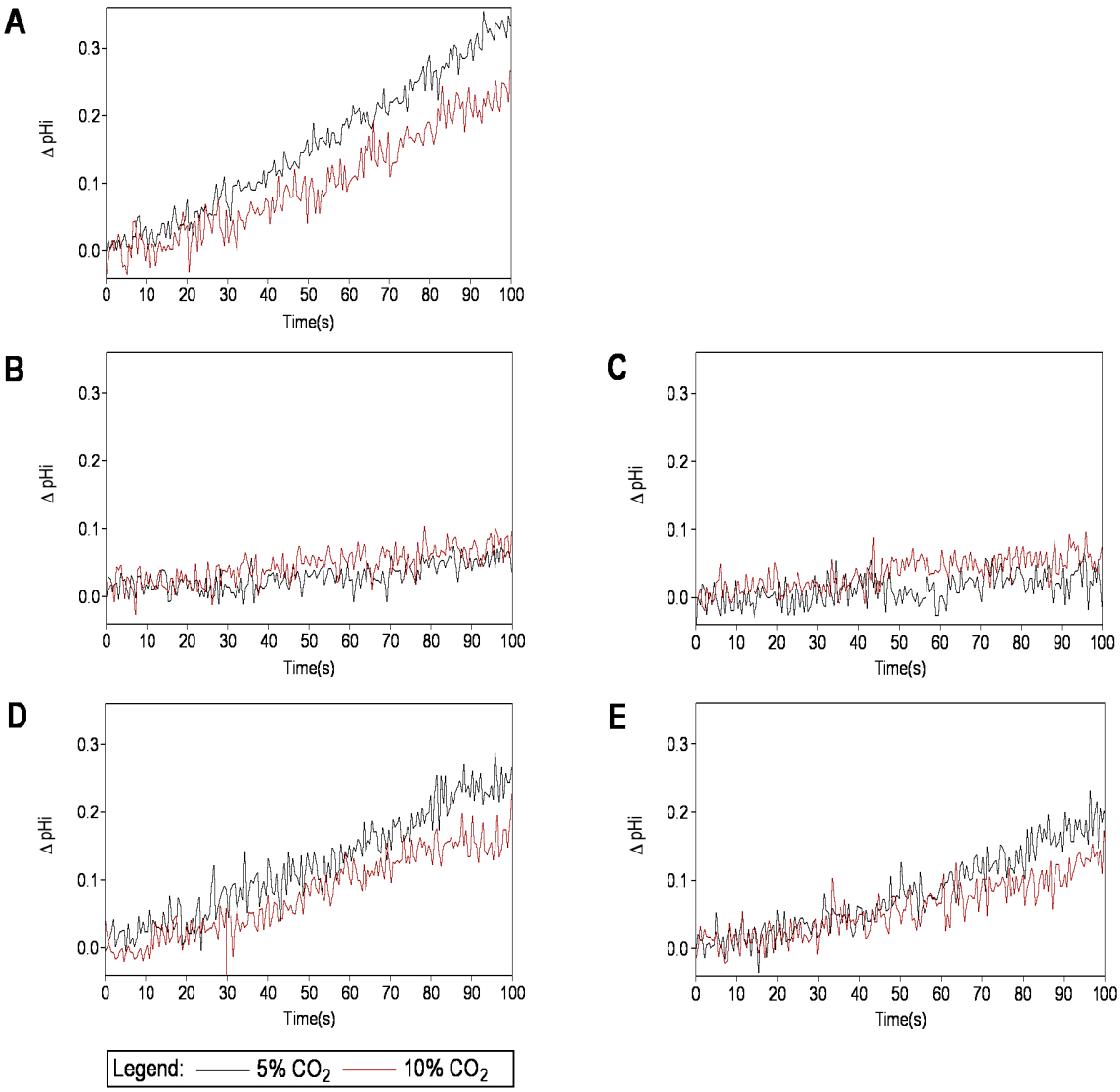

Figure 52: Effect of AC agonist on pHi recovery. Agonist concentrations of 5 nM PTH and 10 μM forskolin with agonist solvent DMSO used as a negative control. Experiments at pH 7.4 and inhibitor allowed time to enter cell prior to NH_4Cl assault. CO_2 percentages given as v/v in air. **A**: DMSO **B**: PTH **C**: FSK **D**: PTH, 10 μM H89 **E**: FSK, 10 μM H89.

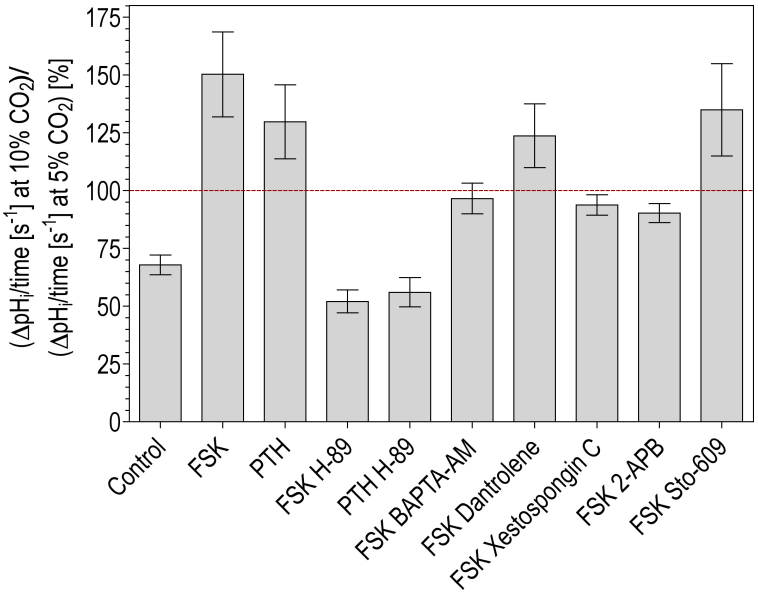

Figure 53: Effect of AC agonist on pHi recovery. Percentage ratio of pHi recovery at 10% (v/v) CO_2 versus 5% (v/v) CO_2 after an NH_4Cl pulse, pH 7.4. Agonist concentrations of 5 nM PTH and 10 μM forskolin with agonist solvent DMSO used as a negative control. Inhibitor concentrations detailed in Table 5 and these antagonists allowed time to enter cell prior to NH_4Cl assault. CO_2 percentages given as v/v in air. $n \geq 3$

Comparison	**Diff.**	**P value**
DMSO vs FSK	-82.35	P $\leq$ 0.001
DMSO vs PTH	-61.82	P $\leq$ 0.05
DMSO vs FSK H-89	15.81	P $\geq$ 0.05
DMSO vs PTH H-89	11.89	P $\geq$ 0.05
DMSO vs BAPTA	-28.66	P $\geq$0.05
DMSO vs Dantrolene	-55.8	P $\leq$ 0.001
DMSO vs Xestospongin	-25.89	P $\geq$ 0.05
DMSO vs 2-APB	-22.36	P $\geq$ 0.05
DMSO vs Sto-609	-67.02	p $\leq$ 0.01
FSK vs PTH	20.53	P $\geq$ 0.05
FSK vs FSK H-89	98.16	P $\leq$ 0.001

Comparison	**Diff.**	**P value**
FSK vs BAPTA	53.69	P $\leq$ 0.05
FSK vs Dantrolene	26.55	P $\geq$ 0.05
FSK vs Xestospongin	56.47	P $\leq$ 0.05
FSK vs 2-APB	59.99	P $\leq$ 0.01
FSK vs Sto-609	15.33	p $\geq$ 0.05
PTH vs PTH H-89	73.71	P $\leq$ 0.05
FSK H-89 vs PTH H-89	-3.92	P $\geq$ 0.05
BAPTA vs Dantrolene	-27.14	P $\geq$ 0.05
BAPTA vs Xestospongin	2.78	P $\geq$ 0.05
BAPTA vs 2-APB	6.3	P $\geq$ 0.05

Table 15: Statistical analysis of the effect of AC agonist on pHi recovery (Figure 53): ANOVA analysis with post hoc Bonferroni testing. BAPTA-AM, Dantrolene, Xestospongin C, 2-APB and Sto-609 experiments carried out in the presence of 10 μM FSK.

Without any OK cell lines avaliable with the target receptor/enzyme genes ablated, pharmacological antagonists and calcium chelators were employed to inhibit the desired element of the Ca^{2+} signalling network. The pHi recovery after an NH_4Cl pulse was thus monitored in the presence of an agonist in addition to the desired antagonist. As both PTH and FSK elicited the same effects on NHE3 with CO_2, FSK was used in these experiments as the AC agonist to avoid complications from PTH activated IP_3 release (Hruska et al., 1987; Pines et al., 1996; Abou-Samra et al., 1992).

Data provided in Figures 53, 54 and Table 15 illustrates that the CO_2 dependent effect of FSK is reliant on Ca^{2+} ion release from IP_3 receptors. Agonist induced relief of the constraint on pHi recovery at 10% (v/v) CO_2 is reduced in the presence of intracellular Ca^{2+} chelator BAPTA-AM. With BAPTA-AM pHi recovery is faster with 5% (v/v) CO_2 than 10% (v/v) CO_2, similar to the trend observed under control conditions. This result, in collaboration with the cAMP accumulation data, implies that at elevated CO_2 Ca^{2+} ions are released which inhibit cAMP generation. The IP_3 receptor inhibitors 2-APB and Xestospongin C gave similar results to BAPTA-AM, indicating that the Ca^{2+} ion release is via these receptors, which agrees with the cAMP data from Chapter 4. Use of the ryanodine receptor antagonist Dantrolene with FSK had no effect, with the 10%/5% (v/v) CO_2 ratio presented in Figure 53 statistically similar to values for FSK alone, thus proving that Ca^{2+} ion release from this source is not required in this system.

Data is additionally provided with the Ca^{2+}/calmodulin-dependent protein kinase kinase (CaM-KK) antagonist Sto-609. As mentioned in Chapter 4, this enzyme has recently been implicated in the transduction of a CO_2 induced Ca^{2+} ion release to Na^+/K^+-ATPase in alveolar epithelial cells (Vadász et al., 2008b) and thus provided an interesting enzyme to test. Furthermore, *Tokumitsu et al.* have provided evidence for the involvement of the CaM-KIV cascade, which includes CaM-KK, in Ca^{2+} dependent gene expression by the phosphorylation of transcription factors such as CREB (Tokumitsu et al., 2002). As cAMP is known to inhibit NHE3 via both phosphorylation (Fan et al., 1999) and reduced expression (Nogueira et al., 2008), this information provides further justification for the inclusion of Sto-609. However, as presented in Figures 53, 54 and Table 15, Sto-609 did not remove the effect of FSK and therefore CaM-KK is not required to transduce the CO_2 signal.

It is feasible that the Ca^{2+} ions released in response to elevated CO_2 are acting directly on the NHE3 antiporter to inhibit pHi recovery and this possibility is covered further in Section 5.3.5.

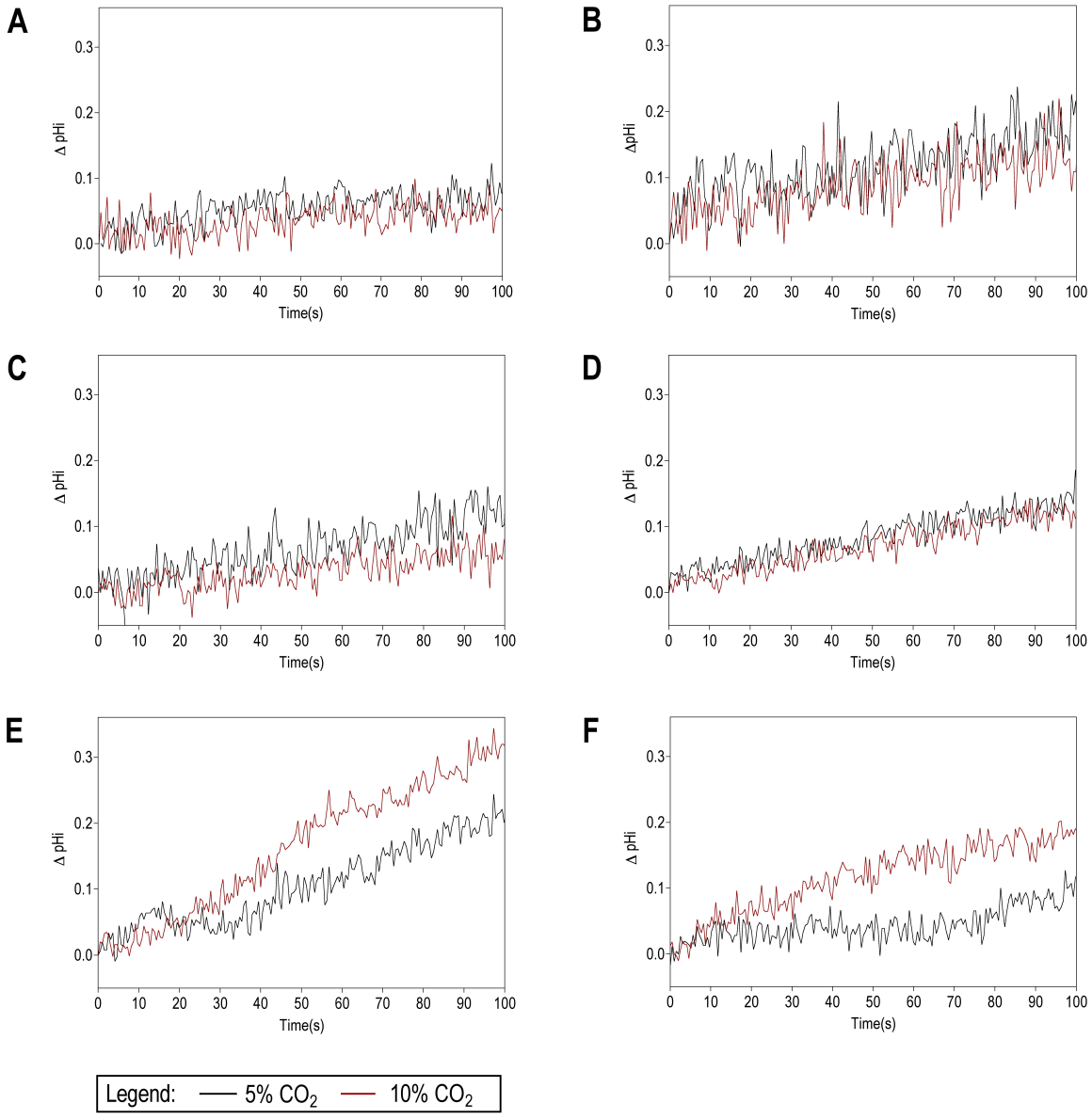

Figure 54: Effect of calcium signalling antagonists on agonist stimulated pHi recovery. Agonist concentrations of 5 nM PTH and 10 μM forskolin with agonist solvent DMSO used as a negative control. Experiments at pH 7.4 and inhibitor allowed time to enter cell prior to NH_4Cl assault. CO_2 percentages given as v/v in air. **A**: PTH, 1mM BAPTA-AM **B**: FSK, 1 mM BAPTA-AM **C**: FSK, 100 μM 2-APB **D**: FSK, 500 nM Xestospongin C **E**: FSK, 10 μM Dantrolene, **F**: FSK, 5 μM Sto-609.

5.3.5 Involvement of PKC pHi Recovery at Different Capnic Levels

Section 5.3.4 demonstrates that the CO_2 dependent effect of FSK (Section 5.3.3) requires Ca^{2+} ion release from IP_3 receptors. Evidence in the literature suggests that NHE3 can be inhibited by both PKA and PKC (Azarani et al., 1995), the latter of which is activated by Ca^{2+} ions. To test the involvement of the PKC pathway, pHi recovery experiments were repeated, this time including the PKC antagonist Gö6983, in conjuction with FSK activation of AC (Figure 55, Table 16). Use of Gö6983 yielded similar trends to BAPTA-AM (explained in Section 5.3.4), removing the effect of FSK on pHi recovery and yielding a trend similar to the control. This implies that PKC is involved in inhibiting NHE3 with FSK activation. However, as inhibition of PKA with H89 (Section 5.3.3) also removes the effect of FSK with elevated CO_2, it can only be inferred that both pathways are involved in this physiological effect of CO_2.

Furthermore it is was interesting to test whether the disparity between control pHi recoveries at 5% (v/v) CO_2 and 10% (v/v) CO_2 (Section 5.3.2) was caused by the increase in intracellular Ca^{2+} observed at elevated CO_2 in the absence of any agonist stimulation (Chapter 4). NH_4Cl pulse experiments were repeated in the absence of any AC agonist with both Gö6983 and Staurosporine, another PKC antagonist. Results from Figure 56 and Table 16 demonstrate that with PKC inhibition the constraint on pHi recovery at 10% (v/v) CO_2 is removed, giving a 5%/10% percentage closer to 100 than under control conditions. Data collected with Staurosporine is less statistically reliable, however this is to be expected as Staurosporine is a non-specific kinase inhibitor, known have effects on PKA, C, G, CaMK and MLCK. With such a range of targets it is therefore difficult to identify the true target protein, however when used in conjuction with the Gö6983 data they would suggest that Ca^{2+} ions released in response to elevated CO_2 inhibit NHE3 via PKC, resulting in the difference in pHi recovery after NH_4Cl pulse observed between 5% (v/v) CO_2 and 10% (v/v) CO_2.

PKC FSK ANOVA (Figure 55)		
Comparison	**Diff.**	**P value**
DMSO vs FSK	-82.35	$P \leq 0.001$
DMSO vs BAPTA-AM	-28.66	$P \geq 0.05$
DMSO vs FSK Gö6983	-27.94	$P \leq 0.05$
FSK vs BAPTA-AM	53.69	$P \leq 0.05$
FSK vs FSK Gö6983	54.41	$P \leq 0.01$
FSK BAPTA vs FSK Gö6983	0.72	$P \geq 0.05$

PKC DMSO ANOVA (Figure 56)		
Comparison	**Diff.**	**P value**
DMSO vs FSK Gö6983	2.71	$P \leq 0.05$
DMSO vs Staurosporine	-18.53	$P \geq 0.05$
Gö6983 vs Staurosporine	13.59	$P \geq 0.05$

Table 16: Statistical analysis of the effect of PKC antagonist on pHi recovery under different conditions (Figures 55 and 56): ANOVA analysis with post hoc Bonferroni testing.

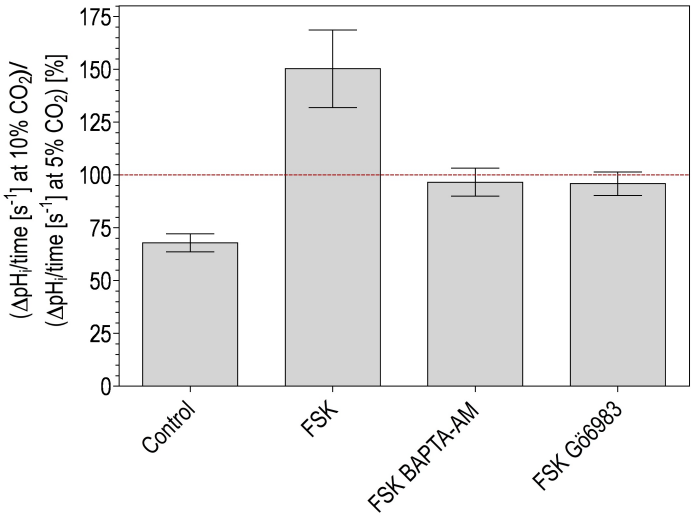

Figure 55: Effect of PKC on FSK inhibited NHE3 activity. Agonist concentration of 10 μM forskolin with agonist solvent DMSO used as a negative control. Experiments at pH 7.4 and inhibitors (1 mM BAPTA-AM or Gö6983) allowed time to enter cell prior to NH_4Cl assault. CO_2 percentages given as v/v in air. $n \geq 6$

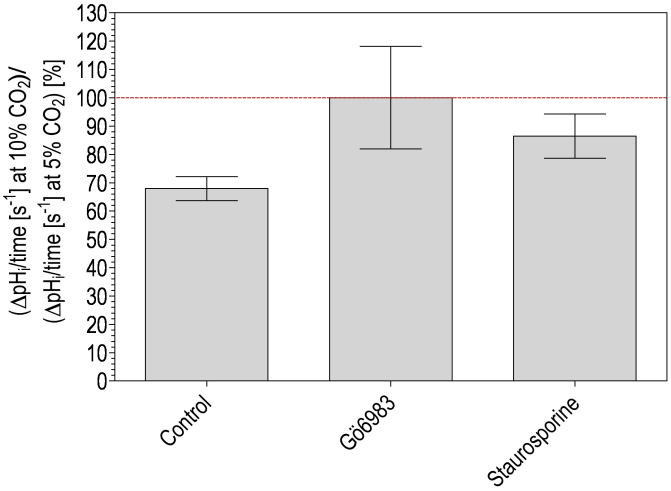

Figure 56: Role of PKC on unstimulated pHi recovery under different capnic conditions. Experiments at pH 7.4 and inhibitors (1 mM Gö6983 or 1 μM Staurosporine) allowed time to enter cell prior to NH_4Cl assault. CO_2 percentages given as v/v in air. $n \geq 3$.

5.4 Chapter Conclusions

Chapters 3 and 4 provided evidence for a pH independent inhibition of cAMP accumulation at elevated CO_2 reliant on Ca^{2+} ion release from IP_3 receptors in the ER. The aim of this chapter was to identify whether this biochemical signalling effect could have a physiological outcome. To investigate this, the activity of two downstream transporters; sodium-phosphate co-transporter NaPi-IIa and sodium-hydrogen exchanger NHE3 were explored under a range of conditions. Whilst results from NaPi-IIa did not support this signalling model, experiments on NHE3 activity were more encouraging. By measuring pHi recovery following an NH_4Cl pulse it was observed that under control conditions recovery rate was faster in cells exposed to 5% (v/v) CO_2 compared to those at 10% (v/v) CO_2. Activation of AC by both PTH and FSK both inhibited NHE3 activity as expected and reversed this control trend, indicative of a reduction of cAMP generated at elevated CO_2 (explained fully in Section 5.3.3). Using pharmacological inhibitors this CO_2 mediated effect of cAMP was found to rely on intracellular Ca^{2+} ions realeased from IP_3 receptors, agreeing with the signalling data generated in Chapter 4. Pictoral representation of this effect of CO_2 is provided as Figure 57.

Inhibition of both PKA and PKC removed the effect of FSK on NHE3. This demonstrates that under these conditions NHE3 activity is inhibited by both cAMP activated PKA and Ca^{2+} ion stimulated PKC. Thus, it is possible that the CO_2 generated Ca^{2+} ions are involved in regulating both control mechanisms. This duel mechanism is, however, unlikely to be the cause for the observed decrease in phosphate uptake at 10% (v/v) CO_2 compared to 5% (v/v) CO_2 as PKC is known to inhibit NaPi-IIa and phosphate transport (Malmstrom & Murer, 1986; Cole et al., 1987; Martin et al., 1994). The effect of CO_2 on phosphate transport can therefore not be explained but does agree with findings from *in vivo* experiments in the literature, as mentioned in Section 5.2.3.

These findings may have profound implications, particularly when trying to understand the homeostatic control mechanisms of systemic pH and inorganic carbon, in the context of metabolic acidosis and hypercapnia. As sodium-hydrogen exchangers of the NHE family are present in most epithelial cells (Schwark et al., 1998), understanding the control mechanisms behind their activity may be vital in understanding the complications arising from hypercapnia in a range of contexts, from therapeutic permissive hypercapnia through to cystic fibrosis and cardiovasular disease (Section 1.7).

Prolonged elevated CO_2 may have an effect on multiple cellular proteins, both directly or indirectly. One possible approach to defining targets to investigate further is through proteomic analysis of

different cell samples after exposure to elevated CO_2. Sample data from one such experiment is provided in Appendix Chapter 8.

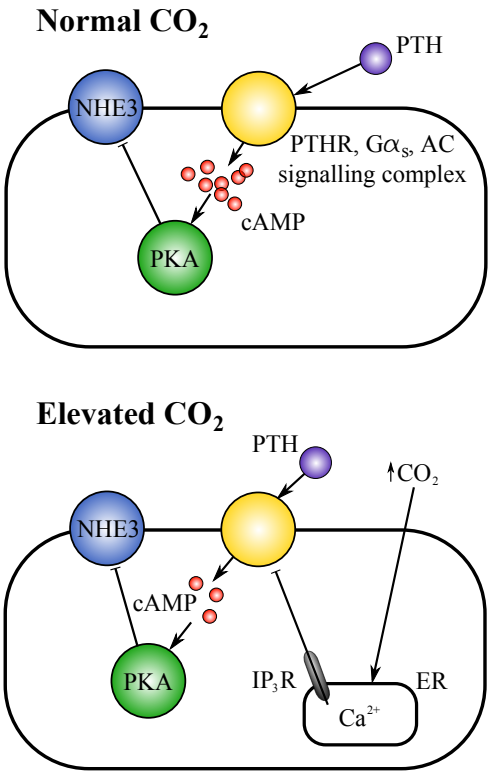

Figure 57: Chapter 5 overview of signalling events at normal and elevated CO_2. Normal CO_2: PTH activation of the AC signalling complex increases cAMP levels which in turn activate PKA and inhibit NHE3 activity. Elevated CO_2: CO_2 induces a Ca^{2+} ion release from the ER via the IP_3 receptor. This Ca^{2+} blunts AC's response to PTH resulting in reduced cAMP production, blunted PKA activity and less inhbition of the NHE3 transporter.

6 Chapter 6: Discussion

6.1 Introduction

This thesis demonstrates that elevated CO_2 can alter physiological processes through IP_3 mediated Ca^{2+} release and an associated decrease in intracellular cAMP levels. Furthermore, these effects of CO_2 were independent of both intra- and extracellular pH. Results were obtained using the PTH response of HEKPR1 and OK cell lines. OK cells were chosen because *in vivo* proximal tubule cells are involved in inorganic carbon homeostasis through HCO_3^- absorption from the glomerular filtrate. Use of cultured cells enabled sufficient levels of control over incubation conditions and CO_2 associated acidoses and avoided any secondary interactions from the effects on the endocrine and autonomic nervous systems. This discussion chapter will summarise the results presented in Chapters 3, 4 and 5 and discuss their findings in relation to the literature currently available, and present ideas for future studies arising from this work.

6.2 Reduction in Agonist Induced cAMP with Elevated CO_2

When stimulated by FSK or PTH, AC mediated cAMP production showed a consistent drop at 10% (v/v) CO_2 compared to 2.5% and 5% (v/v) CO_2. These pCO_2 levels were chosen to represent hyper-, normo- and hypocapnic conditions, spanning the extremes experienced in physiology and pathophysiology (Marshall & Bangert, 2008). Sub-maximal concentrations of cAMP agonists were used to enable the detection of either activation or down-regulation of the cAMP signalling pathway under a given experimental condition. The observation that the inhibition of AC with elevated CO_2 was present regardless of the AC agonist employed, indicated that the inhibitory effect of CO_2 does not occur upstream of AC and is independent of the AC isoform (PTH couples specifically to AC VI in HEKPR1 cells (Tovey et al., 2008), whilst FSK activates all tmAC isoforms (Zhang et al., 1997)).

This response to CO_2 is in direct contrast to the current paradigm where cyclic nucleotide levels are observed to increase in response to increases in CO_2 (Section 1.3.6). There is evidence in the literature, however, that agrees with these findings. In *Mucor racemosus*, exposure to elevated CO_2 caused an immediate four-fold decrease in cAMP compared to control conditions, however this effect may be due to the concomitant acidosis (Larsen & Sypherd, 1974). *Townsend et al.* previously demonstrated a decrease in cAMP mediated CREB phosphylation at 10% (v/v) CO_2 compared to that at 5% (v/v) but no further details were given regarding this observation. In the light of these results, it may be worth considering whether Ci may impart a biphasic effect on ACs with stimulation *in vivo* at lower pCO_2 levels from ambient to physiological levels and inhibition with higher concentrations. Furthermore, whilst in isolation, inorganic carbon may have an activatory role on an AC (Cann et al., 2003); *in vivo* other variables such as Ca^{2+} ions may modulate this activity (Section 6.4).

As CO_2 in solution reacts with water molecules to produce HCO_3^- ions and protons, it was possible that AC activity was being modulated by pH instead of CO_2, especially as pH has been previously shown to have a marked effect on AC activity *in vitro* (Hammes & Rodbell, 1976). The AC rate dependence on pH is due to the fact that the enzyme requires its ATP substrate in two forms for catalysis to proceed, with one ionisable group in its acid form and one in its basic form and that the protonated form of the substrate alone has a strong inhibitory effect (Hammes & Rodbell, 1976). Some ACs are able to respond directly to changes in pH, such as the mycobacterial class III AC, which has a pH sensing domain. When activated, this domain enables conformational changes to occur, which allow the AC to orientate its two catalytic domains properly (Tews et al., 2005).

However, it has also been postulated that in some systems ACs are protected against pH change through association with Na^+/H^+ exchangers, forming microdomains in which pH control on AC activity is effectively eliminated (Willoughby et al., 2005).

The effect of experimental conditions on intracellular pH was determined using microspectrofluorometric measurement of the cell-permeable pH sensitive dye BCECF-AM (Rink et al., 1982). Cells transferred from normo- to hypercapnic media experienced an initial intracellular acidification, as CO_2 reaching the cells reacted in solution to produce protons. This acidification was followed by a gradual return to resting pHas Na^+/H^+ antiporters are activated. Recovery time for pHi, on average, was 10 minutes for both HEKPR1 and OK cells and a similar transient change in pHi could be mimicked using 2 mM propanoic acid. BCECF dye was added to cells as an inactive acetoxyester in order to permit penetration of the cell membrane. This slightly lowered the intracellular pH as intracellular esterases cleave off the acetoxyester group, leaving an acidic functional dye less able to cross the cell membrane (Hegyi et al., 2004). Although this is not ideal, the cells' response to fluctuations in CO_2 concentration is still valid, as pH changes stemming from BECEF cleavage should be minor (Hegyi et al., 2004). All pHi measurements were made after a BECEF-AM incubation step with subsequent media perfusion. The pHi was stable prior to CO_2 change and then recovered afterward to the same pHi. Thus the effects of BCECF on pHi are unlikely to influence the central findings of this thesis.

The timing of the transient pHi change was used to design cAMP accumulation experiments where pHi was allowed to normalise after CO_2 elevation and prior to any agonist application. Replication of the pHi change associated with elevated CO_2 using propanoic acid did not alter cAMP in the same manner as hypercapnia. Therefore, the observations made concerning cAMP accumulation levels are unlikely to be due to altered pHi, as any potential acid signal would need to persist long after pH homeostasis. Extracellular pH is also unlikely to be responsible, as the potential mid-assay medium acidification does not alter the EC_{50} for PTH for either HEKPR1 or OK cell lines. Additionally, the blunted cAMP response at elevated CO_2 can be reproduced when cells are exposed to both acidotic or alkalotic extracellular pH, modelled by pH levels of 7.0 and 7.5 respectively (Marshall & Bangert, 2008). As mentioned, it has previously been demonstrated that G-protein regulated ACs are offered some protection from changes in pHi through the action of Na^+/H^+ antiporters (Willoughby et al., 2005) and this further justifies this conclusion.

The cAMP effects observed were also not due to any mild hypoxia that may have been induced by the gas mixtures used in experimentation. This variable was important to disregard as a down-

regulation of the cAMP signalling network has been reported as a mechanism by which cells adapt to long-term hypoxia (Beitner-Johnson et al., 1998). This potential hypoxic difference was due to the 5% (v/v) CO_2 gas mixture containing 19.90% (v/v) O_2 and the 10% (v/v) CO_2: 18.85% (v/v) O_2. Experiments using a gaseous mixture of 5% CO_2, 18% O_2 and 77% N_2 (v/v) to replicate the hypoxic condition, in the absence of any additional hypercapnia, did not cause any inhibition of cAMP production compared to a 5% (v/v) CO_2 control. Thus hypoxia is unlikely to be a determining factor in this blunted cAMP response.

The effect of CO_2 on cAMP is demonstrated in five independent cell lines: HEKPR1, OK, UMR-106, A549 and DT40 IP_3R1. This suggests a species and tissue independent effect, at least at the metazoan level. Whilst results from the renal and osteoblast cell lines are of interest as these tissues are involved in Ci homeostasis, confirmation using the alveolar epithelial cell line, A549, is of particular interest as a key tissue affected by the use of permissive hypercapnia in a clinical setting. The use of permissive hypercapnia is of increasing interest as a treatment for a range of pathological disorders where artificial hypoventilation is induced to avoid damage from overstretching the lungs. The positive effects of this strategy are not only due to the mechanical ventilation, but have also been attributed to the induced hypercapnia itself, largely due to the anti-inflammatory influence of CO_2 (Sections 1.7.1 and 1.7.2). The effects of CO_2 on cAMP observed here may provide further insight into the positive effects of permissive hypercapnia.

6.3 Use of Pharmacological Inhibitors Suggests Ca^{2+} Ion Release from IP_3 Receptors in the Endoplasmic Reticulum

Based on the conclusions drawn in Section 6.2 it was not possible to determine whether the inhibitory influence of CO_2 on cAMP signalling was due to a direct interaction with AC or indirectly through another signalling pathway affecting cAMP. Pharmacological inhibitors offered the best initial route to investigate the impact of other signalling molecules, taking advantage of the broad spectrum of targets antagonised under moderate inhibitor concentrations. Through studies on HEKPR1 cells, it was possible to eliminate interactions from sAC, PDEs, PKA, CA, sphingosine kinases 1 and 2, PKC and CAMKII. However, antagonism of tmACs did greatly reduce cAMP levels and remove inhibiton at 10% (v/v) CO_2, indicating that the majority of the cellular cAMP produced was from tmACs and the effects of CO_2 were on these isoforms and not the HCO_3^- stimulated sAC (Section 1.3.6).

Interestingly, the blunted cAMP response with hypercapnia was not affected by the CA inhibitor acetazolamide (Maren, 1952). This result may indicate that there is no requirement for CO_2 from the media to be converted to HCO_3^- to cross the membrane (Huckstepp et al., 2010a) and inhibit the AC either directly or indirectly. *Missner et al.* demonstrated that Ci movement across a membrane is via passive diffusion of the CO_2 species (Missner et al., 2008), opposed to through previously hypothesised routes via membrane channels such as aquaporin 1 (Endeward et al., 2006) or the Rhesus complex RhAG (Endeward et al., 2008). The authors demonstrate that movement of Ci across a membrane physiological pH levels is restricted by the near-membrane unstirred layer, which acts as a diffusional barrier to the membrane. Here, CAs convert any HCO_3^- ions from the extracellular bulk to CO_2, allowing diffusion across to the intracellular compartment where the reverse can occur, enabling both CO_2 and HCO_3^- to exist within the cell (Missner et al., 2008). With CAs inhibited, CO_2 within the cell will not be converted to HCO_3^- as readily, supporting the inference that there is no requirement for the CO_2 within the media to be converted to HCO_3^- to inhibit the AC. Nevertheless, the possibility that the blunted cAMP response at 10% (v/v) CO_2 is due in part to HCO_3^- cannot completely be excluded. Use of *in vitro* AC assays under conditions of Ci disequilibrium where a single predominant carbon species, CO_2 or HCO_3^-, is present at a defined pH (Hammer et al., 2006) would further identify this mechanism.

Use of pharmacological inhibitors also identified a role for intracellular Ca^{2+} in the response to CO_2. In the presence of the intracellular Ca^{2+} chelator BAPTA-AM, no reduction in cAMP accumulation

was observed at 10% (v/v) CO_2, whilst in the presence of non-membrane permeable EGTA, the expected drop was obtained. This result suggested that the hypercapnic effect on cAMP signalling involved Ca^{2+} and that the source was most likely derived from an intracellular store. It is possible that by chelating Ca^{2+} ions, CO_2 diffusion rates are affected through inhibition of CA activity (Botre et al., 1991). However, as acetazolamide had no effect on the cAMP trend, this is unlikely.

Further experimentation with antagonists to individually inhibit each of the main intracellular calcium stores led to the inference that Ca^{2+} release was occuring from the endoplasmic reticulum. This inference was made from the observation that thapsigargin ablated the cAMP response to CO_2 in both OK and HEKPR1 cells. Interestingly, this approach was also implemented by *Bouyer et al.* in rabbit S2 PT cells to identify the source of a pH independent Ca^{2+} signal, generated following an application of basolateral CO_2, but in this case the authors were unable to locate the source (Bouyer et al., 2003).

Further chemical antagonists were used to identify the Ca^{2+} source within the ER and whether other potential elements of the Ca^{2+} signalling network could be involved in regulating AC activity. From these studies it was inferred that in OK cells, whilst PLC and Ca^{2+} release from ryanodine receptors were not involved, the Ca^{2+} responsible for blunting agonist induced cAMP production at elevated CO_2 was most likely from IP_3 receptors. The use of IP_3 receptor antagonist 2-APB in OK cells removed the CO_2 effect on cAMP levels, whilst Xestospongin C had no effect. The 2-APB data thus implicated CO_2 dependent release of Ca^{2+} from IP_3 receptors, whilst those from Xestospongin C did not concur. 2-APB antagonises both IP_3 receptors and transient receptor potential channels, TPCs (Prakriya & Lewis, 2001; Venkatachalam et al., 2001; Martin et al., 2009). It is, therefore, possible that Ca^{2+} entry was across the plasma membrane via TPCs, although the lack of a role for extracellular Ca^{2+} (EGTA result) eliminated this possibility and supported a role for Ca^{2+} release from the ER, via the IP_3 receptor.

The involvement of CaM-KK in this response was also tested using antagonist Sto-609. A CaKK-β dependent route was identified recently, by which alveolar epithelial cells respond to hypercapnia (Vadász et al., 2008a). This response involved a rapid and transient increase in intracellular Ca^{2+}, which caused Na^+, K^+-ATPase endocytosis and may explain why hypercapnia impairs alveolar fluid reabsorption, an important consideration with permissive hypercapnia. In the presence of Sto-609, however, the cAMP response to CO_2 was unaltered, demonstrating that this enzyme was not required to inhibit AC activity under hypercapnic conditions in OK cells.

6.4 Release of Calcium by Elevated CO_2

The use of pharmacological inhibitors identified that in HEKPR1 and OK cells the inhibition of cAMP accumulation at elevated CO_2 involved an interaction with an intracellular Ca^{2+} source and that this source was most likely from IP_3 receptors in the endoplasmic reticulum. A role for the IP_3 receptor was subsequently proven through the use of an independent cell line that had been genetically ablated for all three IP_3 receptor isoforms (Sugawara et al., 1997). When exposed to hypercapnic CO_2, this DT40 IP_3 receptor knock-out (DT40 K/O) exhibited no change in cAMP accumulation levels between CO_2 concentrations. However, in a DT40-IP_3R1 cell line where the gene for IP_3 receptor 1 had been re-introduced (Laude et al., 2005), the reduction in cAMP accumulation at elevated CO_2 was observed once more, providing genetic proof that cAMP inhibition requires Ca^{2+} release from IP_3 receptors.

DT40 cells were also used to demonstrate CO_2 induced Ca^{2+} release, using the Ca^{2+} sensitive ratiometric dye Fura-AM (Grynkiewicz et al., 1985). Through this method, an increase in intracellular Ca^{2+} was observed on transition from 5% to 10% (v/v) CO_2 that was independent of pH and any hypoxic changes incurred. Ca^{2+} release was demonstrated both pharmacologically and genetically to be via IP_3 receptors and did not require extracellular Ca^{2+}. The lack of a role for extracellular Ca^{2+} is particularly important as most Ca^{2+}-sensitive ACs are regulated by capacitative calcium entry (Cooper et al., 1994; Sunahara & Taussig, 2002; Willoughby et al., 2005). This Ca^{2+} release did, however, require PLC activity, as demonstrated through the use of antagonist U73-122. As PLC is responsible for generating the IP_3 signal, this result would suggest that the CO_2 sensor is located within or upstream of this pathway. However, when this antagonist was used in cAMP accumulation, there was no demonstrable effect. This discrepancy may be due to the questionable effects of U73-122 on PLC, which may induce both inhibition and activation, as well as a host of other unspecific interactions with signalling molecules (Klein et al., 2011). It is also possible that DT40s contain different PLC isoforms to the OK cells employed for cAMP accumulation, with different sensitivities to U73-122 and/or CO_2. Future work to identify the CO_2 receptor would require further attention to this section of the Ca^{2+} signalling network. It is possible that the signalling response to CO_2 in HEKPR1 and OK cells does not involve the IP_3 receptor. This possibility is unlikely, however, as the IP_3 receptor antagonists used in this study were validated by demonstrating their effect on CO_2 mediated Ca^{2+} release in DT40-IP_3R1 cells. Future experiments, using siRNA or knock-outs generated via zinc finger nucleases, would enable genetic conformation in these renal cells.

This observed release of Ca^{2+} and the inferred effect on AC and cAMP production would suggest that, at elevated CO_2, AC is inhibited by Ca^{2+} or a molecule regulated by Ca^{2+}. All tmAC isoforms are inhibited by high concentrations of calcium, due to competition between these divalent ions and the Mg^{2+} co-factor (Guillou et al., 1999). Certain isoforms are also regulated at lower concentrations e.g. tmACs V and VI (Ishikawa et al., 1992; Yoshimura & Cooper, 1992; Guillou et al., 1999). IP_3 receptor 2 and AC VI have been shown to interact in HEK cells after PTH stimulation forming 'cAMP junctions' (Tovey et al., 2008). These interactions have been hypothesised to directly provide supramaximal concentrations of cAMP to the IP_3 receptor, in order to increase the receptor's sensitivity to IP_3 (Tovey et al., 2008). It is plausible that this interaction may work in reverse under hypercapnic conditions, with IP_3 mediated Ca^{2+} release inhibiting the AC VI and thus generating the data obtained in this report. *Cooper et al.* presents a model whereby AC and Ca^{2+} create a negative feedback control loop that results in oscillations of the two second messengers (Cooper et al., 1995). It is possible that these observations follow a similar feedback loop. Although the PKC antagonists staurosporine and Gö6983 did not identify a role for PKC, the calcium chelator BAPTA-AM is also known to inactivate this kinase (Dieter et al., 1993). As the use of BAPTA-AM removed the CO_2 restraint of cAMP accumulation, it is feasible that this regulation could be mediated by PKC. Experimentation using a genetic model, for example, would be needed to further identify the mechanism behind AC inhibition.

Some PDE isoforms are also regulated by Ca^{2+}/CaM (Section 1.5.3). With hypercapnia, the CO_2 induced Ca^{2+} ions could activate a Ca^{2+}-sensitive PDE, increasing cAMP turnover. However, all cAMP accumulation experiments were carried out in the presence of non-selective PDE inhibitor IBMX and so PDE involvement is unlikely (Gray, 2006). Furthermore, the PDE isoforms PDE8A, 8B and 9, which show limited sensitivity to IBMX, exhibit no known sensitivity to Ca^{2+} (Omori & Kotera, 2007; Wang et al., 2008).

A role for elevated Ca^{2+} signalling in the response to CO_2 has been investigated previously. *Vadász et al.* noted a transient increase in cytoplasmic Ca^{2+} in response to hypercapnia, whilst *Bouyer et al.* identified a rise in intracellular Ca^{2+} in response to basolateral Ci application (Bouyer et al., 2003; Vadász et al., 2008a). Further evidence of acidosis (Tsunoda et al., 1991; Dwyer et al., 1991; Buckler & Vaughan-Jones, 1993; Slotki et al., 1993; Ziegelstein et al., 1993) and hypercapnic acidosis (Rigual et al., 1991; Nishio et al., 2001) stimulating Ca^{2+} release is also available. Whilst pH has been eliminated as the Ca^{2+} mobilising signal, particularly through the use of propanoic acid, which had no effect on Ca^{2+} release, it is still plausible that pH could be contributing. Further monitoring

of pHi with simultaneous measurement of intracellular Ca^{2+} may delinerate this interaction further. It might also be interesting to follow the production of cAMP (Binkowski et al., 2011) and IP_3 through real-time application of biosensors (Tanimura et al., 2009).

6.5 Effect of CO_2 on cAMP Dependent Physiological Processes

The effects of the hypercapnic alterations to cAMP and Ca^{2+} signalling on downstream physiological responses were tested, focusing on the sodium-driven transporters NaPi-IIa and NHE3. These luminal membrane transporters are both downstream of AC and are inhibited in response to PTH. *In vivo* NaPi-IIa and NHE3 are particularly important as they are vitally responsible for controlling the levels of phosphaturia and bicarbonaturia respectively (Section 1.7.3). Hypercapnia appears to have divergent effects on the biochemical signalling network and downstream response from NaPi-IIa. However, the effect of hypercapnia on NHE3 activity and its ability to rescue pHi after an ammonium chloride pulse were more conclusive. When activated by an AC agonist, the pHi recovery rates under control and elevated pCO_2 were reversed, providing a link between the inhibition of cAMP production and a physiological outcome.

6.5.1 Inhibition of Phosphate Uptake with Hypercapnia

As NaPi-IIa activity is inhibited by cAMP signalling, it was hypothesised that the inhibition of agonist induced cAMP accumulation at elevated CO_2 would result in a relative increase in phosphate ion uptake at this CO_2 concentration, compared to normocapnic control. This hypothesis was based on the assumption that the reduction in cAMP would alleviate the inhibition on NaPi-IIa, enabling a higher level of activity. Whilst application of both AC agonists PTH and FSK inhibited phosphate uptake via PKA, the expected increased response with elevated CO_2 was not observed. Instead, there was a consistent decrease in phosphate uptake, independent of agonist presence, absence or the agonist used.

This inhibition of phosphate uptake at elevated CO_2 can not, therefore, be attributed to cAMP and PKA activity. The reduction in phosphate reabsorption with hypercapnia has been demonstrated previously in the literature (Lotspeich & Malvin, 1956; Webb et al., 1977; Guntupalli et al., 1987; Jehle et al., 1999) and may instead be attributed to the observed Ca^{2+} release with elevated CO_2, especially as Ca^{2+} ions are known to inhibit NaPi-IIa mediated phosphate uptake via PKC (Malmstrom & Murer, 1986; Cole et al., 1987; Martin et al., 1994). Repetition of these experiments in the presence of calcium chelators and PKC antagonists may begin to delinearate the observed trend. Furthermore, the effects of hypercapnia may also be a result of alterations to NaPi-IIa expression, which previously have been observed to increase with isohydric normocapnia, compared to hypercapnia in OK cells (Jehle et al., 1999). It is even possible that the activity of the NHE3

exchanger has an indirect effect on NaPi-IIa activity through alteration of the sodium gradient (Hamm et al., 1984). As elevated CO_2 increases AC agonist inhibited NHE3 activity compared to a normocapnic control (Section 6.5.2), the availability of sodium ions would decrease. With fewer sodium ions available for co-transport by NaPi-IIa, it is likely that phosphaturia would develop.

6.5.2 Decreased Inhibition of AC Agonist Induced NHE3 Activity with Hypercapnia

The effect of CO_2 on the cAMP inhibited Na^+-H^+ antiporter NHE3 is consistent with the observed biochemistry of the influence of CO_2 on cAMP. By measuring NHE3 mediated pHi recovery following an NH_4Cl pulse it was observed that under control conditions recovery rate was faster in cells exposed to 5% (v/v) CO_2 compared to those at 10% (v/v) CO_2. Activation of AC by both PTH and FSK both inhibited NHE3 activity as expected and reversed this control trend, indicative of a reduction of cAMP generated at elevated CO_2. Using pharmacological inhibitors, this CO_2 mediated effect of cAMP was observed to rely on intracellular Ca^{2+} ions released from IP_3 receptors, further agreeing with biochemical data. Ca^{2+} release has been documented to increase HCO_3^- flux in PT cells previously (Liu & Cogan, 1990), although this observation may involve either NHE3 or Na-HCO_3^- transporters. Additionally, modulation of proton secretion rates similar to those observed here have been previously demonstrated with CO_2 application. CO_2 has been demonstrated to not only increase cytosolic Ca^{2+} but also elevate proton secretion (Schwartz & Al-Awqati, 1985; Van Adelsberg & Al-Awqati, 1986). However, these effects were attributed to the action of H^+-ATPases. It is unlikely that the observed pHi recovery rates were mediated by H^+-ATPases as AC agonists inhibited recovery and, under control conditions, both DMA and an absence of sodium ions restricted pHi recovery. Confirmation of that the observed CO_2 trend is due to the activity of NHE3 may be provided through use transporter siRNA or knock-outs generated via zinc finger nucleases, in addition to the use of pharmacological inhibitors such as DMA or S3226 (Schwark et al., 1998).

Inhibition of both PKA and PKC removed the effects of FSK on NHE3. This demonstrates that under these conditions NHE3 activity is inhibited by both cAMP activated PKA and Ca^{2+} ion stimulated PKC. Thus, it is possible that the CO_2 generated Ca^{2+} ions are involved in regulating both control mechanisms. It is possible that this duel regulation is due to the fact that the cells used are not polarised, especially as the two systems are purported to be spatially separated (Section 1.7.3). This may be investigated through the use of primary cell cultures and transwells which enable solution perfusion to both apical and basolateral sides of the cell (Rakonczay et al., 2006).

6.6 Further Future Work

Throughout this chapter where relevant future experiments have been outlined. These largely involve confirming the current conclusions using genetic models incorporating either siRNA or knock-outs generated using zinc finger nucleases, particularly with IP_3 receptors from epithelial cell lines and the NHE3 transporter. These constructs are not currently commerically avaliable for the desired targets and therefore were not implemented in this thesis.

From these results it is not possible to know whether the Ci and Ca^{2+} are interacting with the AC directly or via another molecule or even definitively whether the active Ci species is CO_2 or HCO_3^- ions. Use of *in vitro* AC assays on purified enzymes from these HEK and OK cell lines under conditions of Ci disequilibrium (Hammer et al., 2006) would answer some of these questions. Additionally, it is not known whether the observed effects on AC are a general mechanism on all AC isoforms present or on an individual isoform. *In vitro* assays where possible and AC isoform knock-outs using zinc finger nucleases could further help identify the Ci-regulated enzymes.

An important physiological experiment would be to use isolated proximal tubules for perfusion and NHE studies. Whilst cell lines have numerous advantages, they can be heterogenous and unpolarised, potentially leading to misleading results particularly in epithelial cells such as those from the proximal tubule, which have different proteins associated with the apical and basolateral membranes. Experiments to identify whether the observed CO_2 effect is apical or basolateral are particularly important due to spatial separation of the PKA and PKC mediated signalling networks in response to PTH stimulus (Section 1.7.3). In addition, *Chen et al.* demonstrated a pHi alkalinisation of proximal tubule cells in response to Ci which is not due to HCO_3^- transport but most likely from proton extrusion across the apical membrane (Chen & Boron, 1995a,b). However, this effect depended on whether the cells were exposed to Ci on their apical or basolateral face with the tubule lumen insensitive to Ci and the basolateral proposed to contain a Ci sensor (Chen & Boron, 1995b). In continuation of this work, *Bouyer et al.* demonstrated that this basolateral sensor acted by increasing intracellular Ca^{2+} (Bouyer et al., 2003). These results potentially agree with the work presented in this thesis, although *Bouyer et al.* were unable to locate the Ca^{2+} source (Bouyer et al., 2003). It would, therefore, be of interest to ascertain whether the two signalling observations match up. Futhermore, use of polarised cells would also confirm the physiological involvement of the apical NHE proton transporter compared to the basolateral Na^+/HCO_3^- co-transporters in pHi maintenance and recovery after NH_4Cl pulse.

Further work is also required to identify the CO_2 sensor and the mechanism by which the IP_3 receptor is activated. Due to the involvement of this receptor it is resonable to assume that IP_3 is being generated. Therefore, one of the first experiments of interest would be to measure IP_3 generation in response to elevated CO_2 by with commercially avaliable tritium-labelling kits or a FRET biosensor (Remus et al., 2006), in addition to inhibiting the IP_3 generating enzyme PLC with siRNA. Whilst PLC was inhibited at various points during this thesis the inhibitor U-73122 has since been demonstrated to have questionable inhibitory properties and thus a more efficient method would need to be sought out in future (Klein et al., 2011).

6.7 Clinical Implications of these Observations

The observations detailed in this thesis may have profound implications, particulary when trying to understand the homeostatic control mechanisms of systemic pH and inorganic carbon in the context of metabolic acidosis and hypercapnia. This is particularly important as hypercapnia can occur as a complication of numerous disease states, with elevated CO_2 often associated with a worse prognosis and elevated morbidity. The effects of CO_2 on both the cAMP and Ca^{2+} signalling pathways presented may potentially provide a key mechanism by which the toxic effects of CO_2 are manifested. For example, there is growing evidence that chronic daytime hypercapnia associated with obstructive sleep disorders pre-disposes individuals to cardiovascular disease (Gopalakrishnan & Tak, 2011). Furthermore, the leading cause of hospitalisation and morbidity among COPD patients, who commonly experience hypercapnia, is cardiovascular events (Sin & Man, 2005). *Azzam et al.* suggests that as chronic hypercapnia is known to cause permanent damage to muscle cells in *C.elegans* (Sharabi et al., 2009), a similar mechanism might explain the observed cardiovascular complications (Sin & Man, 2005) and reductions in muscle mass noted with COPD patients (Maltais & Debigaré, 2003). As Ca^{2+} is paramount in maintaining muscle, cardiac and circulatory physiology the signalling events presented in this thesis may provide a key route to understanding pathophysiology of hypercapnia and suggest possibilities for therapeutic intervention.

Inconsistent with the detrimental effects of CO_2, permissive hypercapnia is often used as a treatment, particularly when mechanical ventilation is required to support patients suffering with respiratory complications, and this use of CO_2 is related to an improved outcome. This protective effect has been largely attributed to the anti-infammatory influence of CO_2, however, further understanding into the mechanisms involved in these hypercapnic effects is required. These anti-inflammatory effects stem from the pH independent attenuation of the NF-κB pathway with elevated CO_2 (Cummins et al., 2010). As cAMP is known to potently regulate the NF-κB pathway (Satriano & Schlondorff, 1994; Minguet et al., 2005) it is possible that these signalling events initiate a negative control feedback loop. The benefits of therapeutically administed permissive hypercapnia have also, in part, been attributed to an inhibition of alveolar fluid reabsorption via cAMP mediated endocytosis of Na,K-ATPase (Vadász et al., 2008a). Both cAMP and Ca^{2+} signalling are also known to affect fluid reabsorption in the lung through other mechanisms, through the regulation of the cystic fibrosis transmembrane conductance regulator, CFTR (Cheng et al., 1991), and calcium-activated chloride channels, CaCC (Fischer et al., 2010), respectively. Thus, the signalling event demonstrated in this thesis could provide a link to the physiological effects observed with elevated CO_2.

7 Appendix I: Extended Methodology

7.1 Nigericin Calibration and Compensation of Drift

In order to convert data recorded at 440 nm and 490 nm from excitation of BCECF-AM loaded cells into a measurement of the intracellular pH, a nigericin calibration was carried out according to the methods outlined by *Thomas et al.* and *Hegyi et al.* (Thomas et al., 1979; Hegyi et al., 2004). Briefly, cells are exposed to 10 μg mL^{-1} of the K^+/H^+ antiporter nigericin in high potassium solutions (Section 2.4.1) at a pH range of physiologically relevant values. Most commonly these pH values were 6.8, 7.0 and 7.4. Due to the action of the nigericin, pH equilibrates across the plasma membrane through an exchange of internal K^+ for external H^+, resulting in a pH equilibration better than 90% (Thomas et al., 1979). It can then be assumed that the intracellular pH is equivalent to the known extracellular pH of the perfused solution, thus enabling calibration from the 490/440 nm ratio. By using buffers with high potassium concentrations of 130 mM, similar to the intracellular concentration, nigericin induced K^+/H^+ exchange is not limited by internal K^+. The resultant K^+ gradient will therefore not drive the formation of any pH gradients across the plasma membrane (Thomas et al., 1979). Calibration by this method provides accurate estimation of pHi as small as 0.01 pH units (Thomas et al., 1979). A visual representation of the effect of nigericin on the cells is presented in Figure 58, which displays example raw 490/440 ratio data generated with each consecutive nigericin solution compared to the same data after pH calibration.

Due to the effects of dye loading, dye leakage, and photomultiplier aperture size, one calibration curve is not sufficient for accurate determination of pHi, and an appropriate calibration curve must therefore be selected for each individual experiment (Hegyi et al., 2004). Calibration is only linear over a narrow range of pHi values with calibration curves often divergent, particularly at higher pHi values (Boyarsky et al., 1996; Hegyi et al., 2004). Using the method described by *Hegyi et al.*, a graph can be generated from which a calibration curve can be created specific to every data set recorded, based on the assumption that the resting pH of cells in each experiment should be similar provided that the experimental conditions are identical (Hegyi et al., 2004). With this method, the use of nigericin in each experiment is unecessary. Representative graphs from this calibration process are shown in Figure 59.

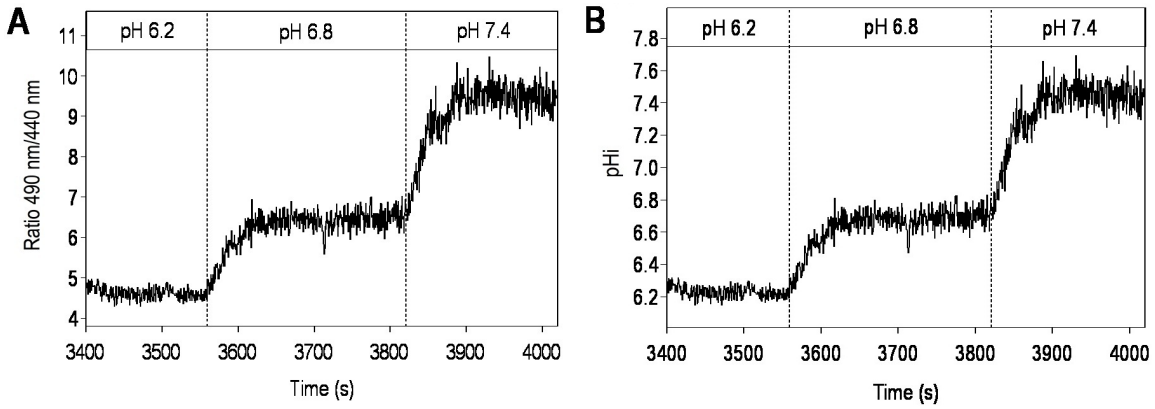

Figure 58: Effect of nigericin on intracellular pH in OK cells. Values presented above the trace refers to the pH of the nigericin containing high potassium solution solution being perfused over cells. **A**: 490/440 nm fluoresence ratio. **B**: Data from A calibrated for pHi.

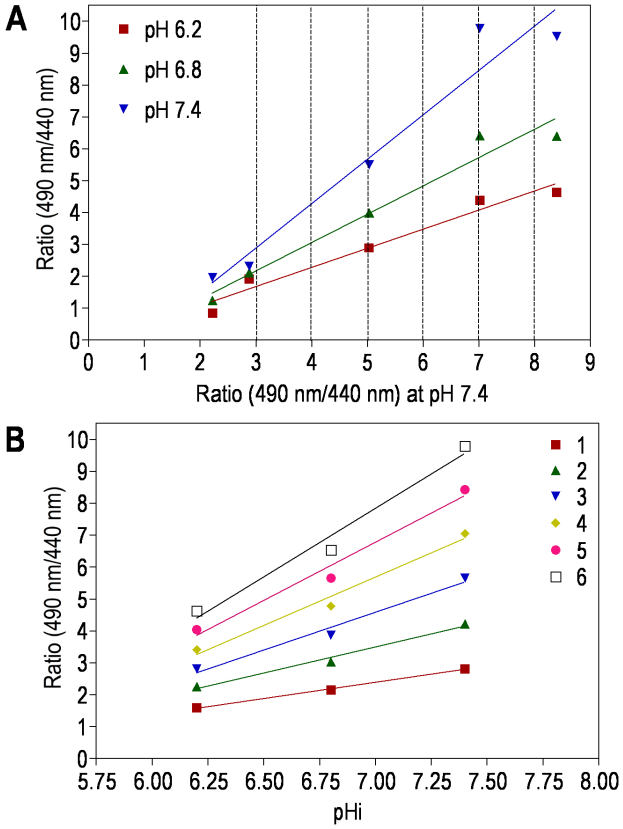

Figure 59: Explanation of pHi calibration. Calibration used the method outlined by *Hegyi et al.*, graphs provided from OK cell data. **A**: Graph of BCECF 490/440 nm emission ratio for nigericin calibration values (each known pHi linked by diagonal linear regression lines) against the 490/440 nm emission ratio at known pHi 7.4. Vertical lines used to construst calibration curves in C and arbitrarily numbered 1-6 from left to right. **B**: BCECF calibration curves. Each line was constructed from the vertical lines in B and their intercepts with diagonal lines of known pHi so that 490/440 nm ratio could be plotted against pHi. From this graph calibration raw data could be calculated individually for each experimental data set.

In addition to nigericin calibrations, raw data was also adjusted to compensate for drift. Drift refers to the continuous and unavoidable leakage of the BCECF-AM dye from the cells and can be seen clearly on the raw data example (Figure 60) as a decrease in emission intensity with 440 nm (Hegyi et al., 2004), therefore potentially leading to a loss of pHi accuracy (Weiner & Hamm, 1989). To compensate for this, data can be adjusted using the method outlined by Hegyi et al. (Hegyi et al., 2004) whereby a resting pHi for cells under each experimental condition is calculated and an imaginary line can be drawn across the data set linking all the time points where the cells are expected to be at this resting pHi. Using this method a correction can be made based on the assumption that the drift is linear, which is generally the case (Hegyi et al., 2004). To compensate for this drift, the product of the following equation is subtracted from the pHi value calculated through nigericin calibration:

$$pHi_{change} = pHi_{start} - pHi_{end} / \text{total number of data sample points within this range}$$

Illustration of this principle is shown in Figure 60 which shows a raw data set with obvious drift (A), the affect on the ratio (B) and an example of the same data set once this drift has been compensated for (C).

It is important to note that in addition to all of the above corrections to the data sets, intital background counts were also removed from raw data, using values measured from the microspectrofluorometer before the shutter to the photomultiplier had been opened.

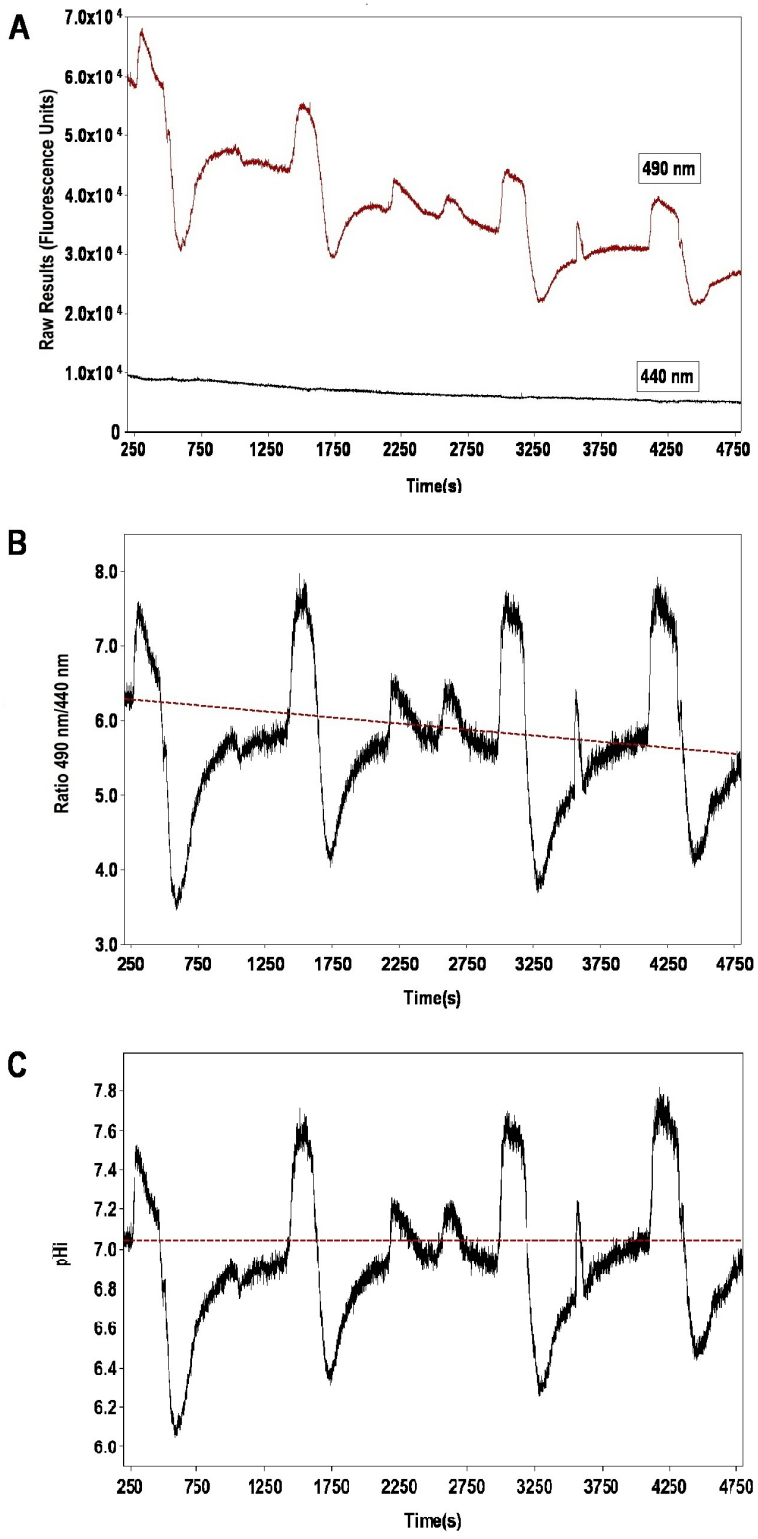

Figure 60: Compensation for drift **A**: Graphical representation of raw fluoresence data displaying obvious drift in the 490 nm values. **B**: Graph of the 490/440 nm ratio for this same data set. Horizontal lines approximately contecting same pHi values. **C**: Data set adjusted for drift and calibrated to show intracellular pH. Horizontal lines approximately connecting same pHi values.

7.2 DT40 Bradford Assay

DT40 cells were grown as a suspension culture. This presented problems when measuring intracellular cAMP levels due to the large amount of insoluble material in lysed cell samples clogging the chromatography columns used to measure cAMP with adherant cells (Section 2.4.6). Instead a cAMP ELISA (GE Healthcare®, RPN2251) was utilised. To account for the possible variations in cell number between samples, ELISA generated cAMP concentrations were normalised for sample protein content. Protein concentration was determined through Bradford assay (Section 2.6.2) where optical density at 595 nm is compared to a standard curve generated using known concentrations of BSA (Figure 61). This value could then be used to generate cAMP concentrations normalised to sample protein content, enabling comparision between assays. Data provided in Table 17 demonstates this method providing a clear increase in normalised cAMP values in cells exposed to forskolin compared to a DMSO control.

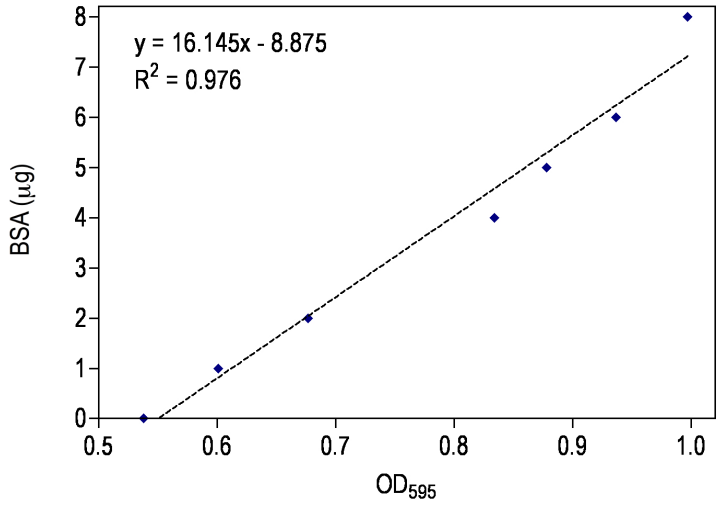

Figure 61: Bradford standard curve example. Experimentally determined standard curve generated using standard protein bovine serum albumin (BSA) at known concentrations.

Sample	Bradford Assay OD_{595}	Protein Conc. (μg/ml)	ELISA Generated cAMP Conc. (fmol/ml)	Normalised cAMP Content (fmol/μg protein)	Mean	S.E.M.
DMSO 1	0.637	1.419	45.11	31.79	84.57	25.10
DMSO 2	0.625	1.225	94.38	77.02		
DMSO 3	0.63	1.306	199.56	152.80		
DMSO 4	0.605	0.902	69.20	76.69		
FSK 1	0.658	1.758	2179.97	1239.95	929.03	122.34
FSK 2	0.642	1.500	1354.27	902.97		
FSK 3	0.632	1.338	859.51	642.22		
FSK 4	0.651	1.645	1531.56	930.99		

Table 17: Normalising DT40 ELISA sample cAMP content to protein content: table to illustrate calculations. Sample protein concentration calculated via Bradford assay and comparison of the optical density at 595 nm to a BSA generated standard curve (Figure 61). Concentration of cAMP generated using cAMP ELISA (GE Healthcare®, RPN2251). S.E.M. refers to the standard error of the mean.

7.3 Fura 2 Calcium Calibration

To convert data recorded at 340 nm and 380 nm from excitation of Fura 2-AM loaded cells into the correct measurement of the intracellular [Ca^{2+}], calibration was carried out according to the methods outlined by *Grynkiewicz et al.* and *Bouyer et al.* (Grynkiewicz et al., 1985; Bouyer et al., 2003). Cells were loaded with Fura 2-AM (Section 2.4.2) with the inclusion of 5 μM ionomycin during the second incubation step. Ionomycin is a calcium ionophore which transports ions across the lipid bilayer of the cell membrane allowing for the assumption that the cytoplasmic [Ca^{2+}] is equal to that of the surrounding medium. The cells were then incubated in Krebs-Ringer-HEPES solutions containing 0 mM (130 mM NaCl, 25 mM Glucose, 20 mM HEPES, 14 mM $NaHCO_3$, 5 mM KCl, 1 mM $MgSO_4$, 5 mM EGTA, pH 7.4) and dye saturating 5 mM (130 mM NaCl, 25 mM Glucose, 20 mM HEPES, 14 mM $NaHCO_3$, 5 mM KCl, 1 mM $MgSO_4$, 5 mM $CaCl_2$, pH 7.4) free Ca^{2+} ions and their fluorescence levels at 340 and 380 nm measured (Figure 62).

From these values intracellular [Ca^{2+}] could be calculated using the method outlined by *Grynkiewicz et al.* in which the equation shown below was employed (Grynkiewicz et al., 1985). Here K_d refers to the dissociation constant, $R_{340/380}$ the experimental 340/380 nm ratio, R_{min} the minimum 340/380 nm ratio at 0 mM Ca^{2+}, R_{max} the maximum 340/380 nm ratio at dye saturating 5 mM Ca^{2+}, S_{f2} the fluorescence measurement at 380 nm with 0 mM Ca^{2+} and S_{b2} 380 nm fluorescence with dye saturating 5 mM [Ca^{2+}].

$$[Ca^{2+}]_i = K_d \left(\frac{R_{340/380} - R_{min}}{R_{max} - R_{340/380}}\right) \text{ x } \frac{S_{f2}}{S_{b2}}$$

To ensure that the light beam used to excite the dye for fluoresence measurements was not causing autofluorescence from another cellular constituent, cells were exposed to the beam in the absence of Fura 2. This test gave fluorescence values of ∼2.50 at 340 nm, ∼3.00 at 380 nm and 340/380 ratios ∼0.85. While small, these values could lead to the generation of potentially misleading Ca^{2+} concentrations. To eliminate this possibilty at the end of every experiment cells were quenched using 5 mM $MnCl_2$, as suggested by *Bouyer et al.* (Bouyer et al., 2003). Quenched fluoresence values for each wavelength were then treated as background and removed from the experimental values prior to ratio generation and calculation of Ca^{2+} concentration.

The dissociation constant (K_d) was calculated for the equipment employed, allowing for potential variations in instrument sensitivity and optical path length. To do this, the commercially avaliable Molecular Probes® 'Fura-2 Calcium Imaging Calibration Kit' was utilised. In this kit free-Fura 2

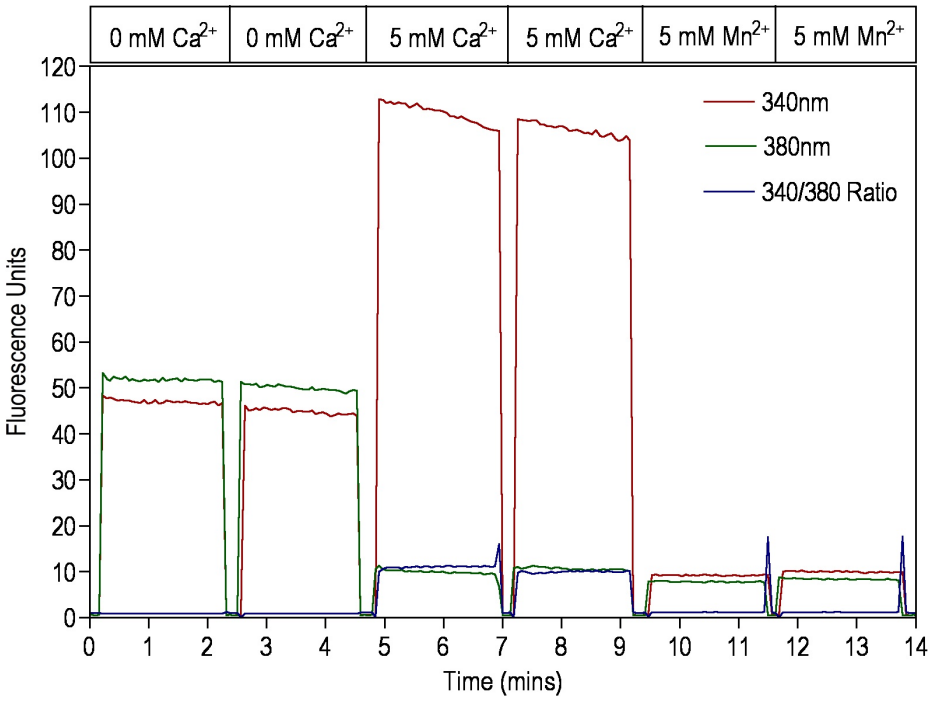

Figure 62: Ionomycin calibration example. 0 mM Ca^{2+} solution refers to a Krebs-Ringer-HEPES solution containing 5 mM EGTA, 5 mM Ca^{2+} solution with 5 mM $CaCl_2$ and 5 mM Mn^{2+} with 5 mM $MnCl_2$

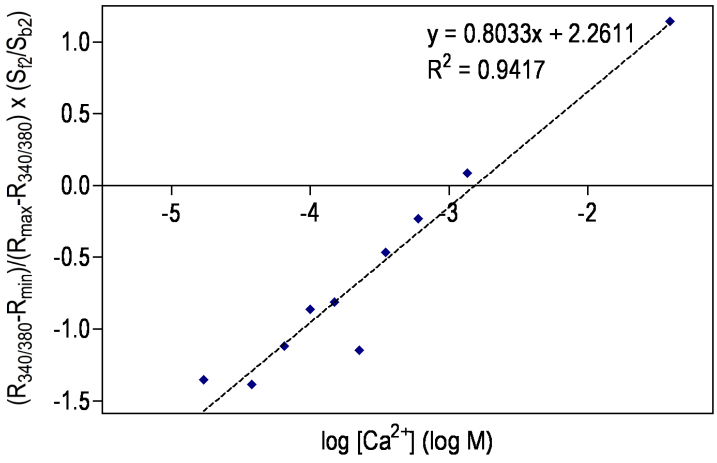

Figure 63: Fura 2-AM dissociation constant calculation. Experimentally determined calibration curve generated using Molecular Probes® 'Fura-2 Calcium Imaging Calibration Kit'. Log of the dissociation constant provided by the y-axis intercept of the best-fit line provided. $R_{340/380}$ refers to the the experimental 340/380 nm ratio, R_{min} the minimum 340/380 nm ratio at zero Ca^{2+}, R_{max} the maximum 340/380 nm ratio at dye saturating Ca^{2+}, S_{f2} the fluorescence measurement at 380 nm with zero Ca^{2+} and S_{b2} 380 nm fluorescence with dye saturating Ca^{2+}

acid is provided in a range of free Ca^{2+} ion/EGTA mixtures providing a range of free calcium from 0 μM through to dye saturating concentrations of 39 μM. These solutions were measured for their 340 and 380 nm fluorescence values under similar conditions to the *in cellulo* experimental conditions at pH 7.2 and 37°C. Data generated from these measurements can then be used to draw a calibration graph Figure (63) where the y-axis intercept forms the log of this empirically determined dissociation constant. Using this method, the dissociation constant was calculated as 182.43 nM.

An example of this calibration process including removal of background quench values and application of the *Grynkiewicz et al.* equation to generate Ca^{2+} concentrations is provided as Figure 64.

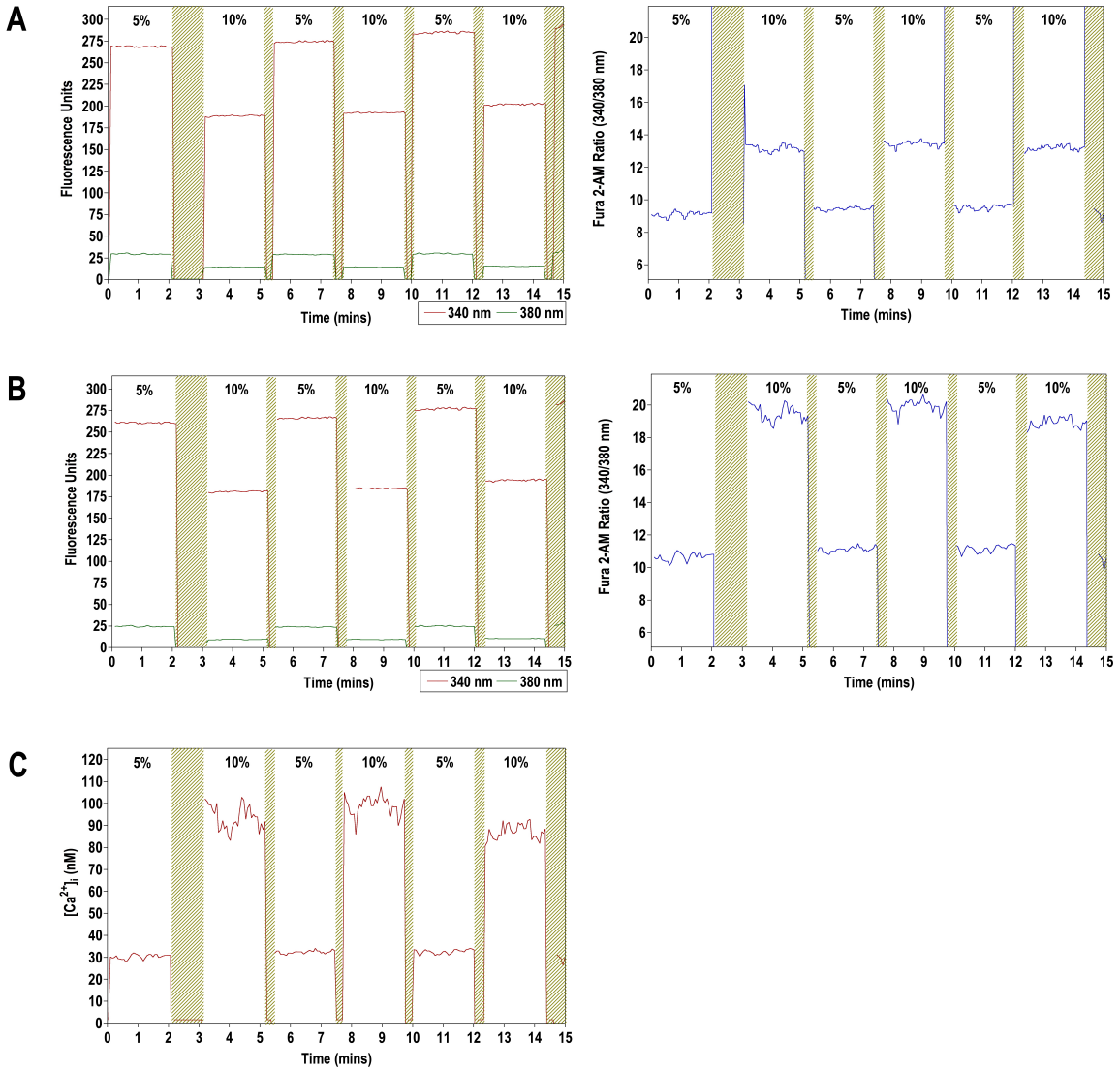

Figure 64: Example of experimental Fura 2 data calibrated for $[Ca^{2+}]$ **A**: Graphical representation of raw fluorescence data (left panel) with 340/380 nm ratio (right) **B**: Graphical representation of fluorescence data with quench values removed, raw data on left and 340/380 nm ratio on right. **C**: Final graph for Ca^{2+} ion concentration.

7.4 Measuring pHi Recovery After Ammonium Chloride Pulse

In order to monitor the activity of sodium-hydrogen exchanger 3 (NHE3), OK cells were exposed to ammonium chloride pulses under different conditions and NHE3 dependent pHi recovery measured using the cell-permeable dye BCECF-AM. Once pHi values had been calculated using the methods provided in Appendix 7.1, recovery was then measured by two methods: linear regression and ΔpHi. These methods were chosen as a combination of methodology from the literature (Preisig et al., 1987; Alpern, 1985). As displayed in Figure 65, recovery rate slows as pHi approaches its resting level, thus initial recovery rates were measured for comparision between samples. This intial rate provides the best representation of NHE3 activity prior to any buffering of protons by cellular constituents (Preisig et al., 1987). With both methods recovery was calculated from an initial starting point (time zero) set as the lowest pHi measurement following pHi decline. Linear regression values were calculated using GraphPad Prism 4® using pHi values from the first 45 seconds of recovery (Figure 65).

The pHi recovery rate was also measured as a change in pHi (ΔpHi) from the 'time zero' (see above) starting point. Subsequent data points were calculated as positive or negative changes in pHi from this initial starting value, allowing for rate to be estimated as ΔpHi sec^{-1}. This method was of most value when creating graphical comparisons of recovery rates (Figure 66).

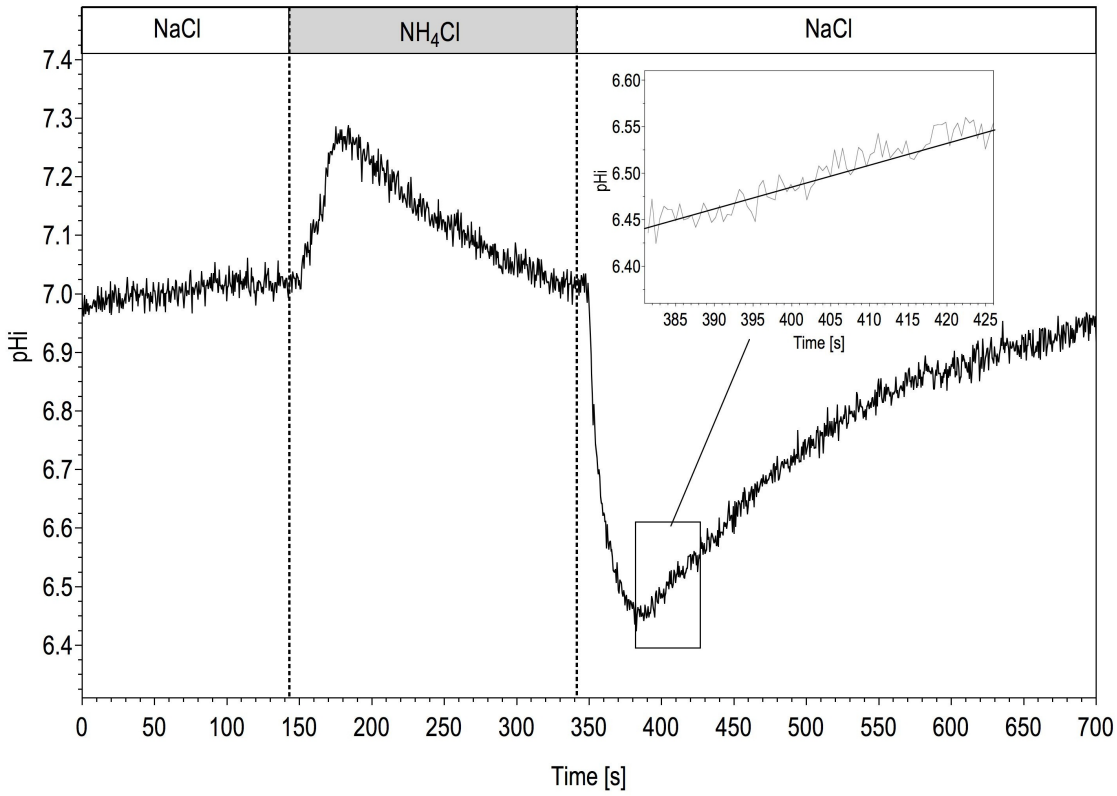

Figure 65: Example of NH_4Cl pulse pHi recovery measurements. Initial recovery rate measured over first 45 seconds of recovery using lowest recorded pHi as time zero. Insert provides magnification of this period with linear regression best fit line illustrated for this data set.

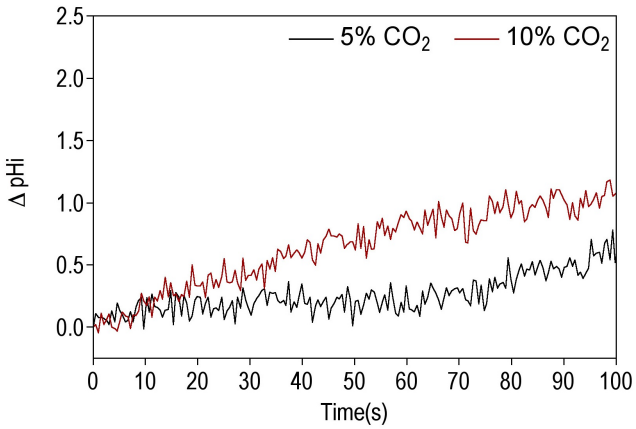

Figure 66: Example of ΔpHi method of measuring pHi recovery following NH_4Cl pulse. Comparision period similar to that shown in Figure 65 with the lowest recorded pHi following NH_4Cl pulse set as time zero (t = 0). Data points from this pHi value at t = 0 were then be measured as change in pHi (ΔpHi). Graphical representations were extended to a 100 second period for better visual comparison.

8 Appendix II: Proteomics

8.1 Introduction

Chapters 3, 4 and 5 focused on the effects of elevated CO_2 on a specific intracellular signalling pathway and its physiological outcome. In contrast, this appendix is concerned with the global effects of CO_2 on protein expression. Using quantitative proteomic analysis of whole cell lysates using iTRAQ reagents and LC/MS/MS, proteins could be identified and their relative abundances calculated between samples. This method was used to identify proteins affected by elevation of CO_2.

Evidence for global effects of CO_2 in the literature have previously focused on transcriptomics (Sheth et al., 2008; Sharabi et al., 2009). An abundance of mRNA, however, is not necessarily indicative of the resultant protein concentration, which depends on its translation and degradation rates. In fact, analyses indicate that differences in protein concentrations are only 20% - 40% attributable to variable mRNA levels, underlining the importance of post-transcriptional regulation (Brockmann et al., 2007). Additionally, the function of many proteins is further governed by a range of post-translational modifications such as phosphorylation and glycosylation indistinguishable by transcriptomic analysis methods.

8.1.1 iTRAQ Reagents

Proteomic analysis utilised the iTRAQ reagent system. These reagents, introduced by Darrly Pappin and colleagues at Applied Biosystems in 2004 (Ross et al., 2004), refer to a set of amine specific isobaric reagents. These reagents, when fragmented in the mass spectrometer, yield unique reporter ions with the same mass but different charges, allowing identification of the iTRAQ label employed. This means that labelled peptides are indistinguishable in MS but exhibit intense signatures with MS/MS supporting quantitation (Ross et al., 2004). In addition to their isobaric nature, these reagents are designed to react with all primary amines, including the N-terminus and the ϵ-amino group of any of the lysine side-chains (Ross et al., 2004). They can, therefore, be used with all protein mixtures with samples typically reduced, alkylated and enzymatically digested with typsin prior to labelling (Section 2.6.5). Labelling with iTRAQ reagents enhances MS/MS fragmentation, improving the confidence of the results (Zieske, 2006). Through use of this method up to eight different samples (using the eight available reagents) can be analysed simultaneously, allowing for quantitative comparison of the labelled peptide peaks.

8.2 Optimisation of Sample Generation Method

As covered in Chapters 3, 4 and 5, elevation of pCO_2 from 5% (v/v) to 10% (v/v) resulted in changes in intracellular pH and calcium in addition to alterations in agonist induced cAMP. To establish whether any protein expression levels altered under elevated CO_2 was due to a combination of these variables opposed to CO_2 itself, various control experiments were simultaneously carried out, varying CO_2, mimicking the CO_2 mediated pHi change with 2 mM propanoic acid, and by chelating intracellular calcium using BAPTA-AM. The 8 conditions chosen for experimentation are detailed in Table 18. As both BAPTA-AM and FSK were added as solutions in a DMSO solvent, where these additions were absent the requisite volume of DMSO was added to eliminate this as a potential variable. HEK-293t cells were used as these cells had the advantage of being both similar to those used in previous chapters, thus yielding potentially comparable results, in addition to being of human origin and, therefore, iTRAQ labelled peptides could be identified with appropriate levels of confidence using the extensive human NCBI library. Each condition was carried out simultaneously and repeated three times to produce independent replicates of samples.

Preparation of samples (Section 2.6.1) required an 8 hour incubation step at the appropriate pCO_2 and agonist/chelator concentration. This step was required to allow cells to respond and where appropriate alter their levels of protein expression. As CO_2 decreases the pH of solutions, preliminary experiments were carried out to monitor the pH over the whole 8 hour period in an attempt to control medium pH between experiments requiring different CO_2 concentrations, to help eliminate pH as a determining factor. Similar to results displayed in Section 5.2.1, optimal experimental conditions were chosen where the media pH was maintained at similar levels between samples for the longest duration. This was achieved by including 100 mM HEPES in the incubating media in addition to a starting pH of 7.50 for 5% (v/v) CO_2 samples and pH 7.65 for 10% (v/v) CO_2 . As displayed in Figure 67, under these conditions the pH was equilibrated by 1 hour, with a difference in pH of only $0.01 \pm 4.08 \times 10^{-3}$ between samples at this time and $0.02 \pm 9.57 \times 10^{-3}$ after the full 8 hours.

In order to perform quantitative proteomic comparisons prior to trypsin digest and labelling with the isobaric tags, each sample was analysed by Bradford assay (Section 6) to calculate protein concentration. Using this value, 50 μg of each sample could be measured and treated further. To test visually that these protein concentrations were correct an SDS-PAGE gel was run using 10 μg of sample protein as calculated by this method. These gels (Figure 68), show that each sample within the three replicates gave similar intensity bands, implying equal loading of protein as desired.

Sample Number	[CO_2] (v/v)	Additional Conditions
1	5%	DMSO
2	5%	10 μM FSK
3	5%	2 mM PA (DMSO)
4	5%	10 μM FSK, 2 mM PA
5	10%	DMSO
6	10%	10 μM FSK
7	10%	1 mM BAPTA-AM
8	10%	10 μM FSK, 1 mM BAPTA-AM

Table 18: Experimental conditions for iTRAQ samples.

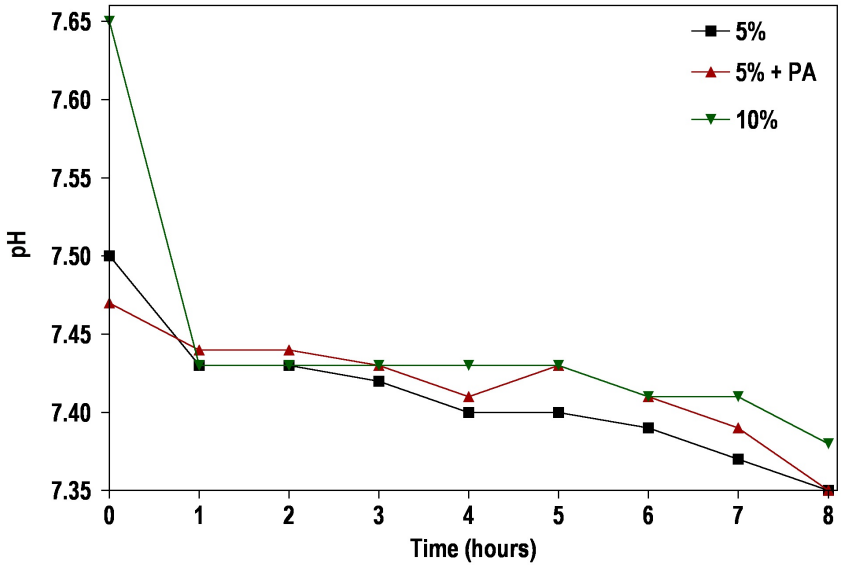

Figure 67: Optimisation of pH for iTRAQ sample preparation. pH changes with each pCO_2 and different starting pH values of pH 7.50 for 5% CO_2 (v/v) and pH 7.65 for 10% (v/v) CO_2, 100mM HEPES. Legend refers to CO_2 concentrations as v/v in air.

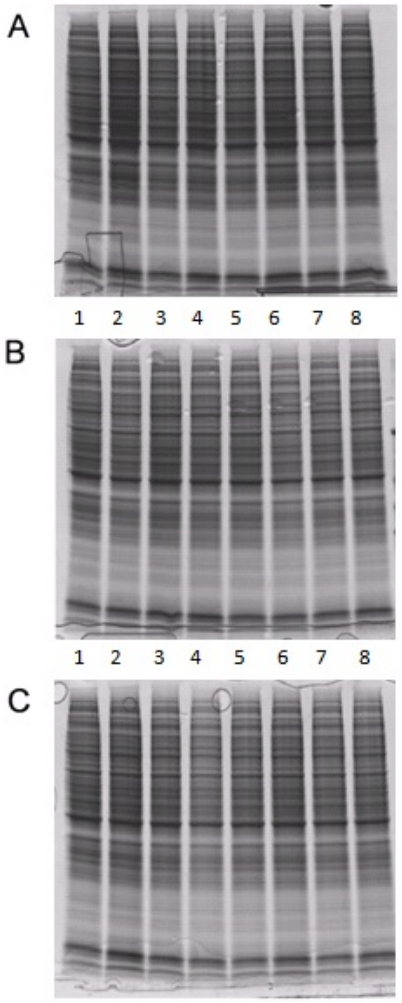

Figure 68: 1D SDS-PAGE gels of samples for iTRAQ labelling. Gels labelled A, B and C representing 10 μg of HEK-293t whole cell lysate samples from each independent experiment run on 12% acrylamide gels. Wells left to right on all gels displaying samples for: [1] 5% (v/v) CO_2 DMSO control, [2] 5% (v/v) CO_2 with 10 μM FSK, [3] 5% (v/v) CO_2 with 2 mM PA, [4] 5% (v/v) CO_2 with 10 μM FSK and 2 mM PA, [5] 10% (v/v) CO_2 DMSO control, [6] 10% (v/v) CO_2 with 10 μM FSK, [7] 10% (v/v) CO_2 with 1mM BAPTA-AM, [8] 10% (v/v) CO_2 with 10 μM FSK and 1 mM BAPTA-AM and where relevant a standard protein ladder.

8.3 Comparision of iTRAQ Proteomic Data

Use of the iTRAQ LC/MS/MS method generated data for 1502, 2116 and 1965 individual proteins for each replicate respectively, thus giving an average estimated coverage of 9.31% of the typical protein content of a human cell (Uhlen, 2005; Bodzon-Kulakowska et al., 2007). This value is low compared to similar procedures from the literature which report proteome coverage of 20-30% (Ross et al., 2004), but still usable. The partial peptide sequences were compared through the program ProteinPilot^{TM} 2.0.1, against the NCBI library for *Homo sapiens* for identification where possible to enable further comparison between samples.

ProteinPilot^{TM} generates a Microsoft Excel^{TM} spreadsheet (example displayed as Table 19) displaying the quantitative amount of each protein as a ratio compared to the control experiment (5% [v/v] CO_2 with no FSK or BAPTA-AM) value. Associated with each ratio are two significance measurements: a p-value and error factor. Briefly, the p-value refers to the probability that the observed ratio was different from unity by chance with values closer to zero indicating greater significance. The error factor is concerned with reporting errors in the ratio with the true ratio expected to be found between the 'ratio x error factor' and the 'ratio / error factor'. Therefore, in this case the closer the number is to 1, the better the confidence of the result.

Accession	**Protein Name**	**Ratio**	**P-value**	**Error Factor**
gi—4503483	Translation elongation factor 2	1.02188611	0.399478436	1.051439881
gi—4885431	Heat shock 70kDa protein 1B	1.009026885	0.713204145	1.049557567

Table 19: Sample of ProteinPilot^{TM} generated data.

Due to the large quantity of data generated, it was unfeasible to manually identify proteins with altered expression levels. Therefore, a program was written using the programming language Python^{TM}. This program (Section 8.3.1) was designed to search through the proteomic data sets and select ratios of up or down-regulated proteins, chosen to have ratios either above 1.1 or below 0.9. From these values only those with appropriate levels of significance (with p-values below 0.05) were then allowed for further selection. The identified peptides with significantly altered expression levels were then compared across all three replicate data sets from each independent experiment to produce the results presented in Section 8.4.

8.3.1 Program Written to Analyse Proteomic Data

The program written to analyse the proteomics data is provided in the boxes below with explanation provided in red following a hash (#).

```
from __future__ import division
# Divides numbers properly instead of treating all numbers as intergers

import csv
import string
# Imports csv and string modules for use later on

# The 'def read_data' routine below defines how to read in the data as a csv
# (comma-separated values) file

def read_data(filename,spacing=0):
        f=open(filename,'U')
        fid=[]
        for line in f:
                fid.append(line)
        f.close()
        fid = fid[spacing:]
        inData=csv.reader(fid,delimiter=',')

data=[]
# Square brackets instruct the program to read the data as a list rather than
# an array

for row in inData:
                data.append(row)
# Reads data in rows not columns
```

```
        return data
# Once data has been read in it is returned to its previous location

# The 'def anyabove' and 'def anybelow' routines below define how to create
# cut-off values for analysing quantitative ratios of protein concentrations
# between samples.  Values of 1.1 for up-regulation and 0.9 for down-regulation
# were chosen arbitrarily (see below) with ratio values above or below these
# values respectively highlighted as of interest

def anyabove(list,value):
        for element in list:
                if element > value:
                        return True
        return False

def anybelow(list,value):
        for element in list:
                if element < value:
                        return True
        return False

# The 'def reg' routine then defines how to apply these cut-off values

def reg(filename):
        data = read_data(filename)  # Reads in data in rows
        print 'Length of file:', filename, len(data)
# Generates a read-out of the file length (number of rows) and the associated
# file name

        above = 1.1
        below = 0.9
# Defines the cut-off values
```

```
cols = [6,9,12,15,18,21,24]
# Defines which columns to apply this command to, those chosen contain the
# ratios of protein content between samples

        printout=False
# The program had some difficulty reading some parts of the data due to absent
# and blank cells in the original csv/excel file.  The following lines of code
# deal with this problem

for i in range(2,len(data)):         # Adds any missing columns
        try:
                dummy = data[i][25]  # Looks at all columns to number 25
        except:
                data[i].append('')   # Adds blank cells at the end of rows if
                data[i].append('')   # cells are absent

        for c in cols:
                if data[i][c]=='':
                        data[i][c] = data[i-1][c]
                        data[i][c+1] = data[i-1][c+1]
                        data[i][c+2] = data[i-1][c+2]

# Where empty cells are present this command instructs the program to read in
# the value from the previous row in a repetitive loop and is repeated for
# ratios, p-values and error factors.  This is important in sections of the data
# where the peptide sequence had numerous potential identities when searching
# the human NCBI database

# The section below then acts as a filter, telling the program to apply the
# previously defined routines and create a list of protein IDs (unique
#  identifiers for each protein, using the 'GenInfo Identifier' from the NCBI
# Genbank database located in the data set as column 3) for those proteins which
```

```
# fit the stipulated criteria of having one or more ratios above or below the
# previously defined cut-off values


        j=0
        i_out = []
        ID_out = []
        for i in range(1,len(data)):
                values=[]
                for c in cols:
                        values.append(float(data[i][c]))


                if anyabove(values,above) or anybelow(values,below):
                        i_out.append(i)
                        ID_out.append(data[i][3])


        data_out=[0]*len(i_out)
        a=0
        for i in i_out:
                data_out[a] = data[i]
                a+=1


        return data_out,ID_out


# The routine below, 'def pv' acts as another filter taking the data which
# fulfils the above criteria and then tests for the significance of the data,
# only selecting ratios with an associated p-value below a defined cut-off value,
# set below as 0.05


def pv(data,below=0.2):
        p_cols = [7,10,13,16,19,22,25]  # These columns contain p-values
        i_out = []
        ID_out = []
```

```
        for i in range(0,len(data)):
                values=[]
                for c in p_cols:
                        try:
                                values.append(float(data[i][c]))
                        except:
                                pass

                if anybelow(values,below):
                        i_out.append(i)
                        ID_out.append(data[i][3])

        data_out=[0]*len(i_out)
        a=0
        for i in i_out:
                data_out[a] = data[i]
                a+=1

        print 'Number of significant rows:', len(ID_out)

        return data_out,ID_out

# The 'def pvalues()' tells the program which files to apply these filters on
# with File-1.csv containing the data for the first replicate of experiments
# etc.  By including all three files the filters can be applied to all three
# data sets at the same time

def pvalues():
        filename1 = './File-1.csv'
        data1,ID1 = reg(filename1)
        filename2 = './File-2.csv'
        data2,ID2 = reg(filename2)
```

```
        filename3 = './File-3.csv'
        data3,ID3 = reg(filename3)

        cutoff = 0.05                          # Defines the p-value cut-off

        d1_sig,ID1_sig = pv(data1,below=cutoff) # Selects rows which have any
        d2_sig,ID2_sig = pv(data2,below=cutoff) # p-values below the prescribed
        d3_sig,ID3_sig = pv(data3,below=cutoff) # cut-off

# The following 'fileout' routines print the rows from each file containing
# data that meets the prescribed criteria as three separate csv files entitled
# 'significant1.csv' for data set 1 etc.


        fileout=open('./significant1.csv','a')
        for i in range(0,len(d1_sig)):
                print >>fileout, d1_sig[i]
        fileout.close()
        fileout=open('./significant2.csv','a')
        for i in range(0,len(d2_sig)):
                print >>fileout, d2_sig[i]
        fileout.close()
        fileout=open('./significant3.csv','a')
        for i in range(0,len(d3_sig)):
                print >>fileout, d3_sig[i]
        fileout.close()

# The rest of the code then compares the unique protein IDs (using the NCBI
# 'GenInfo Identifier' numbers) for the data which fits the above criteria and
# searches through the three lists generated from each data set to identify
# which proteins appear in all three.  It then produces a file containing these
# protein IDs and their associated data, bringing together the values from each
```

```
# independent experimental replicate


        ID_common = []
        for ID in ID1_sig:
                if ID in ID2_sig and ID in ID3_sig:
                        ID_common.append(ID)


        print 'Amount of cross matches:', len(ID_common)


        ind1=[]
        row_number1=[]
        for i in range(0,len(d1_sig)):
                ind1.append(d1_sig[i][3])
        for ID in ID_common:
                row_number1.append(ind1.index(ID))



        ind2=[]
        row_number2=[]
        for i in range(0,len(d2_sig)):
                ind2.append(d2_sig[i][3])
        for ID in ID_common:
                row_number2.append(ind2.index(ID))
        ind3=[]
        row_number3=[]
        for i in range(0,len(d3_sig)):
                ind3.append(d3_sig[i][3])
        for ID in ID_common:
                row_number3.append(ind3.index(ID))


        fileout=open('./significant.csv','a')
        for i in range(0,len(row_number1)):
```

```
                ia = row_number1[i]; ib = row_number2[i]; ic = row_number3[i]
                print >>fileout, d1_sig[ia][3],',',d1_sig[ia][4],',',
                        string.join(d1_sig[ia][6:],',')
                print >>fileout, d2_sig[ib][3],',',d2_sig[ib][4],',',
                        string.join(d2_sig[ib][6:],',')
                print >>fileout, d3_sig[ic][3],',',d3_sig[ic][4],',',
                        string.join(d3_sig[ic][6:],',')
        fileout.close()

if __name__ == '__main__':
        pvalues()
```

This program generated a file containing 108 NCBI 'GenInfo Identifiers' for proteins which could then be searched manually for any trends, the results from which are provided in Section 8.4.

8.4 Proteins Identified to have Altered Expression

Whilst the analysis program displayed in Section 8.3.1 generated 108 proteins of interest, when looking at the data very few of these proteins showed any consistant trends across the experimental conditions. Those with such trends are displayed in Table 20. Only two proteins exhibited altered expression with CO_2: carbonic anhydrase II which was upregulated and methylenetetra- hydrofolate dehydrogenase I which was downregulated. Results from FSK activated samples were more promising with proteins histone H3 and KIA0098 upregulated and chaperonin containing TCP1 and solute carrier family 16 downregulated.

Multiple papers have looked at the effect of elevated CO_2 on the cell although, as mentioned, most of these have looked at the gene expression level rather than the downstream protein production. *Tomanek et al.* focuses on the effect of elevated CO_2 on estuarine eastern oyster *Crassostrea virginica* protein expression; however hypercapnia in this context ($\sim$357 Pa PCO_2) is a lot lower than in humans ($\sim$6 kPa). Here the authors observe differential expression of 12% of proteins (54 of 456) with 17 identified (Tomanek et al., 2011). In this study elements of the cytoskeleton were found to be upregulated including actin, actin-polymerisation factor and calponin 2 and in addition a host of proteins involved in cellular response to oxidative stress such as superoxide dismutase (catalyses superoxide generation), peroxiredoxins 2, 4 and 5 (antioxidants involved in detoxification of organic peroxides and H_2O_2), thioredoxin-related nucleoredoxin, mitochondrial malate dehydrogenase (Tomanek et al., 2011). Furthermore, there was an observed upregulation of certain regulators of protein synthesis and degradation, including the 40S ribsomal protein and proteosome alpha type 3 protein (Tomanek et al., 2011). Taken as a whole, these changes to the proteome indicate that elevated CO_2 is causing significant oxidative stress by producing reactive oxygen species (ROS) either directly or indirectly, with the concomitant lowered pH effecting electron transport chain efficiency. The results from the study presented in this report do not support any of these findings, although due to the poor peptide identification this is not surprising.

From transcriptomics there is evidence in the literature that elevated CO_2 levels lead to increased expression of apoptotic proteins in the cortical neurons of newborn piglets (Fritz et al., 2005), cell adhesion molecules procollagen and fibulin, surfactant proteins A and D and chloride channel-activated 3 in neonate mice (Li et al., 2006a), innate immune and inflammatory response genes downstream of the NF-κB pathway in human alveolar adenocarcinomic cells (Cummins et al., 2010) and sGC, ubiquitin ligase and elements of the innate immune system in *Caenorhabditis elegans*

(Sharabi et al., 2009). There is also evidence for decreased gene expression of immune response genes and elements of the WNT1-inducible signalling pathway in neonate mice (Li et al., 2006a) and heat shock proteins in *Candida albicans* (Sheth et al., 2008) and *Caenorhabditis elegans* (Sharabi et al., 2009). Interestingly *Sharabi et al.* reported downregulation of carbonic anhydrase genes in *Caenorhabditis elegans* after 6 and 72 hours of elevated CO_2 (Sharabi et al., 2009) whilst this report showed upregulated protein expression at 8 hours. Repetition of this experiment would be needed to confirm this result.

As noted, unfortunately this experiment returned very little useful data. Whilst the experimental method for cell treatment has been optimised throughout this report and the lysis method is near identical to that which is recommended in the literature (Witzmann et al., 2002; Bodzon-Kulakowska et al., 2007), there are numerous options for the cell lysate sample preparations and LC/MS/MS separation. It may be possible that the conditions used were not optimum for the complexity of the samples due to the facilities available. Further experimentation would be required to improve the quality of the data returned.

Accession	**Protein Name**	**Function**	**Condition**	**Amount Compared to 5% CO_2 (v/v) DMSO control (%)**
gi—14250065	Calmodulin 2	Calcium-binidng messenger protein transducing calcium messages	Downregulated by FSK but not at elevated CO_2	5% 90.50, 10% 106.00
gi—16306837	Chaperonin containing TCP1	Chaperonin (involved in protein folding) essential for enabling cytoskeletal proteins actin and tubulin to fold to their native state	Downregulated by FSK	93.95
gi—19923753	Solute carrier family 16	Membrane mono-carboxylate (e.g. lactate, pyruvate and ketones) transporters	Downregulated by FSK	88.00
gi—30048109	Methylenetetrahydrofolate dehydrogenase 1	Enzyme involved in the production of reducing agent NADPH	Downregulated at 10% CO_2	93.95
gi—37724561	Lung cancer oncogene 7	Protein postulated to be involved in the progression of lung cancer	Upregulated by FSK	119.35
gi—51459502	Histone H3	Involved in the structure of chromatin	Upregulated by FSK	160.54
gi—58257644	KIAA0098 protein	Unknown - possible chaperonin	Upregulated by FSK	125.27
gi—15080386	Carbonic anhydrase II	Enzyme catalysing the reversible hydration of CO_2 to HCO_3^-	Upregulated at 10% CO_2	111.42

Table 20: Results from proteomic analysis. CO_2 concentration v/v in air.

References

Abou-Samra, A. B., Jüppner, H., Force, T., Freeman, M. W., Kong, X. F., Schipani, E., Urena, P., Richards, J., Bonventre, J. V., & Potts, J. T. (1992). Expression cloning of a common receptor for parathyroid hormone and parathyroid hormone-related peptide from rat osteoblast-like cells: a single receptor stimulates intracellular accumulation of both cAMP and inositol trisphosphates and increases intracel. *PNAS USA*, 89(7), 2732–6.

Acin-Perez, R., Russwurm, M., Günnewig, K., Gertz, M., Zoidl, G., Ramos, L., Buck, J., Levin, L. R., Rassow, J., Manfredi, G., & Steegborn, C. (2011). A phosphodiesterase 2A isoform localized to mitochondria regulates respiration. *J Biol Chem*, 286(35), 30423–32.

Adrogue, H. J. & Madias, N. E. (1998). Management of life-threatening acid-base disorders. *N Engl J Med*, 338(1), 26–34.

Agus, Z. S., Gardner, L. B., Beck, L. H., & Goldberg, M. (1973). Effects of parathyroid hormone on renal tubular reabsorption of calcium, sodium, and phosphate. *Am J Physiol*, 224(5), 1143–8.

Agus, Z. S., Puschett, J. B., Senesky, D., & Goldberg, M. (1971). Mode of action of parathyroid hormone and cyclic adenosine 3',5'-monophosphate on renal tubular phosphate reabsorption in the dog. *J Clin Invest*, 50(3), 617–26.

Alberts, B. (2002). *Molecular biology of the cell*. New York; London: Garland, 4th edition.

Allgrove, J., Chayen, J., & O'Riordan, J. L. (1983). The cytochemical bioassay of parathyroid hormone: further experience. *J immunoassay*, 4(1), 1–19.

Alpern, R. J. (1985). Mechanism of basolateral membrane H+/OH-/HCO-3 transport in the rat proximal convoluted tubule. A sodium-coupled electrogenic process. *J Gen Physiol*, 86(5), 613–36.

Alvarez, R. & Bruno, J. J. (1977). Activation of cardiac adenylate cyclase: horminal modification of the magnesium ion requirement. *PNAS USA*, 74(1), 92–95.

Alvarez, R. & Daniels, D. V. (1992). A Separation Method for the Assay of Adenylyl Cyclase, Intracellular Cyclic-AMP, and Cyclic-AMP Phosphodiesterase Using Tritium-Labeled Substrates. *Anal Biochem*, 203(1), 76–82.

Amato, M. B., Barbas, C. S., Medeiros, D. M., Magaldi, R. B., Schettino, G. P., Lorenzi-Filho, G., Kairalla, R. A., Deheinzelin, D., Munoz, C., Oliveira, R., Takagaki, T. Y., & Carvalho, C. R. (1998). Effect of a protective-ventilation strategy on mortality in the acute respiratory distress syndrome. *N Engl J Med*, 338(6), 347–54.

Anderson, K., Lai, F., Liu, Q., Rousseau, E., Erickson, H., & Meissner, G. (1989). Structural and functional characterization of the purified cardiac ryanodine receptor-Ca2+ release channel complex. *J Biol Chem*, 264(2), 1329–35.

Andersson, I. (2008). Catalysis and regulation in Rubisco. *J Exp Bot*, 59(7), 1555–68.

Ando, H., Mizutani, A., Kiefer, H., Tsuzurugi, D., Michikawa, T., & Mikoshiba, K. (2006). IRBIT suppresses IP3 receptor activity by competing with IP3 for the common binding site on the IP3 receptor. *Mol Cell*, 22(6), 795–806.

Ardura, J. A., Wang, B., Watkins, S. C., Vilardaga, J.-P., & Friedman, P. A. (2011). Dynamic Na+-H+ exchanger regulatory factor-1 association and dissociation regulate parathyroid hormone receptor trafficking at membrane microdomains. *J Biol Chem*, 286(40), 35020–9.

Armston, A. E. & Wood, P. J. (1994). Studies on the Use of Cultured Cells in a Bioassay for Parathyroid-Hormone. *J Endocrinol*, 143(2), 261–268.

Atkins, E. L. (1969). Assessment of acid-base disorders. A practical approach and review. *CMAJ*, 100(21), 992–8.

Aurbach, G. D. & Potts, J. T. (1964). The Parathyroid. *Adv Metab Disord*, 15, 45–93.

Azarani, A., Goltzman, D., & Orlowski, J. (1995). Parathyroid-Hormone and Parathyroid Hormone-Related Peptide Inhibit the Apical Na+/H+ Exchanger NHE-3 Isoform in Renal-Cells (OK) Via a Dual Signaling Cascade Involving Protein-Kinase-A and Protein-Kinase-C. *J Biol Chem*, 270(34), 20004–20010.

Azzam, Z. S., Sharabi, K., Guetta, J., Bank, E. M., & Gruenbaum, Y. (2010). The physiological and molecular effects of elevated CO2 levels. *Cell cycle*, 9(8), 1528–32.

Baba, T. W., Giroir, B. P., & Humphries, E. H. (1985). Cell lines derived from avian lymphomas exhibit two distinct phenotypes. *Virology*, 144(1), 139–51.

Bacic, D., Schulz, N., Biber, J., Kaissling, B., Murer, H., & Wagner, C. A. (2003). Involvement of the MAPK-kinase pathway in the PTH-mediated regulation of the proximal tubule type IIa Na+/Pi cotransporter in mouse kidney. *Pflügers Arch*, 446(1), 52–60.

Badger, M. R., Price, G. D., Long, B. M., & Woodger, F. J. (2006). The environmental plasticity and ecological genomics of the cyanobacterial CO2 concentrating mechanism. *J Exp Bot*, 57(2), 249–65.

Bakalyar, H. A. & Reed, R. R. (1990). Identification of a specialized adenylyl cyclase that may mediate odorant detection. *Science*, 250(4986), 1403–6.

Barker, E. S., Singer, R. B., Elkinton, J. R., & Clark, J. K. (1957). The renal response in man to acute experimental respiratory alkalosis and acidosis. *J Clin Invest*, 36(4), 515–29.

Barry, E. L., Gesek, F. A., Yu, A. S., Lytton, J., & Friedman, P. A. (1998). Distinct calcium channel isoforms mediate parathyroid hormone and chlorothiazide-stimulated calcium entry in transporting epithelial cells. *J Membr Biol*, 161(1), 55–64.

Bârzu, O. & Danchin, A. (1994). Adenylyl cyclases: a heterogeneous class of ATP-utilizing enzymes. *Prog Nucleic Acid Res Mol Biol.*, 49, 241–83.

Baumann, K., de Rouffignac, C., Roinel, N., Rumrich, G., & Ullrich, K. J. (1975). Renal phosphate transport: inhomogeneity of local proximal transport rates and sodium dependence. *Pflügers Arch*, 356(4), 287–98.

Beard, N. A., Laver, D. R., & Dulhunty, A. F. (2004). Calsequestrin and the calcium release channel of skeletal and cardiac muscle. *Prog Biophys Mol Biol*, 85(1), 33–69.

Beavo, J. A., Rogers, N. L., Crofford, O. B., Hardman, J. G., Sutherland, E. W., & Newman, E. V. (1970). Effects of xanthine derivatives on lipolysis and on adenosine 3', 5'-monophosphate phosphodiesterase activity. *Mol pharmacol*, 6(6), 597–603.

Behar, V., Pines, M., Nakamoto, C., Greenberg, Z., Bisello, A., Stueckle, S. M., Bessalle, R., Usdin, T. B., Chorev, M., Rosenblatt, M., & Suva, L. J. (1996). The human PTH2 receptor: binding and signal transduction properties of the stably expressed recombinant receptor. *Endocrinology*, 137(7), 2748–57.

Beitner-Johnson, D., Leibold, J., & Millhorn, D. E. (1998). Hypoxia regulates the cAMP and Ca2+/calmodulin signaling systems in PC12 cells. *Biochem Biophys Res Commun*, 242(1), 61–6.

Belkin, R. A., Henig, N. R., Singer, L. G., Chaparro, C., Rubenstein, R. C., Xie, S. X., Yee, J. Y., Kotloff, R. M., Lipson, D. A., & Bunin, G. R. (2006). Risk factors for death of patients with cystic fibrosis awaiting lung transplantation. *Am J Respir Crit Care Med*, 173(6), 659–66.

Beltrán, A. R., Ramírez, M. A., Carraro-Lacroix, L. R., Hiraki, Y., Rebouças, N. A., & Malnic, G. (2008). NHE1, NHE2, and NHE4 contribute to regulation of cell pH in T84 colon cancer cells. *Pflügers Arch*, 455(5), 799–810.

Beltran, C., Vacquier, V. D., Moy, G., Chen, Y. Q., Buck, J., Levin, L. R., & Darszon, A. (2007). Particulate and soluble adenylyl cyclases participate in the sperm acrosome reaction. *Biochem Biophys Res Commun*, 358(4), 1128–1135.

Berjukow, S., Döring, F., Froschmayr, M., Grabner, M., Glossmann, H., & Hering, S. (1996). Endogenous calcium channels in human embryonic kidney (HEK293) cells. *Br J Pharmacol*, 118(3), 748–54.

Berridge, M., Catterall, B., Stull, J., Coughlin, S., Olso, E., & Sunahara, Roger Sambrano, G. (2012). Calcium Signaling in Cardiac Myocytes.

Berridge, M. J. (2002). The endoplasmic reticulum: a multifunctional signaling organelle. *Cell calcium*, 32(5-6), 235–49.

Berridge, M. J., Cobbold, P. H., & Cuthbertson, K. S. (1988). Spatial and temporal aspects of cell signalling. *Philos Trans R Soc Lond B Biol Sci.*, 320(1199), 325–43.

Bezprozvanny, I. & Ehrlich, B. E. (1993). ATP modulates the function of inositol 1,4,5-trisphosphate-gated channels at two sites. *Neuron*, 10(6), 1175–84.

Biemesderfer, D., Nagy, T., DeGray, B., & Aronson, P. S. (1999). Specific association of megalin and the Na+/H+ exchanger isoform NHE3 in the proximal tubule. *J Biol Chem*, 274(25), 17518–24.

Biemesderfer, D., Pizzonia, J., Abu-Alfa, A., Exner, M., Reilly, R., Igarashi, P., & Aronson, P. S. (1993). NHE3: a Na+/H+ exchanger isoform of renal brush border. *Am J Physiol*, 265(5 Pt 2), F736–42.

Binkowski, B. F., Butler, B. L., Stecha, P. F., Eggers, C. T., Otto, P., Zimmerman, K., Vidugiris, G., Wood, M. G., Encell, L. P., Fan, F., & Wood, K. V. (2011). A luminescent biosensor with increased dynamic range for intracellular cAMP. *ACS Chem Biol*, 6(11), 1193–7.

Blank, J. L., Brattain, K. A., & Exton, J. H. (1992). Activation of cytosolic phosphoinositide phospholipase C by G-protein beta gamma subunits. *J Biol Chem*, 267(32), 23069–75.

Bleasdale, J. E., Bundy, G. L., Bunting, S., Fitzpatrick, F. A., Huff, R. M., Sun, F. F., & Pike, J. E. (1989). Inhibition of phospholipase C dependent processes by U-73, 122. *Adv Prostaglandin Thromboxane Leukot Res*, 19, 590–3.

Bodzon-Kulakowska, A., Bierczynska-Krzysik, A., Dylag, T., Drabik, A., Suder, P., Noga, M., Jarzebinska, J., & Silberring, J. (2007). Methods for samples preparation in proteomic research. *J Chromatogr B Biomed Sci Appl.*, 849(1-2), 1–31.

Boehning, D. & Joseph, S. K. (2000). Direct association of ligand-binding and pore domains in homo- and heterotetrameric inositol 1,4,5-trisphosphate receptors. *EMBO J*, 19(20), 5450–9.

Bonar, P. T. & Casey, J. R. (2008). Plasma membrane Cl-/HCO- exchangers: structure, mechanism and physiology. *Channels (Austin)*, 2(5), 337–45.

Boron, W. F. (2006). Acid-base transport by the renal proximal tubule. *J Am Soc Nephrol*, 17(9), 2368–2382.

Boron, W. F. & Boulpaep, E. L. (1983). Intracellular pH regulation in the renal proximal tubule of the salamander. Basolateral HCO3- transport. *J Gen Physiol*, 81(1), 53–94.

Boron, W. F., Endeward, V., Gros, G., Musa-Aziz, R., & Pohl, P. (2011). Intrinsic CO2 permeability of cell membranes and potential biological relevance of CO2 channels. *Chemphyschem*, 12(5), 1017–9.

Botre, C., Botre, F., Lorenti, G., Pranzoni, C., & Scibona, G. (1991). Interactions between calcium entry blocking drugs and carbonic anhydrase. *Arzneimittel-Forschung*, 41(9), 891–894.

Bouyer, P., Zhou, Y., & Boron, W. F. (2003). An increase in intracellular calcium concentration that is induced by basolateral CO2 in rabbit renal proximal tubule. *Am J Physiol Renal Physiol*, 285(4), F674–87.

Boyarsky, G., Ganz, M. B., Sterzel, R. B., & Boron, W. F. (1988). pH regulation in single glomerular mesangial cells. I. Acid extrusion in absence and presence of HCO3-. *Am J Physiol*, 255(6 Pt 1), C844–56.

Boyarsky, G., Hanssen, C., & Clyne, L. A. (1996). Inadequacy of high K+/nigericin for calibrating BCECF. I. Estimating steady-state intracellular pH. *Am J Physiol*, 271(4 Pt 1), C1131–45.

Boyer, J. L., Waldo, G. L., & Harden, T. K. (1992). Beta gamma-subunit activation of G-protein-regulated phospholipase C. *J Biol Chem*, 267(35), 25451–6.

Brandt, J. P., Aziz-Zaman, S., Juozaityte, V., Martinez-Velazquez, L. A., Petersen, J. G., Pocock, R., & Ringstad, N. (2012). A Single Gene Target of an ETS-Family Transcription Factor Determines Neuronal CO2 Chemosensitivity. *PloS One*, 7(3), e34014.

Braun, T. & Dods, R. F. (1975). Development of a Mn-2+-sensitive, "soluble" adenylate cyclase in rat testis. *Proc Natl Acad Sci U S A*, 72(3), 1097–1101.

Bretscher, A. J., Kodama-Namba, E., Busch, K. E., Murphy, R. J., Soltesz, Z., Laurent, P., & de Bono, M. (2011). Temperature, oxygen, and salt-sensing neurons in C. elegans are carbon dioxide sensors that control avoidance behavior. *Neuron*, 69(6), 1099–113.

Briva, A., Lecuona, E., & Sznajder, J. I. (2010). Permissive and non-permissive hypercapnia: mechanisms of action and consequences of high carbon dioxide levels. *Arch Bronconeumol*, 46(7), 378–82.

Briva, A., Vadász, I., Lecuona, E., Welch, L. C., Chen, J., Dada, L. a., Trejo, H. E., Dumasius, V., Azzam, Z. S., Myrianthefs, P. M., Batlle, D., Gruenbaum, Y., & Sznajder, J. I. (2007). High CO2 levels impair alveolar epithelial function independently of pH. *PloS One*, 2(11), e1238.

Broadus, A. E., Mahaffey, J. E., Bartter, F. C., & Neer, R. M. (1977). Nephrogenous cyclic adenosine monophosphate as a parathyroid function test. *J Clin Invest*, 60(4), 771–83.

Broccard, A. F., Hotchkiss, J. R., Vannay, C., Markert, M., Sauty, A., Feihl, F., & Schaller, M. D. (2001). Protective effects of hypercapnic acidosis on ventilator-induced lung injury. *Am J Respir Crit Care Med*, 164(5), 802–6.

Brockmann, R., Beyer, A., Heinisch, J. J., & Wilhelm, T. (2007). Post-transcriptional expression regulation: what determines translation rates? *PLoS Comput Biol.*, 3(3), e57.

Buck, J., Sinclair, M. L., Schapal, L., Cann, M. J., & Levin, L. R. (1999). Cytosolic adenylyl cyclase defines a unique signaling molecule in mammals. *PNAS USA*, 96(1), 79–84.

Buckler, K. J. & Vaughan-Jones, R. D. (1993). Effects of acidic stimuli on intracellular calcium in isolated type I cells of the neonatal rat carotid body. *Pflügers Arch*, 425(1-2), 22–7.

Buckler, K. J., Vaughan-Jones, R. D., Peers, C., Lagadic-Gossmann, D., & Nye, P. C. (1991). Effects of extracellular pH, PCO2 and HCO3- on intracellular pH in isolated type-I cells of the neonatal rat carotid body. *J Physiol*, 444, 703–21.

Bugrim, A. E. (1999). Regulation of Ca2+ release by cAMP-dependent protein kinase. A mechanism for agonist-specific calcium signaling? *Cell calcium*, 25(3), 219–26.

Bull, R., Finkelstein, J. P., Humeres, A., Behrens, M. I., & Hidalgo, C. (2007). Effects of ATP, Mg2+, and redox agents on the Ca2+ dependence of RyR channels from rat brain cortex. *Am J Physiol Cell Physiol*, 293(1), C162–71.

Bushinsky, D. A., Smith, S. B., Gavrilov, K. L., Gavrilov, L. F., Li, J., & Levi-Setti, R. (2002). Acute acidosis-induced alteration in bone bicarbonate and phosphate. *Am J Physiol Renal Physiol*, 283(5), F1091–7.

Cali, J. J., Zwaagstra, J. C., Mons, N., Cooper, D. M., & Krupinski, J. (1994). Type VIII adenylyl cyclase. A Ca2+/calmodulin-stimulated enzyme expressed in discrete regions of rat brain. *J Biol Chem*, 269(16), 12190–5.

Camps, M., Carozzi, A., Schnabel, P., Scheer, A., Parker, P. J., & Gierschik, P. (1992). Isozyme-selective stimulation of phospholipase C-beta 2 by G-protein beta gamma-subunits. *Nature*, 360(6405), 684–6.

Cancela, J. M., Gerasimenko, O. V., Gerasimenko, J. V., Tepikin, A. V., & Petersen, O. H. (2000). Two different but converging messenger pathways to intracellular Ca(2+) release: the roles of nicotinic acid adenine dinucleotide phosphate, cyclic ADP-ribose and inositol trisphosphate. *J EMBO*, 19(11), 2549–57.

Cann, M. J., Hammer, A., Zhou, J., & Kanacher, T. (2003). A defined subset of adenylyl cyclases is regulated by bicarbonate ion. *J Biol Chem*, 278(37), 35033–35038.

Carafoli, E. (1991). Calcium pump of the plasma membrane. *Physiol Rev*, 71(1), 129–53.

Carafoli, E., Tiozzo, R., Lugli, G., Crovetti, F., & Kratzing, C. (1974). The release of calcium from heart mitochondria by sodium. *J Mol Cell Cardiol*, 6(4), 361–71.

Carlisle Michel, J. J., Dodge, K. L., Wong, W., Mayer, N. C., Langeberg, L. K., & Scott, J. D. (2004). PKA-phosphorylation of PDE4D3 facilitates recruitment of the mAKAP signalling complex. *J Biochem*, 381(Pt 3), 587–92.

Casale, T. B., Romero, F. A., & Spierings, E. L. H. (2008). Intranasal noninhaled carbon dioxide for the symptomatic treatment of seasonal allergic rhinitis. *J Allergy Clin Immunol*, 121(1), 105–9.

Caverzasio, J., Rizzoli, R., & Bonjour, J. P. (1986). Sodium-dependent phosphate transport inhibited by parathyroid hormone and cyclic AMP stimulation in an opossum kidney cell line. *J Biol Chem*, 261(7), 3233–7.

Cha, B., Zhu, X. C., Chen, W., Jones, M., Ryoo, S., Zachos, N. C., Chen, T.-E., Lin, R., Sarker, R., Kenworthy, A. K., Tse, M., Kovbasnjuk, O., & Donowitz, M. (2010). NHE3 mobility in brush borders increases upon NHERF2-dependent stimulation by lyophosphatidic acid. *J Cell Sci*, 123(Pt 14), 2434–43.

Chambers, D. J., Dunham, J., Zanelli, J. M., Parsons, J. A., Bitensky, L., & Chayen, J. (1978). A sensitive bioassay of parathyroid hormone in plasma. *Clin Endocrinol*, 9(4), 375–9.

Chandrashekar, J., Yarmolinsky, D., von Buchholtz, L., Oka, Y., Sly, W., Ryba, N. J. P., & Zuker, C. S. (2009). The taste of carbonation. *Science*, 326(5951), 443–5.

Chase, L. R. & Aurbach, G. D. (1967). Parathyroid function and the renal excretion of 3'5'-adenylic acid. *PNAS USA*, 58(2), 518–525.

Chase, L. R. & Aurbach, G. D. (1970). The effect of parathyroid hormone on the concentration of adenosine 3',5'-monophosphate in skeletal tissue in vitro. *J Biol Chem*, 245(7), 1520–1526.

Chattopadhyaya, R., Meador, W. E., Means, A. R., & Quiocho, F. A. (1992). Calmodulin structure refined at 1.7 A resolution. *J Mol Biol*, 228(4), 1177–92.

Chen, J., Levin, L. R., & Buck, J. (2012). Role of soluble adenylyl cyclase in the heart. *Am J Physiol Heart Circ Physiol*, 302(3), H538–43.

Chen, L. K. & Boron, W. F. (1995a). Acid extrusion in S3 segment of rabbit proximal tubule. I. Effect of bilateral CO2/HCO3-. *Am J Physiol*, 268(2 Pt 2), F179–92.

Chen, L. K. & Boron, W. F. (1995b). Acid extrusion in S3 segment of rabbit proximal tubule. II. Effect of basolateral CO2/HCO3-. *Am J Physiol*, 268(2 Pt 2), F193–203.

Chen, S., Zhang, L., & MacLennan, D. (1992). Characterization of a Ca2+ binding and regulatory site in the Ca2+ release channel (ryanodine receptor) of rabbit skeletal muscle sarcoplasmic reticulum. *J Biol Chem*, 267(32), 23318–26.

Chen, Y. Q., Cann, M. J., Litvin, T. N., Iourgenko, V., Sinclair, M. L., Levin, L. R., & Buck, J. (2000). Soluble adenylyl cyclase as an evolutionarily conserved bicarbonate sensor. *Science*, 289(5479), 625–628.

Cheng, S. H., Rich, D. P., Marshall, J., Gregory, R. J., Welsh, M. J., & Smith, A. E. (1991). Phosphorylation of the R domain by cAMP-dependent protein kinase regulates the CFTR chloride channel. *Cell*, 66(5), 1027–1036.

Chijiwa, T., Mishima, A., Hagiwara, M., Sano, M., Hayashi, K., Inoue, T., Naito, K., Toshioka, T., & Hidaka, H. (1990). Inhibition of forskolin-induced neurite outgrowth and protein phosphorylation by a newly synthesized selective inhibitor of cyclic AMP-dependent protein kinase, N-[2-(p-bromocinnamylamino)ethyl]-5-isoquinolinesulfonamide (H-89), of PC12D pheochromocytoma. *J Biol Chem*, 265(9), 5267–72.

Christensen, K. A., Myers, J. T., & Swanson, J. A. (2002). pH-dependent regulation of lysosomal calcium in macrophages. *J Cell Sci*, 115(Pt 3), 599–607.

Christian, G. D., Knoblock, E. C., & C, P. W. (1965). Coulometric Generation of Ethylene Glycol bis-(beta-aminoethyl ether)-N,N'-Tetraacetic acid. Titration of Calcium in the Presence of Magnesium. *Anal Chem*, 37, 292–4.

Christianson, D. W. & Cox, J. D. (1999). Catalysis by metal-activated hydroxide in zinc and manganese metalloenzymes. *Annu Rev Biochem*, 68, 33–57.

Churchill, G. C. & Galione, A. (2000). Spatial control of Ca2+ signaling by nicotinic acid adenine dinucleotide phosphate diffusion and gradients. *J Biol Chem*, 275(49), 38687–92.

Churchill, G. C., Okada, Y., Thomas, J. M., Genazzani, A. A., Patel, S., & Galione, A. (2002). NAADP mobilizes Ca(2+) from reserve granules, lysosome-related organelles, in sea urchin eggs. *Cell*, 111(5), 703–8.

Clapper, D. L., Walseth, T. F., Dargie, P. J., & Lee, H. C. (1987). Pyridine nucleotide metabolites stimulate calcium release from sea urchin egg microsomes desensitized to inositol trisphosphate. *J Biol Chem*, 262(20), 9561–8.

Clark, G. C., Briggs, D. C., Karasawa, T., Wang, X., Cole, A. R., Maegawa, T., Jayasekera, P. N., Naylor, C. E., Miller, J., Moss, D. S., Nakamura, S., Basak, A. K., & Titball, R. W. (2003). Clostridium absonum alpha-toxin: new insights into clostridial phospholipase C substrate binding and specificity. *J Mol Biol*, 333(4), 759–69.

Cockcroft, S. & Stutchfield, J. (1988). G-proteins, the inositol lipid signalling pathway, and secretion. *Philos Trans R Soc Lond B Biol Sci.*, 320(1199), 247–65.

Cole, J. A. (1999). Parathyroid hormone activates mitogen-activated protein kinase in opossum kidney cells. *Endocrinology*, 140(12), 5771–9.

Cole, J. A., Eber, S. L., Poelling, R. E., Thorne, P. K., & Forte, L. R. (1987). A Dual Mechanism for Regulation of Kidney Phosphate-Transport by Parathyroid-Hormone. *Am J Physiol*, 253(2), E221–E227.

Cole, J. A., Forte, L. R., Krause, W. J., & Thorne, P. K. (1989). Clonal sublines that are morphologically and functionally distinct from parental OK cells. *Am J Physiol*, 256(4 Pt 2), F672–9.

Connors, A. F., Dawson, N. V., Thomas, C., Harrell, F. E., Desbiens, N., Fulkerson, W. J., Kussin, P., Bellamy, P., Goldman, L., & Knaus, W. A. (1996). Outcomes following acute exacerbation of severe chronic obstructive lung disease. The SUPPORT investigators (Study to Understand Prognoses and Preferences for Outcomes and Risks of Treatments). *Am J Respir Crit Care Med*, 154(4 Pt 1), 959–67.

Cooper, D. M., Mons, N., & Karpen, J. W. (1995). Adenylyl cyclases and the interaction between calcium and cAMP signalling. *Nature*, 374(6521), 421–4.

Cooper, D. M., Yoshimura, M., Zhang, Y., Chiono, M., & Mahey, R. (1994). Capacitative Ca2+ entry regulates Ca(2+)-sensitive adenylyl cyclases. *J Biochem*, 297(3), 437–40.

Cooper, D. M. F. (2003). Regulation and organization of adenylyl cyclases and cAMP. *J Biochem*, 375(Pt 3), 517–29.

Coronado, R., Morrissette, J., Sukhareva, M., & Vaughan, D. M. (1994). Structure and function of ryanodine receptors. *Am J Physiol*, 266(6 Pt 1), C1485–504.

Costello, J., Higgins, B., Contreras, M., Chonghaile, M. N., Hassett, P., O'Toole, D., & Laffey, J. G. (2009). Hypercapnic acidosis attenuates shock and lung injury in early and prolonged systemic sepsis. *Crit Care Med*, 37(8), 2412–20.

Crompton, M., Moser, R., Lüdi, H., & Carafoli, E. (1978). The inter-relations between the transport of sodium and calcium in mitochondria of various mammalian tissues. *Eur J Biochem*, 82(1), 25–31.

Cumbay, M. G. & Watts, V. J. (2004). Novel regulatory properties of human type 9 adenylate cyclase. *J Pharmacol Exp Ther*, 310(1), 108–15.

Cummins, E. P., Oliver, K. M., Lenihan, C. R., Fitzpatrick, S. F., Bruning, U., Scholz, C. C., Slattery, C., Leonard, M. O., McLoughlin, P., & Taylor, C. T. (2010). NF-κB links CO2 sensing to innate immunity and inflammation in mammalian cells. *J Immunol*, 185(7), 4439–45.

Cunningham, R., Steplock, D., Wang, F., Huang, H., E, X., Shenolikar, S., & Weinman, E. J. (2004). Defective parathyroid hormone regulation of NHE3 activity and phosphate adaptation in cultured NHERF-1-/- renal proximal tubule cells. *J Biol Chem*, 279(36), 37815–21.

Darè, E., Kifor, O., Brown, E. M., & Weber, G. (1998). Characterization of the phosphatidylinositol-specific phospholipase C isozymes present in the bovine parathyroid and in human kidney HEK293

cells stably transfected with the human parathyroid Ca2+-sensing receptor. *J Endocrinol*, 21(1), 7–17.

de Haen, C. (1974). Adenylate cyclase. A new kinetic analysis of the effects of hormones and fluoride ion. *J Biol Chem*, 249(9), 2756–2762.

De Zengotita, V. M., Abston, L. R., Schmelzer, A. E., Shaw, S., & Miller, W. M. (2002). Selected amino acids protect hybridoma and CHO cells from elevated carbon dioxide and osmolality. *Biotechnol Bioeng*, 78(7), 741–52.

Dekker, T., Geier, M., & Cardé, R. T. (2005). Carbon dioxide instantly sensitizes female yellow fever mosquitoes to human skin odours. *J Exp Biol*, 208(Pt 15), 2963–72.

Dessauer, C. W., Scully, T. T., & Gilman, A. G. (1997). Interactions of forskolin and ATP with the cytosolic domains of mammalian adenylyl cyclase. *J Biol Chem*, 272(35), 22272–22277.

Di Benedetto, G., Zoccarato, A., Lissandron, V., Terrin, A., Li, X., Houslay, M. D., Baillie, G. S., & Zaccolo, M. (2008). Protein kinase A type I and type II define distinct intracellular signaling compartments. *Circ Res*, 103(8), 836–44.

Diaz-Sylvester, P. L., Porta, M., & Copello, J. A. (2011). Modulation of cardiac ryanodine receptor channels by alkaline earth cations. *PloS One*, 6(10), e26693.

Dieter, P., Fitzke, E., & Duyster, J. (1993). BAPTA induces a decrease of intracellular free calcium and a translocation and inactivation of protein kinase C in macrophages. *Biol Chem Hoppe-Seyler*, 374(3), 171–4.

Dionisio, N., Albarrán, L., López, J. J., Berna-Erro, A., Salido, G. M., Bobe, R., & Rosado, J. A. (2011). Acidic NAADP-releasable Ca(2+) compartments in the megakaryoblastic cell line MEG01. *Biochim Biophys Acta*, 1813(8), 1483–94.

Dodge-Kafka, K. L., Soughayer, J., Pare, G. C., Carlisle Michel, J. J., Langeberg, L. K., Kapiloff, M. S., & Scott, J. D. (2005). The protein kinase A anchoring protein mAKAP coordinates two integrated cAMP effector pathways. *Nature*, 437(7058), 574–8.

Doerr, C. H., Gajic, O., Berrios, J. C., Caples, S., Abdel, M., Lymp, J. F., & Hubmayr, R. D. (2005). Hypercapnic acidosis impairs plasma membrane wound resealing in ventilator-injured lungs. *Am J Respir Crit Care Med*, 171(12), 1371–7.

Doyle, M. E. & Jan de Beur, S. M. (2008). The skeleton: endocrine regulator of phosphate homeostasis. *Curr Osteoporos Rep*, 6(4), 134–141.

Dwyer, S. D., Zhuang, Y., & Smith, J. B. (1991). Calcium mobilization by cadmium or decreasing extracellular Na+ or pH in coronary endothelial cells. *Exp Cell Res*, 192(1), 22–31.

Dyer, J. L., Mobasheri, H., Lea, E. J. A., Dawson, A. P., & Michelangeli, F. (2003). Differential effect of PKA on the Ca2+ release kinetics of the type I and III InsP3 receptors. *Biochem Biophys Res Commun*, 302(1), 121–6.

Eldridge, F. L., Kiley, J. P., & Millhorn, D. E. (1985). Mechanisms of respiratory response to isoproterenol in glomectomized cats. *J Appl Physiol*, 58(1), 83–8.

Endeward, V., Cartron, J.-P., Ripoche, P., & Gros, G. (2008). RhAG protein of the Rhesus complex is a CO2 channel in the human red cell membrane. *FASEB J*, 22(1), 64–73.

Endeward, V. & Gros, G. (2005). Low carbon dioxide permeability of the apical epithelial membrane of guinea-pig colon. *J Physiol*, 567(Pt 1), 253–65.

Endeward, V., Musa-Aziz, R., Cooper, G. J., Chen, L.-M., Pelletier, M. F., Virkki, L. V., Supuran, C. T., King, L. S., Boron, W. F., & Gros, G. (2006). Evidence that aquaporin 1 is a major pathway for CO2 transport across the human erythrocyte membrane. *FASEB J*, 20(12), 1974–81.

Enzo-Life-Sciences (2010). Stauroporine Product Entry.

Esposito, G., Jaiswal, B. S., Xie, F., Krajnc-Franken, M. a. M., Robben, T. J. a. a., Strik, A. M., Kuil, C., Philipsen, R. L. a., van Duin, M., Conti, M., Gossen, J. a., & Jaiswal, B. S. (2004). Mice deficient for soluble adenylyl cyclase are infertile because of a severe sperm-motility defect. *PNAS USA*, 101(9), 2993–8.

Fagan, K. A., Mahey, R., Cooper, D. M. F., & Chem, D. M. F. J. B. (1996). Functional Co-localization of Transfected Ca2+ - Stimulable Adenylyl Cyclases with Capacitative Ca2+ Entry Sites. *J Biol Chem*, 271, 12438 –12444.

Fan, L., Wiederkehr, M. R., Collazo, R., Wang, H., Crowder, L. A., & Moe, O. W. (1999). Dual mechanisms of regulation of Na/H exchanger NHE-3 by parathyroid hormone in rat kidney. *J Biol Chem*, 274(16), 11289–95.

Feldman, J. L., Mitchell, G. S., & Nattie, E. E. (2003). Breathing: rhythmicity, plasticity, chemosensitivity. *Annu Rev Neurosci*, 26, 239–66.

Fenyk, S., Campillo, A. d. S. E., Pohl, E., Hussey, P. J., & Cann, M. J. (2012). A nucleotide phosphatase activity in the nucleotide binding domain of an orphan resistance protein from rice. *J Biol Chem*, 287(6), 4023–32.

Feske, S., Gwack, Y., Prakriya, M., Srikanth, S., Puppel, S.-H., Tanasa, B., Hogan, P. G., Lewis, R. S., Daly, M., & Rao, A. (2006). A mutation in Orai1 causes immune deficiency by abrogating CRAC channel function. *Nature*, 441(7090), 179–85.

Fill, M. & Copello, J. A. (2002). Ryanodine receptor calcium release channels. *Physiol Rev*, 82(4), 893–922.

Fischer, H., Illek, B., Sachs, L., Finkbeiner, W. E., & Widdicombe, J. H. (2010). CFTR and calcium-activated chloride channels in primary cultures of human airway gland cells of serous or mucous phenotype. *American journal of physiology. Lung cellular and molecular physiology*, 299(4), L585–94.

Fiskum, G. & Lehninger, A. L. (1979). Regulated release of Ca2+ from respiring mitochondria by Ca2+/2H+ antiport. *J Biol Chem*, 254(14), 6236–9.

Fleckenstein, A., Tritthart, H., Döring, H. J., & Byon, K. Y. (1972). BAY a 1040 - a highly potent Ca ++ - antagonistic inhibitor of electro-mechanical coupling processes in mammalian myocardium. *Arzneimittel-Forschung*, 22(1), 22–33.

Forrest, S. M., Ng, K. W., Findlay, D. M., Michelangeli, V. P., Livesey, S. A., Partridge, N. C., Zajac, J. D., & Martin, T. J. (1985). Characterization of an osteoblast-like clonal cell line which responds to both parathyroid hormone and calcitonin. *Calcif Tissue Int*, 37(1), 51–56.

Forte, L. R., Bylund, D. B., & Zahler, W. L. (1983). Forskolin does not activate sperm adenylate cyclase. *Mol Pharmacol*, 24(1), 42–7.

French, K. J., Schrecengost, R. S., Lee, B. D., Zhuang, Y., Smith, S. N., Eberly, J. L., Yun, J. K., & Smith, C. D. (2003). Discovery and Evaluation of Inhibitors of Human Sphingosine Kinase Discovery and Evaluation of Inhibitors of Human Sphingosine Kinase 1. *Cancer Res*, 63, 5962–5969.

French, K. J., Upson, J. J., Keller, S. N., Zhuang, Y., Yun, J. K., & Charles, D. (2006). Antitumor Activity of Sphingosine Kinase Inhibitors. *J Pharmacol Exp Ther*, 318(2), 596–603.

Friedlander, G. & Amiel, C. (1994). Cellular mode of action of parathyroid hormone. *Adv Nephrol Necker Hosp*, 23, 265–279.

Fritz, K. I., Zubrow, A., Mishra, O. P., & Delivoria-Papadopoulos, M. (2005). Hypercapnia-induced modifications of neuronal function in the cerebral cortex of newborn piglets. *Pediatr res.*, 57(2), 299–304.

Gafni, J., Munsch, J. A., Lam, T. H., Catlin, M. C., Costa, L. G., Molinski, T. F., & Pessah, I. N. (1997). Xestospongins: potent membrane permeable blockers of the inositol 1,4,5-trisphosphate receptor. *Neuron*, 19(3), 723–33.

Galione, A. (2006). NAADP, a new intracellular messenger that mobilizes Ca2+ from acidic stores. *Biochem Soc Trans*, 34(Pt 5), 922–6.

Gani, O. & Engh, R. A. (2010). Protein kinase inhibition of clinically important staurosporine analogues. *Nat Prod Rep*, 27(4), 489–98.

Garbers, D. L., Tubb, D. J., & Hyne, R. V. (1982). A requirement of bicarbonate for Ca2+-induced elevations of cyclic AMP in guinea pig spermatozoa. *J Biol Chem*, 257(15), 8980–8984.

Gehring, C. (2010). Adenyl cyclases and cAMP in plant signaling - past and present. *Cell Commun Signal*, 8, 15.

Genazzani, A. A. & Galione, A. (1997). A Ca2+ release mechanism gated by the novel pyridine nucleotide, NAADP. *Trends Pharmacol Sci*, 18(4), 108–10.

Geng, W. D., Wang, Z. G., Zhang, J. N., Reed, B. Y., Pak, C. Y. C., & Moe, O. W. (2005). Cloning and characterization of the human soluble adenylyl cyclase. *Am J Physiol Cell Physiol*, 288(6), C1305–C1316.

Geoffroy, E. (1895). Contribution to the study of Robinia nicou Aublet from a botanical, chemical, and physiological point of view. In *Extrait des Annales de L'Institut Colonial de Marseille 2* (pp. 1–86).

Geoffroy, V., Fouque, F., Nivet, V., Clot, J. P., Lugnier, C., Desbuquois, B., & Benelli, C. (1999). Activation of a cGMP-stimulated cAMP phosphodiesterase by protein kinase C in a liver Golgi-endosomal fraction. *Eur J Biochem*, 259(3), 892–900.

Gerstner, J. R., Lyons, L. C., Wright, K. P., Loh, D. H., Rawashdeh, O., Eckel-Mahan, K. L., & Roman, G. W. (2009). Cycling behavior and memory formation. *J Neurosci*, 29(41), 12824–30.

Giard, D. J., Aaronson, S. A., Todaro, G. J., Arnstein, P., Kersey, J. H., Dosik, H., & Parks, W. P. (1973). In vitro cultivation of human tumors: establishment of cell lines derived from a series of solid tumors. *J Natl Cancer Inst*, 51(5), 1417–23.

Goldhaber, P. & Rabadjija, L. (1987). H+ stimulation of cell-mediated bone resorption in tissue culture. *Am J Physiol*, 253(1 Pt 1), E90–8.

Goldring, S. R., Dayer, J. M., Russell, R. G., Mankin, H. J., & Krane, S. M. (1978). Response to hormones of cells cultured from human giant cell tumors of bone. *J Clin Endocrinol Metab*, 46(3), 425–33.

Gopalakrishnan, P. & Tak, T. (2011). Obstructive sleep apnea and cardiovascular disease. *Cardiology in review*, 19(6), 279–90.

Gourine, A. V., Llaudet, E., Dale, N., & Spyer, K. M. (2005). ATP is a mediator of chemosensory transduction in the central nervous system. *Nature*, 436(7047), 108–11.

Gouy, H., Cefai, D., Christensen, S. B., Debré, P., & Bismuth, G. (1990). Ca2+ influx in human T lymphocytes is induced independently of inositol phosphate production by mobilization of intracellular Ca2+ stores. A study with the Ca2+ endoplasmic reticulum-ATPase inhibitor thapsigargin. *Eur J Immunol*, 20(10), 2269–75.

Goyret, J., Markwell, P. M., & Raguso, R. A. (2008). Context- and scale-dependent effects of floral CO2 on nectar foraging by Manduca sexta. *PNAS USA*, 105(12), 4565–70.

Graham, F. L., Smiley, J., Russell, W. C., & Nairn, R. (1977). Characteristics of a human cell line transformed by DNA from human adenovirus type 5. *J Virol*, 36(1), 59–74.

Gray, J. E., Holroyd, G. H., van der Lee, F. M., Bahrami, A. R., Sijmons, P. C., Woodward, F. I., Schuch, W., & Hetherington, A. M. (2000). The HIC signalling pathway links CO2 perception to stomatal development. *Nature*, 408(6813), 713–6.

Gray, M. A. (2006). Primary cilia and regulation of renal Na+ transport. Focus on 'Heightened epithelial Na+ channel-mediated Na+ absorption in a murine polycystic kidney disease model epithelium lacking apical monocilia'. *Am J Physiol Cell Physiol*, 290(4), C947–9.

Grichtchenko, I. I., Choi, I., Zhong, X., Bray-Ward, P., Russell, J. M., & Boron, W. F. (2001). Cloning, characterization, and chromosomal mapping of a human electroneutral Na(+)-driven Cl-HCO3 exchanger. *J Biol Chem*, 276(11), 8358–63.

Gros, G., Rollema, H., & Forster, R. (1981). The carbamate equilibrium of alpha- and epsilon-amino groups of human hemoglobin at 37 degrees C. *J Biol Chem*, 256(11), 5471–80.

Grynkiewicz, G., Poenie, M., & Tsien, R. Y. (1985). A new generation of Ca2+ indicators with greatly improved fluorescence properties. *J Biol Chem*, 260(6), 3440–50.

Gschwendt, M., Dieterich, S., Rennecke, J., Kittstein, W., Mueller, H. J., & Johannes, F. J. (1996). Inhibition of protein kinase C mu by various inhibitors. Differentiation from protein kinase C isoenzymes. *FEBS Lett*, 392(2), 77–80.

Guerenstein, P. G., A Yepez, E., Van Haren, J., Williams, D. G., & Hildebrand, J. G. (2004). Floral CO2 emission may indicate food abundance to nectar-feeding moths. *Naturwissenschaften*, 91(7), 329–33.

Guillou, J. L., Nakata, H., & Cooper, D. M. (1999). Inhibition by calcium of mammalian adenylyl cyclases. *J Biol Chem*, 274(50), 35539–45.

Gullino, P. M., Grantham, F. H., Smith, S. H., & Haggerty, A. C. (1965). Modifications of the acid-base status of the internal milieu of tumors. *J Natl Cancer Inst*, 34(6), 857–69.

Guntupalli, J., Matthews, B., Carlin, B., & Bourke, E. (1987). Effect of Acute Hypercapnia on PTH-Stimulated Phosphaturia in Dietary Pi-Deprived Rat. *Am J Physiol*, 253(1), F34–F40.

Guo, D., Zhang, J. J., & Huang, X.-Y. (2009). Stimulation of guanylyl cyclase-D by bicarbonate. *Biochemistry*, 48(20), 4417–22.

Gutowska, I., Machoy, Z., & Machaliski, B. (2005). The role of bivalent metals in hydroxyapatite structures as revealed by molecular modeling with the HyperChem software. *J Biomed Mater Res A*, 75(4), 788–93.

Hacker, B. M., Tomlinson, J. E., Wayman, G. a., Sultana, R., Chan, G., Villacres, E., Disteche, C., & Storm, D. R. (1998). Cloning, chromosomal mapping, and regulatory properties of the human type 9 adenylyl cyclase (ADCY9). *Genomics*, 50(1), 97–104.

Hajnóczky, G., Hager, R., & Thomas, A. P. (1999). Mitochondria suppress local feedback activation of inositol 1,4, 5-trisphosphate receptors by Ca2+. *J Biol Chem*, 274(20), 14157–62.

Hall, R. A., De Sordi, L., Maccallum, D. M., Topal, H., Eaton, R., Bloor, J. W., Robinson, G. K., Levin, L. R., Buck, J., Wang, Y., Gow, N. A. R., Steegborn, C., & Mühlschlegel, F. A. (2010). CO(2) acts as a signalling molecule in populations of the fungal pathogen Candida albicans. *PLoS pathogens*, 6(11), e1001193.

Hallem, E. A., Spencer, W. C., McWhirter, R. D., Zeller, G., Henz, S. R., Rätsch, G., Miller, D. M., Horvitz, H. R., Sternberg, P. W., & Ringstad, N. (2011). Receptor-type guanylate cyclase is required for carbon dioxide sensation by Caenorhabditis elegans. *PNAS USA*, 108(1), 254–9.

Hallem, E. A. & Sternberg, P. W. (2008). Acute carbon dioxide avoidance in Caenorhabditis elegans. *PNAS USA*, 105(23), 8038–43.

Hamilton (2011). Hamilton Biotrode Product Booklet.

Hamm, L. L., Kokko, J. P., & Jacobson, H. R. (1984). Effect of luminal pH and HCO3- on phosphate reabsorption in the rabbit proximal convoluted tubule. *Am J Physiol*, 247(1 Pt 2), F25–34.

Hammer, A., Hodgson, D. R. W., & Cann, M. J. (2006). Regulation of prokaryotic adenylyl cyclases by CO2. *Biochem J*, 396, 215–218.

Hammerman, M. R. (1986). Phosphate transport across renal proximal tubular cell membranes. *Am J Physiol*, 251(3 Pt 2), F385–98.

Hammes, G. G. & Rodbell, M. (1976). Simple model for hormone-activated adenylate cyclase systems. *PNAS*, 73(4), 1189–92.

Hancock, J. T. (2005). *Cell Signalling*. Oxford University Press, second edition.

Hanly, E. J., Fuentes, J. M., Aurora, A. R., Bachman, S. L., De Maio, A., Marohn, M. R., & Talamini, M. A. (2006). Carbon dioxide pneumoperitoneum prevents mortality from sepsis. *Surgical endos*, 20(9), 1482–7.

Hanson, P. I., Kapiloff, M. S., Lou, L. L., Rosenfeld, M. G., & Schulman, H. (1989). Expression of a multifunctional Ca2+/calmodulin-dependent protein kinase and mutational analysis of its autoregulation. *Neuron*, 3(1), 59–70.

Haramati, A. & Nienhuis, D. (1984). Renal handling of phosphate during acute respiratory acidosis and alkalosis in the rat. *Am J Physiol*, 247(4 Pt 2), F596–601.

Harris, D. N., Asaad, M. M., Phillips, M. B., Goldenberg, H. J., & Antonaccio, M. J. (1979). Inhibition of adenylate cyclase in human blood platelets by 9-substituted adenine derivatives. *J Cyclic Nucleotide Res*, 5(2), 125–34.

Hatley, M. E., Gilman, A. G., & Sunahara, R. K. (2002). Expression, purification, and assay of cytosolic (catalytic) domains of membrane-bound mammalian adenylyl cyclases. *Methods Enzymol*, 345, 127–40.

Hayashi, H. & Miyata, H. (1994). Fluorescence imaging of intracellular Ca2+. *J Pharmacol Toxicol Methods*, 31(1), 1–10.

Hayashi, K., Wakino, S., Sugano, N., Ozawa, Y., Homma, K., & Saruta, T. (2007). Ca2+ channel subtypes and pharmacology in the kidney. *Circ Res*, 100(3), 342–53.

He, P., Klein, J., & Yun, C. C. (2010). Activation of Na+/H+ exchanger NHE3 by angiotensin II is mediated by inositol 1,4,5-triphosphate (IP3) receptor-binding protein released with IP3 (IRBIT) and Ca2+/calmodulin-dependent protein kinase II. *J Biol Chem*, 285(36), 27869–78.

He, P., Zhang, H., & Yun, C. C. (2008). IRBIT, inositol 1,4,5-triphosphate (IP3) receptor-binding protein released with IP3, binds Na+/H+ exchanger NHE3 and activates NHE3 activity in response to calcium. *J Biol Chem*, 283(48), 33544–53.

Healthcare, G. E. (2007). Amersham cAMP Biotrak Enzymeimmunoassay (EIA) System Product booklet .

Hegyi, P., Rakonczay, Z., Gray, M. A., & Argent, B. E. (2004). Measurement of intracellular pH in pancreatic duct cells: a new method for calibrating the fluorescence data. *Pancreas*, 28(4), 427–34.

Helenius, I. T., Krupinski, T., Turnbull, D. W., Gruenbaum, Y., Silverman, N., Johnson, E. A., Sporn, P. H. S., Sznajder, J. I., & Beitel, G. J. (2009). Elevated CO2 suppresses specific Drosophila innate immune responses and resistance to bacterial infection. *PNAS USA*, 106(44), 18710–5.

Herrera, M. & Garvin, J. L. (2011). Aquaporins as gas channels. *Pflügers Arch*, 462(4), 623–30.

Hess, K. C., Jones, B. H., Marquez, B., Chen, Y. Q., Ord, T. S., Kamenetsky, M., Miyamoto, C., Zippin, J. H., Kopf, G. S., Suarez, S. S., Levin, L. R., Williams, C. J., Buck, J., & Moss, S. B. (2005). The 'soluble' adenylyl cyclase in sperm mediates multiple signaling events required for fertilization. *Dev Cell*, 9(2), 249–259.

Hetherington, A. M. & Raven, J. A. (2005). The biology of carbon dioxide. *Curr Biol*, 15(11), R406–10.

Hoppe, A., Rybczynska, A., Knox, F. G., & Angielski, S. (1988). Beta-Receptors in Resistance to Phosphaturic Effect of PTH in Respiratory Alkalosis. *Am J Physiol*, 255(4), R557–R562.

Houslay, M. D., Baillie, G. S., & Maurice, D. H. (2007). cAMP-Specific phosphodiesterase-4 enzymes in the cardiovascular system: a molecular toolbox for generating compartmentalized cAMP signaling. *Circ Res*, 100(7), 950–66.

Hruska, K. A., Moskowitz, D., Esbrit, P., Civitelli, R., Westbrook, S., & Huskey, M. (1987). Stimulation of inositol trisphosphate and diacylglycerol production in renal tubular cells by parathyroid hormone. *J Clin Invest*, 79(1), 230–9.

Hu, J., Zhong, C., Ding, C., Chi, Q., Walz, A., Mombaerts, P., Matsunami, H., & Luo, M. (2007). Detection of near-atmospheric concentrations of CO2 by an olfactory subsystem in the mouse. *Science*, 317(5840), 953–7.

Huckfinne (2010). A acid-base nomograph of human serum, commonly used in physiology and medicine.

Huckstepp, R. T. R. & Dale, N. (2011). Redefining the components of central CO2 chemosensitivity - towards a better understanding of mechanism. *J Physiol*, 589(Pt 23), 5561–79.

Huckstepp, R. T. R., Eason, R., Sachdev, A., & Dale, N. (2010a). CO2-dependent opening of connexin 26 and related β connexins. *J Physiol*, 588(Pt 20), 3921–31.

Huckstepp, R. T. R., id Bihi, R., Eason, R., Spyer, K. M., Dicke, N., Willecke, K., Marina, N., Gourine, A. V., & Dale, N. (2010b). Connexin hemichannel-mediated CO2-dependent release of ATP in the medulla oblongata contributes to central respiratory chemosensitivity. *J Physiol*, 588(Pt 20), 3901–20.

Hulikova, A., Vaughan-Jones, R. D., & Swietach, P. (2011). Dual role of CO2/HCO3(-) formula buffer in the regulation of intracellular pH of three-dimensional tumor growths. *J Biol Chem*, 286(16), 13815–26.

Hull, R. N., Cherry, W. R., & Weaver, G. W. (1976). The origin and characteristics of a pig kidney cell strain, LLC-PK. *In vitro*, 12(10), 670–7.

Hurley, J. H. (1999). Adenylyl Cyclase *. (pp. 1–4).

Hyne, R. V. & Garbers, D. L. (1979). Regulation of guinea pig sperm adenylate cyclase by calcium. *Biol Reprod*, 21(5), 1135–42.

Invitrogen, M.-P. (2006). BCECF Product Data MP 01150.

Invitrogen, M.-P. (2012). Fura 2 Product Data.

Iscoe, S. & Fisher, J. A. (2005). Hyperoxia-induced hypocapnia - An underappreciated risk. *Chest*, 128(1), 430–433.

Ishikawa, Y., Katsushika, S., Chen, L., Halnon, N. J., Kawabe, J., & Homcy, C. J. (1992). Isolation and characterization of a novel cardiac adenylyl cyclase cDNA. *J Biol Chem*, 267(19), 13553–7.

Ismaiel, N. M. & Henzler, D. (2011). Effects of hypercapnia and hypercapnic acidosis on attenuation of ventilator-associated lung injury. *Minerva anestesiol*, 77(7), 723–33.

Jähnichen, S. (2006). Activation cycle of G-proteins by G-protein-coupled receptors.

Jaiswal, B. S. & Conti, M. (2001). Identification and functional analysis of splice variants of the germ cell soluble adenylyl cyclase. *J Biol Chem*, 276(34), 31698–31708.

Jehle, A. W., Hilfiker, H., Pfister, M. F., Biber, J., Lederer, E., Krapf, R., & Murer, H. (1999). Type II Na-Pi cotransport is regulated transcriptionally by ambient bicarbonate/carbon dioxide tension in OK cells. *Am J Physiol*, 276(1 Pt 2), F46–53.

Jobert, A. S., Leroy, C., Butlen, D., & Silve, C. (1997). Parathyroid hormone-induced calcium release from intracellular stores in a human kidney cell line in the absence of stimulation of cyclic adenosine 3',5'-monophosphate production. *Endocrinology*, 138(12), 5282–92.

Johnson, R. A., Alvarez, R., & Salomon, Y. (1994). Determination of adenylyl cyclase catalytic activity using single and double column procedures. *Methods Enzymol*, 238, 31–56.

Jones, W. D., Cayirlioglu, P., Kadow, I. G., & Vosshall, L. B. (2007). Two chemosensory receptors together mediate carbon dioxide detection in Drosophila. *Nature*, 445(7123), 86–90.

Kaczorowski, T., Furmanek, B., & Sektas, M. (1994). A Method for Removal of Radioactive Nucleotides from Electrophoretic Buffers. *Biotechniques*, 16(6), 1030–1031.

Kamenetsky, M., Middelhaufe, S., Bank, E. M., Levin, L. R., Buck, J., & Steegborn, C. (2006). Molecular details of cAMP generation in mammalian cells: A tale of two systems. *J Mol Biol*, 362(4), 623–639.

Karim, Z., Gerard, B., Bakouh, N., Alili, R., Leroy, C., Beck, L., Silve, C., Planelles, G., Urena-Torres, P., Grandchamp, B., Friedlander, G., & Prie, D. (2008). NHERF1 mutations and responsiveness of renal parathyroid hormone. *N Engl J Med*, 359(11), 1128–1135.

Katsuta, H., Takaoka, T., Tagaya, I., & Kikuchi, K. (1960). Cultivation of monkey kidney cells in the simplified replicate tissue culture. *Jpn J Exp Med.*, 30, 485–95.

Kempson, S. A., Lötscher, M., Kaissling, B., Biber, J., Murer, H., & Levi, M. (1995). Parathyroid hormone action on phosphate transporter mRNA and protein in rat renal proximal tubules. *Am J Physiol*, 268(4 Pt 2), F784–91.

Kessler, R., Faller, M., Fourgaut, G., Mennecier, B., & Weitzenblum, E. (1999). Predictive factors of hospitalisation for acute exacerbation in a series of 64 patients with chronic obstructive pulmonary disease. *Am J Respir Crit Care Med*, 159(1), 158–64.

Keusch, I., Traebert, M., Lötscher, M., Kaissling, B., Murer, H., & Biber, J. (1998). Parathyroid hormone and dietary phosphate provoke a lysosomal routing of the proximal tubular Na/Pi-cotransporter type II. *Kidney Int*, 54(4), 1224–32.

Kijima, Y., Saito, A., Jetton, T. L., Magnuson, M. A., & Fleischer, S. (1993). Different intracellular localization of inositol 1,4,5-trisphosphate and ryanodine receptors in cardiomyocytes. *J Biol Chem*, 268(5), 3499–506.

Kilmarti, J., Fogg, J., Luzzana, M., & Rossi-Bernardi, L. (1973). Role of the alpha-amino groups of the alpha and beta chains of human hemoglobin in oxygen-linked binding of carbon dioxide. *J Biol Chem*, 248(20), 7039–43.

Kimata, N., Yamashita, T., Matsuyama, T., Imamoto, Y., & Shichida, Y. (2012). The C-terminus of G-protein α subunit controls the affinity of nucleotides. *Biochemistry*, 51(13), 2768–74.

Klein, R. R., Bourdon, D. M., Costales, C. L., Wagner, C. D., White, W. L., Williams, J. D., Hicks, S. N., Sondek, J., & Thakker, D. R. (2011). Direct activation of human phospholipase C by its well known inhibitor U73122. *J Biol Chem*, 286(14), 12407–16.

Kleyman, T. R. & Cragoe, E. J. (1988). Amiloride and its analogs as tools in the study of ion transport. *J Membr Biol*, 105(1), 1–21.

Kobayashi, M., Buck, J., & Levin, L. R. (2004). Conservation of functional domain structure in bicarbonate-regulated 'soluble' adenylyl cyclases in bacteria and eukaryotes. *Dev Genes Evol*, 214(10), 503–9.

Kondo, Y. & Frömter, E. (1987). Axial heterogeneity of sodium-bicarbonate cotransport in proximal straight tubule of rabbit kidney. *Pflügers Arch*, 410(4-5), 481–6.

Koyama, H., Goodpasture, C., Miller, M. M., Teplitz, R. L., & Riggs, A. D. (1978). Establishment and characterization of a cell line from the American opossum (Didelphys virginiana). *In vitro*, 14(3), 239–46.

Krapf, R., Vetsch, R., Vetsch, W., & Hulter, H. N. (1992). Chronic metabolic acidosis increases the serum concentration of 1,25-dihydroxyvitamin D in humans by stimulating its production rate. Critical role of acidosis-induced renal hypophosphatemia. *J Clin Invest*, 90(6), 2456–63.

Krieger, N. S., Sessler, N. E., & Bushinsky, D. A. (1992). Acidosis inhibits osteoblastic and stimulates osteoclastic activity in vitro. *Am J Physiol*, 262(3 Pt 2), F442–8.

Kwan, C. Y., Takemura, H., Obie, J. F., Thastrup, O., & Putney, J. W. (1990). Effects of MeCh, thapsigargin, and La3+ on plasmalemmal and intracellular Ca2+ transport in lacrimal acinar cells. *Am J Physiol*, 258(6 Pt 1), C1006–15.

Kwon, J. Y., Dahanukar, A., Weiss, L. A., & Carlson, J. R. (2007). The molecular basis of CO2 reception in Drosophila. *PNAS USA*, 104(9), 3574–8.

Laffey, J. G., Honan, D., Hopkins, N., Hyvelin, J.-M., Boylan, J. F., & McLoughlin, P. (2004). Hypercapnic acidosis attenuates endotoxin-induced acute lung injury. *Am J Respir Crit Care Med*, 169(1), 46–56.

Laffey, J. G. & Kavanagh, B. P. (1999). Carbon dioxide and the critically ill - too little of a good thing? *Lancet*, 354(9186), 1283–1286.

Laffey, J. G. & Kavanagh, B. P. (2002). Medical progress - Hypocapnia. *N Engl J Med*, 347(1), 43–53.

Larsen, A. D. & Sypherd, P. S. (1974). Cyclic adenosine 3',5'-monophosphate and morphogenesis in Mucor racemosus. *J Bacteriol*, 117(2), 432–8.

Laude, A. J., Tovey, S. C., Dedos, S. G., Potter, B. V. L., Lummis, S. C. R., & Taylor, C. W. (2005). Rapid functional assays of recombinant IP3 receptors. *Cell calcium*, 38(1), 45–51.

Lawrence, T., Bebien, M., Liu, G. Y., Nizet, V., & Karin, M. (2005). IKKalpha limits macrophage NF-kappaB activation and contributes to the resolution of inflammation. *Nature*, 434(7037), 1138–43.

Lechner, A. J. (1976). Respiratory adaptations in burrowing pocket gophers from sea level and high altitude. *J Appl Physiol*, 41(2), 168–73.

Lee, H. C., Aarhus, R., Gee, K. R., & Kestner, T. (1997). Caged nicotinic acid adenine dinucleotide phosphate. Synthesis and use. *J Biol Chem*, 272(7), 4172–8.

Lee, H. C., Walseth, T. F., Bratt, G. T., Hayes, R. N., & Clapper, D. L. (1989). Structural determination of a cyclic metabolite of NAD+ with intracellular Ca2+-mobilising activity. *J Biol Chem*, 264(3), 1608–15.

Leonard, T. A., Róycki, B., Saidi, L. F., Hummer, G., & Hurley, J. H. (2011). Crystal structure and allosteric activation of protein kinase C βII. *Cell*, 144(1), 55–66.

Leong, P. K. K., Yang, L. E., Lin, H. W., Holstein-Rathlou, N. H., & McDonough, A. A. (2004). Acute hypotension induced by aortic clamp vs. PTH provokes distinct proximal tubule Na+ transporter redistribution patterns. *Am J Physiol Regul Integr Comp Physiol*, 287(4), R878–85.

Leva Di, F., Domi, T., Fedrizzi, L., Lim, D., & Carafoli, E. (2008). The plasma membrane Ca2+ ATPase of animal cells: structure, function and regulation. *Arch Biochem Biophys*, 476(1), 65–74.

Lew, V. L., Tsien, R. Y., Miner, C., & Bookchin, R. M. (1982). Physiological [Ca2+]i level and pump-leak turnover in intact red cells measured using an incorporated Ca chelator. *Nature*, 298(5873), 478–81.

Lewit-Bentley, A. & Réty, S. (2000). EF-hand calcium-binding proteins. *Curr Opin Struct Biol*, 10(6), 637–643.

Li, G., Zhou, D., Vicencio, A. G., Ryu, J., Xue, J., Kanaan, A., Gavrialov, O., & Haddad, G. G. (2006a). Effect of carbon dioxide on neonatal mouse lung: a genomic approach. *J Appl Physiol*, 101(6), 1556–64.

Li, J., Allen, K. T., Sun, X. C., Cui, M., & Bonanno, J. A. (2008). Dependence of cAMP meditated increases in Cl- and HCO3- permeability on CFTR in bovine corneal endothelial cells. *Exp Eye Res*, 86(4), 684–690.

Li, X.-D., Lupo, D., Zheng, L., & Winkler, F. (2006b). Structural and functional insights into the AmtB/Mep/Rh protein family. *Transfus Clin Biol*, 13(1-2), 65–9.

Lieber, M., Smith, B., Szakal, A., Nelson-Rees, W., & Todaro, G. (1976). A continuous tumor-cell line from a human lung carcinoma with properties of type II alveolar epithelial cells. *Int J Cancer*, 17(1), 62–70.

Lim, K. G., Sun, C., Bittman, R., Pyne, N. J., & Pyne, S. (2011). (R)-FTY720 methyl ether is a specific sphingosine kinase 2 inhibitor: Effect on sphingosine kinase 2 expression in HEK 293 cells and actin rearrangement and survival of MCF-7 breast cancer cells. *Cell Signal*, 23(10), 1590–5.

Lin-Moshier, Y., Walseth, T. F., Churamani, D., Davidson, S. M., Slama, J. T., Hooper, R., Brailoiu, E., Patel, S., & Marchant, J. S. (2012). Photoaffinity labeling of nicotinic acid adenine dinucleotide phosphate (NAADP) targets in mammalian cells. *J Biol Chem*, 287(4), 2296–307.

Linder, J. U. & Schultz, J. E. (2003). The class III adenylyl cyclases: multi-purpose signalling modules. *Cell Signal*, 15(12), 1081–1089.

Liou, J., Kim, M. L., Heo, W. D., Jones, J. T., Myers, J. W., Ferrell, J. E., & Meyer, T. (2005). STIM is a Ca2+ sensor essential for Ca2+-store-depletion-triggered Ca2+ influx. *Curr Biol*, 15(13), 1235–41.

Litvin, T. N., Kamenetsky, M., Zarifyan, A., Buck, J., & Levin, L. R. (2003). Kinetic properties of 'soluble' adenylyl cyclase. Synergism between calcium and bicarbonate. *J Biol Chem*, 278(18), 15922–6.

Liu, F. Y. & Cogan, M. G. (1990). Effects of intracellular calcium on proximal bicarbonate absorption. *Am J Physiol*, 259(3 Pt 2), F451–7.

Long, S. P., Ainsworth, E. A., Rogers, A., & Ort, D. R. (2004). Rising atmospheric carbon dioxide: plants FACE the future. *Annu Rev Plant Biol*, 55, 591–628.

Lorimer, G. H. (1983). Carbon dioxide and carbamate formation: the makings of a biochemical control system. *Trends Biochem Sci*, 8(2), 65–68.

Lotspeich, W. D. & Malvin, R. L. (1956). Relation between tubular transport of inorganic phosphate and bicarbonate in the dog. *Am J Physiol*, 187(1), 51–6.

Lundqvist, T. & Schneider, G. (1991). Crystal structure of the ternary complex of ribulose-1,5-bisphosphate carboxylase, Mg(II), and activator CO2 at 2.3-A resolution. *Biochemistry*, 30(4), 904–8.

Lytton, J., Westlin, M., & Hanley, M. R. (1991). Thapsigargin inhibits the sarcoplasmic or endoplasmic reticulum Ca-ATPase family of calcium pumps. *J Biol Chem*, 266(26), 17067–71.

Maeda, N., Kawasaki, T., Nakade, S., Yokota, N., Taguchi, T., Kasai, M., & Mikoshiba, K. (1991). Structural and functional characterisation of inositol 1,4,5-trisphosphate receptor channel from mouse cerebellum. *J Biol Chem*, 266(2), 1109–16.

Mahon, M. J., Cole, J. A., Lederer, E. D., & Segre, G. V. (2003a). Na+/H+ exchanger-regulatory factor 1 mediates inhibition of phosphate transport by parathyroid hormone and second messengers by acting at multiple sites in opossum kidney cells. *Molecular Endocrinology*, 17(11), 2355–2364.

Mahon, M. J., Cole, J. A., Lederer, E. D., & Segre, G. V. (2003b). Na+/H+ exchanger-regulatory factor 1 mediates inhibition of phosphate transport by parathyroid hormone and second messengers by acting at multiple sites in opossum kidney cells. *Mol Endocrinol*, 17(11), 2355–64.

Maine-University (2011). Tertiary Structure of Proteins - I.

Mak, D. O., McBride, S., & Foskett, J. K. (1999). ATP regulation of type 1 inositol 1,4,5-trisphosphate receptor channel gating by allosteric tuning of Ca(2+) activation. *J Biol Chem*, 274(32), 22231–7.

Malmstrom, K. & Murer, H. (1986). Parathyroid-Hormone Inhibits Phosphate-Transport in OK Cells but not in LLC-PK1 and JTC-12.P3 Cells. *Am J Physiol*, 251(1), C23–C31.

Maltais, F. & Debigaré, R. (2003). Biology of muscle impairment in COPD. *Monaldi Arch Chest Dis*, 59(4), 338–41.

Marchant, J., Callamaras, N., & Parker, I. (1999). Initiation of IP(3)-mediated Ca(2+) waves in Xenopus oocytes. *EMBO J*, 18(19), 5285–99.

Marchant, J. S. & Taylor, C. W. (1997). Cooperative activation of IP3 receptors by sequential binding of IP3 and Ca2+ safeguards against spontaneous activity. *Curr Biol*, 7(7), 510–8.

Maren, T. H. (1952). Pharmacological and renal effects of diamox (6063), a new carbonic anhydrase inhibitor. *Trans N Y Acad Sci*, 15(2), 53.

Marshall, W. J. & Bangert, S. K. (2008). *Clinical Biochemistry*. Philadelphia: Churchill Livingstone, second edition.

Martin, A. C. L., Willoughby, D., Ciruela, A., Ayling, L.-J., Pagano, M., Wachten, S., Tengholm, A., & Cooper, D. M. F. (2009). Capacitative Ca2+ entry via Orai1 and stromal interacting molecule 1 (STIM1) regulates adenylyl cyclase type 8. *Mol Pharmacol*, 75(4), 830–42.

Martin, K. J., McConkey, C. L., Jacob, A. K., Gonzalez, E. A., Khan, M., & Baldassare, J. J. (1994). Effect of U-73,122, an inhibitor of phospholipase C, on actions of parathyroid hormone in opossum kidney cells. *Am J Physiol*, 266(2 Pt 2), F254–8.

Maruyama, T., Kanaji, T., Nakade, S., Kanno, T., & Mikoshiba, K. (1997). 2-APB, 2-aminoethoxydiphenyl borate, a membrane-penetrable modulator of Ins(1,4,5)P3-induced Ca2+ release. *J Biochem*, 122(3), 498–505.

Marx, S. O., Reiken, S., Hisamatsu, Y., Jayaraman, T., Burkhoff, D., Rosemblit, N., & Marks, A. R. (2000). PKA phosphorylation dissociates FKBP12.6 from the calcium release channel (ryanodine receptor): defective regulation in failing hearts. *Cell*, 101(4), 365–76.

Mason, M. J., Garcia-Rodriguez, C., & Grinstein, S. (1991). Coupling between intracellular Ca2+ stores and the Ca2+ permeability of the plasma membrane. Comparison of the effects of thapsigargin, 2,5-di-(tert-butyl)-1,4-hydroquinone, and cyclopiazonic acid in rat thymic lymphocytes. *J Biol Chem*, 266(31), 20856–62.

McSheehy, P. M. & Chambers, T. J. (1986). Osteoblastic cells mediate osteoclastic responsiveness to parathyroid hormone. *Endocrinology*, 118(2), 824–828.

Meinkoth, J. L., Alberts, A. S., Went, W., Fantozzi, D., Taylor, S. S., Hagiwara, M., Montminy, M., & Feramisco, J. R. (1993). Signal transduction through the cAMP-dependent protein kinase. *Mol Cell Biochem*, 127-128, 179–86.

Meissner, G. (1986). Evidence of a role for calmodulin in the regulation of calcium release from skeletal muscle sarcoplasmic reticulum. *Biochemistry*, 25(1), 244–51.

Meissner, G. (2004). Molecular regulation of cardiac ryanodine receptor ion channel. *Cell calcium*, 35(6), 621–8.

Melson, G. L., Chase, L. R., & Aurbach, G. D. (1970). Parathyroid hormone-sensitive adenyl cyclase in isolated renal tubules. *Endocrinology*, 86(3), 511–8.

Messinger, S. M., Buckley, T. N., & Mott, K. A. (2006). Evidence for involvement of photosynthetic processes in the stomatal response to CO2. *Plant Physiol*, 140(2), 771–8.

Mészáros, L. G., Bak, J., & Chu, A. (1993). Cyclic ADP-ribose as an endogenous regulator of the non-skeletal type ryanodine receptor Ca2+ channel. *Nature*, 364(6432), 76–9.

Meyer, T., Holowka, D., & Stryer, L. (1988). Highly cooperative opening of calcium channels by inositol 1,4,5-trisphosphate. *Science*, 240(4852), 653–6.

Mignery, G. A., Newton, C. L., Archer, B. T., & Südhof, T. C. (1990). Structure and expression of the rat inositol 1,4,5-trisphosphate receptor. *J Biol Chem*, 265(21), 12679–85.

Milligan, G., Mitchell, F. M., Mullaney, I., McClue, S. J., & McKenzie, F. R. (1990). The role and specificity of guanine nucleotide binding proteins in receptor-effector coupling. *Symp Soc Exp Biol*, 44, 157–72.

Minguet, S., Huber, M., Rosenkranz, L., Schamel, W. W. A., Reth, M., & Brummer, T. (2005). Adenosine and cAMP are potent inhibitors of the NF-kappa B pathway downstream of immunoreceptors. *European journal of immunology*, 35(1), 31–41.

Missner, A., Kugler, P., Saparov, S. M., Sommer, K., Mathai, J. C., Zeidel, M. L., & Pohl, P. (2008). Carbon dioxide transport through membranes. *J Biol Chem*, 283(37), 25340–25347.

Miyawaki, A., Furuichi, T., Ryou, Y., Yoshikawa, S., Nakagawa, T., Saitoh, T., & Mikoshiba, K. (1991). Structure-function relationships of the mouse inositol 1,4,5-trisphosphate receptor. *PNAS USA*, 88(11), 4911–5.

Mongillo, M., McSorley, T., Evellin, S., Sood, A., Lissandron, V., Terrin, A., Huston, E., Hannawacker, A., Lohse, M. J., Pozzan, T., Houslay, M. D., & Zaccolo, M. (2004). Fluorescence resonance energy transfer-based analysis of cAMP dynamics in live neonatal rat cardiac myocytes reveals distinct functions of compartmentalised phosphodiesterases. *Circ Res*, 95(1), 67–75.

Monkawa, T., Miyawaki, A., Sugiyama, T., Yoneshima, H., Yamamoto-Hino, M., Furuichi, T., Saruta, T., Hasegawa, M., & Mikoshiba, K. (1995). Heterotetrameric complex formation of inositol 1,4,5-trisphosphate receptor subunits. *J Biol Chem*, 270(24), 14700–4.

Mott, K. A. (1988). Do Stomata Respond to CO(2) Concentrations Other than Intercellular? *Plant Physiol*, 86(1), 200–3.

Mount, D. B. & Romero, M. F. (2004). The SLC26 gene family of multifunctional anion exchangers. *Pflügers Arch*, 447(5), 710–21.

Murer, H., Hopfer, U., & Kinne, R. (1976). Sodium/proton antiport in brush-border-membrane vesicles isolated from rat small intestine and kidney. *J Biochem*, 154(3), 597–604.

Musa-Aziz, R., Chen, L. M., Pelletier, M. F., & Boron, W. F. (2009). Relative CO2/NH3 selectivities of AQP1, AQP4, AQP5, AmtB, and RhAG. *PNAS USA*.

Musgaard, M., Thø gersen, L., & Schiø tt, B. (2011). Protonation states of important acidic residues in the central Ca2+ ion binding sites of the Ca2+-ATPase: a molecular modeling study. *Biochemistry*, 50(51), 11109–20.

Mutlu, G. M., Factor, P., Schwartz, D. E., & Sznajder, J. I. (2002). Severe status asthmaticus: management with permissive hypercapnia and inhalation anesthesia. *Crit Care Med*, 30(2), 477–80.

Nalefski, E. A. & Falke, J. J. (1996). The C2 domain calcium-binding motif: structural and functional diversity. *Protein Sci*, 5(12), 2375–90.

Neumann, J.-O., Chambers, I. R., Citerio, G., Enblad, P., Gregson, B. A., Howells, T., Mattern, J., Nilsson, P., Piper, I., Ragauskas, A., Sahuquillo, J., Yau, Y. H., & Kiening, K. (2008). The use of hyperventilation therapy after traumatic brain injury in Europe: an analysis of the BrainIT database. *Intensive Care Med*, 34(9), 1676–82.

Nichol, A. D., O'Cronin, D. F., Howell, K., Naughton, F., O'Brien, S., Boylan, J., O'Connor, C., O'Toole, D., Laffey, J. G., & McLoughlin, P. (2009). Infection-induced lung injury is worsened after renal buffering of hypercapnic acidosis. *Crit Care Med*, 37(11), 2953–61.

Nishio, K., Suzuki, Y., Takeshita, K., Aoki, T., Kudo, H., Sato, N., Naoki, K., Miyao, N., Ishii, M., & Yamaguchi, K. (2001). Effects of hypercapnia and hypocapnia on [Ca2+]i mobilization in human pulmonary artery endothelial cells. *J Appl Physiol*, 90(6), 2094–100.

Nogueira, C., Bezerra, A., Girardi, A. C. C., Carraro-Lacroix, L. R., & Reboucas, N. A. (2008). Mechanisms underlying the long-term regulation of NHE3 by parathyroid hormone. *Am J Physiol Renal Physiol*, 294(5), F1232–F1237.

Nowak, J. Z. & Zawilska, J. B. (1999). Adenylyl cyclase - isoforms, regulation and function. *Postepy Hig Med Dosw*, 53(2), 147–72.

Nunes, A. R., Monteiro, E. C., Johnson, S. M., & Gauda, E. B. (2009). Bicarbonate-regulated soluble adenylyl cyclase (sAC) mRNA expression and activity in peripheral chemoreceptors. *Adv Exp Med Biol*, 648, 235–241.

O'Croinin, D. F., Nichol, A. D., Hopkins, N., Boylan, J., O'Brien, S., O'Connor, C., Laffey, J. G., & McLoughlin, P. (2008). Sustained hypercapnic acidosis during pulmonary infection increases bacterial load and worsens lung injury. *Crit Care Med*, 36(7), 2128–35.

Ohnishi, H., Miyake, M., Kamitani, S., & Horiguchi, Y. (2008). The morphological changes in cultured cells caused by Bordetella pertussis adenylate cyclase toxin. *FEMS Microbiol Lett*, 279(2), 174–9.

Ohta, T., Ito, S., & Ohga, A. (1990). Inhibitory action of dantrolene on Ca-induced Ca2+ release from sarcoplasmic reticulum in guinea pig skeletal muscle. *Eur J Pharmacol*, 178(1), 11–9.

Oliver, K. M., Lenihan, C. R., Bruning, U., Cheong, A., Laffey, J. G., McLoughlin, P., Taylor, C. T., & Cummins, E. P. (2012). Hypercapnia induces cleavage and nuclear localization of REL B giving insight into CO2 sensing and signalling. *J Biol Chem*, 287(17), 14004–11.

Omori, K. & Kotera, J. (2007). Overview of PDEs and their regulation. *Circ Res*, 100(3), 309–27.

Omura, S., Iwai, Y., Hirano, A., Nakagawa, A., Awaya, J., Tsuchya, H., Takahashi, Y., & Masuma, R. (1977). A new alkaloid AM-2282 OF Streptomyces origin. Taxonomy, fermentation, isolation and preliminary characterization. *J Antibiot (Tokyo)*, 30(4), 275–82.

O'Toole, D., Hassett, P., Contreras, M., Higgins, B. D., McKeown, S. T. W., McAuley, D. F., O'Brien, T., & Laffey, J. G. (2009). Hypercapnic acidosis attenuates pulmonary epithelial wound repair by an NF-kappaB dependent mechanism. *Thorax*, 64(11), 976–82.

Paredes, R. M., Etzler, J. C., Watts, L. T., Zheng, W., & Lechleiter, J. D. (2008). Chemical calcium indicators. *Methods (San Diego, Calif.)*, 46(3), 143–51.

Park, C. Y., Hoover, P. J., Mullins, F. M., Bachhawat, P., Covington, E. D., Raunser, S., Walz, T., Garcia, K. C., Dolmetsch, R. E., & Lewis, R. S. (2009). STIM1 clusters and activates CRAC channels via direct binding of a cytosolic domain to Orai1. *Cell*, 136(5), 876–90.

Partridge, N. C., Alcorn, D., Michelangeli, V. P., Kemp, B. E., Ryan, G. B., & Martin, T. J. (1981). Functional properties of hormonally responsive cultured normal and malignant rat osteoblastic cells. *Endocrinology*, 108(1), 213–9.

Partridge, N. C., Frampton, R. J., Eisman, J. A., Michelangeli, V. P., Elms, E., Bradley, T. R., & Martin, T. J. (1980). Receptors for 1,25(OH)2-vitamin D3 enriched in cloned osteoblast-like rat osteogenic sarcoma cells. *FEBS Lett*, 115(1), 139–42.

Pastor-Soler, N., Beaulieu, V., Litvin, T. N., Da Silva, N., Chen, Y., Brown, D., Buck, J., Levin, L. R., & Breton, S. (2003). Bicarbonate-regulated adenylyl cyclase (sAC) is a sensor that regulates pH-dependent V-ATPase recycling. *J Biol Chem*, 278(49), 49523–49529.

Paunescu, T. G., Da Silva, N., Russo, L. M., Mckee, M., Lu, H. A. J., Breton, S., & Brown, D. (2008). Association of soluble adenylyl cyclase with the V-ATPase in renal epithelial cells. *Am J Physiol Renal Physiol*, 294(1), F130–F138.

Pessah, I. N., Waterhouse, A. L., & Casida, J. E. (1985). The calcium-ryanodine receptor complex of skeletal and cardiac muscle. *Biochem Biophys Res Commun*, 128(1), 449–56.

Pfister, M. F., Ruf, I., Stange, G., Ziegler, U., Lederer, E., Biber, J., & Murer, H. (1998). Parathyroid hormone leads to the lysosomal degradation of the renal type II Na/Pi cotransporter. *PNAS USA*, 95(4), 1909–14.

Picard, N., Capuano, P., Stange, G., Mihailova, M., Kaissling, B., Murer, H., Biber, J., & Wagner, C. A. (2010). Acute parathyroid hormone differentially regulates renal brush border membrane phosphate cotransporters. *Pflügers Arch*, 460(3), 677–87.

Pignatti, C., Tantini, B., Zanfanti, M. L., Sacchi, P., & Clo, C. (1993). Influence of Mg2+ on the in-Vitro Responsiveness of Adenylate-Cyclase from Hearts of Aging Rats. *Cardioscience*, 4(2), 105–109.

Pines, M., Fukayama, S., Costas, K., Meurer, E., Goldsmith, P. K., Xu, X., Muallem, S., Behar, V., Chorev, M., Rosenblatt, M., Tashjian, A. H., & Suva, L. J. (1996). Inositol 1-,4-,5-trisphosphate-dependent Ca2+ signaling by the recombinant human PTH/PTHrP receptor stably expressed in a human kidney cell line. *Bone*, 18(4), 381–9.

Pollock, A. S., Warnock, D. G., & Strewler, G. J. (1986). Parathyroid-Hormone Inhibition of Na+-H+ Antiporter Activity in a Cultured Renal-Cell Line. *Am J Physiol*, 250(2), F217–F225.

Prakriya, M. & Lewis, R. S. (2001). Potentiation and inhibition of Ca(2+) release-activated Ca(2+) channels by 2-aminoethyldiphenyl borate (2-APB) occurs independently of IP(3) receptors. *J Physiol*, 536(Pt 1), 3–19.

Preisig, P. A., Ives, H. E., Cragoe, E. J., Alpern, R. J., & Rector, F. C. (1987). Role of the Na+/H+ antiporter in rat proximal tubule bicarbonate absorption. *J Clin Invest*, 80(4), 970–8.

Putney, J. W. (1986). A model for receptor-regulated calcium entry. *Cell calcium*, 7(1), 1–12.

Querfurth, H. W., Haughey, N. J., Greenway, S. C., Yacono, P. W., Golan, D. E., & Geiger, J. D. (1998). Expression of ryanodine receptors in human embryonic kidney (HEK293) cells. *Biochem J*, 334 (Pt 1, 79–86.

Raisz, L. G. (1965). Bone reabsorption in tissue culture. Factors influencing the response to parathyroid hormone. *J Clin Invest*, 44, 103–16.

Rakonczay, Z., Fearn, A., Hegyi, P., Boros, I., Gray, M. A., & Argent, B. E. (2006). Characterization of H+ and HCO3- transporters in CFPAC-1 human pancreatic duct cells. *World J Gastroenterol*, 12(6), 885–95.

Rasmussen, U., Brøogger Christensen, S., & Sandberg, F. (1978). Thapsigargine and thapsigargicine, two new histamine liberators from Thapsia garganica L. *Acta Pharm Suec*, 15(2), 133–40.

Remus, T. P., Zima, A. V., Bossuyt, J., Bare, D. J., Martin, J. L., Blatter, L. A., Bers, D. M., & Mignery, G. A. (2006). Biosensors to measure inositol 1,4,5-trisphosphate concentration in living cells with spatiotemporal resolution. *The Journal of biological chemistry*, 281(1), 608–16.

Richerson, G. B. (2004). Serotonergic neurons as carbon dioxide sensors that maintain pH homeostasis. *Nat Rev Neurosci*, 5(6), 449–61.

Rigual, R., López-López, J. R., & Gonzalez, C. (1991). Release of dopamine and chemoreceptor discharge induced by low pH and high pCO2 stimulation of the cat carotid body. *J Physiol*, 433, 519–31.

Rink, T. J., Tsien, R. Y., & Pozzan, T. (1982). Cytoplasmic pH and free Mg2+ in lymphocytes. *J Biol Chem*, 95(1), 189–96.

Ripoche, P., Bertrand, O., Gane, P., Birkenmeier, C., Colin, Y., & Cartron, J.-P. (2004). Human Rhesus-associated glycoprotein mediates facilitated transport of NH(3) into red blood cells. *PNAS USA*, 101(49), 17222–7.

Rizzuto, R., Pinton, P., Carrington, W., Fay, F. S., Fogarty, K. E., Lifshitz, L. M., Tuft, R. A., & Pozzan, T. (1998). Close contacts with the endoplasmic reticulum as determinants of mitochondrial Ca2+ responses. *Science*, 280(5370), 1763–6.

Rodriguez, H. J., Walls, J., Yates, J., & Klahr, S. (1974). Effects of acetazolamide on the urinary excretion of cyclic AMP and on the activity of renal adenyl cyclase. *J Clin Invest*, 53(1), 122–30.

Romero, M. F., Fulton, C. M., & Boron, W. F. (2004). The SLC4 family of HCO3- transporters. *Pflügers Arch*, 447(5), 495–509.

Rosado, J. A. (2006). Discovering the mechanism of capacitative calcium entry. *Am J Physiol Cell Physiol*, 291(6), C1104–6.

Ross, C. A., Meldolesi, J., Milner, T. A., Satoh, T., Supattapone, S., & Snyder, S. H. (1989). Inositol 1,4,5-trisphosphate receptor localized to endoplasmic reticulum in cerebellar Purkinje neurons. *Nature*, 339(6224), 468–70.

Ross, P. L., Huang, Y. N., Marchese, J. N., Williamson, B., Parker, K., Hattan, S., Khainovski, N., Pillai, S., Dey, S., Daniels, S., Purkayastha, S., Juhasz, P., Martin, S., Bartlet-Jones, M., He,

F., Jacobson, A., & Pappin, D. J. (2004). Multiplexed protein quantitation in Saccharomyces cerevisiae using amine-reactive isobaric tagging reagents. *Mol Cell Proteomics*, 3(12), 1154–69.

Rottenberg, H. & Scarpa, A. (1974). Calcium uptake and membrane potential in mitochondria. *Biochemistry*, 13(23), 4811–7.

Ruas, M., Rietdorf, K., Arredouani, A., Davis, L. C., Lloyd-Evans, E., Koegel, H., Funnell, T. M., Morgan, A. J., Ward, J. A., Watanabe, K., Cheng, X., Churchill, G. C., Zhu, M. X., Platt, F. M., Wessel, G. M., Parrington, J., & Galione, A. (2010). Purified TPC isoforms form NAADP receptors with distinct roles for Ca(2+) signaling and endolysosomal trafficking. *Curr Biol*, 20(8), 703–9.

Salomon, Y., Londos, C., & Rodbell, M. (1974). Highly Sensitive Adenylate Cyclase Assay. *Anal Biochem*, 58(2), 541–548.

Sampson, L. E. & Chaplin, D. J. (1996). The influence of oxygen and carbon dioxide tension on the production of TNF-alpha by activated macrophages. *Br J Cancer Suppl*, 27, S133–5.

Satriano, J. & Schlondorff, D. (1994). Activation and attenuation of transcription factor NF-kB in mouse glomerular mesangial cells in response to tumor necrosis factor-alpha, immunoglobulin G, and adenosine 3':5'-cyclic monophosphate. Evidence for involvement of reactive oxygen species. *The Journal of clinical investigation*, 94(4), 1629–36.

Scarpa, A. & Azzone, G. F. (1970). The mechanism of ion translocation in mitochondria. Coupling of K+ efflux with Ca2+ uptake. *Eur J Biochem*, 12(2), 328–35.

Schatzmann, H. (1966). ATP-dependent Ca++-extrusion from human red cells. *Experientia*, 22(6), 364–5.

Schmid, A., Sutto, Z., Nlend, M. C., Horvath, G., Schmid, N., Buck, J., Levin, L. R., Conner, G. E., Fregien, N., & Salathe, M. (2007). Soluble adenylyl cyclase is localized to cilia and contributes to ciliary beat frequency regulation via production of cAMP. *J Gen Physiol*, 130(1), 99–109.

Schultheis, P. J., Clarke, L. L., Meneton, P., Miller, M. L., Soleimani, M., Gawenis, L. R., Riddle, T. M., Duffy, J. J., Doetschman, T., Wang, T., Giebisch, G., Aronson, P. S., Lorenz, J. N., & Shull, G. E. (1998). Renal and intestinal absorptive defects in mice lacking the NHE3 Na+/H+ exchanger. *Nat Genet*, 19(3), 282–5.

Schwark, J. R., Jansen, H. W., Lang, H. J., Krick, W., Burckhardt, G., & Hropot, M. (1998). S3226, a novel inhibitor of Na+/H+ exchanger subtype 3 in various cell types. *Pflügers Arch*, 436(5), 797–800.

Schwartz, G. J. (1981). Na+-dependent H+ efflux from proximal tubule: evidence for reversible Na+-H+ exchange. *Am J Physiol*, 241(4), F380–5.

Schwartz, G. J. & Al-Awqati, Q. (1985). Carbon dioxide causes exocytosis of vesicles containing H+ pumps in isolated perfused proximal and collecting tubules. *J Clin Invest*, 75(5), 1638–44.

Seiler, S., Wegener, A., Whang, D., DR, H., & Jones, L. (1984). High molecular weight proteins in cardiac and skeletal muscle junctional sarcoplasmic reticulum vesicles bind calmodulin, are phosphorylated, and are degraded by Ca2+-activated protease. *J Biol Chem*, 259(13), 8550–7.

Seki, G., Coppola, S., Yoshitomi, K., Burckhardt, B. C., Samarzija, I., Müller-Berger, S., & Frömter, E. (1996). On the mechanism of bicarbonate exit from renal proximal tubular cells. *Kidney Int*, 49(6), 1671–7.

Seki, G. & Frömter, E. (1990). The chloride/base exchanger in the basolateral cell membrane of rabbit renal proximal tubule S3 segment requires bicarbonate to operate. *Pflügers Arch*, 417(1), 37–41.

Selwyn, M. J., Dawson, A. P., & Dunnett, S. J. (1970). Calcium transport in mitochondria. *FEBS Lett*, 10(1), 1–5.

Seo, M.-D., Velamakanni, S., Ishiyama, N., Stathopulos, P. B., Rossi, A. M., Khan, S. A., Dale, P., Li, C., Ames, J. B., Ikura, M., & Taylor, C. W. (2012). Structural and functional conservation of key domains in InsP3 and ryanodine receptors. *Nature*.

Shams, H. (1985). Differential effects of CO2 and H+ as central stimuli of respiration in the cat. *J Appl Physiol*, 58(2), 357–64.

Sharabi, K., Hurwitz, A., Simon, A. J., Beitel, G. J., Morimoto, R. I., Rechavi, G., Sznajder, J. I., & Gruenbaum, Y. (2009). Elevated CO2 levels affect development, motility, and fertility and extend life span in Caenorhabditis elegans. *PNAS USA*, 106(10), 4024–9.

Shaw, G., Morse, S., Ararat, M., & Graham, F. L. (2002). Preferential transformation of human neuronal cells by human adenoviruses and the origin of HEK 293 cells. *FASEB J*, 16(8), 869–71.

Sherwood, L. M., Potts, J., Care, A. D., Mayer, G. P., & Aurbach, G. D. (1966). Evaluation by Radioimmunoassay of Factors Controlling the Secretion of Parathyroid Hormone: Intravenous

Infusions of Calcium and Ethylenediamine Tetraacetic Acid in the Cow and Goat. *Nature*, 209(5018), 52–55.

Sheth, C. C., Mogensen, E. G., Fu, M. S., Blomfield, I. C., & Muhlschlegel, F. A. (2008). Candida albicans HSP12 is co-regulated by physiological CO2 and pH. *Fungal Genet Biol*, 45(7), 1075–1080.

Shibata, K., Cregg, N., Engelberts, D., Takeuchi, A., Fedorko, L., & Kavanagh, B. P. (1998). Hypercapnic acidosis may attenuate acute lung injury by inhibition of endogenous xanthine oxidase. *Am J Respir Crit Care Med*, 158(5 Pt 1), 1578–84.

Shlatz, L. J., Schwartz, I. L., Kinne-Saffran, E., & Kinne, R. (1975). Distribution of parathyroid hormone-stimulated adenylate cyclase in plasma membranes of cells of the kidney cortex. *J Membr Biol*, 24(2), 131–44.

Short, A. D. & Taylor, C. W. (2000). Parathyroid hormone controls the size of the intracellular Ca2+ stores available to receptors linked to inositol trisphosphate formation. *J Biol Chem*, 275(3), 1807–1813.

Shuai, J., Rose, H. J., & Parker, I. (2006). The number and spatial distribution of IP3 receptors underlying calcium puffs in Xenopus oocytes. *Biophys J*, 91(11), 4033–44.

Shuai, J. W. & Jung, P. (2003). Optimal ion channel clustering for intracellular calcium signaling. *PNAS USA*, 100(2), 506–10.

Siggaard-Andersen, O. (2005). Acid-Base Balance. *Respiratiory Medicine: Acid-base balance*, (pp. 1–6).

Sin, D. D. & Man, S. F. P. (2005). Chronic obstructive pulmonary disease: a novel risk factor for cardiovascular disease. *Can J Physiol Pharmacol*, 83(1), 8–13.

Sinclair, M. L., Wang, X. Y., Mattia, M., Conti, M., Buck, J., Wolgemuth, D. J., & Levin, L. R. (2000). Specific expression of soluble adenylyl cyclase in male germ cells. *Molecular Reproduction and Development*, 56(1), 6–11.

Sinclair, S. E., Kregenow, D. A., Lamm, W. J. E., Starr, I. R., Chi, E. Y., & Hlastala, M. P. (2002). Hypercapnic acidosis is protective in an in vivo model of ventilator-induced lung injury. *Am J Respir Crit Care Med*, 166(3), 403–8.

Slotki, I., Schwartz, J. H., & Alexander, E. A. (1993). Inter-relationship between cell pH and cell calcium in rat inner medullary collecting duct cells. *Am J Physiol*, 265(2 Pt 1), C432–8.

Sly, W. S. & Hu, P. Y. (1995). Human carbonic anhydrases and carbonic anhydrase deficiencies. *Annu Rev Biochem*, 64, 375–401.

Snyder, H. R., Davis, C. S., Bickerton, R. K., & Halliday, R. P. (1967). 1-[(5-arylfurfurylidene)amino]hydantoins. A new class of muscle relaxants. *J Med Chem*, 10(5), 807–10.

Spät, A., Eberhardt, I., & Kiesel, L. (1992). Low concentrations of adenine nucleotides enhance the receptor binding of inositol 1,4,5-trisphosphate. *J Biochem*, 287 (Pt 1, 335–6.

Sprang, S. R., Chen, Z., & Du, X. (2007). Structural basis of effector regulation and signal termination in heterotrimeric G-alpha proteins. *Adv Protein Chem*, 74, 1–65.

Stange, G. (1999). Carbon Dioxide Is a Close-Range Oviposition Attractant in the Queensland Fruit Fly Bactrocera tryoni. *Naturwissenschaften*, 86, 190–192.

Stathopulos, P. B., Li, G.-Y., Plevin, M. J., Ames, J. B., & Ikura, M. (2006). Stored Ca2+ depletion-induced oligomerisation of stromal interaction molecule 1 (STIM1) via the EF-SAM region: An initiation mechanism for capacitive Ca2+ entry. *J Biol Chem*, 281(47), 35855–62.

Steegborn, C., Litvin, T. N., Hess, K. C., Capper, A. B., Taussig, R., Buck, J., Levin, L. R., & Wu, H. (2005). A novel mechanism for adenylyl cyclase inhibition from the crystal structure of its complex with catechol estrogen. *J Biol Chem*, 280(36), 31754–9.

Stefan, E., Wiesner, B., Baillie, G. S., Mollajew, R., Henn, V., Lorenz, D., Furkert, J., Santamaria, K., Nedvetsky, P., Hundsrucker, C., Beyermann, M., Krause, E., Pohl, P., Gall, I., MacIntyre, A. N., Bachmann, S., Houslay, M. D., Rosenthal, W., & Klussmann, E. (2007). Compartmentalisation of cAMP-dependent signaling by phosphodiesterase-4D is involved in the regulation of vasopressin-mediated water reabsorption in renal principal cells. *J Am Soc Nephrol*, 18(1), 199–212.

Sterling, D. & Casey, J. R. (2002). Bicarbonate transport proteins. *Biochem Cell Biol*, 80(5), 483–97.

Stessin, A. M., Zippin, J. H., Kamenetsky, M., Hess, K. C., Buck, J., & Levin, L. R. (2006). Soluble adenylyl cyclase mediates nerve growth factor-induced activation of Rap1. *J Biol Chem*, 281(25), 17253–17258.

Streb, H., Irvine, R. F., Berridge, M. J., & Schulz, I. (1983). Release of Ca2+ from a non-mitochondrial intracellular store in pancreatic acinar cells by inositol-1,4,5-trisphosphate. *Nature*, 306(5938), 67–9.

Strehler, E. & Zacharias, D. (2001). Role of alternative splicing in generating isoform diversity among plasma membrane calcium pumps. *Physiol Rev*, 81(1), 21–50.

Strider, J. W., Masterson, C. G., & Durham, P. L. (2011). Treatment of mast cells with carbon dioxide suppresses degranulation via a novel mechanism involving repression of increased intracellular calcium levels. *Allergy*, 66(3), 341–50.

Sugawara, H., Kurosaki, M., Takata, M., & Kurosaki, T. (1997). Genetic evidence for involvement of type 1, type 2 and type 3 inositol 1,4,5-trisphosphate receptors in signal transduction through the B-cell antigen receptor. *EMBO J*, 16(11), 3078–88.

Suh, G. S. B., Wong, A. M., Hergarden, A. C., Wang, J. W., Simon, A. F., Benzer, S., Axel, R., & Anderson, D. J. (2004). A single population of olfactory sensory neurons mediates an innate avoidance behaviour in Drosophila. *Nature*, 431(7010), 854–9.

Sun, L., Wang, H., Hu, J., Han, J., Matsunami, H., & Luo, M. (2009). Guanylyl cyclase-D in the olfactory CO2 neurons is activated by bicarbonate. *PNAS USA*, 106(6), 2041–6.

Sun, X. C., Zhai, C. B., Cui, M., Chen, Y. Q., Levin, L. R., Buck, J., & Bonanno, J. A. (2003). HCO3–dependent soluble adenylyl cyclase activates cystic fibrosis transmembrane conductance regulator in corneal endothelium. *American Journal of Physiology-Cell Physiology*, 284(5), C1114–C1122.

Sunahara, R. K., Dessauer, C. W., Whisnant, R. E., Kleuss, C., & Gilman, A. G. (1997). Interaction of Gsalpha with the cytosolic domains of mammalian adenylyl cyclase. *J Biol Chem*, 272(35), 22265–71.

Sunahara, R. K. & Taussig, R. (2002). Isoforms of Mammalian Adenylyl Cyclase: Multiplicities of Signaling. *Mol. Interv.*, 2(3), 168–184.

Sutherland, W. & Rall, T. W. (1958). Fractionation and characterisation of a cyclic adenine ribonucleotide formed by tissue particles. *J Biol Chem*, 232(2), 1077–91.

Tada, M. & Toyofuku, T. (1998). Molecular regulation of phospholamban function and expression. *Trends Cardiovasc Med*, 8(8), 330–40.

Takasago, T., Imagawa, T., Furukawa, K., Ogurusu, T., & Shigekawa, M. (1991). Regulation of the cardiac ryanodine receptor by protein kinase-dependent phosphorylation. *J Biochem*, 109(1), 163–70.

Takemura, H., Hughes, A. R., Thastrup, O., & Putney, J. W. (1989). Activation of calcium entry by the tumor promoter thapsigargin in parotid acinar cells. Evidence that an intracellular calcium pool and not an inositol phosphate regulates calcium fluxes at the plasma membrane. *J Biol Chem*, 264(21), 12266–71.

Takeshita, K. (2003). Hypercapnic Acidosis Attenuates Endotoxin-Induced Nuclear Factor- B Activation. *Am J Respir Cell Mol Biol*, 29(1), 124–132.

Tamaoki, T., Nomoto, H., Takahashi, I., Kato, Y., Morimoto, M., & Tomita, F. (1986). Staurosporine, a potent inhibitor of phospholipid/Ca++dependent protein kinase. *Biochem Biophys Res Commun*, 135(2), 397–402.

Tang, W. J. & Gilman, A. G. (1995). Construction of a soluble adenylyl cyclase activated by Gs alpha and forskolin. *Science*, 268(5218), 1769–1772.

Tang, W. J. & Hurley, J. H. (1998). Catalytic mechanism and regulation of mammalian adenylyl cyclases. *Mol Pharmacol*, 54(2), 231–240.

Tanimura, A., Morita, T., Nezu, A., & Tojyo, Y. (2009). Monitoring of IP3 dynamics during Ca2+ oscillations in HSY human parotid cell line with FRET-based IP3 biosensors. *J Med Invest*, 56 Suppl, 357–61.

Taylor, C. T. & Cummins, E. P. (2011). Regulation of gene expression by carbon dioxide. *J Physiol*, 589(Pt 4), 797–803.

Taylor, C. W. & Laude, A. J. (2002). IP3 receptors and their regulation by calmodulin and cytosolic Ca2+. *Cell calcium*, 32(5-6), 321–34.

Taylor, C. W., Rahman, T., Tovey, S. C., Dedos, S. G., Taylor, E. J. A., & Velamakanni, S. (2009). IP3 receptors: some lessons from DT40 cells. *Immunol Rev*, 231(1), 23–44.

Teitelbaum, A. P. & Strewler, G. J. (1984). Parathyroid hormone receptors coupled to cyclic adenosine monophosphate formation in an established renal cell line. *Endocrinology*, 114(3), 980–5.

Tesmer, J. J., Sunahara, R. K., Gilman, a. G., & Sprang, S. R. (1997). Crystal structure of the catalytic domains of adenylyl cyclase in a complex with Gsalpha.GTPgammaS. *Science*, 278(5345), 1907–16.

Tesmer, J. J., Sunahara, R. K., Johnson, R. A., Gosselin, G., Gilman, A. G., & Sprang, S. R. (1999). Two-metal-ion catalysis in adenylyl cyclase. *Science*, 285(5428), 756–60.

Tews, I., Findeisen, F., Sinning, I., Schultz, A., Schultz, J. E., & Linder, J. U. (2005). The structure of a pH-sensing mycobacterial adenylyl cyclase holoenzyme. *Science*, 308(5724), 1020–3.

Thastrup, O., Cullen, P. J., Drø bak, B. K., Hanley, M. R., & Dawson, A. P. (1990). Thapsigargin, a tumor promoter, discharges intracellular Ca2+ stores by specific inhibition of the endoplasmic reticulum Ca2(+)-ATPase. *PNAS*, 87(7), 2466–70.

Thom, C., Guerenstein, P. G., Mechaber, W. L., & Hildebrand, J. G. (2004). Floral CO2 reveals flower profitability to moths. *J Chem Ecol*, 30(6), 1285–8.

Thomas, J. A., Buchsbaum, R. N., Zimniak, A., & Racker, E. (1979). Intracellular Ph Measurements in Ehrlich Ascites Tumor-Cells Utilizing Spectroscopic Probes Generated Insitu. *Biochemistry*, 18(11), 2210–2218.

Tokumitsu, H., Inuzuka, H., Ishikawa, Y., Ikeda, M., Saji, I., & Kobayashi, R. (2002). STO-609, a specific inhibitor of the Ca(2+)/calmodulin-dependent protein kinase kinase. *J Biol Chem*, 277(18), 15813–8.

Tomanek, L., Zuzow, M. J., Ivanina, A. V., Beniash, E., & Sokolova, I. M. (2011). Proteomic response to elevated PCO2 level in eastern oysters, Crassostrea virginica: evidence for oxidative stress. *J Exp Biol*, 214(Pt 11), 1836–44.

Tovey, S. C., Dedos, S. G., Rahman, T., Taylor, E. J. A., Pantazaka, E., & Taylor, C. W. (2010). Regulation of inositol 1,4,5-trisphosphate receptors by cAMP independent of cAMP-dependent protein kinase. *J Biol Chem*, 285(17), 12979–89.

Tovey, S. C., Dedos, S. G., Taylor, E. J. A., Church, J. E., & Taylor, C. W. (2008). Selective coupling of type 6 adenylyl cyclase with type 2 IP3 receptors mediates direct sensitisation of IP3 receptors by cAMP. *J Cell Biol*, 183(2), 297–311.

Tovey, S. C., Sun, Y., & Taylor, C. W. (2006). Rapid functional assays of intracellular Ca2+ channels. *Nat Protoc*, 1(1), 259–63.

Townsend, P. D., Holliday, P. M., Fenyk, S., Hess, K. C., Gray, M. A., Hodgson, D. R., & Cann, M. J. (2009). Stimulation of mammalian G-protein-responsive adenylyl cyclases by carbon dioxide. *J Biol Chem*, 284(2), 784–791.

Tresguerres, M., Buck, J., & Levin, L. R. (2010). Physiological carbon dioxide, bicarbonate, and pH sensing. *Pflügers Arch*, 460(6), 953–64.

Tse, C. M., Brant, S. R., Walker, M. S., Pouyssegur, J., & Donowitz, M. (1992). Cloning and sequencing of a rabbit cDNA encoding an intestinal and kidney-specific Na+/H+ exchanger isoform (NHE-3). *J Biol Chem*, 267(13), 9340–6.

Tsien, R. Y. (1980). New calcium indicators and buffers with high selectivity against magnesium and protons: design, synthesis, and properties of prototype structures. *Biochemistry*, 19(11), 2396–404.

Tsunoda, Y., Matsuno, K., & Tashiro, Y. (1991). Cytosolic acidification leads to Ca2+ mobilisation from intracellular stores in single and populational parietal cells and platelets. *Exp Cell Res*, 193(2), 356–63.

Tugba Durlu-Kandilci, N., Ruas, M., Chuang, K.-T., Brading, A., Parrington, J., & Galione, A. (2010). TPC2 proteins mediate nicotinic acid adenine dinucleotide phosphate (NAADP)- and agonist-evoked contractions of smooth muscle. *J Biol Chem*, 285(32), 24925–32.

Turner, S. L., Li, N., Guda, T., Githure, J., Cardé, R. T., & Ray, A. (2011). Ultra-prolonged activation of CO2-sensing neurons disorients mosquitoes. *Nature*, 474(7349), 87–91.

Twort, C. H. & van Breemen, C. (1988). Cyclic guanosine monophosphate-enhanced sequestration of Ca2+ by sarcoplasmic reticulum in vascular smooth muscle. *Circ Res*, 62(5), 961–4.

Uhlen, M. (2005). Antibody-based Proteomics for Human Tissue Profiling. *Mol Cell Proteomics*, 4(4), 384–393.

Vadász, I., Dada, L. A., Briva, A., Trejo, H. E., Welch, L. C., Chen, J., Tóth, P. T., Lecuona, E., Witters, L. A., Schumacker, P. T., Chandel, N. S., Seeger, W., & Sznajder, J. I. (2008a). AMP-activated protein kinase regulates CO2-induced alveolar epithelial dysfunction in rats and human cells by promoting Na,K-ATPase endocytosis. *The Journal of clinical investigation*, 118(2), 752–62.

Vadász, I., Dada, L. A., Briva, A., Trejo, H. E., Welch, L. C., Chen, J., Tóth, P. T., Lecuona, E., Witters, L. A., Schumacker, P. T., Chandel, N. S., Seeger, W., & Sznajder, J. I. (2008b). AMP-activated protein kinase regulates CO2-induced alveolar epithelial dysfunction in rats and human cells by promoting Na,K-ATPase endocytosis. *J Clin Invest*, 118(2), 752–62.

Valentich, J. D. (1986). Innovative approaches for the study of cultured renal epithelia. *Miner Electrolyte Metab*, 12(1), 6–13.

Van Adelsberg, J. & Al-Awqati, Q. (1986). Regulation of cell pH by Ca+2-mediated exocytotic insertion of H+-ATPases. *J Cell Biol*, 102(5), 1638–45.

Vandecaetsbeek, I., Vangheluwe, P., Raeymaekers, L., Wuytack, F., & Vanoevelen, J. (2011). The Ca2+ pumps of the endoplasmic reticulum and Golgi apparatus. *Cold Spring Harb Perspect Biol*, 3(5).

Vater, W., Kroneberg, G., Hoffmeister, F., Saller, H., Meng, K., Oberdorf, A., Puls, W., Schlossmann, K., & Stoepel, K. (1972). Pharmacology of 4-(2'-nitrophenyl)-2,6-dimethyl-1,4-dihydropyridine-3,5-dicarboxylic acid dimethyl ester, Nifedipine, BAY a 1040. *Arzneimittel-Forschung*, 22(1), 1–14.

Venkatachalam, K., Ma, H. T., Ford, D. L., & Gill, D. L. (2001). Expression of functional receptor-coupled TRPC3 channels in DT40 triple receptor InsP3 knockout cells. *J Biol Chem*, 276(36), 33980–5.

Vigne, P., Frelin, C., Cragoe, E. J., & Lazdunski, M. (1984). Structure-activity relationships of amiloride and certain of its analogues in relation to the blockade of the Na+/H+ exchange system. *Mol Pharmacol*, 25(1), 131–6.

Vince, J. W. & Reithmeier, R. A. (1998). Carbonic anhydrase II binds to the carboxyl terminus of human band 3, the erythrocyte C1-/HCO3- exchanger. *J Biol Chem*, 273(43), 28430–7.

Vohwinkel, C. U., Lecuona, E., Sun, H., Sommer, N., Vadasz, I., Chandel, N. S., & Sznajder, J. I. (2011). Elevated CO2 levels cause mitochondrial dysfunction and impair cell proliferation. *J Biol Chem*.

Volpe, P., Villa, A., Damiani, E., Sharp, A. H., Podini, P., Snyder, S. H., & Meldolesi, J. (1991). Heterogeneity of microsomal Ca2+ stores in chicken Purkinje neurons. *EMBO J*, 10(11), 3183–9.

Waisbren, S. J., Geibel, J. P., Modlin, I. M., & Boron, W. F. (1994). Unusual permeability properties of gastric gland cells. *Nature*, 368(6469), 332–5.

Walsh, C., Barrow, S., Voronina, S., Chvanov, M., Petersen, O. H., & Tepikin, A. (2009). Modulation of calcium signalling by mitochondria. *Biochim Biophys Acta*, 1787(11), 1374–82.

Wang, H., Yan, Z., Yang, S., Cai, J., Robinson, H., & Ke, H. (2008). Kinetic and structural studies of phosphodiesterase-8A and implication on the inhibitor selectivity. *Biochemistry*, 47(48), 12760–8.

Wang, K. W. & Deen, W. M. (1980). Chemical kinetic and diffusional limitations on bicarbonate reabsorption by the proximal tubule. *Biophys J*, 31(2), 161–82.

Wang, Y., Cohen, J., Boron, W. F., Schulten, K., & Tajkhorshid, E. (2007). Exploring gas permeability of cellular membranes and membrane channels with molecular dynamics. *J Struct Biol*, 157(3), 534–44.

Wang, Y., Lam, C. S., Wu, F., Wang, W., Duan, Y. Y., & Huang, P. B. (2005). Regulation of CFTR channels by HCO3–sensitive soluble adenylyl cyclase in human airway epithelial cells. *Am J Physiol Cell Physiol*, 289(5), C1145–C1151.

Ward, D. T. (2004). Calcium receptor-mediated intracellular signalling. *Cell Calcium*, 35(3), 217–228.

Watson, A. J., Metzl, N., & Schuster, U. (2011). Monitoring and interpreting the ocean uptake of atmospheric CO2. *Philos Transact A Math Phys Eng Sci*, 369(1943), 1997–2008.

Webb, R. K., Woodhall, P. B., Tisher, C. C., Glaubiger, G., Neelon, F. A., & Robinson, R. R. (1977). Relationship between phosphaturia and acute hypercapnia in the rat. *J Clin Invest*, 60(4), 829–37.

Wehrens, X. H. T., Lehnart, S. E., Reiken, S., Vest, J. A., Wronska, A., & Marks, A. R. (2006). Ryanodine receptor/calcium release channel PKA phosphorylation: a critical mediator of heart failure progression. *PNAS USA*, 103(3), 511–8.

Weiner, I. D. & Hamm, L. L. (1989). Use of fluorescent dye BCECF to measure intracellular pH in cortical collecting tubule. *Am J Physiol*, 256(5 Pt 2), F957–64.

Weintraub, W. H. & Machen, T. E. (1989). pH regulation in hepatoma cells: roles for Na-H exchange, Cl-HCO3 exchange, and Na-HCO3 cotransport. *Am J Physiol*, 257(3 Pt 1), G317–27.

Wenker, I. C., Sobrinho, C. R., Takakura, A. C., Moreira, T. S., & Mulkey, D. K. (2012). Regulation of ventral surface CO2/H+-sensitive neurons by purinergic signalling. *J Physiol*, 590(Pt 9), 2137–50.

Werner, G., Hagenmaier, H., Drautz, H., Baumgartner, A., & Zähner, H. (1984). Metabolic products of microorganisms. 224. Bafilomycins, a new group of macrolide antibiotics. Production, isolation, chemical structure and biological activity. *J Antibiot (Tokyo)*, 37(2), 110–7.

White, A. A. & Zenser, T. V. (1971). Separation of cyclic 3',5'-nucleoside monophosphates from other nucleotides on aluminum oxide columns. Application to the assay of adenyl cyclase and guanyl cyclase. *Anal Biochem*, 41(2), 372–396.

Willgoss, D., Jacobi, J., de Jersey, J., Bartley, P., & Lloyd, H. (1980). Effect of calcium on cyclic nucleotide phosphodiesterase in parathyroid tissue. *Biochem Biophys Res Commun*, 94(3), 763–768.

Willoughby, D. & Cooper, D. M. F. (2007). Organization and Ca2+ regulation of adenylyl cyclases in cAMP microdomains. *Physiol Rev*, 87(3), 965–1010.

Willoughby, D., Masada, N., Crossthwaite, A. J., Ciruela, A., & Cooper, D. M. F. (2005). Localised Na+/H+ exchanger 1 expression protects Ca2+-regulated adenylyl cyclases from changes in intracellular pH. *J Biol Chem*, 280(35), 30864–72.

Wincek, T. J. & Sweat, F. W. (1975). Assay of Adenyl-Cyclase by Sequential Dowex-Alumina Chromatography. *Anal Biochem*, 64(2), 631–635.

Winkler, F. K. (2006). Amt/MEP/Rh proteins conduct ammonia. *Pflügers Arch*, 451(6), 701–7.

Witzmann, F. A., Clack, J. W., Geiss, K., Hussain, S., Juhl, M. J., Rice, C. M., & Wang, C. (2002). Proteomic evaluation of cell preparation methods in primary hepatocyte cell culture. *Electrophoresis*, 23(14), 2223–32.

Wojcikiewicz, R. J. & Luo, S. G. (1998). Phosphorylation of inositol 1,4,5-trisphosphate receptors by cAMP-dependent protein kinase. Type I, II, and III receptors are differentially susceptible to phosphorylation and are phosphorylated in intact cells. *J Biol Chem*, 273(10), 5670–7.

Woodward, F. I. (2002). Potential impacts of global elevated CO2 concentrations on plants. *Curr Opin Plant Biol*, 5(3), 207–211.

Wu, M. M., Luik, R. M., & Lewis, R. S. (2007). Some assembly required: constructing the elementary units of store-operated Ca2+ entry. *Cell calcium*, 42(2), 163–72.

Wu, M. S., Biemesderfer, D., Giebisch, G., & Aronson, P. S. (1996). Role of NHE3 in mediating renal brush border Na+-H+ exchange. Adaptation to metabolic acidosis. *J Biol Chem*, 271(51), 32749–52.

Xie, F. & Conti, M. (2004). Expression of the soluble adenylyl cyclase during rat spermatogenesis: evidence for cytoplasmic sites of cAMP production in germ cells. *Dev Biol*, 265(1), 196–206.

Xie, F., Garcia, M. A., Carlson, A. E., Schuh, S. M., Babcock, D. F., Jaiswal, B. S., Gossen, J. A., Esposito, G., van Duin, M., & Conti, M. (2006). Soluble adenylyl cyclase (sAC) is indispensable for sperm function and fertilization. *Developmental Biology*, 296(2), 353–362.

Yáñez, M., Gil-Longo, J., & Campos-Toimil, M. (2012). Calcium binding proteins. *Adv Exp Med Biol*, 740, 461–82.

Yamasaki, M., Masgrau, R., Morgan, A. J., Churchill, G. C., Patel, S., Ashcroft, S. J. H., & Galione, A. (2004). Organelle selection determines agonist-specific Ca2+ signals in pancreatic acinar and beta cells. *J Biol Chem*, 279(8), 7234–40.

Yan, S. Z., Huang, Z. H., Andrews, R. K., & Tang, W. J. (1998). Conversion of forskolin-insensitive to forskolin-sensitive (mouse-type IX) adenylyl cyclase. *Mol Pharmacol*, 53(2), 182–7.

Yan, S. Z., Huang, Z. H., Rao, V. D., Hurley, J. H., & Tang, W. J. (1997). Three discrete regions of mammalian adenylyl cyclase form a site for Gsalpha activation. *J Biol Chem*, 272(30), 18849–18854.

Yang, D., Shcheynikov, N., & Muallem, S. (2011). IRBIT: It Is Everywhere. *Neurochem Res*, 36(7), 1166–74.

Yao, C. A. & Carlson, J. R. (2010). Role of G-proteins in odor-sensing and CO2-sensing neurons in Drosophila. *J Neurosci*, 30(13), 4562–72.

Yoshimura, M. & Cooper, D. M. (1992). Cloning and expression of a Ca(2+)-inhibitable adenylyl cyclase from NCB-20 cells. *PNAS USA*, 89(15), 6716–20.

Young, J. M., Waters, H., Dong, C., Fülle, H.-J., & Liman, E. R. (2007). Degeneration of the olfactory guanylyl cyclase D gene during primate evolution. *PloS One*, 2(9), e884.

Yu, S. & Choi, D. (1997). Na(+)-Ca2+ exchange currents in cortical neurons: concomitant forward and reverse operation and effect of glutamate. *Eur J Neurosci*, 9(6), 1273–81.

Zacchetti, D., Clementi, E., Fasolato, C., Lorenzon, P., Zottini, M., Grohovaz, F., Fumagalli, G., Pozzan, T., & Meldolesi, J. (1991). Intracellular Ca2+ pools in PC12 cells. A unique, rapidly exchanging pool is sensitive to both inositol 1,4,5-trisphosphate and caffeine-ryanodine. *J Biol Chem*, 266(30), 20152–8.

Zhang, G., Liu, Y., Ruoho, A. E., & Hurley, J. H. (1997). Structure of the adenylyl cyclase catalytic core. *Nature*, 386(6622), 247–53.

Zhao, N. & Tenenhouse, H. S. (2000). Npt2 gene disruption confers resistance to the inhibitory action of parathyroid hormone on renal sodium-phosphate cotransport. *Endocrinology*, 141(6), 2159–65.

Zhao, P.-L., Wang, X.-T., Zhang, X.-M., Cebotaru, V., Cebotaru, L., Guo, G., Morales, M., & Guggino, S. E. (2002). Tubular and cellular localisation of the cardiac L-type calcium channel in rat kidney. *Kidney Int*, 61(4), 1393–406.

Zhou, Y., Frey, T. K., & Yang, J. J. (2009). Viral calciomics: interplays between Ca2+ and virus. *Cell calcium*, 46(1), 1–17.

Zhou, Y., Sondek, J., & Harden, T. K. (2008). Activation of human phospholipase C-eta2 by Gbetagamma. *Biochemistry*, 47(15), 4410–7.

Zhu, M. X., Evans, A. M., Ma, J., Parrington, J., & Galione, A. (2010). Two-pore channels for integrative Ca signaling. *Commun Integr Biol*, 3(1), 12–7.

Zhu, X., Cha, B., Zachos, N. C., Sarker, R., Chakraborty, M., Chen, T.-E., Kovbasnjuk, O., & Donowitz, M. (2011). Elevated calcium acutely regulates dynamic interactions of NHERF2 and NHE3 proteins in opossum kidney (OK) cell microvilli. *J Biol Chem*, 286(40), 34486–96.

Ziegelstein, R. C., Cheng, L., Blank, P. S., Spurgeon, H. A., Lakatta, E. G., Hansford, R. G., & Capogrossi, M. C. (1993). Modulation of calcium homeostasis in cultured rat aortic endothelial cells by intracellular acidification. *Am J Physiol*, 265(4 Pt 2), H1424–33.

Zieske, L. R. (2006). A perspective on the use of iTRAQ reagent technology for protein complex and profiling studies. *J Exp Bot*, 57(7), 1501–8.

Zima, A. V., Copello, J. A., & Blatter, L. A. (2004). Effects of cytosolic NADH/NAD(+) levels on sarcoplasmic reticulum Ca(2+) release in permeabilised rat ventricular myocytes. *J Physiol*, 555(Pt 3), 727–41.

Zippin, J. H., Farrell, J., Huron, D., Kamenetsky, M., Hess, K. C., Fischman, D. A., Levin, L. R., & Buck, J. (2003). Article defines a nuclear cAMP microdomain. *Cell*.

Zong, X., Schreieck, J., Mehrke, G., Welling, A., Schuster, A., Bosse, E., Flockerzi, V., & Hofmann, F. (1995). On the regulation of the expressed L-type calcium channel by cAMP-dependent phosphorylation. *Pflügers Arch*, 430(3), 340–7.